Innate lymphoid cell-produced interleukin-26 modulates proliferation and DNA damage in intestinal epithelial cells

Yazan Salloum

PSL UNIVERSITÉ PARIS

THÈSE DE DOCTORAT
DE L'UNIVERSITÉ PSL

Préparée à l'institut Curie
École doctorale Complexité du Vivant ED515

Innate lymphoid cell-produced interleukin-26 modulates proliferation and DNA damage in intestinal epithelial cells

L'interleukine-26 produite par les cellules lymphoïdes innées module la prolifération et les dommages à l'ADN dans les cellules épithéliales intestinales

Soutenue par
Yazan SALLOUM
Le 06/09/2024

École doctorale n° 515
Complexité du Vivant

Spécialité
Cancérologie, génétique, hématologie, immunologie

Composition du jury :

Ana-Maria, LENNON Directrice de recherche, Institut Curie, Paris	*Présidente*
Neves, JOANA Principal investigator, King's College London	*Rapporteuse*
Mai Eva, NGUYEN CHI Chargée de recherche, Université de Montpellier	*Rapporteuse*
Christelle, LANGEVIN Directrice de recherche, INRAE, France	*Examinatrice*
Silvia, FRE Directrice de recherche, Institut Curie, Paris	*Examinatrice*
Pedro, HERNANDEZ Chargé de recherche, Institut Curie, Paris	*Directeur de thèse*

institutCurie

Génétique et Biologie du Développement
CNRS UMR 3215, INSERM U934

Dedicated to those who start with nothing but dreams

Table of content

Acknowledgments

Throughout my PhD, each failure, misjudgment, and heartbreak has been a teacher. Therefore, first and foremost, I acknowledge all the hardships, challenges, and setbacks that have crossed my path.

I want to express my gratitude to my supervisor, Dr. Pedro Hernandez, whose expertise, understanding, and patience added considerably to my graduate experience. His guidance, encouragement, and insightful feedback were instrumental in shaping this work.

I would like to sincerely thank the members of my thesis jury for accepting to evaluate my work and travel long distances for my PhD defense.

A big heartfelt thanks to the members of my thesis committee: Dr. Elisa Gomez-Perdiguero, Dr. Benoit Moindrot, and Dr. Morgane Thion for their guidance, support, and insightful comments throughout my PhD.

My sincere acknowledgements go to the Curie Institute for providing the resources necessary for my research. Special thanks to the Departments of Genetics and Developmental Biology (UMR3215 / U934) and Immunity and Cancer (U932) for all the invaluable conversations and input during unit seminars, as those have substantially contributed to my work and honed my presentation skills.

I would also like to acknowledge my lab mates and colleagues for the discussions, support, and help. A special thank you to Gwendoline Gros, whose assistance with intricate experiments significantly contributed to the success of my PhD.

Of course, I am forever grateful to my BdD family. Our simple coffee breaks in the middle room turned into extended sessions anywhere and everywhere, filled with lively (another way to say loud) conversations. What started as casual drinks evolved into night outs and eventually unforgettable vacations with cherished memories. You have transformed the lab into a second home for me. We have experienced so much together, and I am filled with gratitude for all of it. We have transcended the world of colleagues into the realm of habibis. I wish, though I know it is impossible, to find a similarly friendly and vibrant atmosphere at my next stop.

Cheers to all Thursday night drinkers. You are the proof that we should not quit alcohol. I will always remember all the laughs we shared, all the kebabs and shawarmas.

To my Syrian gang outside the BdD, we have known each other for almost half our lives. We have shared so much together—love, friendship, hardship, and war. We have always found each other, and we always will. Love you!

My beloved family, you have always believed in me (maybe sometimes beyond reason) and I think that gave me the confidence I have today. For that, I will be forever in your debt.

I would like to give a special shout-out to some unique people I met in Curie. Manuela Ye, the beating heart of our floor and my walking diary. You are an absolutely amazing person and our friendship means a lot for me. Thank you for all the unlimited and unconditional support and genuine care. Xavier Sabate, the BG, thank you for all the conservations and laughs we had, I learned a lot from you. Soraya Rabahi, the banana queen, my best office and conference mate (as long as you are awake!!). Thanks for being as ridiculous as humanly possible with me. Ignacio Medina Yanez, AMIIIGO, Cheers for your inappropriate jokes and the best Instagram reel updates which always made my day. Emma Torun, our friendship and discussions have been invaluable in the most vulnerable moments of my PhD, thank you! Hedvika Martin, I am sad that I will not be in Curie for the second part of your PhD and won't see you grow into the amazing scientist you will become. I wish you all the best!

To everyone who has been part of this journey, whether mentioned here or not, your contributions have been invaluable. Thank you all for your support and encouragement.

List of abbreviations

AHR: Aryl Hydrocarbon Receptor
AKT1: Serine/Threonine Kinase 1
AMPs: Antimicrobial Peptides
anxa4: The zebrafish Annexin A4 gene
APC: Adenomatous Polyposis Coli
bactDNA: Bacterial DNA
brca2: The zebrafish Breast Cancer Gene 2 DNA Repair Associated gene
CAC: Colitis-Associated Colon Cancer
ccnh: The zebrafish Cyclin H gene
CD: Crohn's Disease
CFU: Colony-Forming Units
CRC: Colorectal Cancer
CV: Conventional
dpf: Days Post-fertilization
dpi: Days Post-Infection
DSS: Dextran Sodium Sulfate
EOMES: The human Eomesodermin gene
elovl2: The zebrafish ELOVL Fatty Acid Elongase 2 gene
ercc1: The zebrafish Excision Repair Cross-complementation Group 1 gene
ERK: Extracellular Signal-Regulated Kinase
fabp2: The zebrafish Fatty Acid Binding Protein 2 gene
FoxP3: Forkhead Box P3
GALT: Gut-Associated Lymphoid Tissues
GATA3: GATA-binding Protein-3
gDNA: Genomic DNA
GF: Germ-free
GO: Gene Ontology
GSEA: Gene Set Enrichment Analysis
GWAS: Genome-Wide Association Studies
hIL-26Tg: A humanized transgenic mouse model, harboring the human *IL26* gene
hpi: Hours Post-Injection
IBD: Inflammatory Bowel Disease
IECs: Intestinal Epithelial Cells
IELs: Intraepithelial Lymphocytes
IFNG: Interferon-gamma
IFNλ: Lambda Interferons
IL-26: Interleukin-26
IL26: The human IL-26 gene

IL26: The human IL-26 protein
Il26: The mouse IL-26 gene
il26: The zebrafish IL-26 gene
Il26: The zebrafish IL-26 protein
ILCregs: Regulatory ILCs
ILCs: Innate Lymphoid Cells
ILFs: Isolated Lymphoid Follicles
ISCs: Intestinal Stem Cells
KEGG: Kyoto Encyclopedia of Genes and Genomes
LREs: Lysosome-Rich Enterocytes
LTi: Lymphoid Tissue Inducer cells
M cells: Microfold cells
MAIT: Mucosal-Associated Invariant T cells
MDP: Muramyl Dipeptide
myca: The zebrafish Myc Proto-Oncogene A gene
MYD88: Myeloid Differentiation Primary Response 88
NETs: Neutrophil Extracellular Traps
NF-κB: The transcription factor Nuclear Factor Kappa-Light-Chain-Enhancer of Activated B Cells
nitr4: The zebrafish Novel Immune Type Receptor-4 gene
nitr9: The zebrafish Novel Immune Type Receptor-9 gene
NK: Natural Killer cells
NOD2: Nucleotide Binding Oligomerization Domain Containing Protein 2
PAMPs: Pathogen Associated Molecular Patterns
PBMCs: Peripheral Blood Mononuclear Cells
pks: Polypeptide-non-Ribosomal Peptide Synthase Operon
rad51b: The zebrafish RAD51 Paralog B gene
rhIL26: The human recombinant IL-26 protein
RNA-seq: RNA-Sequencing
RNI: Reactive Nitrogen Intermediates
RORA: Retinoic Acid Receptor-related Orphan Receptor-alpha
RORC: Retinoic Acid Receptor-related Orphan Receptor-gamma
ROS: Reactive Oxygen Species
rzIl26: The recombinant zebrafish IL-26 protein
SAPK/JNK: Stress-Activated Protein Kinase/c-Jun N-terminal Kinase
scRNA-seq: Single-cell RNA Sequencing
SILTs: Solitary Isolated Lymphoid Tissues
SNPs: Single-nucleotide Polymorphisms
STAT1: Signal Transducers and Activators of Transcription 1
STAT3: Signal Transducers and Activators of Transcription 3
STING: Cytosolic Stimulator of Interferon Genes

TA: Transient Amplifying Cells
TBX21: T-box Transcription Factor T-bet
TGFβ1: Transforming Growth Factor-beta1
Th1: T helper 1 cells
Th17: T helper 17 cells
Th2: T helper 2 cells
TLRs: Toll-like Receptors
TNF: Tumor Necrosis Factor
TOX: The human Thymocyte Selection Associated High Mobility Group Box gene
Tregs: Regulatory T cells
Tregs: Regulatory T Cells
UC: Ulcerative Colitis
wpi: Week Post-Fertilization

List of figures

Introduction

Results

Discussion

Introduction

In multicellular animals, the gastrointestinal tract is responsible for ingesting and digesting food, absorbing water and nutrients, and eliminating waste. A significant fraction of these processes occurs in the intestine, which harbors numerous populations of immune cells alongside a large community of beneficial microorganisms, collectively known as the gut microbiota. As a consequence, the intestine must maintain a delicate balance, tolerating the presence of these microorganisms while preserving its absorptive functions and defending against harmful dietary antigens and invading pathogens. This intricate task is facilitated by a dynamic communication network involving the intestinal epithelium, immune cells, and the microbiota.

This crosstalk is largely mediated by cytokines, and its dysregulation can lead to pathologies such as inflammatory bowel disease (IBD), a group of disorders characterized by chronic inflammation in the gut and affecting millions of people worldwide (*1*). Despite extensive research, the etiology of IBD remains not fully understood. However, insights into the underlying factors of IBD can be drawn from genome-wide association studies (GWAS) which have identified over 200 loci associated with increased IBD risk. These loci predominantly influence the integrity of the intestinal epithelial barrier, the function of immune cells, and the immunological pathways that regulate microbial recognition and elimination (*2*). This underscores the critical role of the epithelium, microbiota, and immune cells, as well as the interactions between these elements, in maintaining gut homeostasis and preventing disease.

Interleukin-26 (IL-26) was identified as a risk factor for IBD (*3*) and is notably overexpressed in IBD lesions (*4*, *5*). The role of IL-26 in intestinal homeostasis and disease remains poorly understood, largely due to its absence in rodents, the main models for *in vivo* functional studies on cytokines (*6*).

In this project, we exploited the zebrafish model, which possesses a unique orthologue of the human *IL26* gene (*7*), to investigate role of IL-26 in gut homeostasis. Our findings revealed that the loss of IL-26 results in increased cell proliferation and DNA damage in intestinal epithelial cells (IECs) of zebrafish larvae. We identified innate lymphoid cells (ILCs)

as the primary cell source of IL-26 at this developmental stage. Moreover, we demonstrated that the adverse effects of IL-26 loss on epithelial homeostasis depend on the presence of microbiota, indicating that IL-26 is at the core of a regulatory circuit between IECs, ILCs, and the microbiota.

To provide a comprehensive literature review of this research project, I will begin by briefly describing the anatomy of the intestine. This will be followed by introducing the three primary players in intestinal homeostasis that are relevant to this work. This includes the intestinal epithelium, the gut immune system with an emphasis on ILCs, and the gut microbiota. Next, I will discuss the characteristics of IBD, highlighting the dysregulation of cellular proliferation and DNA damage. Subsequently, I will present the state of the art regarding IL-26 and its functions. Finally, I will provide an overview of the zebrafish as a model for intestinal functional studies, highlighting the main similarities and differences between zebrafish and mammalian guts.

1. Anatomy of the intestine

The mammalian intestinal wall consists of four layers: the mucosa, submucosa, muscularis, and serosa (Fig. 1). The mucosa is composed of the epithelium, the underlying lamina propria, and the muscularis mucosa. The lamina propria, a connective tissue layer located just beneath the epithelium, provides structural support to the mucosa and contains an extensive network of blood vessels and lymphatics. The muscularis mucosa is a thin layer of smooth muscle which constitutes the boundary between the mucosa and the submucosa. The submucosa is a connective tissue layer significant for housing blood vessels, lymphatic vessels, submucosal glands, and the submucosal plexus of enteric neurons. This layer is bordered by the muscularis which has two smooth muscle layers: an inner circular layer and an outer longitudinal layer. The myenteric plexus of enteric neurons lies between these two layers, coordinating muscular contraction in the gut and resulting in rhythmic peristalsis. Finally, The outermost layer of the gut is the serosa, which is a fibrous covering that separates the intestine from the surrounding peritoneal cavity (*8*).

The intestine is functionally divided into two primary segments: the small intestine, which includes the duodenum, jejunum, and ileum; and the large intestine, which comprises the cecum, appendix, colon, rectum, and anus. The small intestine's main functions are

digestion and nutrient absorption, whereas the large intestine is where water reabsorption primarily takes place (*9*). The structure, function, and cellular diversity of the epithelium differs between the small and large intestines, as outlined in the next section.

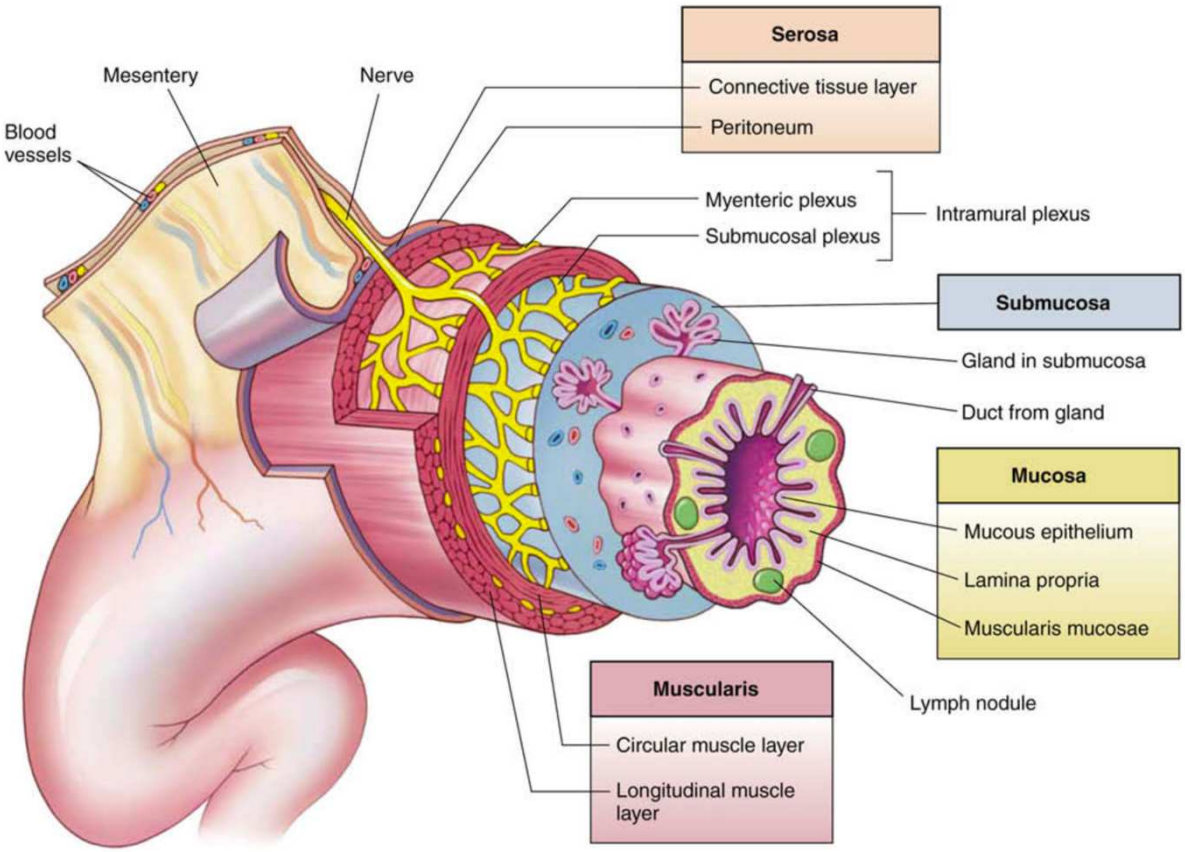

Fig. 1. The mammalian intestinal wall. The four layers constituting the wall of the intestine are: the mucosa, submucosa, muscularis, and serosa. The serosa continues as a serous membrane called the mesentery, which supports and stabilizes the intestines within the abdominal cavity. (Reprinted. (*10*))

2. The intestinal epithelium

The intestinal epithelium is composed of a single layer of epithelial cells which effectively contain the microbiota and luminal content within the intestinal lumen. In the small intestine, this layer forms finger-like protrusions that extend into the lumen, referred to as villi (Fig. 2). This significantly increases the surface area of the intestinal epithelium in contact with the lumen, thereby enhancing nutrient absorption. Conversely, the colon does not have villi, resulting in a relatively flat mucosal surface that helps prevent damage from semi-solid stool moving through the large intestine (*11*).

The epithelial layer throughout the intestine forms invaginations known as crypts of Lieberkühn (Fig. 2). At the base of these crypts reside intestinal stem cells (ISCs), which are crucial for the continuous renewal of IECs, maintaining the integrity and functionality of intestinal epithelium (*11*). As ISCs divide, they give rise to a population of highly proliferative cells, known as transient amplifying (TA) cells, which differentiate as they migrate upwards through the crypt. Mature IECs reach the apex of the crypts or villi, where they are ultimately shed into the intestinal lumen. This whole process is estimated to require 4-5 days in the human small intestine (*12*).

2.1. Classification of differentiated intestinal epithelial cells

Differentiated IECs carry out specialized functions and are broadly classified into two categories: absorptive and secretory enterocytes (*11*). Absorptive enterocytes are the most abundant cell type in the intestinal epithelium and are responsible for nutrient and water absorption. Secretory cells include:

- Goblet cells: Secrete mucins that form a protective mucus layer, which lines the intestinal epithelium and shields it from pathogens and physical damage.
- Enteroendocrine cells: Release hormones that regulate the secretion of digestive enzymes, control gut motility, and manage appetite and satiety.
- Paneth cells: Located at the base of the crypts adjacent to ISCs, Paneth cells secrete antimicrobial peptides to protect ISCs from luminal bacterial invasion (*13*, *14*). These cells also produce important Wnt factors to maintain the proliferation of ISCs (*15*). It is worth mentioning that, unlike other enterocytes, these cells are long-lived and migrate downwards along the crypt to reach their final position in proximity to ISCs (*16*).
- Tuft cells: Play an essential role in defending against helminths.
- Microfold (M) cells: Critical for the uptake and presentation of luminal antigens to the immune system.

While all these cell types are present in the small intestine, Paneth cells and M cells are not found in the large intestine (Fig. 2). Notably, in the colon of mice, there is a population of cells that expresses markers of both goblet cells and Paneth cells, known as colonic crypt base secretory cells. These cells have been demonstrated to enhance gut organoid formation

in vitro, suggesting that they may perform functions analogous to Paneth cells (*17*). In addition, macrophages in the distal colon have been observed to extend their cell membranes and form balloon-like structures embedded within the epithelium. These macrophages can sample fluids within IECs and respond to their content. Consequently, these macrophages could hypothetically fulfill roles typically carried out by M cells (*18*).

It is important to note that previously mentioned populations of IECs can be further subdivided based on their transcriptional programs, as demonstrated by single-cell RNA sequencing studies (*11*, *19*). However, for the purposes of this project, we will adhere to this classification.

2.2. Intestinal epithelial cells in gut homeostasis

The regulation of epithelial function is critical for maintaining gut health. This is underscored by the fact that several IBD risk genes are highly expressed in IECs. This includes genes associated with lineage specification (hepatocyte nuclear factor 4 alpha, *HNF4A*), junctional integrity (Chromosome 1 Open Reading Frame 106, *C1orf106*), and mucus production (Mucin 2, *MUC2*) (*2*). The role of these genes in intestinal inflammation was further demonstrated through functional studies. For instance, the expression of *MUC2*, a mucin vital for the formation of the mucus layer, has been observed to be dysregulated in ulcerative colitis patients (*20*). In addition, *Muc2*-diffecient mice were shown to develop spontaneous colitis after 5 weeks of age and exhibit increased susceptibility to dextran sodium sulfate (DSS)-induced colitis (*21*). Understanding the mechanisms and identifying the signals that regulate IEC function is crucial for developing targeted therapies for gastrointestinal diseases.

One technological advancement that contributed significantly to our understanding of IEC functions in recent years is organoid *in vitro* culture systems. Organoids are 3D structures closely resembling the architectural features and cellular heterogeneity of IECs found in native tissues. They can be generated by culturing ISCs, isolated crypts, or human pluripotent stem cells (*22*, *23*). Organoids offer a reductionist, scalable, and reproducible platform for addressing questions about intestinal homeostasis, such as the role of immune cells is the regulation of IEC function. For example, when co-cultured with murine small intestinal organoids, T helper 1 (Th1), Th2, and Th17 lead to decreased ISC numbers. In contrast,

incubation with Interleukin-10 (IL-10) or regulatory T cells (Tregs) support the growth of ISCs (*24*). These observations underscore the intricate relationship between IECs and immune cells in the gut, which will be discussed in the next chapter.

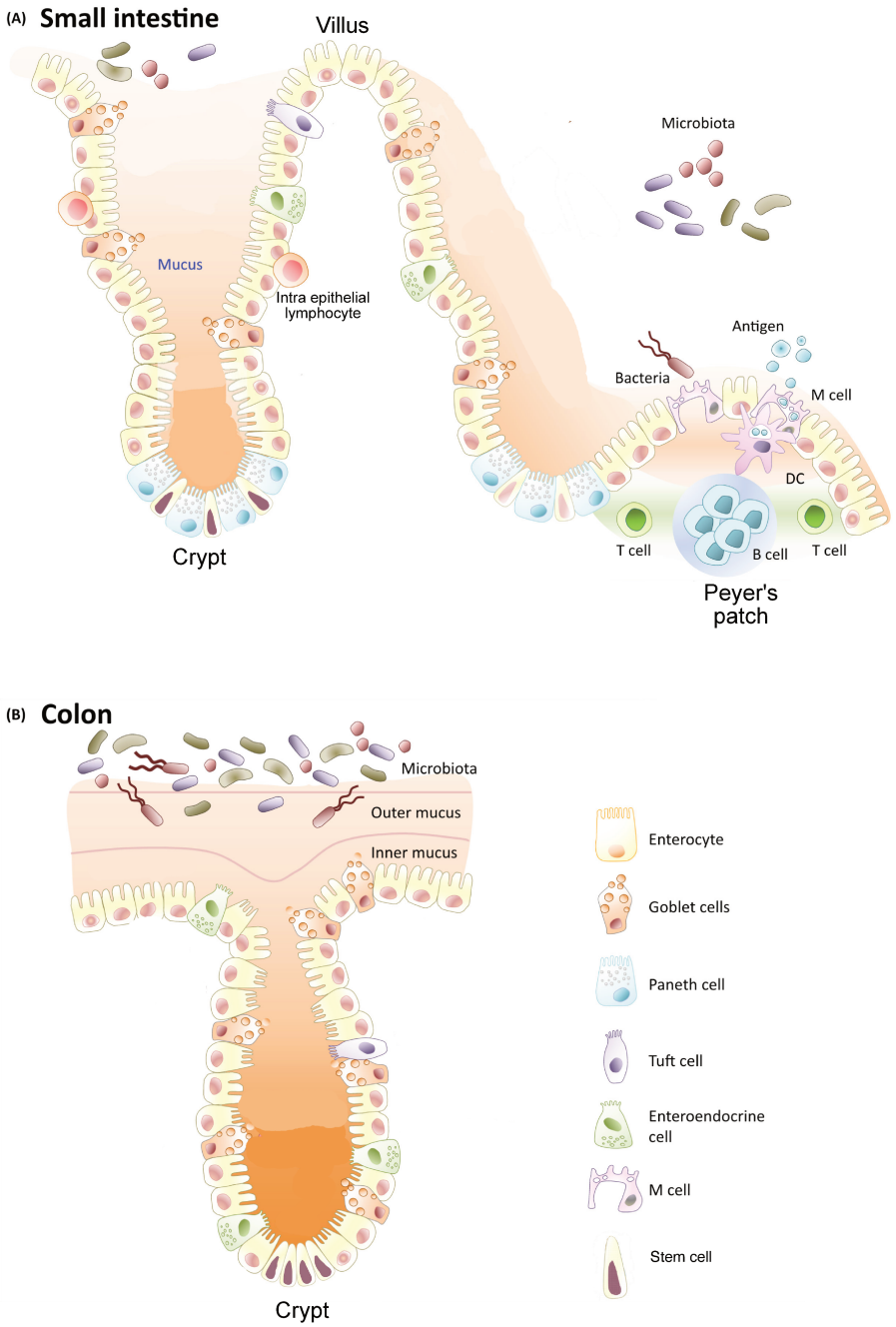

Fig. 2. The mammalian intestinal epithelium. (**A**) In the small intestine, the epithelial layer forms villi and crypts. The small intestine is characterized by the presence of Peyer's patches (see section 3). (**B**) The epithelium in the colon lacks villi and forms only crypts. Note that the mucus in the colon forms two layers: an inner layer, which is dense and attached to the epithelium, and an outer layer, which is looser and serves as a barrier to pathogens. (Adapted. (*11*))

3. The gut immune system and innate lymphoid cells

Immune cell populations in the intestine display significant variability in both their frequency and anatomical distribution. The majority of these immune cells reside within the lamina propria, encompassing both lymphoid and myeloid lineages. This diverse array includes B cells, T cells, ILCs, dendritic cells, macrophages, eosinophils, and mast cells. A smaller proportion of immune cells, predominantly T cells and ILCs, resides within the intestinal epithelium and are referred to as intraepithelial lymphocytes (IELs) (*25*).

A characteristic feature of the immune system in the gut is the presence of lymphoid structures known as gut-associated lymphoid tissues (GALT). These entities consist of subepithelial lymphoid aggregates found within the mucosa and submucosa. The epithelium overlaying these structures is characterized by the presence of M cells. These cells, as mentioned before, specialize in capturing and transporting luminal antigens to the GALT, where these antigens are subsequently presented to adaptive immune cells (*26*).

The most well-studied of the GALT are Peyer's patches, which are macroscopically visible and unique to the small intestine. Peyer's patches comprise numerous B cell lymphoid follicles, flanked by smaller T cell areas. In distinction to lymph nodes, Peyer's patches are not encapsulated and consistently contain germinal centers, suggesting continuous immune activation (*26*). In the large intestine, similar macroscopic structures are called caecal patches near the ileocaecal valve (*27*) and colonic patches throughout the colon and rectum (*28*).

Additionally, the GALT encompasses smaller lymphoid aggregates referred to as solitary isolated lymphoid tissues (SILTs), which are only detectable microscopically. SILTs vary in size, from small cryptopatches to mature isolated lymphoid follicles (ILFs). Unlike Peyer's patches, ILFs mainly consist of B cells and lack distinct T cell zones. However, similar to Peyer's patches, they contain germinal centers, indicating continuous humoral immune activation. In contrast, cryptopatches are primarily composed of T cells and ILCs and lack fully differentiated B cells (*26*).

During fetal development, lymphoid tissue inducer (LTi) cells play a significant role in the formation of GALT. LTi cells induce mesenchymal stromal cells to express essential factors for the homing of hematopoietic cells to the developing lymphoid structures. LTi cells are a subset of ILCs, the most recently described subset of immune cells. ILCs are distinguished by

their lymphoid morphology and their lack of recombined antigen-specific receptors. ILCs function as rapid cytokine producers in response to constant challenges, unlike adaptive lymphocytes that require longer periods to expand in response to antigen-specific stimulation. In the intestine, ILCs are mainly located in the lamina propria, although some can be found within the intestinal epithelium (*29*).

3.1. Classification of innate lymphoid cells

ILCs are categorized based on their transcription factor and cytokine production profiles. These groups include natural killer (NK) cells, type 1 ILCs (ILC1), type 2 ILCs (ILC2), type 3 ILCs (ILC3), and LTis. Each of these ILC groups shares functional similarities with a specific subset of T cells. For instance, ILC1 resemble $CD4^+$ Th1 cells, ILC2 are analogous to $CD4^+$ Th2 cells, ILC3 are similar to $CD4^+$ Th17 cells, and NK cells display functional similarity to $CD8^+$ cytotoxic T cells (*30*).

NK cells express the transcription factor eomesodermin (*EOMES*). ILC1 express the T-box transcription factor T-bet (*TBX21*). Both NK and ILC1 respond to IL-12 and IL-18, and produce interferon-gamma (*IFNG*) and tumor necrosis factor (*TNF*). ILC2 are marked by the expression of two transcription factors, GATA-binding protein-3 (*GATA3*) and retinoic acid receptor-related orphan receptor-alpha (*RORA*). They bear the IL-33 receptor and express type 2 cytokines (e.g., IL-5 and IL-13). ILC3 produce ROR-gamma (*RORC*) and aryl hydrocarbon receptor (*AHR*) transcription factors, express receptors for IL-1 and IL-23, and secrete IL-17, IL-22, and IL-26. LTis require *RORC* as well as thymocyte selection associated high mobility group box (TOX) transcription factors and produce Lymphotoxin, IL-17, and IL-22 (*31*).

3.2. Innate lymphoid cells in gut homeostasis

The importance of ILCs in health and disease is emphasized by multiple lines of evidence. First, ILCs numbers are dysregulated in the inflammatory lesions of IBD patients (*32*). Second, GWAS in IBD patients have identified several risk polymorphisms in genes associated with ILCs function. These comprise polymorphisms in IL-17RA, IL-23R, and IL-26. ILC3 respond to IL-23 by expressing IL-17, IL-22, and IL-26, indicating the potential involvement of these cells in IBD pathology.

Functional studies further support the involvement of ILCs in disease. For example, *Rag2*$^{-/-}$ mice lack adaptive lymphocytes and are used to study the role of innate immunity in

intestinal inflammation. These mice develop colitis upon infection with *Helicobacter hepaticus* in an IL-23-dependent manner (*33*). The cells responding to IL-23 in this model were shown to be ILC3 (*34*) and the depletion of these cells using specific antibodies protected the mice from colitis. Furthermore, in contrast to *Rag2-/-* mice that develop colitis upon the administration of anti-CD40 which activates myeloid cells, *Rag2-/-Rorc-/-* mice are protected from colitis due to the genetic depletion of ILC3 (*34*). These observations emphasize the critical involvement of ILC3 in intestinal inflammation.

The role of ILC-produced cytokines and their dynamic interactions with IECs in maintaining gut homeostasis is best exemplified by IL-22. This ILC3-produced cytokine promotes epithelial cell proliferation (*35*), protects ISCs from genotoxic stress (*36*), enhances mucus production, and sustains goblet cell numbers upon infection with *Citrobacter rodentium* (*37*). Interestingly, co-culturing ILC3 with small intestinal organoids enriches for a secretory goblet cell signature, which in turn induces IL-22 expression by ILCs (*38*). This demonstrates the presence of bidirectional communication between these two populations and underscores the need for a better understanding of regulatory communication networks in the gut.

Although models such as *Rag2-/-* mice and organoids contributed to our understanding of ILCs function, there are significant limitations. *Rag2-/-* mice lack adaptive lymphocytes that may interact with ILCs and modulate their function in WT animals. In addition, organoids do not reflect the complexity and heterogeneity of all cell types in native tissues. Therefore, the specific functions of the different ILC subtypes in both mice and humans remain incompletely understood. This knowledge gap is primarily attributed to the lack of ILC-specific markers, precluding the targeted ablation of these cells. Consequently, further research is needed to develop these markers and advance our understanding of the role of ILCs in gut homeostasis and disease.

4. The gut microbiota

4.1. Composition of the human gut microbiota

The collection of bacteria, archaea, eukarya, and viruses colonizing the gut is termed the gut microbiota. It is involved in many beneficial processes to the host such as breaking down of nutrients, synthesis of certain vitamins, and protection against pathogen colonization (*39*).

The density of microbiota increases progressively along the intestine, peaking in the distal colon (*40*). The most represented bacterial phyla in the human gut are Firmicutes and Bacteroidetes. Firmicutes comprise a diverse group of bacteria, including genera such as *Lactobacillus*, *Clostridium*, and *Enterococcus*. Bacteroidetes include genera such as *Bacteroides* and *Prevotella*. Seven additional phyla are present in the human gut microbiota, including Actinobacteria, Proteobacteria, Fusobacteria, Verrucomicrobia, Spirochaetes, VadinBE97, and Cyanobacteria (*41–43*).

Although the majority of intestinal microorganisms engage in a mutualistic beneficial relationship with the host, certain symbiotic organisms, such as *Mucispirillum schaedleri* and *Helicobacter* species, have the potential to cause disease under certain conditions. These organisms are therefore termed pathobionts (*44*).

4.2. Microbiota and gut homeostasis

The composition of the gut microbiota varies significantly between individuals. This is influenced by a number of factors, including the diet, genetics, and environment. This variability is considered to play a role in determining host susceptibility to various diseases, including IBD (*44*). Notably, several insights into the role of the microbiota in gut homeostasis have been derived from the tight connection between the microbiota and IBD.

First, in various models of intestinal inflammation in mice, gut inflammation can be resolved when these mice are reared in a germ-free (GF) environment (*45–49*).

Second, a hallmark of IBD in humans is the alteration of the composition of the gut microbiota, referred to as dysbiosis. This is characterized by a decreased diversity of bacterial communities and a shift in bacterial taxa, including alterations in certain genera of the phylum Firmicutes and increased abundance of *Enterobacteriaceae* species (*50*). Functional evidence

for the contribution of an altered microbiota to the onset of inflammation was demonstrated when transferring microbiota from colitis-bearing mice to healthy wild-type (WT) mice was sufficient to trigger disease in the recipient mice in several colitis models (*45*–*47*).

Third, GWAS have identified several innate bacterial sensing pathways as risk loci for IBD (*2*). For instance, polymorphisms in the nucleotide binding oligomerization domain containing protein 2 (*NOD2*) gene were one of the first to be conclusively linked to IBD (*51*). NOD2 functions as an intracellular cytosolic sensor of muramyl dipeptide (MDP), a component of bacterial cell walls. The binding of NOD2 to MDP activates the transcription factor nuclear factor kappa-light-chain-enhancer of activated B cells (NF-κB) and promotes the secretion of the proinflammatory cytokine IL-1β (*52*). *Nod2*-deficient mice are more susceptible to DSS-induced colitis (*53*), indicating that innate bacterial sensing and adequate immune activation in response to microbial species is paramount for gut homeostasis.

Innate bacterial sensing pathways also comprise Toll-like receptors (TLRs). TLRs are a family of innate immune receptors that recognize various bacterial components and utilize the downstream signaling molecule myeloid differentiation primary response 88 (MYD88) (*54*). *Myd88*$^{-/-}$ mice suffer greater tissue damage and mortality upon exposure to DSS due to reduced IEC proliferation and repair (*55*), further demonstrating the significance of innate sensing pathways in IECs homeostasis.

4.3. A communication network between the microbiota, ILCs, and IECs in the gut

The effects of microbial colonization on epithelial and immune homeostasis extends beyond disease conditions. For example, the gut epithelium of GF mice contains lower numbers of secretory cells (*56*, *57*) and manifests impaired lipid absorption (*58*). Moreover, IECs in GF mice show reduced proliferation and impaired mucus production at steady state (*49*, *59*).

The gut microbiota is also essential for the maturation of the immune system in the developing gut. GF mice exhibit defective formation of mucosa-associated lymphoid tissues (*60*), incomplete development of Th1, Th17, and Treg cells (*61*, *62*), and reduced numbers of intraepithelial T cells (*63*) and IgA-producing plasma cells (*64*).

One example that illustrates the interactions between the microbiota and ILCs can be observed in *Tbx21*$^{-/-}$ *Rag2*$^{-/-}$ mice. These animals are deficient for type 1 immunity and develop spontaneous colitis with increases accumulation of IL-17- and IL-22-producing ILC3 (*65*). ILC3 depletion using anti-CD90 antibodies protects these mice from colitis. Rearing these mice GF can reduce IL-17 and IL-22 expression and subsequently attenuate colitis. This shows the involvement of microbiota in regulating ILC function in the gut.

In the preceding sections, I have discussed the intestinal epithelium, ILCs, and microbiota, emphasizing their continuous interaction to maintain gut health. Next, I will examine the consequences of disrupted communication within this network, focusing on inflammatory bowel disease.

5. Inflammatory bowel disease

5.1. Definition and classification

IBD is a group of chronic inflammatory conditions of the gastrointestinal tract that can significantly impact life quality with symptoms such as abdominal pain, diarrhea, and weight loss. It is a chronic relapsing and remitting disease, associated with dysregulation of the mucosal immune system and commensal ecosystem in the intestine. The characteristic breakdown of the symbiotic relationship between the microbiota and the immune system results in an exaggerated immune response that damages the integrity and functionality of the epithelial barrier (*66*). The impaired barrier integrity results in the presence of bacterial DNA in the blood of up to 40% of patients (*67*, *68*), which is associated with poor disease prognosis (*69*). The translocation of bacterial components to the blood of IBD patients underscores the necessity of studying factors that control bacterial invasion in the gut.

IBD is typically classified into two subtypes: ulcerative colitis (UC) and Crohn's disease (CD). UC affects the colon while CD may affect any region of the gastrointestinal tract, but occurs primarily in the terminal ileum and colon. The onset of IBD predominantly occurs in the second and third decades of life with the majority of affected individuals progressing to relapsing and chronic disease. The increasing prevalence of IBD in pediatric populations suggests that the dysregulation of intestinal homeostasis could start early in life (*70*). This hypothesis requires further investigation utilizing animal models that allow for microbiota manipulation in the developing gut.

Traditional treatments to IBD typically involve pharmacotherapy to attenuate the immune response, utilizing drugs such as aminosalicylates and corticosteroids, supplemented with surgical intervention when necessary. More recently, the introduction of specific TNF inhibitors has represented a major breakthrough in IBD therapeutics, enabling prolonged remission in a significant fraction of patients. However, primary non-response to TNF inhibitors has been observed in up to 40% of patients. Additionally, secondary loss of response occurs in 23-46% of patients after one year of treatment, underscoring the need for novel therapeutic approaches (*71*).

5.2. Colitis-associated cancer

An important healthcare burden associated with IBD is its positive correlation with colitis-associated cancer (CAC). Chronic inflammation during IBD can lead to the formation of precancerous polyps in the colon, which over time can develop into cancer if left untreated. It is estimated that within 30 years of IBD onset, over 20% of patients develop carcinoma. Consistently, individuals with IBD exhibit a 2- to 3-fold increased lifetime risk of developing colorectal cancer (*72*).

This elevated risk can be explained by the significantly higher mutation rate observed in inflamed IBD lesions, which can be up to 25 times greater than that of healthy tissues. More precisely, it has been estimated that healthy colon crypts accumulate an average of 40 somatic mutations per crypt per year, whereas non-dysplastic inflamed IBD crypts showed 95 mutations per year (*73*–*75*). Consistently, non-dysplastic crypts in IBD-affected colons exhibit approximately a 2.4-fold increase in mutation rate compared to a healthy colon.

By comparing the distribution of mutations in dysplastic versus non-dysplastic IBD epithelium, it is evident that dysplastic tissue harbors mutations in several cellular processes, including cell proliferation and DNA repair. Specifically, mutations in the adenomatous polyposis coli (*APC*) gene, associated with proliferation, and in the *TP53* gene, involved in DNA repair, have been identified to be enriched in dysplastic tissues (*76*). These observations highlight the role of dysregulated cell proliferation and DNA repair in the progression from chronic inflammation to cancer.

The *APC* gene encodes an essential component of the β-catenin destruction complex, which plays a vital role in the Wnt signaling pathway. Loss of activity in this complex promotes

β-catenin nuclear localization and enhances Wnt signaling (*77*). This is known to induce proliferation in gut epithelial cells (*78*). Consequently, in a mouse model of *Apc* deficiency, these mice develop approximately 25–75 spontaneous adenomas in the small intestine and 1–5 in the colon by 180 days of age (*79*, *80*). This underscores the importance of regulating cellular proliferation in the pathogenesis of colon cancer.

TP53 encodes the p53 protein, a crucial regulator of cellular stress responses and often called the "guardian of the genome." p53 plays a pivotal role in maintaining genomic stability by responding to DNA damage through various mechanisms. When DNA damage is detected, p53 can induce cell cycle arrest, allowing time for repair processes to correct the damage. It also activates DNA repair pathways directly by upregulating genes involved in nucleotide excision repair, base excision repair, and double-strand break repair. Therefore, p53 is essential for protecting cells from accumulating genetic mutations and maintaining overall genomic integrity (*81*).

The high mutation rate observed in IBD can be attributed to the high concentration of reactive oxygen species (ROS) and reactive nitrogen intermediates (RNI) produced by activated immune cells in the inflammatory milieu of IBD lesions (*82*). Alternatively, genetic damage can be induced by bacteria-derived genotoxins accumulating in the context of a dysbiotic microbiota (*83*, *84*) or a bacterial infection (*85*).

One example of bacteria-derived genotoxins can be illustrated with *pks*$^{+}$ *E. coli*, which harbors the polypeptide-non-ribosomal peptide synthase operon (*pks*). This bacterium produces colibactin, a DNA alkylating and double-stranded break-inducing genotoxin. *pks*$^{+}$ *E. coli* is more prevalent in the colonic mucosa of both IBD and colorectal cancer (CRC) patients, with an estimated prevalence of 20% in healthy individuals and 40% in IBD patients (*83*, *86*). The pro-tumorigenic role of *pks*$^{+}$ *E. coli* has been demonstrated using a mouse model of CAC where inoculation of *pks*$^{+}$ *E. coli* into colitis-prone *il10*-defiecent mice resulted in a greater tumor burden, compared to *pks*$^{-}$ *E. coli* (*84*). This highlights the importance of controlled microbial communities in the gut to maintain gut homeostasis.

Overall, identifying agents that regulate proliferation, mitigate DNA damage, and influence microbiota composition in both health and disease is of great value. In this study, we focused on deciphering the functions of IL-26 in the gut and found that it modulates these

critical processes. Therefore, in the next chapter, I will introduce IL-26 and discuss the main reasons supporting our hypothesis of its significance in maintaining gut homeostasis.

6. Interleukin-26

6.1. Classification and gene conservation

IL-26, initially known as AK155 (*87*), is a member of the IL-10 cytokine family which includes IL-10, IL-19, IL-20, IL-22, IL-24, IL-28A, IL-28B, and IL-29. IL-28A, IL-28B, and IL-29 are additionally classified as lambda interferons (IFNλ). The human *IL26* gene consists of five exons and is located on chromosome 12q15, between the *IFNG* and *IL22* genes. This specific synteny (*IFNG*, *IL26*, and *IL22*) is conserved across all vertebrate species in which an IL-26 homologue has been identified (*88*).

In rodents, the *Il26* gene is inactivated due to transposon insertions (*89*) and gene duplication events (*90*). This precluded the use of this animal model for experimental studies involving endogenous IL-26 *in vivo.* Consequently, the functions of IL-26 in gut physiology and homeostasis are poorly characterized.

Moreover, sequence analysis of the IL-26 gene across available genomes has uncovered several inactivating mutations in the IL-26 gene in several vertebrate species (Fig. 3), including the African Elephant (*Loxodonta africana*) and the European Hedgehog (*Erinaceus europaeus*) (*91*). Phylogenetic analysis of these species indicates that the loss of IL-26 has occurred independently multiple times throughout evolution. Among the animals that have lost the IL-26 gene, no shared characteristics or a clear evolutionary gain have been described. Interestingly, some lower vertebrates, such as zebrafish, frogs, and birds, possess functionally intact IL-26 genes, providing potential animal models for studying IL-26. However, no such studies have been conducted to date.

6.2. Cellular sources

IL-26 expression has been predominantly reported in lymphocytes, including Th17 and Th1 cells (*92*), ILC3 (*93–95*), intraepithelial γδ T cells (*96*), mucosal-associated invariant T (MAIT) cells (*97*, *98*), and $CD8^+$ T cells (*99*). The expression of IL-26 in other immune cells, such as monocytes, is contested; some studies report no expression (*100*, *101*), while others indicate its presence (*102*). Among nonimmune cells, although IL-26 expression has been

reported (*103*, *104*), no clear evidence of this has been shown in the intestine. The contribution of each of these cell types to IL-26 expression across development and upon different inflammatory conditions, as well as the *in vivo* consequences of this expression, remain largely unknown.

6.3. Receptor

The IL-26 receptor complex is composed of two cytokine receptor proteins: IL-10RB and IL-20RA (*105*, *106*). IL-10RB is shared among IL-10, IL-22, IL-28A, IL-28B, IL-29, and IL-26, whereas IL-20RA is utilized by IL-26, IL-19, IL-20, and IL-24. Notably, the combination of IL-10RB and IL-20RA is unique to IL-26.

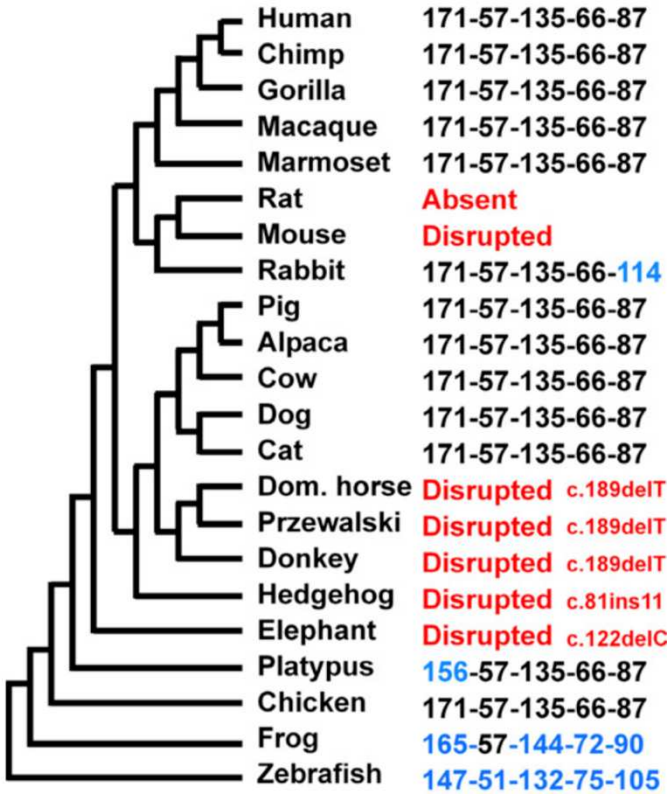

Fig. 3. Sequence analysis of the IL-26 gene across vertebrate species. Phylogenetic tree of the analyzed species. Branch length does not reflect evolutionary distance. The lengths of the 5 exons of the IL-26 gene are shown. Inactivating mutations are indicated in red next to their positions with respect to the human *IL26* mRNA sequence NM_018402. Variations in exon lengths are indicated in blue. (Adapted. (*91*))

In terms of cellular expression, IL-10RB is ubiquitously expressed, while IL-20Ra is primarily expressed in epithelial cells. Notably, IL-20Ra expression has also been reported in mesenchymal cells and monocytes (*107*).

In contrast to the *IL26* gene, the genes encoding the receptor complex are highly conserved throughout evolution. Consequently, although a functional *Il26* gene is absent in rodents, the genes encoding its receptor are present. Interestingly, several murine cells have been confirmed to express the IL-26 receptor complex and respond to human IL26 both *in vitro* and *in vivo* (*99*, *108*, *109*).

6.4. Signaling

It has been shown that several intestinal epithelial cell lines express the IL-26 receptor complex and respond to IL-26 by phosphorylating the transcription factors signal transducers and activators of transcription 1 (STAT1) and STAT3 (*110*). This response has also been observed in human colonic subepithelial myofibroblasts (*104*). In addition, the binding of IL-26 to its receptor leads to the phosphorylation of extracellular signal-regulated kinase (ERK)-1/2, stress-activated protein kinase/c-Jun N-terminal kinase (SAPK/JNK)-1/2, and serine/threonine Kinase 1 (AKT1) (*108*, *110*). These signaling events result in the expression of TNF-α and IL-8 in intestinal epithelial cells (*110*), IL-6 and IL-1β in monocytes (*111*), and, IL-6, and IFN-α in dendritic cells (*112*).

The role of IL-26 in regulating proliferation and DNA repair *in vivo* in the gut is not yet characterized. However, one report indicates that IL-26 inhibits proliferation of the intestinal epithelial cell line HT29 (*110*). Further research is required to confirm these findings and uncover the underlying mechanisms.

6.5. Protein structure and physiochemical features

IL-26 is a 171-amino acid protein with a mass of approximately 19 kDa. Although the crystal structure of IL-26 has not yet been elucidated, it is predicted to contain six alpha-helices. The human IL26 protein comprises a high number of positively charged amino acids, including 30 lysine and arginine residues. In consequence, the isoelectric point of IL26 is 10.7, indicating a cationic alkaline nature. In addition, the predicted structure reveals a predominance of cationic charges on one side, while the opposite side features a hydrophobic patch. This arrangement suggests that IL26 is a cationic, amphipathic protein (*88*).

6.6. Receptor-independent functions of IL-26

6.6.1. Intrinsic bactericidal activity

Several naturally occurring antimicrobial peptides (AMPs) are cationic and amphipathic. Therefore, the cationic amphipathic nature of IL26 has prompted research into whether it possesses antimicrobial properties (*112*). At concentrations of 5-10 µM, recombinant human IL26 protein (rhIL26) has been demonstrated to kill several gram-negative bacterial strains, including *Pseudomonas aeruginosa*, *Escherichia coli*, and *Klebsiella pneumoniae*, as well as the gram-positive bacterium *Staphylococcus aureus*. No effect of rhIL26 was observed with the gram-positive *Enterococcus faecalis* or the fungus *Candida albicans* at concentrations up to 50 µM. This effect was attributed to bacterial killing as the number of colonies incubated with rhIL26 decreased over time, accompanied by a loss of membrane integrity, formation and disruption of blebs, and leakage of bacterial cytosol into the extracellular environment. These findings suggest that IL26 disrupts bacterial membranes through pore formation. The full spectrum of IL26-sensitive species and the bacterial characteristics or components that render the bacteria susceptible to IL26 remain unidentified.

Interestingly, in a lung bacterial infection model, mice treated with rhIL26 show a strong reduction in bacterial loads in their lungs, blood, and spleen (*112*). However, whether this protective function of rhIL26 is a consequence of its intrinsic bactericidal activity or receptor-dependent signaling is unclear. Therefore, further research on the *in vivo* consequences of IL-26 antimicrobial activity is warranted.

6.6.2. IL-26-DNA complexes

The cationic nature of IL-26 suggests that it can bind negatively charged molecules, such as DNA. The formation of IL-26-DNA complexes has been confirmed through microscopy and gel migration assays, where incubation of genomic DNA (gDNA) with rhIL26 blocked the migration of gDNA through the gel (*112*). These complexes can protect extracellular DNA from degradation by DNases. Additionally, IL-26-DNA complexes can be endocytosed by plasmacytoid dendritic cells and subsequently trigger IFN-α production. This process occurs in an IL-26 receptor-independent manner, mediated through TLR9 (*112*), an innate immune receptor that recognises unmethylated CpG DNA motifs (*113*).

The ability of rhIL26 to bind nucleic acids is not limited to gDNA. rhIL26 has also been demonstrated to bind RNA, mitochondrial DNA, and neutrophil extracellular traps (NETs). These complexes have also been shown to activate monocytes and neutrophils via the inflammasome and the cytosolic stimulator of interferon genes (STING) pathways (*111*).

These findings suggest that IL-26 could sensitize the immune system to the presence of extracellular DNA. The release of DNA to the extracellular milieu occurs as a consequence tissue damage during chronic inflammation and bacterial infections. Whether IL-26 plays a role in immune activation in these conditions remains unknown.

6.7. IL-26 in health and disease

IL-26 is overexpressed in several inflammatory conditions such as psoriasis (*114*), rheumatoid arthritis (*115*), and most relevant to this work, IBD (*104*, *110*, *116*). More precisely, the inflamed mucosa of IBD patients, both in UC and CD, displays higher levels of IL-26 (*104*, *110*, *116*). Furthermore, IL-26 concentrations are higher in the blood of IBD patients (*110*, *116*).

The overexpression of this cytokine in these conditions highlights the urgent need to understand its *in vivo* functions. This urgency is further emphasized by the association of single-nucleotide polymorphisms (SNPs) within the *IL26* gene region with various disease conditions, including multiple sclerosis (*117*) , rheumatoid arthritis (*118*), and IBD (*119*).

The SNP in the *IL26* gene that is associated with increased IBD risk is intronic (*119*). To explore the correlation between this polymorphism and IBD, IBD patients were grouped based on their genotype, those with the risk allele were designated as varIL26 and those without it as wtIL26 (*120*). Examining the presence of bacterial DNA (bactDNA) in patients' blood revealed that the rate of bactDNA translocation to the blood in varIL26 patients was similar to that in wtIL26 patients. However, among bactDNA^{+} patients, the amount of bactDNA was significantly higher in varIL26. This suggests a role of IL-26 in controlling bactDNA loads in the blood of IBD patients.

In the same study, the presence of circulating bactDNA was associated with increased levels of IL-26 in the serum of only wtIL26 patients. Consistently, peripheral blood mononuclear cells (PBMCs) from varIL26 patients exposed to different concentrations of bactDNA from *E. coli* expressed lower *IL26* levels compared to wtIL26 patients. This was

associated with lower ability of these cells to kill *E. coli in vitro* (*120*). This proposes that the IBD-associated single nucleotide polymorphism (SNP) may regulate IL-26 expression levels in response to bactDNA in the blood, which in turn influences the concentrations of bactDNA. Functional verification of these hypotheses in suitable animal models is necessary.

In order to elucidate the function of IL-26 in gut inflammation, Corridoni et al. utilized a humanized transgenic mouse model, harboring the human *IL26* gene (hIL-26Tg) (*121*). These mice showed lower pathology upon DSS-induced colitis compared to WT mice, suggesting a protective role of IL-26 in acute colitis. This effect was associated with lower expression of immune response-associated genes in hIL-26Tg mice, indicating an immunoregulatory role for IL-26 (*99*).

Although this model provides a valuable tool to address the functions of IL-26 *in vivo*, it has significant limitations. First, the transgene used to generate this mouse line is 190-kb (*121*) and contains other elements besides *IL26*, such as *IFNG*, which could interfere with any observed phenotype. Second, the study did not address the composition and role of the microbiota, nor did it explore IL-26 receptor-dependent versus -independent functions. Lastly, this mouse model allows for the investigation of the consequences of a gain-of-function of IL-26 in a model organism that naturally lacks it, but it cannot address the results of IL-26 loss-of-function.

Interestingly, the zebrafish possess a unique homolog of the human *IL26* gene (*7*), providing a suitable model for studying IL-26 loss-of-function. In the next chapter of this thesis, I will introduce the zebrafish as a mode to study the function of IL-26 in the gut, highlighting major similarities and dissimilarities between mammalian and zebrafish guts.

7. The zebrafish model

The zebrafish (*Danio rerio*), a small freshwater teleost fish, has emerged as a prominent model organism in biological research due to its manageable laboratory husbandry, high fecundity, optical transparency up to two weeks of life, and rapid ex-utero development, facilitating microbiota manipulation and gnotobiotic research. Its utility in the laboratory is further enhanced by its fully annotated genome and the availability of extensive genomic resources and tools for genetic manipulations (*122*).

Zebrafish and humans diverged from a common ancestor approximately 400 million years ago (*123*). For comparison, the divergence between humans and mice occurred around 170 million years ago (*124*). Despite this evolutionary distance, anatomical and functional resemblance between zebrafish and mammalian digestive systems allowed the exploitation of zebrafish to study gut biology.

The zebrafish digestive tract is divided into the mouth, esophagus, three gut segments (anterior, middle, and posterior), and the anus. Notably, zebrafish lack a stomach and gastric glands. In consequence, the pH in the digestive tract does not drop below 7.5 under homeostatic conditions (*125*).

The zebrafish gut can be divided into segments that are functionally equivalent to the mammalian small and large intestines. This homology was demonstrated by microarray analysis on adult zebrafish guts, which were divided into seven segments (Fig. 4). Segments S1 to S5 closely resemble the small intestines of mammals, displaying high expression of genes involved in lipid, fatty acid, cholesterol, and glycerol, lipid metabolism, as well as peptidase and oxidoreductase activity. Segment S6 shows expression of genes related to glycolysis, oxidoreductase activity, and metabolism of amino acid, similar to the mammalian cecum. Segment S7 resembles the rectum, primarily involved in water retention. Therefore, segments S1 to S5 of the zebrafish intestine possess features of a mammalian small intestine, while segments S6 and S7 correspond to the mammalian large intestine (*126*).

In addition to this functional similarity, combined transcriptomic analysis with chromatin accessibility assessment in zebrafish, stickleback, mice, and human reveals a shared transcriptional regulatory network in intestinal epithelial cells across these species. These discoveries underscores the conservation of gut function between zebrafish and mammals (*127*).

The zebrafish gut wall comprises three layers: the mucosa (consisting of the epithelium and lamina propria), the muscularis (composed of circular and longitudinal smooth muscle), and the serosa. Notably, zebrafish lack the submucosal layer and the muscularis mucosa. As mentioned beforehand, the submucosa connects the mucosa with the underlying smooth muscle layer in mammals. However, in zebrafish, the smooth muscle layer is less complex and directly attach to the mucosa (*126*).

The zebrafish gut organogenesis occurs relatively quickly; zebrafish larvae develop a complete gut by 3-days post-fertilization (dpf), and begin digesting food by 5-6 dpf (*128*). This rapid development enables gut functional studies during larval stages, taking full advantage of zebrafish high fecundity, optical transparency, and easy gnotobiotic manipulation. Notably, the larval zebrafish gut is segmented into anterior, middle, and posterior sections, each with functional similarities to adult counterparts (Fig. 4).

7.1. The zebrafish gut Epithelium

The intestinal epithelium in zebrafish is organized into folds that resemble the villi of the mammalian small intestine but lack crypt structures (Fig. 5). These folds decrease in size from the anterior to the posterior gut, forming a relatively smooth surface in segment S7 (*126*).

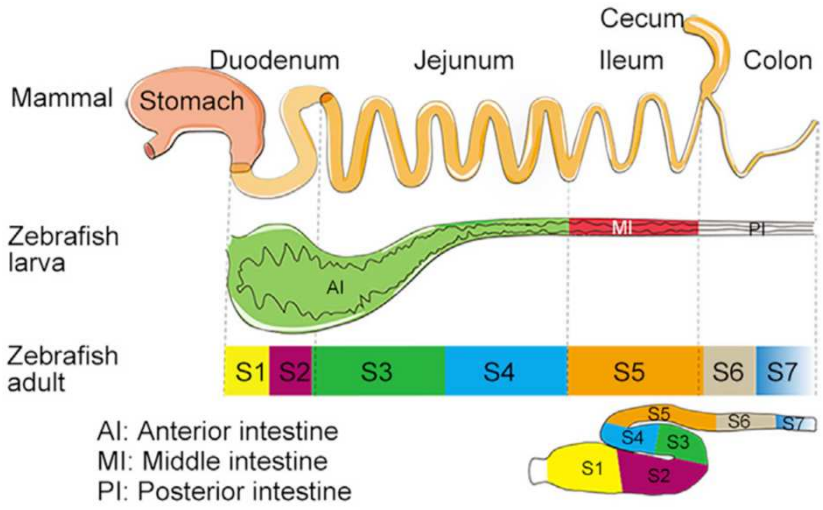

Fig. 4. Homology between mammalian and zebrafish gastrointestinal tracts. The anterior, middle, and posterior gut of zebrafish larvae are equivalent to mammalian duodenum plus jejunum, ileum, and colon, respectively. The S1-S2, S3-S4, S5, and S6-S7 segments of the adult zebrafish gut correspond to mammalian duodenum, jejunum, ileum, and colon, respectively. (Reprinted. (*129*))

Zebrafish ISCs reside at the base of the folds and express stemness markers such as *stat3*, *sox9b*, *her15.1, and prmt1* (*130–133*). Lineage-tracing experiments using the transgenic line *prmt1:mCherry-CreER*^{T2} have confirmed that *prmt1*-expressing cells are bona fide ISCs. The migration of these cells from the base to the tip of the folds takes approximately 2-3 days (*133*).

In the zebrafish gut, epithelial cell types such as absorptive enterocytes, goblet cells, enteroendocrine cells, and tuft cells have been described. However, Paneth cells and M cells have not been identified (*130*). Moreover, unlike adult mammals, lysosome-rich enterocytes (LREs) are present in the middle intestine of adult zebrafish (*127*). LREs are highly endocytic vacuolated cells that preferentially internalize dietary proteins via fluid-phase and receptor-mediated endocytosis. These proteins are subsequently broken down intracellularly into amino acids, thereby facilitating their absorption (*134*). LREs are found in the ileum of suckling mammals and middle intestine of zebrafish larvae. They are replaced by mature enterocytes at weaning in mammals (*135*, *136*), but remain into adulthood in zebrafish. Their persistence in zebrafish could be attributed to the low protease activity in the zebrafish intestinal lumen, leading to insufficient protein breakdown and amino acid uptake by enterocytes. This necessitates LREs to facilitate protein absorption by performing the digestion step intracellularly rather than in the intestinal lumen.

Recent studies have identified the presence of BEST4^{+} cells in the zebrafish gut epithelium (*130*, *137*). This finding is significant because these cells are absent in mice but present in humans. This population of cells represents a novel subset of mature absorptive enterocytes characterized by the expression of Bestrophin 4 (*BEST4*). They are sparsely distributed in the small and large intestines in humans. BEST4^{+} cells are involved in pH regulation, electrolyte secretion, and mucus hydration (*138*). The presence of this population in the zebrafish highlights the similarities between human and zebrafish intestinal epithelium and provides a valuable system to further explore their role in gut homeostasis.

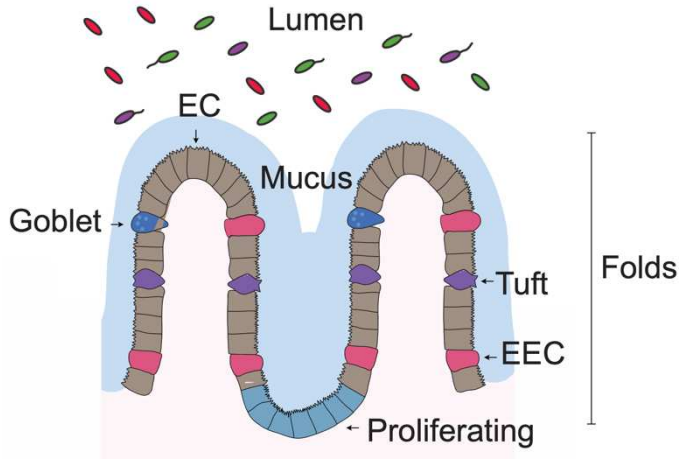

Fig. 5. Structure of the zebrafish epithelium. The epithelial layer in zebrafish is organized into folds. Abbreviations: EC, enterocyte; EEC, enteroendocrine cell.

7.2. Immune cells in the zebrafish gut

Zebrafish immune cells in the gut do not form discrete, macroscopically identifiable structures such as Peyer's patches. Instead, they are scattered in the mucosal layer throughout the gut. Major immune cell populations such as T cells, B cells, macrophages, and neutrophils are well described in the zebrafish gut and show functional resemblance to their mammalian counterparts. Interestingly, a recent study demonstrated the presence of ILCs in the intestines of adult zebrafish, with subtypes resembling those of mammalian ILCs (*139*). This work identified the novel immune type receptor-9 (*nitr9*) and *nitr4a* as specific markers for a population of ILCs that is capable of converting to ILC2 or ILC3 when stimulated with *Anisakis simplex* or *Vibrio anguillarum,* respectively. Notably, this population, referred to as ILC2/3, upregulates *il26* expression upon exposure to *Vibrio anguillarum* (*139*).

The identification of *nitr9* and *nitr4a* as ILC-specific markers paves the way for a better understanding of ILCs function in intestinal development and homeostasis. Questions that remain to be addressed include the timing of ILC emergence in the larval gut, the conditions that induce *il26* expression, and the subsequent consequences of this expression.

7.3. The zebrafish gut microbiota

In zebrafish, gut colonization starts at 4 dpf when the mouth opens, allowing microbes to enter into the digestive tract (*140*). At the phylum level, the gut microbiota consists of 11 divisions, 6 of them are shared with humans. These shared phyla encompass Proteobacteria, Fusobacteria, Firmicutes, Bacteroidetes, Actinobacteria and Verrucomicrobia (*42*). While the human microbiota is primarily dominated by Firmicutes and Bacteroidetes (*43*), the zebrafish microbiota is predominantly composed of by Proteobacteria (*Aeromonas*, *Pseudomona*s, and *Vibrio* genera), followed by Fusobacteria (Fig. 6). The diversity of the gut microbiota in zebrafish changes across larval, juvenile, and adult stages. Although Proteobacteria remain the most abundant phylum throughout all developmental stages, members of the phyla Firmicutes and Fusobacteria expand during later adult stages (*141*).

The divergence in microbiota composition between different species is influenced by both environmental factors and intrinsic host factors. This was demonstrated by transplanting mouse intestinal microbiota, which is dominated by Firmicutes, into zebrafish. Although the percentage of Firmicutes remained significantly higher after transplantation compared to

conventionally raised zebrafish, the small number of Proteobacteria that were present in the mouse intestine proliferated and became dominant after being transplanted to zebrafish (*42*). This indicates that environmental exposure to different bacterial species plays a crucial role in determining the composition of the gut microbiota, which is subsequently subjected to selective pressure by the host.

Despite the differences in microbiota composition between species, the effects of microbial colonization on intestinal homeostasis as well as the implicated mechanisms are conserved. For instance, by taking advantage of the zebrafish larvae model, it has been shown that microbial colonization in zebrafish induces IEC proliferation (*142*), promotes secretory cell fate (*143*), modulates lipid metabolism (*144*), increases mucin production (*143*), and increases immune cell numbers (*145*). Similar observations have been made in mouse models (see section 4), highlighting the functional conservation of microbial colonization between mammals and zebrafish.

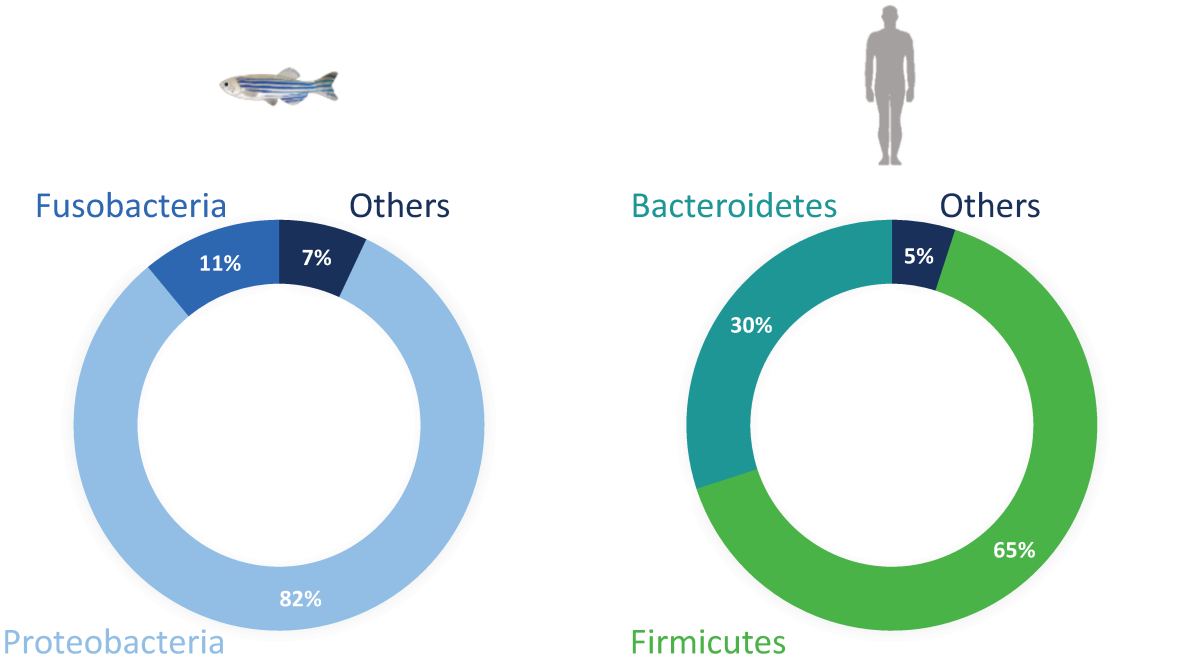

Fig. 6. Microbiota composition in the zebrafish and human gut. While the microbiota in zebrafish is dominated by Proteobacteria (*42*), Firmicutes and Bacteroidetes are the most represented phyla in the human intestinal microbiota (*43*).

7.4. Zebrafish as a model for gut bacterial infection

Zebrafish have been increasingly used as a model to study infectious diseases. Major pathogens in aquaculture include species from the *Edwardsiella* and *Aeromonas* genera. Among the *Edwardsiella* species, only *E. tarda* is known to infect humans. The consumption of *E. tarda*-contaminated food can lead to gastroenteritis and diarrhea, particularly among the elderly and immunocompromised individuals (*122*, *146*). *E. tarda* is a Gram-negative, rod-shaped bacterium (*146*) capable of infecting zebrafish both in adult (*147*) and larval stages (*148*, *149*). This bacterium enters the fish host through the skin and gills (*150*) subsequently infecting several organs, including the gut (*148*, *149*, *151*). *E. tarda* infection induces the proinflammatory cytokines IL-1β and TNF-α in adult spleen and liver (*151*) as well as in whole larvae (*149*), leads to the development of haemorrhagic septicaemia, and increases mortality (*151*). The gut-specific consequences of *E. tarda* infections and the role played by IL-26 in containing bacterial infections in the gut remain unexplored.

8. Final remarks

In this work, we utilized zebrafish larvae as a model to investigate the functions of IL-26 in gut homeostasis. We identified a circuit involving the microbiota, ILCs, and IECs, where IL-26 regulates proliferation and DNA damage in the gut at steady state and upon *E. tarda* infections. In the next section, I will present the results obtained during my PhD in the format of a paper manuscript.

Results

Innate lymphoid cell-produced interleukin-26 modulates intestinal epithelial homeostasis through interactions with the microbiota

Authors:

Yazan Salloum[1], Gwendoline Gros[1], Keinis Quintero-Castillo[2], Camila Garcia-Baudino[1], Soraya Rabahi[1], Akshai Janardhana Kurup[1], Sophie Richon[3], David Pérez-Pascual[4], Jean-Marc Ghigo[4], Danijela Matic Vignjevic[3], Carmen Feijoo[2], Pedro P. Hernandez[1]*

Affiliations:

[1]Institut Curie, PSL Research University CNRS UMR 3215, INSERM U934, 26 Rue d'Ulm, 75248 Paris Cedex 05, France.

[2]Fish Immunology Laboratory, Faculty of Life Science, Andres Bello University, Santiago 8370146, Chile.

[3]Institut Curie, PSL Research University, CNRS UMR 144, F-75005, Paris, France

[4]Institut Pasteur, Université Paris-Cité, UMR CNRS 6047, Genetics of Biofilms Laboratory, Department of Microbiology, Paris, France

*Corresponding author. Email: pedro.hernandez-cerda@curie.fr (P.P.H)

ABSTRACT

Interleukin-26 (IL-26) was identified as a risk factor for human inflammatory bowel disease (IBD) and is overexpressed in IBD lesions. In addition, IL-26 has been shown to have unique physiochemical properties enabling it to kill bacteria *in vitro* and bind to extracellular DNA. The *in vivo* functions of IL-26 in the intestine are not well understood primarily due to its absence in rodents. In this study, we utilized the zebrafish, which possess a unique orthologue of IL-26, to investigate its role in gut homeostasis. We show that IL-26 is a negative regulator of proliferation and DNA damage in gut epithelial cells in zebrafish larvae. We identified innate lymphoid cells (ILCs) as the primary source of IL-26 at this early developmental stage. Moreover, we demonstrate that the adverse effects of IL-26 loss on epithelial homeostasis are microbiota-dependent, indicating that IL-26 is central to a

regulatory circuit involving the microbiota, ILCs, and intestinal epithelial cells. Understanding the role of IL-26 in maintaining gut health is crucial for elucidating the aetiology of IBD and may inform the development of novel therapeutic strategies for this disorder.

INTRODUCTION

The gastrointestinal tract represents a complex system housing numerous populations of immune cells and commensal microorganisms, and it is a port of entry for different types of pathogens. In this environment, a dynamic crosstalk between immune cells, epithelial cells, and the microbiota ensures proper organ homeostasis. Dysregulation of this crosstalk can lead to inflammatory bowel diseases (IBD), a group of disorders characterized by chronic inflammation in the gut and a higher risk of developing colon cancer. A hallmark of this carcinogenesis is greater genomic instability and increased proliferation of abnormal cells (*76*). Therefore, it is essential to identify agents that control cell proliferation and DNA damage in the intestine.

Genome-wide association studies have identified interleukin-26 (IL-26) as a risk locus for ulcerative colitis (*3*), indicating a potential role of this cytokine in intestinal homeostasis. Moreover, IL-26 has been found to be overexpressed in the inflamed mucosa of IBD patients (*4*, *5*). Interestingly, intestinal epithelial cells (IECs) were shown to express the IL-26 receptor complex (IL10RB and IL20RA) and to respond to this cytokine *in vitro* (*5*). However, the *in vivo* functions of IL-26 and its impact on IECs hemostasis remain unclear, primarily due to the absence of IL-26 in rodent models (*6*), the main animal models for *in vivo* functional studies in the intestine. Interestingly, the zebrafish possess a unique orthologue of the human *IL26* gene (*7*), providing a suitable model to study the functions of this cytokine.

The human IL26 protein has been demonstrated to exhibit receptor-independent functions. For example, it has been shown that IL26 can form complexes with DNA, cross the cellular membrane, and activate intracellular TLR9 in dendritic cells (*92*), a toll-like receptor that recognizes unmethylated CpG motifs in DNA (*113*). This capability of IL26 might potentially serve as an alarm signal, activating the immune system in response to the presence extracellular DNA, a frequent occurrence upon inflammation (*152*, *153*). Moreover, IL-26 was shown to directly kill bacteria by pore formation *in vitro* in a dose-dependent manner (*92*, *154*). These anti-bacterial properties could potentially alter microbiota

composition, which is crucial for maintaining gut homeostasis and represents the main driver of inflammation in advanced IBD (*155*). The *in vivo* functional relevance of these receptor-independent functions of IL-26, and whether they are conserved in zebrafish, require further investigation.

In the human gut, ILCs have been reported to express IL-26 (*93*–*95*). We have recently demonstrated that ILCs are present in the adult zebrafish gut, resembling human ILCs (*139*). However, whether ILCs are present in the developing zebrafish gut, whether and how these cells express IL-26, and the *in vivo* functions of this cytokine, particularly during early-life, are still unknown.

In this study, we combined zebrafish genetics, transcriptomics, and microscopy with gnotobiotics and gut bacterial infection tools to uncover a novel role of IL-26 in regulating gut homeostasis during early life. We report that the loss of IL-26 resulted in increased proliferation in gut epithelial progenitors and elevated DNA damage in absorptive enterocytes. We further characterized these phenotypes in zebrafish lacking IL-26 receptor and zebrafish reared germ-free. We observed that the regulation of epithelial cell proliferation and DNA damage by IL-26 was dependent on the presence of microbiota and occurred independently of IL-26 receptor-mediated signaling. Importantly, we characterized the zebrafish IL-26 protein and found functional conservation of IL-26 intrinsic bactericidal properties between humans and zebrafish. Finally, we identified ILCs as the main cell source of IL-26 in the larval gut, with this expression being dependent on innate bacterial sensing of the microbiota. Overall, our findings suggest a circuit in which the microbiota induces IL-26 production in ILCs, which in turn helps keeping a healthy microbiota composition, maintaining epithelial gut homeostasis.

RESULTS

IL-26 regulates cell proliferation and DNA damage in the zebrafish larval gut

In order to understand the function of IL-26 in gut homeostasis, we generated *il26*-deficientzebrafish using the CRISPR/Cas9 system. Our approach resulted in a 110-bp deletion across exon 1 and exon 2 of the zebrafish IL-26 gene (*il26*^{ic4}) (Fig. S1A). This deletion is predicted to create a premature stop codon giving rise to a truncated protein consisting of

53-amino acids (Fig. S1B). The homozygous *il26*^{ic4}/*il26*^{ic4} mutant fish are hereafter referred to as *il26*$^{-/-}$.

In order to characterize IL-26 functions, we took an unbiased approach and performed bulk RNA-sequencing (RNA-seq) on dissected guts from 5-days post-fertilization (dpf) *il26*$^{-/-}$ and wild-type (WT) larvae. We identified 291 upregulated and 275 downregulated genes in the guts *il26*$^{-/-}$ larvae (Fig. 1A and Table S1). Complementary, we performed transcriptomic analysis upon IL-26 overexpression. To this end, recombinant zebrafish IL-26 (rzIl26) or bovine serum albumin (BSA) were injected in the gut and swim bladder of 5-dpf WT larvae, followed by RNA-seq on dissected guts 1-hour post-injection (hpi). In this condition, 1759 genes were upregulated and 2022 were downregulated (Fig. 1B and Table S2).

To infer the affected biological pathways and processes, we performed Kyoto encyclopedia of genes and genomes (KEGG) and gene set enrichment analyses (GSEA) on both datasets (Fig. 1, C-D and Fig. S1, C-D). KEGG pathway analysis on *il26*$^{-/-}$ guts revealed activation of the gene ontology (GO) term "cell cycle" (Fig. 1C), with upregulation of genes such as *myca* (Myc proto-oncogene a), a transcription factor that promotes proliferation (*156*); and *ccnh* (cyclin H), which controls cell cycle progression and promotes cancer growth (*157–159*) (Fig. 1E). In contrast, KEGG pathway analysis upon rzIl26 injection showed suppression of the GO term "DNA replication" (Fig. S1C), with downregulation of genes such as *myca* and *ccnh* (Fig. 1F). Furthermore, GSEA showed the suppression of the GO term "DNA repair" upon IL-26 overexpression (Fig. 1D), with downregulation of several DNA repair genes such as *brca2* (breast cancer gene 2 DNA repair associated (*160*)); *rad51b* (RAD51 paralog B (*161*)); and *ercc1* (excision repair cross-complementation group 1 (*162*)) (Fig. 1G). Collectively, our transcriptomic analysis upon IL-26 loss-of-function and overexpression suggested a potential role for IL-26 in regulating cell proliferation and DNA repair in the gut.

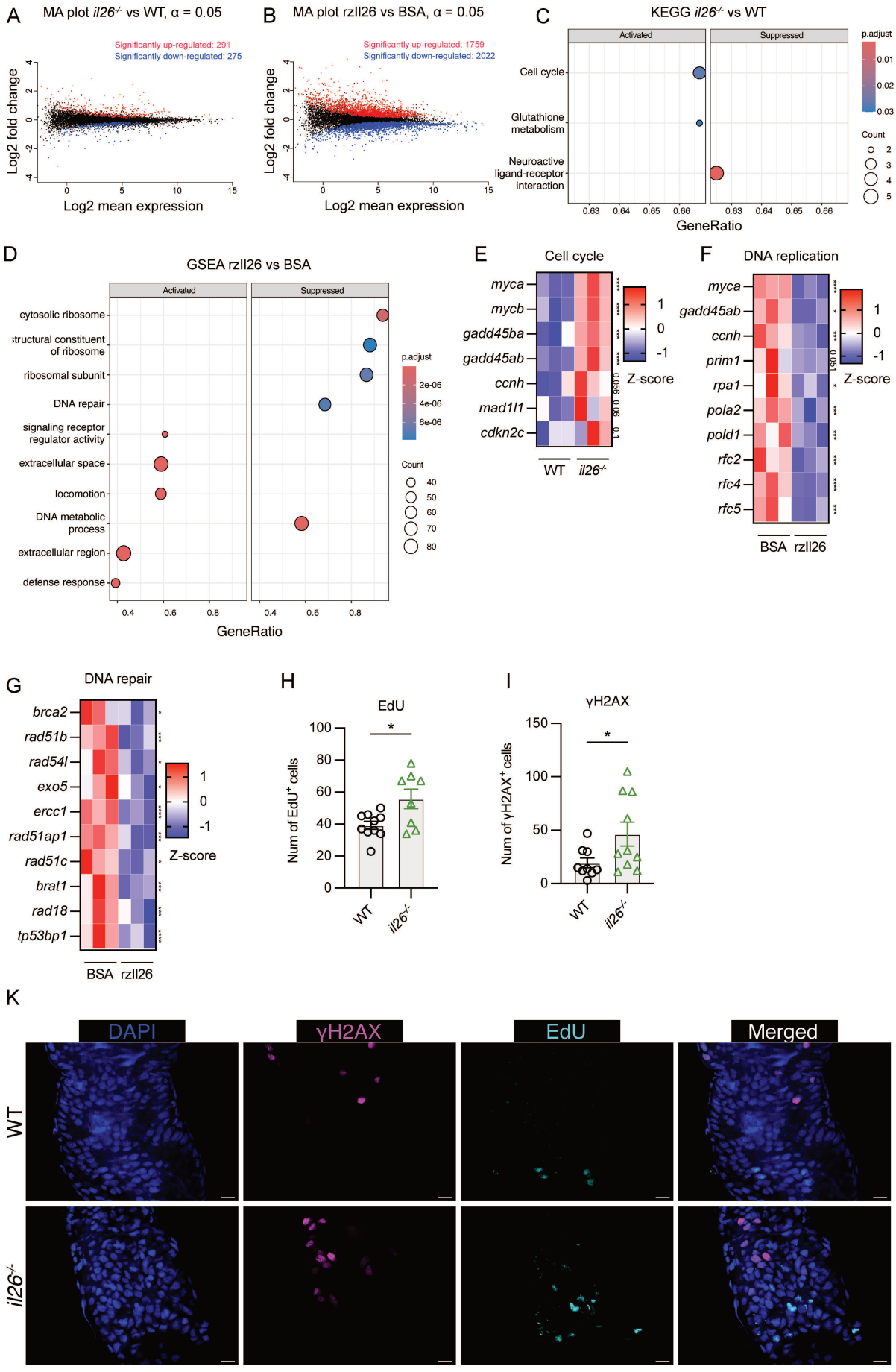
A
MA plot il26-/- vs WT, α = 0.05
Significantly up-regulated: 291
Significantly down-regulated: 275
Log2 fold change
Log2 mean expression
B
MA plot rzIl26 vs BSA, α = 0.05
Significantly up-regulated: 1759
Significantly down-regulated: 2022
Log2 fold change
Log2 mean expression
C
KEGG il26-/- vs WT
Activated
Suppressed
Cell cycle
Glutathione metabolism
Neuroactive ligand-receptor interaction
p.adjust
Count
GeneRatio
D
GSEA rzIl26 vs BSA
Activated
Suppressed
cytosolic ribosome
structural constituent of ribosome
ribosomal subunit
DNA repair
signaling receptor regulator activity
extracellular space
locomotion
DNA metabolic process
extracellular region
defense response
p.adjust
Count
GeneRatio
E
Cell cycle
myca
mycb
gadd45ba
gadd45ab
ccnh
mad1l1
cdkn2c
Z-score
WT
il26-/-
F
DNA replication
myca
gadd45ab
ccnh
prim1
rpa1
pola2
pold1
rfc2
rfc4
rfc5
Z-score
BSA
rzIl26
G
DNA repair
brca2
rad51b
rad54l
exo5
ercc1
rad51ap1
rad51c
brat1
rad18
tp53bp1
Z-score
BSA
rzIl26
H
EdU
Num of EdU+ cells
WT
il26-/-
I
γH2AX
Num of γH2AX+ cells
WT
il26-/-
K
DAPI
γH2AX
EdU
Merged
WT
il26-/-

Fig. 1. **Increased proliferation and DNA damage in the guts of *il26*$^{-/-}$ zebrafish larvae.** MA plots of bulk RNA-seq data on dissected guts from 5-dpf *il26*$^{-/-}$ and WT larvae (**A**) and 5-dpf WT larvae injected with rzIl26 or BSA (**B**). (**C**) KEGG pathway analysis on the loss-of-function dataset. (**D**) GSEA analysis on the overexpression dataset. Heatmaps of z-scores of genes associated with cell cycle in the loss-of-function dataset (**E**) and genes associated with DNA replication in the overexpression dataset (**F**). P-values are indicated. (**G**) Heatmap of z-scores of genes associated with DNA repair in the overexpression dataset. P-values are indicated. Quantification of EdU (**H**) and γH2AX (**I**) staining in WT and *il26*$^{-/-}$ 5-dpf larval guts. (**K**) Representative images of EdU and γH2AX staining in WT and *il26*$^{-/-}$ 5-dpf larval guts. Scale bars, 10 µm. Error bars in (H and I) show means ± SEM. Statistical significance was determined by edgeR package in R (E-G) and Wilcoxon test (H and I). **P* < 0.05, ***P* < 0.01, ****P* < 0.001, and *****P* < 0.0001

We next set out to validate these findings by incubating 5-dpf *il26*$^{-/-}$ and WT larvae with EdU for 3-hours, followed by EdU and γH2AX staining to assess proliferation and DNA damage, respectively. We observed a higher number of EdU-positive cells in the guts of *il26*$^{-/-}$ larvae compared to WT controls (Fig. 1, H and K). This is consistent with the activation of cell cycle in our RNA-seq dataset of *il26*$^{-/-}$ guts. Moreover, there was an increase in γH2AX-positive cells in *il26*$^{-/-}$ guts (Fig. 1, I and K), indicating elevated DNA damage. Despite these perturbations, we did not observe any difference in gut lengths of 5-dpf *il26*$^{-/-}$ larvae compared to WT (Fig. S1, E and F). Furthermore, these fish displayed normal phenotypic traits and survived to adulthood (3-months post-fertilization) in proportions consistent with Mendelian genetics (Chi-Square = 0.7036, P value = 0.7034, Table S3). Additionally, body lengths of adult *il26*$^{-/-}$ fish were comparable to WT fish (Fig. S1, G and H). Together, our data demonstrate that IL-26 loss leads to increased cell proliferation and accumulation of DNA damage in the larval gut without causing gross developmental phenotypes.

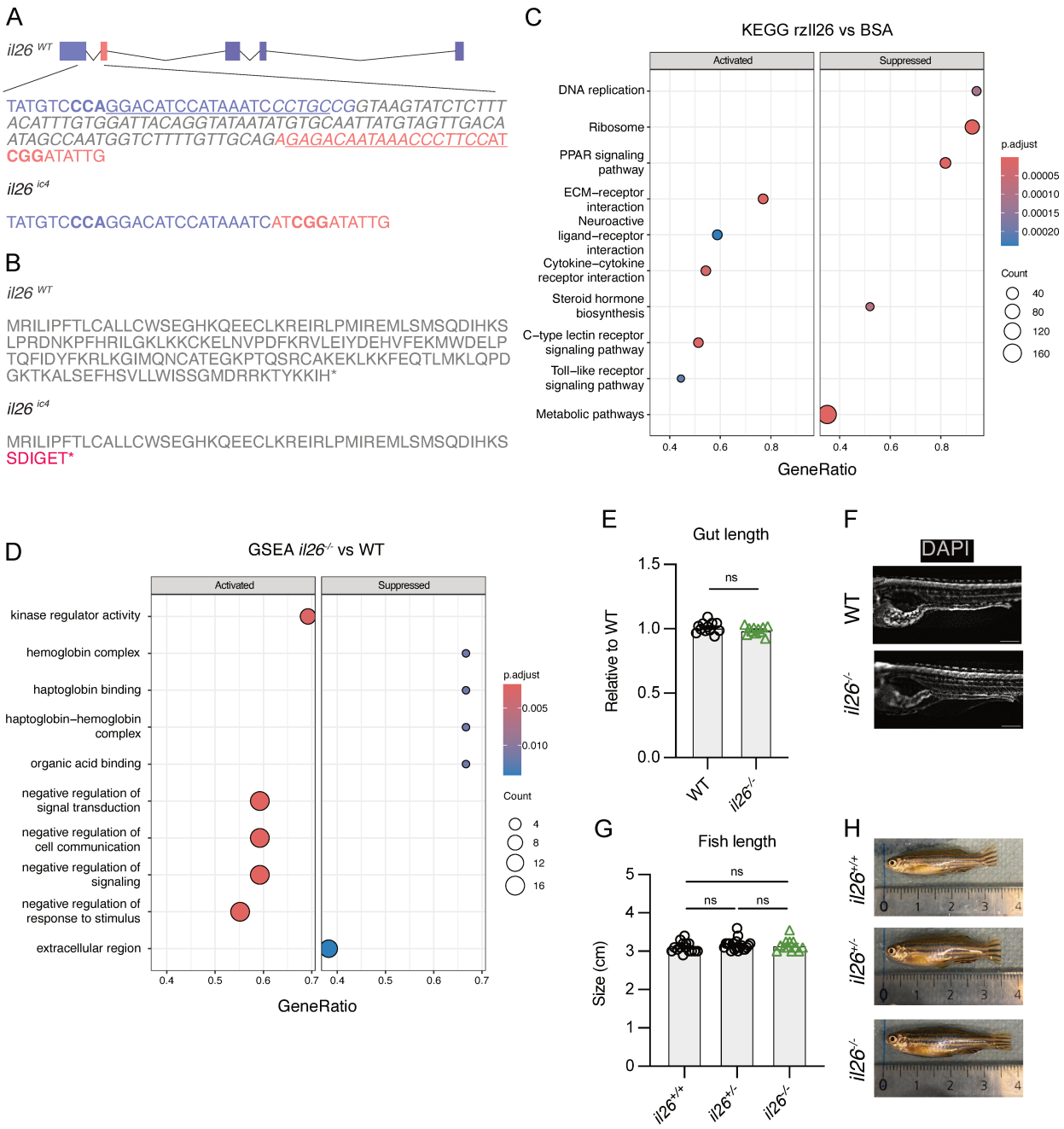

Fig. S1. **Generation and characterization of *il26*-deficientzebrafish.** (**A**) Schematics and DNA sequence of the WT and mutant zebrafish *il26* alleles. The single guide RNA (sgRNA) target sites are underlined. The protospacer adjacent motif (PAM) sequences are indicated in bold. The deleted nucleotides in *il26*^{ic4} are highlighted in *italics.* (**B**) The predicted protein sequence of *il26*^{ic4}. (**C**) KEGG pathway analysis on the overexpression dataset. (**D**) GSEA analysis on the loss-of-function dataset. Gut lengths (**E**) and representative images (**F**) of 5-dpf WT and *il26*$^{-/-}$ larvae. Scale bars, 100 μm. Fish lengths (**G**) and representative images (**H**) of adult zebrafish with the genotypes: *il26*$^{+/+}$, *il26*$^{+/-}$, and *il26*$^{-/-}$. Error bars in (E and G) show means ± SEM. Statistical significance was determined by Wilcoxon test (E) and Kruskal-Wallis test (G). ns $P > 0.05$.

IL-26 suppresses gut cell proliferation in epithelial progenitors and DNA damage in absorptive enterocytes

To gain a deeper insight into the phenotypes of increased proliferation and DNA damage in *il26*$^{-/-}$ guts and to pinpoint the affected cell types, we performed single-cell RNA sequencing (scRNA-seq) on dissected guts of 5-dpf *il26*$^{-/-}$ and WT larvae. After excluding low-quality cells and cells from tissues external to the gut, such as the pancreas, liver, and epidermis, we profiled the gene expression of 11,471 individual cells (6,506 WT; 4,965 *il26*$^{-/-}$) (Fig. 2A), with a median of 1,867 detected genes per cell. We next applied graph-based clustering on our integrated dataset (Fig. 2B) and identified 29 distinct clusters based on the expression of known markers (Table S4).

To identify which cell types show increased proliferation in *il26*$^{-/-}$, we analyzed expression changes of several genes associated with cell cycle and proliferation, including members of the MYC family, cyclins, and replication factors (Fig. 2C). The expression of these genes was elevated in *il26*$^{-/-}$ in gut epithelial progenitors. This population of cells was annotated as gut epithelial progenitors based on the expression of several markers including *tnfrsf11a* (tumor necrosis factor receptor superfamily, member 11a) (Fig. S2A and B), previously shown to label epithelial progenitors in the larval gut (*137*). Consistent with this observation, our scRNA-seq analysis revealed a higher number of epithelial progenitor cells in *il26*$^{-/-}$ compared to WT, with 53 progenitors per 1000 detected cells in *il26*$^{-/-}$ larvae versus 31 per 1000 detected cells in WT larvae. This *in silico* analysis suggests that the loss of IL-26 increases cell proliferation in the epithelial compartment. To confirm this, we performed EdU staining in *il26*$^{-/-}$ *TgBAC(cldn15la-GFP)* larvae, which specifically labels the basolateral membrane of intestinal epithelial cells (*163*). We observed that EdU-positive cells were GFP-positive (Fig. 2E), strongly indicating that IL-26 loss enhances cell proliferation of epithelial progenitors.

Next, to uncover which cell types exhibit higher DNA damage in *il26*$^{-/-}$ guts, we analyzed the expression changes of several genes associated with DNA damage in *il26*$^{-/-}$ compared to WT across each cell cluster (Fig. 2D). EC1, a subtype of absorptive enterocytes, displayed heightened expression of DNA damage-related genes. We annotated this cell population as absorptive enterocytes based on the expression of several markers such as

fabp2 (fatty acid binding protein 2), *elovl2* (ELOVL fatty acid elongase 2), and others (Fig. S2C and D). To validate these findings, we performed γH2AX staining in *il26*$^{-/-}$ *TgBAC(cldn15la-GFP)* larvae (Fig. 2F). We observed that γH2AX-positive cells were GFP-positive, showing that IL-26 loss increased DNA damage in gut epithelial cells. Furthermore, we co-stained for γH2AX and 2F11, which specifically labels secretory cells in the zebrafish larval gut (*164*). No colocalization between these two markers was observed (Fig. S2E), excluding the possibility that these γH2AX-positive cells were secretory. Moreover, the expression profile of *anxa4* (annexin A4), the gene encoding for the 2F11 antigen (*165*), showed very low expression in EC1 compared to secretory cell types like goblet cells and enteroendocrine cells (Fig. S2F). These results demonstrate that IL-26 suppresses DNA damage in gut epithelial cells, likely in absorptive enterocytes rather than secretory cells. Overall, our single-cell transcriptomic and *in situ* analyses suggest that IL-26 suppresses cell proliferation and DNA damage in gut epithelial progenitors and absorptive enterocytes, respectively.

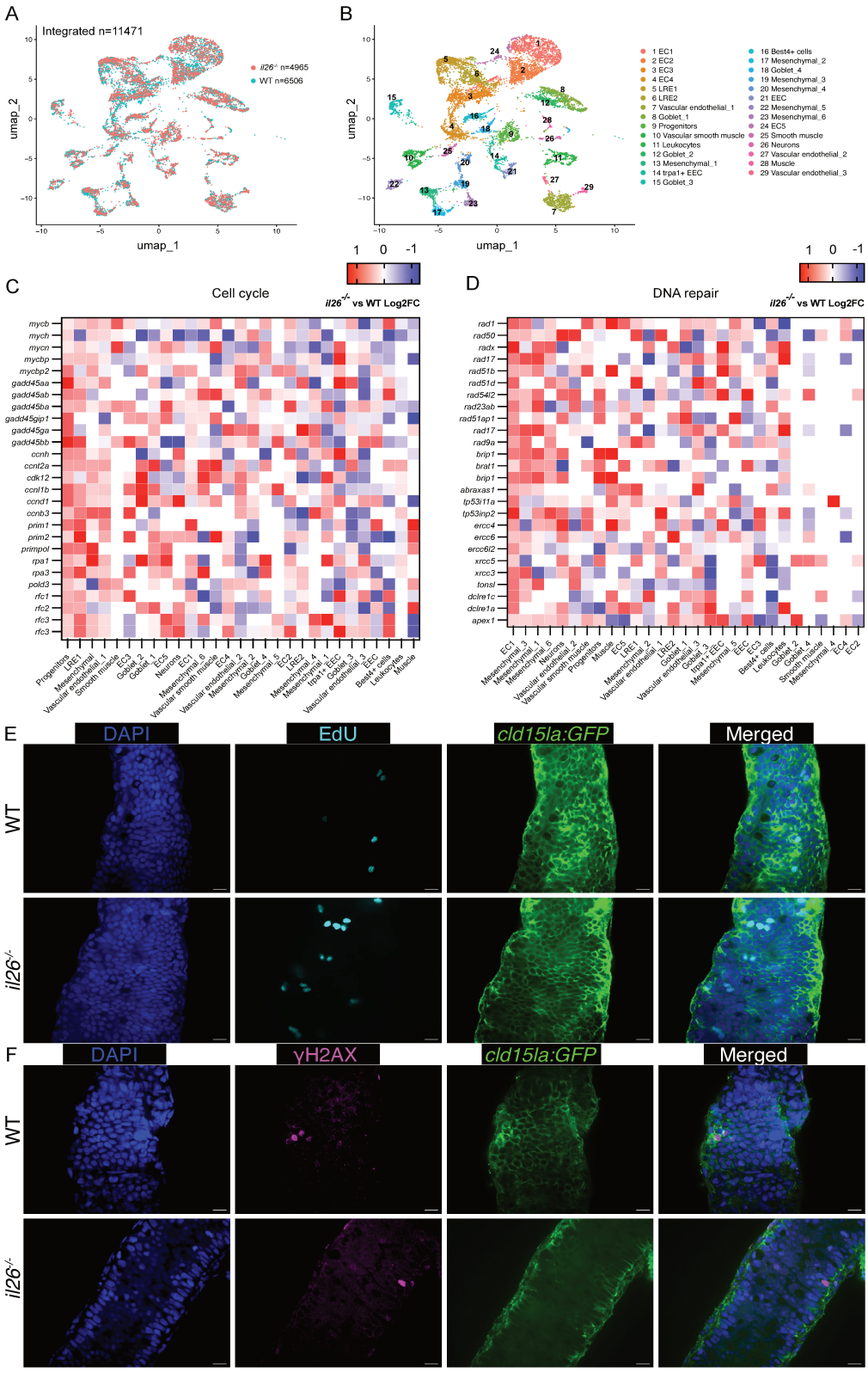

Fig. 2. Single-cell RNA sequencing reveals increased proliferation and DNA damage in the epithelial compartment of *il26*$^{-/-}$ gut. UMAP Dimensional reduction projection of scRNA-seq dataset of disscted guts of 5-dpf *il26*$^{-/-}$ and WT larvae. Cells are colored by genotype (**A**) or cell type (**B**). Expression of genes associated with cell cycle (**C**) or DNA repair (**D**), colored by log2FC expression in *il26*$^{-/-}$ compared to WT across each cell cluster. Immunostaining for EdU (**E**) and γH2AX (**F**) of 5-dpf *TgBAC(cldn15la-GFP)* in WT and *il26*$^{-/-}$ genetic background. Scale bars, 10 µm.

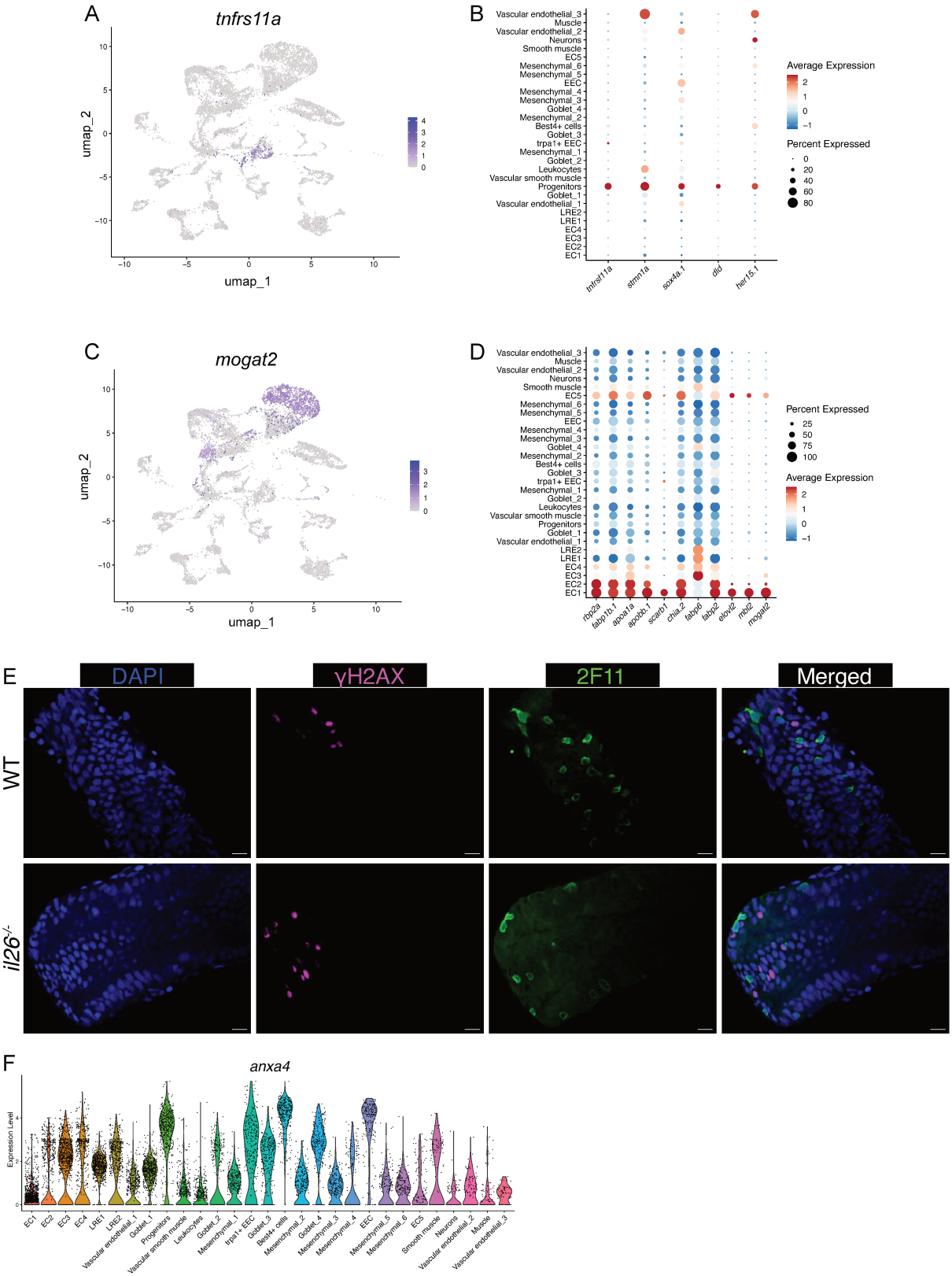

Fig. S2. Single-cell RNA sequencing uncovers that epithelial progenitors and absorptive enterocytes show increased proliferation and DNA damage, respectively in *il26*$^{-/-}$ gut. (**A**) Feature plot of the epithelial progenitor marker *tnfrs11a*. (**B**) Dot plot of a panel of epithelial progenitor markers. (**C**) Feature plot of the absorptive enterocyte marker *mogat2*. (**D**) Dot plot of a panel of markers of EC1. (**E**) Co-immunostaining for γH2AX and 2F11in WT and *il26*$^{-/-}$. Scale bars, 10 µm. (**F**) Violin plot of *anxa4* expression.

IL-26 modulation of epithelial homeostasis in the gut is receptor-independent

Human IL-26 has been reported to exert a modest antiproliferative effect on the human colon cancer cell line HT29 *in vitro* (*5*). Additionally, HT29 cells have been shown to express the two receptor subunits of IL-26, IL10RB and IL20RA (*5*). These findings suggest that IL-26 suppresses proliferation in a direct, receptor-dependent manner. To elucidate the role of IL-26 receptor-dependent signaling in the observed higher proliferation and DNA damage in *il26*$^{-/-}$, we investigated the expression profile and functional significance of IL20RA in zebrafish. *il20ra* was mainly expressed in epithelial cells in our scRNA-seq dataset (Fig. S3A). To investigate the function of this receptor subunit, we generated *il20ra*-deficient zebrafish using the CRISPR/Cas9 system. This led to a deletion in the 2nd exon of the zebrafish *il20ra* gene (*il20ra*^{aps40}) (Fig. S3B). This mutation is predicted to create a premature stop codon giving rise to a truncated protein of 40 amino acids (Fig. S3C). The homozygous *il20ra*^{aps40}/ *il20ra*^{aps40} mutant fish will be designated as *il20ra*$^{-/-}$ throughout this study. Notably, injection of rzIl26 induced *il20ra* in WT and not in *il20ra*$^{-/-}$ (Fig. S3D), consistent with IL-20RA loss-of-function in this mutant.

To determine the role of IL20RA in proliferation and DNA damage in the gut, we analyzed EdU (Fig. 3A and Fig. S3F) and γH2AX (Fig. 3B and Fig. S3F) in *il20ra*$^{-/-}$ larvae. Mutants showed similar proliferation and DNA damage levels compared to WT, showing that IL-26 receptor is dispensable for the function of IL-26 to suppress these processes in the larval gut. In line with these results, *il26* expression in *il20ra*$^{-/-}$ larval guts was similar to WT (Fig. S3E), suggesting that IL-26 can effectively suppress proliferation and DNA damage in the gut in the absence of its receptor.

Given that this conclusion did not align with a previous report suggesting a receptor-dependent role of IL-26 in suppressing proliferation in the intestinal epithelial cell line HT29, we aimed to reproduce this result. We incubated a series of concentrations of the human IL26 protein with HT29 cells and did not observe any changes in cell proliferation (Fig. 3C), in contrast to the before-mentioned report (*5*). We observed similar results when using the cell lines SW480 and HCT116 (Fig. S3G and H). These findings support the hypothesis that IL-26 regulates epithelial cell proliferation in an indirect, receptor-independent manner.

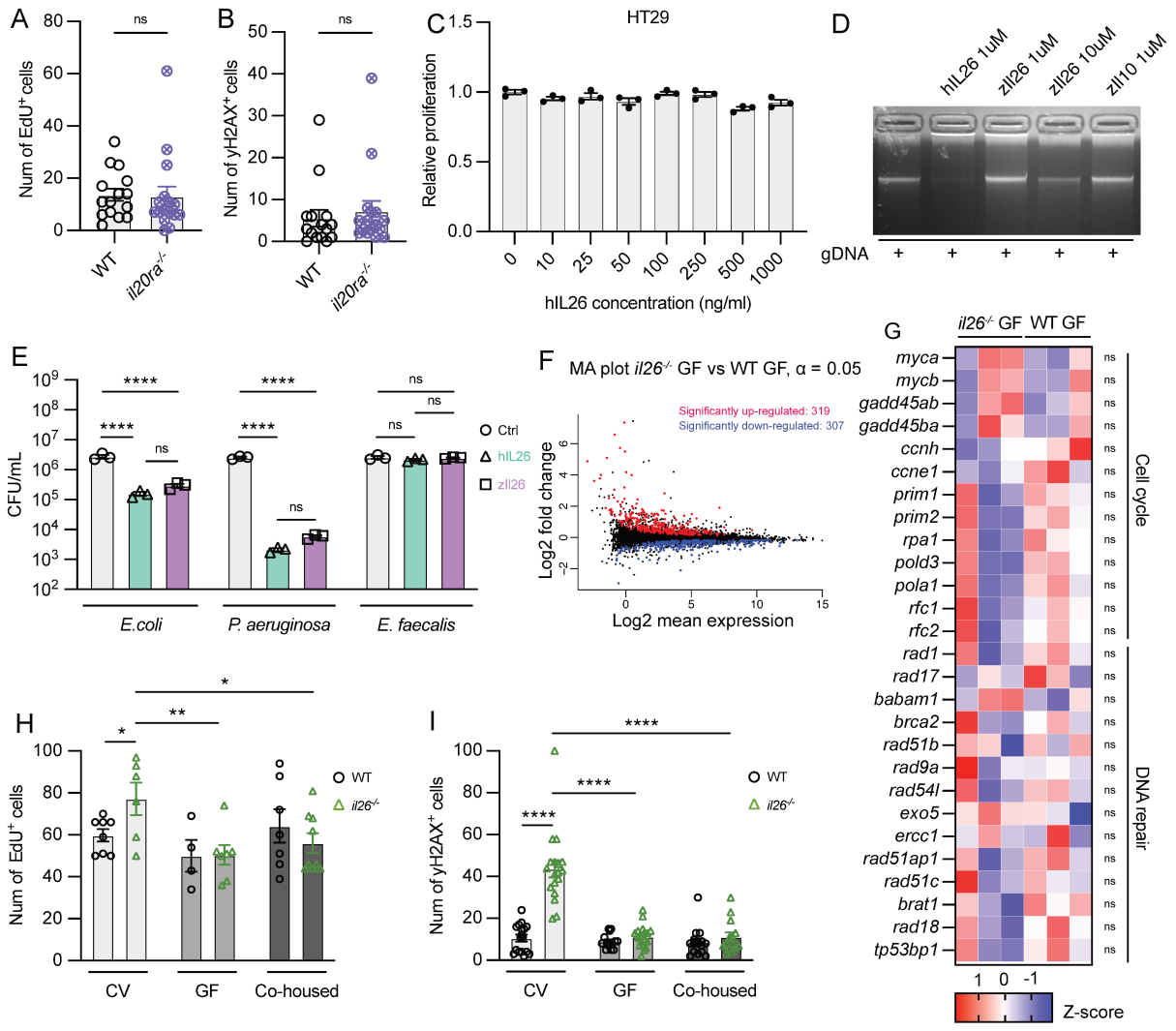

Fig. 3. Receptor-dependent vs receptor-independent functions of IL-26 in regulating proliferation and DNA damage. Quantification of EdU staining (**A**) and γH2AX staining (**B**) in WT and *il20ra*$^{-/-}$ 5-dpf larval guts. (**C**) MTT assay of HT29 cells incubated with human IL26 protein at different concentrations. (**D**) Gel migration assay of genomic DNA incubated with several cytokines. (**E**) Quantification of colony forming units of different bacterial species after incubation with human or zebrafish IL-26 proteins at a concentration of 8 µM. (**F**) MA plot of bulk RNA-seq data on dissected guts from 5-dpf *il26*$^{-/-}$ and WT larvae reared GF. Quantification of EdU staining (**H**) and γH2AX staining (**I**) in WT and *il26*$^{-/-}$ larval guts reared CV, GF, or cohoused. (**G**) Heatmap of z-scores of genes associated with cell cycle and DNA repair in *il26*$^{-/-}$ GF compared to WT GF. p-values are indicated. Error bars show means ± SEM. Statistical significance was determined by Wilcoxon test (A and B), Kruskal-Wallis test (C), 2way ANOVA (E, H, and I), and edgeR package in R (G). ns $P > 0.05$, *$P < 0.05$, **$P < 0.01$, ***$P < 0.001$, and ****$P < 0.0001$.

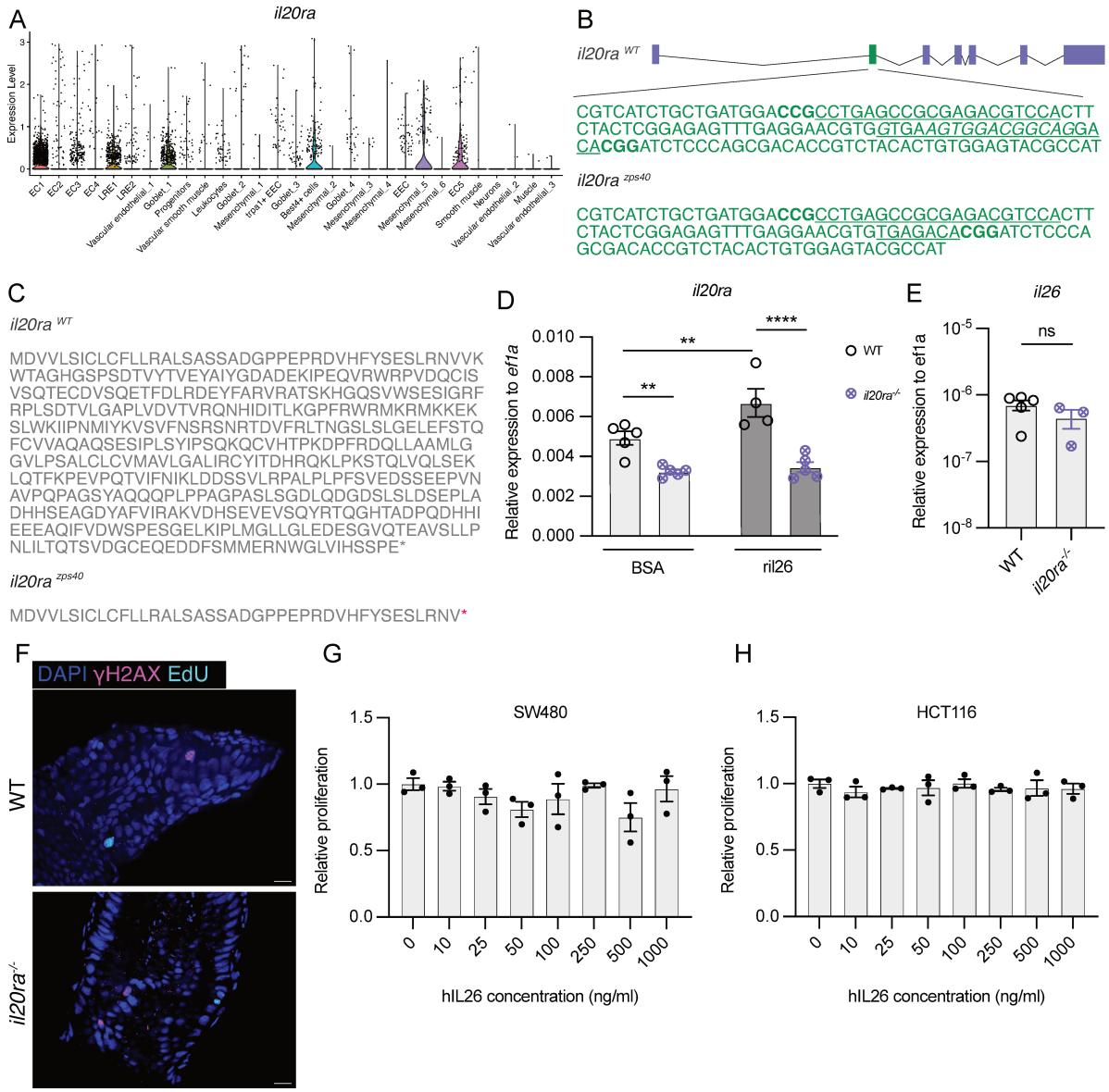

Fig. S3. **Generation and characterization of *il20ra*-deficient zebrafish.** (**A**) Violin plot of *il20ra* expression in the integrated scRNA-seq dataset of WT and *il26*$^{-/-}$ guts. (**B**) Schematics and DNA sequence of the WT and mutant zebrafish *il20ra* alleles. The single guide RNA (sgRNA) target sites are underlined. The protospacer adjacent motif (PAM) sequences are indicated in bold. The deleted nucleotides in *il20ra*^{zps40} are highlighted in *italics*. (**C**) The predicted protein sequence for *il20ra*^{zps40}. (**D**) qRT-PCR analysis of *il20ra* in dissected guts of WT or *il20ra*$^{-/-}$ larvae injected with rzIl26 or BSA. (**E**) qRT-PCR analysis of *il26* in dissected guts of WT or *il20ra*$^{-/-}$ larvae. (**F**) Representative images of EdU and γH2AX staining in WT and *il20ra*$^{-/-}$ 5-dpf larval guts. Scale bars, 10 μm. MTT assay of SW480 cells (**G**) and HCT116 cells (**H**) incubated with human IL26 protein at different concentrations. Error bars in (D, E, G, and H) show means ± SEM. Statistical significance was determined by 2way ANOVA (D), Wilcoxon test (E), and Kruskal-Wallis test (G and H). ns $P > 0.05$, *$P < 0.05$, **$P < 0.01$, ***$P < 0.001$, and ****$P < 0.0001$.

Analysis of IL-26 receptor-independent functions reveals conservation of IL-26 antibacterial activity in zebrafish

Human IL-26 was demonstrated to have receptor-independent functions. For example, human IL-26 can form complexes with DNA and activate intracellular TLR9 in the absence of IL-26 canonical receptor (*92*). Since TLR9 has been shown to regulate cell proliferation (*166*, *167*) and DNA damage (*168*), we investigated the involvement of IL-26-DNA complexes in the observed phenotypes. We assessed whether the DNA-binding abilities of human IL26 are conserved in zebrafish using gel migration assays (Fig. 3D). Contrary to human IL-26, incubating the zebrafish protein with genomic DNA did not block the DNA from migrating in the gel, showing that zebrafish IL-26 did not bind and form complexes with DNA. This observation excludes the involvement of IL-26 DNA-binding properties in the regulation of cell proliferation and DNA damage in the zebrafish larval gut.

Another receptor-independent function of human IL26 is its direct bactericidal activity (*92*). For instance, human IL-26 was demonstrated to kill *E. coli* and *P. aeruginosa* (*92*). To determine whether this function is conserved in zebrafish, we incubated human or zebrafish IL-26 proteins with *E. coli* and *P. aeruginosa* and quantified colony-forming units (CFU). We observed that both proteins killed these bacteria at similar levels (Fig. 3E). Moreover, when incubated with *E. faecalis,* which has been reported to be resistant to IL26 at this concentration (*92*), neither protein killed the bacteria (Fig. 3E). These results show that the intrinsic bactericidal activity of IL-26 is conserved in zebrafish, with similar specificity and efficacy.

IL-26 controls proliferation and DNA damage in the gut in a microbiota-dependent manner

We next reasoned that the impaired bactericidal activity in *il26*$^{-/-}$ might result in an altered microbiota composition, leading to the observed increased proliferation and DNA damage in a receptor-independent manner. Consistently, these phenotypes would be rescued in germ-free (GF) *il26*$^{-/-}$ larvae. To test this, we first performed bulk RNA-seq analysis on dissected guts from 5-dpf WT and *il26*$^{-/-}$ larvae reared under GF conditions. The analysis revealed 319 upregulated and 307 downregulated genes in the guts *il26*$^{-/-}$ GF larvae (Fig. 3F and Table S5). Notably, genes related to cell cycle and DNA repair were not differentially

expressed between *il26*$^{-/-}$ GF and WT GF (Fig. 3G), suggesting that the increased proliferation and DNA damage in *il26*$^{-/-}$ is reverted in GF conditions. To validate this, we reared WT and *il26*$^{-/-}$ larvae under conventional (CV) or GF conditions and quantified gut cell proliferation (Fig. 3H and Fig. S4A) and DNA damage (Fig. 3I and Fig. S4B). EdU- and γH2AX-positive cells were less abundant in *il26*$^{-/-}$ GF compared to *il26*$^{-/-}$ CV. Furthermore, *il26*$^{-/-}$ GF showed similar levels of proliferation and DNA damage as WT GF. These data indicate that IL-26 suppresses cell proliferation and DNA damage in the zebrafish gut in a microbiota-dependent manner.

Next, we hypothesized that if an altered microbiota in *il26*$^{-/-}$ larvae is responsible for the observed elevated proliferation and DNA damage, then introducing WT microbiota to *il26*$^{-/-}$ larvae might rescue these phenotypes. To test this, we cohoused *il26*$^{-/-}$ GF with WT CV larvae to promote microbiota transfer from WT to mutant animals and carried out EdU (Fig. 3H and Fig. S4A) and γH2AX (Fig. 3I and Fig. S4B) staining. Cohoused *il26*$^{-/-}$ larvae displayed cell proliferation and DNA damage levels similar to those in WT CV, suggesting that WT microbiota mitigated the increased proliferation and DNA damage in *il26*$^{-/-}$ larvae. Additionally, cohousing WT GF with *il26*$^{-/-}$ CV did not result in increased cell proliferation and DNA damage in WT, showing that microbiota transfer from *il26*$^{-/-}$ to WT is not sufficient to induce cell proliferation and DNA damage in WT larvae. These observations indicate that *il26*-deficiency leads to dysbiosis, consequently resulting in impaired epithelial homeostasis.

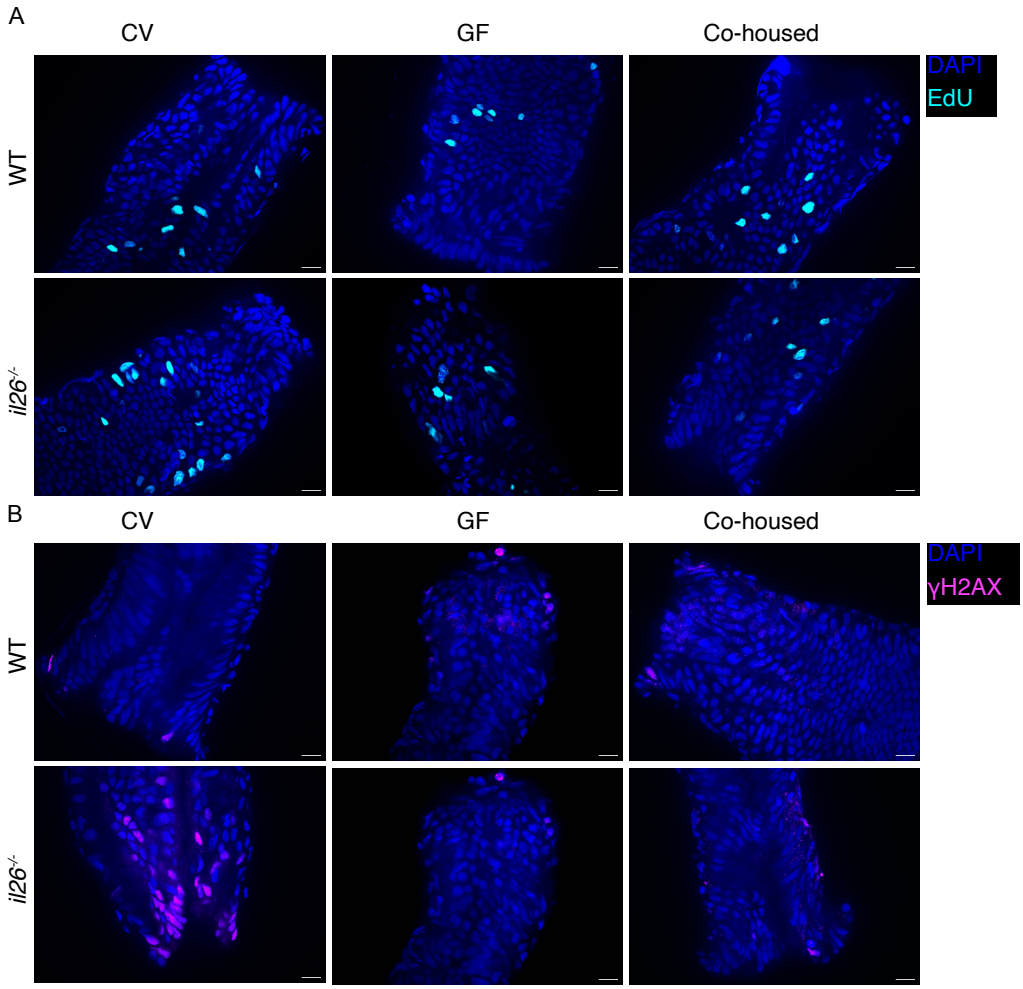

Fig. S4. **Immunostaining WT and *il26*$^{-/-}$ larval guts reared CV, GF, or cohoused.** Representative images of EdU (**A**) and γH2AX staining (**B**) in WT and *il26*$^{-/-}$ larval guts reared CV, GF, or cohoused. Scale bars, 10 µm.

Innate lymphoid cells are the primary source of IL-26 in the larval gut

To identify the cellular sources of IL-26 in the larval gut, we examined *il26* expression in our scRNA-seq dataset, however, it was not detected. This is likely due to the low expression levels of *il26* at steady state as well as the low sequencing depth of current 10X genomics technologies (median of 1867 detected genes per cell). Since cytokine expression is induced upon inflammation, we re-analyzed a published scRNA-seq dataset of dissected guts from 6-dpf larvae treated with dextran sulfate sodium (DSS) for 24-hours (*169*) (Fig. S5A). *il26* was mainly expressed in a population of lymphocytes characterized by the expression of *il7r* and *rorc* (Fig. 4, A and B). Interestingly, these cells expressed *nitr4a,* a specific marker of zebrafish ILCs (*139*) (Fig. 4B). These data suggest that ILCs are present in the larval gut during early life, being the primary cell source of *il26*.

To verify that ILCs express *il26* in 5-dpf larval guts, we employed several complementary experimental approaches. First, we measured *il26* in dissected guts of 5-dpf *rag1*$^{-/-}$ larvae, which lack adaptive lymphocytes but still possess ILCs (*170*). *il26* levels in *rag1*$^{-/-}$ were similar to those in WT larvae (Fig. 4C), indicating that adaptive lymphocytes were not required for *il26* expression. Second, we utilized *il2rga*$^{-/-}$*prkdc*$^{-/-}$ larvae, which are devoid of both adaptive lymphocytes and ILCs (*171*). *il2rga*$^{-/-}$*prkdc*$^{-/-}$ fish are immunodeficient and only heterozygous *il2rga*$^{+/-}$*prkdc*$^{-/-}$ could be maintained as adults in our animal facility. Therefore, performing experiments on homozygous *il2rga*$^{-/-}$*prkdc*$^{-/-}$ 5-dpf larvae necessitates in-crossing *il2rga*$^{+/-}$*prkdc*$^{-/-}$ adults and genotyping the larvae at 3-dpf. However, measuring *il26* expression by qPCR on 5-dpf dissected guts requires pooling up to 10 guts per replicate. This poses a challenge to the procedure of obtaining enough guts from 5-dpf *il2rga*$^{-/-}$*prkdc*$^{-/-}$ larvae to measure *il26* at steady state. To overcome this, we adopted an alternative approach where we induced *il26* expression in the gut, allowing us to measure this cytokine by pooling only 3 guts. *Vibrio anguillarum* is a fish pathogen that was reported to induce *il26* expression in adult zebrafish guts (*139*, *172*). Therefore, our approach involved injecting a killed bacterial extract of *Vibrio anguillarum* in the gut of 5-dpf larvae. This injection induced *il26* expression in WT larval guts, peaking at 2-hpi (Fig. S5B). *il26* levels were lower in injected *il2rga*$^{-/-}$*prkdc*$^{-/-}$ compared to *il2rga*$^{+/+}$*prkdc*$^{-/-}$ at 2-hpi (Fig. 4D), showing that lymphocytes were indispensable for *il26* expression. Together with our observation in *rag1*$^{-/-}$ larvae, these data demonstrate that ILCs are required for *il26* expression in the larval gut.

In order to observe *il26* expression *in situ* in gut ILCs in 5-dpf larvae, we performed RNA-FISH for *il26* and *nitr9*, a specific marker of zebrafish ILCs (*139*). We detected *il26* expression in *nitr9*-positive cells (Fig. 4E), further confirming that functional ILC are present in the developing larval gut as early as 5-dpf, being the main source of *il26*.

Innate sensing of the microbiota induces IL-26 expression in the larval gut

Next, we sought to determine the cues that induce *il26* expression in gut ILCs. Microbial colonization of the gut is known to induce significant transcriptional changes. Therefore, to characterize the role of microbiota in regulating *il26* expression, we quantified *il26* mRNA levels in CV and GF larval guts. *Il26* expression was lower in GF larval guts (Fig. 4F), indicating that microbiota induces *il26* expression in the gut. To uncover the signaling pathways involved in this process, we measured *il26* in TLR-deficient *myd88*$^{-/-}$ larvae. We

found that *il26* expression was lower in *myd88*$^{-/-}$ larval guts compared to WT controls (Fig. 4G). Altogether, our results suggest that microbial colonization induces *il26* expression in gut ILCs as a result of TLR-dependent innate immune sensing.

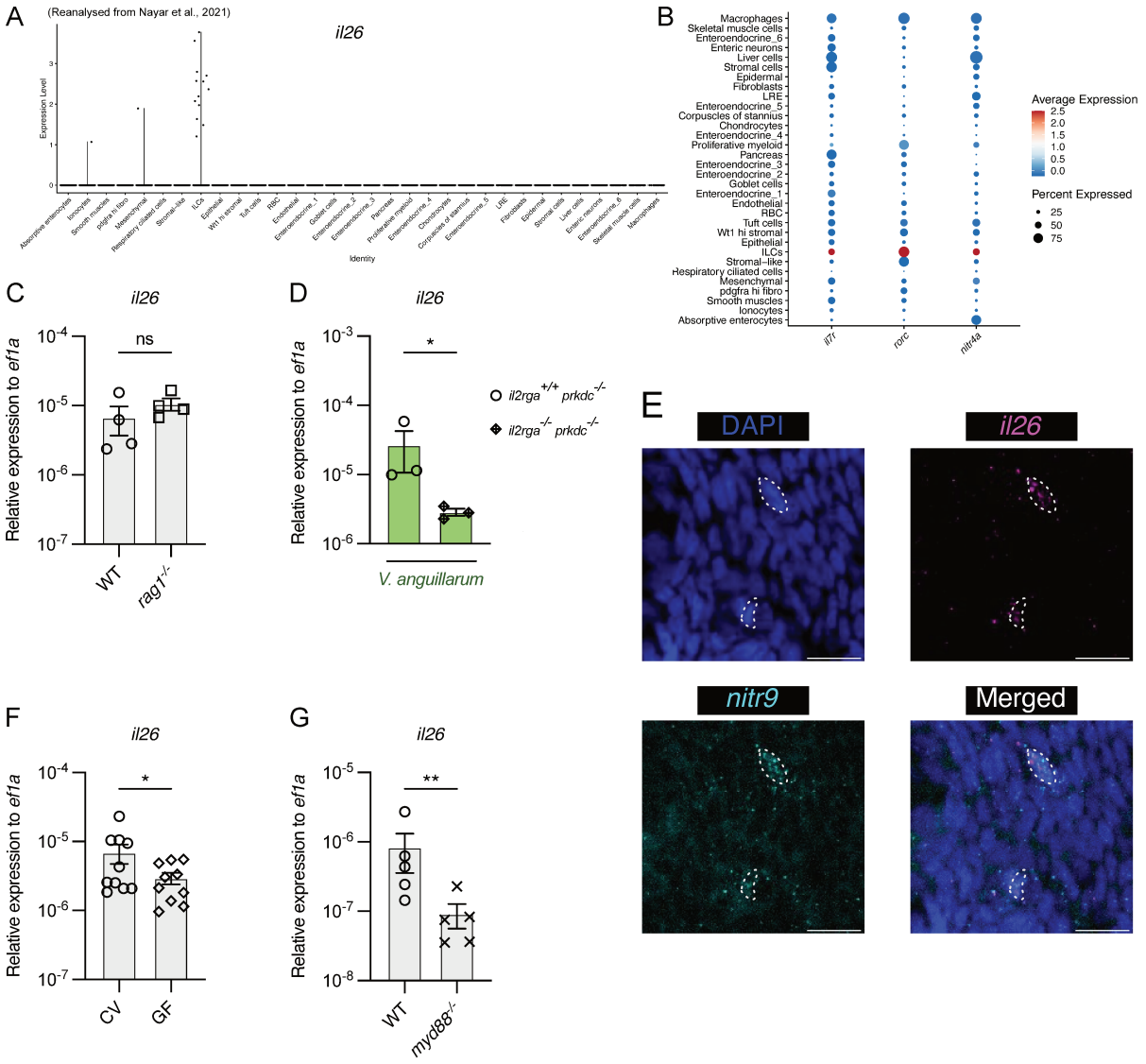

Fig. 4. IL-26 is expressed in the larval gut by ILCs. (**A**) Violin plot of *il26* expression, reanalyzed from Nayar et al., 2021 (*169*). (**B**) Dot plot of a ILCs markers, reanalyzed from Nayar et al., 2021 (*169*). (**C**) qRT-PCR analysis of *il26* in dissected guts of WT or *rag1*$^{-/-}$ 5-dpf larvae. (**D**) qRT-PCR analysis of *il26* in dissected guts of *il2rga*$^{+/+}$*prkdc*$^{-/-}$ and *il2rga*$^{-/-}$*prkdc*$^{-/-}$ 5-dpf larvae after *V. anguillarum* injection. (**E**) RNA-FISH of *il26* and *nitr9* on dissected guts of 5-dpf larvae. Scale bars, 10 µm. (**F**) qRT-PCR analysis of *il26* in dissected guts of 5-dpf WT larvae reared CV or GF. (**G**) qRT-PCR analysis of *il26* in dissected guts of WT or *myd88*$^{-/-}$ 5-dpf larvae. Error bars in (C, D, F, and G) show means ± SEM. Statistical significance was determined by Wilcoxon test (C, D, F, and G). ns $P > 0.05$, *$P < 0.05$, **$P < 0.01$, ***$P < 0.001$, and ****$P < 0.0001$.

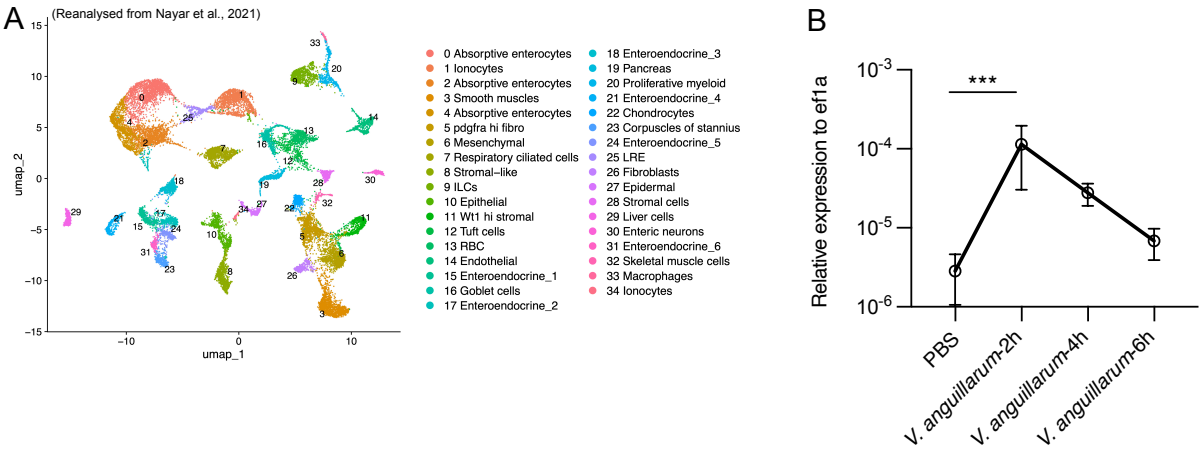

Fig. S5. Analysis of IL-26 expression in the larval gut. (**A**) UMAP Dimensional reduction projection, reanalyzed from Nayar et al., 2021 (*169*). (**B**) qRT-PCR analysis of *il26* in dissected guts of 5-dpf WT injected with PBS or *V. anguillarum*. Error bars show means ± SEM. Statistical significance was determined by Kruskal-Wallis test (B). ***$P < 0.001$.

IL-26 protects from gut bacterial infection

To elucidate the role of IL-26 in the gut under inflammatory conditions, we utilized *Edwardsiella tarda*, a Gram-negative bacterium known to infect zebrafish and human guts (*146–148*). We infected WT and *il26*$^{-/-}$ larvae with mCherry-labeled *E. tarda* via water bath immersion (Fig. 5A). mCherry-labeled *E. tarda* accumulated primarily in the gut at 3-days post-infection (dpi) both in WT and *il26*$^{-/-}$ larvae (Fig. 5B). To verify whether *il26* expression is induced upon *E. tarda*, we quantified mRNA levels in dissected guts at 1- and 3-dpi in WT larvae. *il26* expression levels where higher in 3-dpi larvae compared to uninfected controls (Fig. 5C). These data illustrate that *E. tarda* provides a relevant model to study the functions of IL-26 upon infection-induced gut inflammation.

Next, we monitored the survival of *E. tarda*-infected WT and *il26*$^{-/-}$ larvae. We discovered that *il26*$^{-/-}$ larvae exhibited higher mortality compared to WT upon infection (Fig. 5D). To elucidate whether higher bacterial loads in *il26*$^{-/-}$ could explain this increased susceptibility, we quantified mCherry fluorescence area (Fig. 5E) and mCherry mean intensity (Fig. 5F) in WT and *il26*$^{-/-}$ guts. However, we did not observe any difference between WT and *il26*$^{-/-}$.

An alternative explanation for the increased susceptibility of *il26*$^{-/-}$ to *E. tarda* infection is dysregulated proliferation and DNA damage. To investigate this, we performed EdU and γH2AX staining at 3-dpi in both WT and *il26*$^{-/-}$ larvae. WT guts did not exhibit differences in

the number of EdU-positive cells upon *E. tarda* compared to uninfected controls (Fig. S6, A and B). Similarly, *il26*$^{-/-}$ infected guts showed comparable levels of EdU-positive cells to uninfected *il26*$^{-/-}$.This finding undermines the hypothesis that altered proliferation in *il26*$^{-/-}$ larvae contributes to the higher mortality rate upon *E. tarda* infections. Interestingly, *E. tarda* infection increased the number of γH2AX-positive cells in WT guts (Fig. 5G and Fig. S6A), indicating infection-induced elevated DNA damage. Moreover, infected *il26*$^{-/-}$ guts exhibited greater DNA damage compared to infected WT guts. This result demonstrates that the loss of IL-26 renders epithelial cells in the gut more susceptible to DNA damage upon *E. tarda* infections.

Finally, with the aim of characterizing the immune response in the gut of *il26*$^{-/-}$ upon infection, we measured the expression levels of several cytokines in WT and *il26*$^{-/-}$ larval guts at 3-dpi. We found that *E. tarda* infection induced the upregulation of *il1b*, *il22*, *tnfa*, and *il10* in WT larvae (Fig. S6, C-F). Similarly, the levels of these cytokines where higher in *il26*$^{-/-}$ guts upon infection compared to uninfected *il26*$^{-/-}$ controls. However, these cytokines were significantly lower in *E. tarda*-infected *il26*$^{-/-}$ compared to infected WT larvae. In sum, we show that *il26*$^{-/-}$ larvae exhibited higher susceptibility to gut bacterial infection, accumulating greater DNA damage and failing to mount a sufficient immune response. These findings underscore the critical role of IL-26 in regulating the immune response and maintaining gut integrity during bacterial infections.

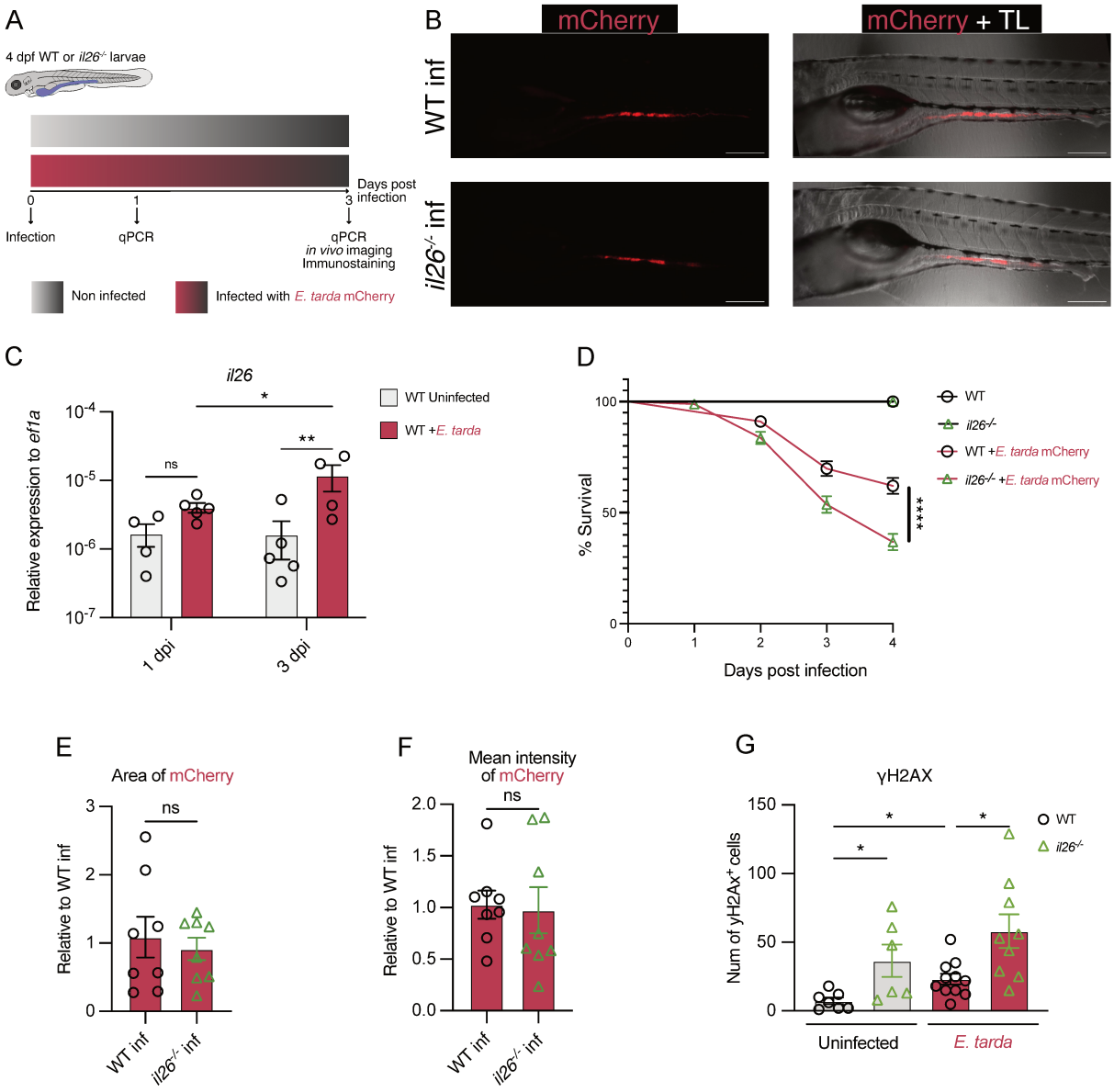

Fig. 5. *il26*$^{-/-}$ larvae are more susceptible to *E. tarda* infections and show elevated DNA damage accumulation in the gut. (**A**) Schematic representation of *E. tarda* infection and subsequent analyses. (**B**) WT and *il26*$^{-/-}$ larvae infected with mCherry-labeled *E. tarda* at 3-dpi. Scale bars, 200 µm. (**C**) qRT-PCR analysis of *il26* in dissected guts of WT larvae at 1- and 3-dpi. (**D**) Survival analysis of WT and *il26*$^{-/-}$ larvae infected with *E. tarda*. Analysis of the area of mCher€(**E**) and mean intensity of mCherry (**F**) in WT and *il26*$^{-/-}$ larvae infected with mCherry-labeled *E. tarda* at 3-dpi. (**G**) Quantification of γH2AX staining in WT and *il26*$^{-/-}$ larval guts at 3-dpi. Error bars in (C-G) show means ± SEM. Statistical significance was determined by one-way ANOVA (C and G), Gehan-Breslow-Wilcoxon test (D), and Wilcoxon test (E and F). ns $P > 0.05$, *$P < 0.05$, **$P < 0.01$, ***$P < 0.001$, and ****$P < 0.0001$.

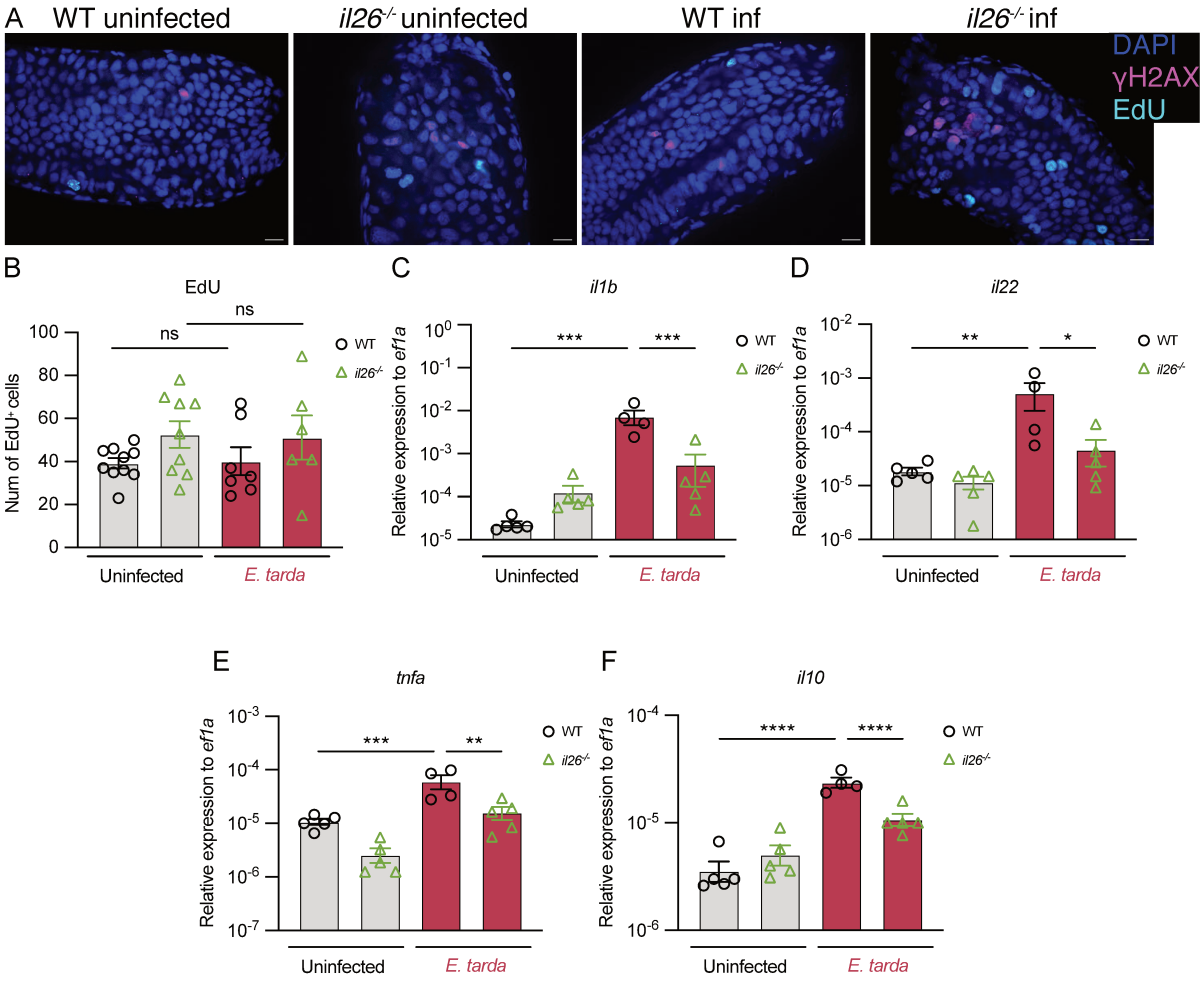

Fig. S6. *il26*$^{-/-}$ larvae mount an insufficient immune response upon *E. tarda*. (**A**) Representative images of EdU and γH2AX staining in WT and *il26*$^{-/-}$ at 3-dpi. Scale bars, 10 μm. (**B**) Quantification of EdU staining in WT anhow means ± SEM. Statistical significance was determined by one-way ANOVA (B-F). ns $P > 0.05$, *$P < 0.05$, **$P < 0.01$, ***$P < 0.001$, and ****$P < 0.0001$.

DISCUSSION

In this study, we created the first *in vivo* animal model to study the impact of IL-26 loss-of-function on gut homeostasis. Bulk and single-cell transcriptomic analysis coupled with microscopy revealed that zebrafish IL-26 suppresses cell proliferation and DNA damage in gut epithelial progenitors and absorptive enterocytes, respectively. The dysregulated cell proliferation and DNA damage in the gut of *il26*$^{-/-}$ larvae suggests a central role of IL-26 in maintaining tissue homeostasis and genome integrity. Interestingly, these mutants did not exhibit any overt developmental abnormalities and developed normally to adulthood. Compensatory mechanisms may exist to mitigate the impact of IL-26 deficiency on proliferation and DNA damage later in life. Another possibility is that the consequences of

these phenotypes are more subtle and require longer periods to manifest as pathological conditions. Further research is warranted to examine the long-term effects of IL-26 deficiency on mutational burden, genome integrity, and epithelial barrier integrity in the gut.

We show that the loss of the IL-26 receptor does not impact cell proliferation or DNA damage, suggesting that the control of these cellular processes by IL-26 is independent of IL-26 receptor-mediated signaling. These results pave the way for future research focusing on dissecting in detail IL-26 receptor-dependent versus -independent functions.

Human IL-26 has been reported to have receptor-independent functions, such as binding to DNA and killing bacteria by pore formation (*92*). Our data suggest that the ability to bind DNA is not conserved in zebrafish IL-26. However, in-depth analysis using high-resolution microscopy is required to validate this finding. Interestingly, the zebrafish IL-26 killed the bacterial strains *E. coli* and *P. aeruginosa* to similar level as its human counterpart, demonstrating that the bactericidal activity of human IL-26 is highly conserved in zebrafish. The full range of bacterial species affected by the two proteins requires further analysis. Furthermore, the role of specific domains of the IL-26 protein in controlling distinct cellular processes could be further studied using comparative structural and sequence-based approaches.

We revealed a key role of the microbiota in IL-26-mediated control of cell proliferation and DNA damage. Microbiota transfer from WT animals mitigated the elevated gut epithelial cell proliferation and DNA damage of *il26*-deficient larvae, suggesting that an altered microbiota composition contributes to these observed phenotypes. These results highlight the therapeutic potential of microbiota transfer to restore genetically-caused impairments. Future studies should focus on profiling the microbiota composition in these different conditions to pinpoint specific bacterial species, strains, or components driving the observed phenotypes.

ILCs are known to regulate gut homeostasis through cytokine production in the adult zebrafish gut (*16*). However, the emergence of ILCs in the gut during early life and their cytokine production profile were not identified. We report the presence of functional ILCs in the larval gut as early as 5-dpf, being the main source of IL-26. Our study underscores the importance of ILCs and their produced cytokines in gut homeostasis in early life. A more detailed characterization of ILCs function across the lifespan through targeted ablation is

warranted. Additionally, the cellular sources of IL-26 across the lifespan and under different immunological challenges remain to be identified.

ILCs are known to express several TLRs and respond to pathogen associated molecular patterns (PAMPs) by cytokine production (*173–175*). We demonstrate that TLR-dependent sensing of the microbiota is crucial for maintaining baseline IL-26 expression levels in gut ILCs during early life. Additional studies are required to determine whether ILCs directly sense the microbiota via TLRs or if microbiota recognition occurs in other cell types, which then signal to ILCs to produce IL-26.

Our findings established that IL-26 protects the gut from bacterial infections, which correlated with increased DNA damage and an impaired immune response. One limitation of our study is the unclear role of the increased DNA damage in the higher mortality observed in *il26*$^{-/-}$ larvae. Future investigations should examine cell death and gut epithelial barrier integrity in *il26*$^{-/-}$ larval guts upon bacterial infections. Another limitation is the undetermined impact of the microbiota on the increased DNA damage and mortality rate observed upon *E. tarda* infection in *il26*$^{-/-}$ larvae. Additional work is required to elucidate the consequences of IL-26 loss in the gut upon *E. tarda* infection in different gnotobiotic conditions. Our study also underscores the need to decipher the role of receptor-mediated IL-26 signaling versus IL-26 bactericidal properties during *E. tarda* infection. Utilizing *il20ra*$^{-/-}$ will be a valuable tool to gain insights into this matter.

In summary, our findings reveal key mechanisms by which host-microbiota interactions during development, mediated by ILC-produced IL-26, protect against excessive cell proliferation and DNA damage in epithelial cells, thereby preserving gut homeostasis.

MATERIALS AND METHODS

Zebrafish lines and husbandry

The zebrafish lines: wild-type (AB), *TgBAC(cldn15la-GFP)* (*163*), *rag1*$^{-/-}$ (*176*), *myd88*$^{-/-}$ (*54*), *il2rga*$^{-/-}$*prkdc*$^{-/-}$ (*171*), *il26*$^{-/-}$, and *il20ra*$^{-/-}$ were reared and kept in the zebrafish core facility at the Institut Curie animal facility in accordance with European Union regulations on laboratory animals using protocol numbers: APAFIS#27495-2020100614519712 v14.2.2, #2019_010 and #2022-008 (approved the French Ministry of Research). Zebrafish larvae used

in foreign collaborations abroad were maintained according to the "Acta de Aprobación 004/2021" provided by the Universidad Andrés Bello, Chile. Zebrafish embryos were collected by natural spawning of adults and were kept at 28°C in E3 water.

Generation of *il26*- and *il20ra*-deficient zebrafish

The coding sequence for the zebrafish interleukin-26 gene (gene name: *il26*, ENSEMBL ID: ENSDARG00000045672.6) was targeted using CRISPR/Cas9 technology with two specific sgRNAs: GCAGGGATTTATGGATGTCC and GAGACAATAAACCCTTCCAT. Interleukin-20 receptor A (gene name: *il20ra*, ENSEMBL ID: ENSDART00000043626.6) was targeted using two specific sgRNAs: TGGACGTCTCGCGGCTCAGG and GTGAAGTGGACGGCAGGACA. One-cell stage zebrafish embryos were injected with 1 nL of a mixture containing guide RNA (6.65 µM) and Cas9 protein (5 µM).

Genotyping

Adult zebrafish were anesthetized with tricaine (100 ug/ml, Sigma, #A5040), their tails were cut and incubated during 1 hour at 56°C with FinClip buffer (10 mM Tris, pH 8.0, 10 mM EDTA, 200 mM NaCl, 0.5% SDS) containing Proteinase K (0,2 mg/mL, Invitrogen, #25530-049). DNA was precipitated by adding 70% ethanol. The pellet was resuspended in water and the product solution was used for genotyping. Zebrafish larvae were anesthetized with tricaine, their tails were cut and incubated during 15 min at 95°C in Base buffer (25 mM KOH, 0.2 mM EDTA). An equal volume of Neutralization buffer (40 mM Tris-HCl) was then added, and the solution was used for genotyping. *il26*$^{-/-}$ fish were genotyped by gel electrophoresis using the primers: GTCAAAAGTGAGGTTGTGGCA and CCATGAATGCAGCCTTCAGC. *il20ra*$^{-/-}$ fish were genotyped by sequencing using the primers GTTGTGGCTGCTGTACGCTA and GGAACAGGGTTGGGAAGCTAAA.

Zebrafish Il26 protein injections

Injections were performed using 2 µL of recombinant zebrafish IL-26 protein (1 mg/mL, Kingfisher Biotech, #RP1773Z-025) mixed with 0.5 µL of phenol red. BSA at 1 mg/mL was used as a control.

Bulk RNA-sequencing

10-15 guts per replicate were dissected and RNA was extracted using the Single Cell RNA Purification Kit (Norgen, #51800) following the manufacturer's instructions. RNA integrity and concentration were analyzed on the Agilent 4200 Tapestation system using the High Sensitivity RNA ScreenTape Analysis kit (Agilent, #5067-5579). RNA sequencing libraries were prepared from 500 ng to 1 µg of total RNA using the Illumina TruSeq Stranded mRNA Library Preparation Kit. cDNA quality was checked on the Agilent 2100 Bioanalyzer using the Agilent High Sensitivity DNA Kit (Agilent #5067-4626). After quality control, libraries were sequenced with 100-bp paired-end (PE100) reads on the NovaSeq 6000 (Illumina) sequencer. Raw data were checked for quality using FastQC (v0.11.8) and aligned to the reference genome for *Danio rerio* danRer11 from the Genome Reference Consortium. Analysis was performed in R using the EdgeR (*177*) and ClusterProfile (*178*) packages.

Immunostaining on dissected larval guts

Larvae were incubated with 100 µM EdU in E3 for 3 hours. After incubation, larvae were washed with E3. Next, the guts were dissected and fixed in 4% paraformaldehyde for 1 hour at room temperature. Samples were washed twice with PBST (0.1% Triton-X100 in PBS), followed by incubation in PBS with 3% BSA for 1 hour. After one wash with PBS, the samples were incubated overnight at 4°C with primary antibodies diluted in 200 ul of PBS: γH2AX (1:200, GeneTex, #GTX127342) or 2F11 (1:200, Abcam, #ab71286). The next day, the samples were washed three times for 10 minutes each in PBST. They were then incubated with secondary antibodies diluted in 500 ul of PBS at 4°C for 3 to 4 hours: Goat Anti-Rabbit IgG H&L (1:500, Abcam, #ab175471) or Donkey Anti-Rabbit IgG H&L (1:500, Abcam, #ab150075). Following this, the samples were washed twice for 10 minutes in PBST, and then washed three more times for 10 minutes in PBS. The Click-iT™ EdU Cell Proliferation Kit (Invitrogen, #C10337, # C10340, #C10638) was used according to the manufacturer's instructions. Samples were washed twice in PBS for 10 minutes. The dissected guts were then mounted with ProLong™ Gold Antifade Mountant (ThermoFisher, #P36931). Images were acquired using the Upright Spinning Disk Confocal Microscope (Roper/Zeiss) with a 63X objective (63x/1.4 OIL DICII PL APO, 420782-9900). Multi-dimensional imaging of the posterior gut was performed to encompass the entire intestinal tube. Quantification was carried out in ImageJ.

Gut length analysis in larvae

Larvae were anesthetized with tricaine and mounted in 3% methylcellulose for live imaging. Gut length was measured from the intestinal bulb to the end of the intestine at the anal pore. The analysis was done in ImageJ.

Adult body length measurements

Adult fish were anesthetized with tricaine. Body length was measured from the head to the tail, excluding the tail fin using a ruler.

Single-cell RNA-sequencing

10 guts were dissected and placed in 200 µL of a dissociation cocktail (1 mg/mL fresh collagenase A, 40 µg/mL proteinase K, and 0.25% trypsin in PBS) at 37°C for 30 minutes. 50 guts were dissected per condition for a total of 5 replicate tubes per condition. Cells were centrifuged at 300 RCF for 15 minutes at 4°C. The pellet was resuspended in 200 µL PBS with 0.04% non-acetylated BSA. Replicates were pooled and filtered through a 40 µm cell strainer (Fisherbrand, #22363547). Samples were centrifuged at 300 RCF for 15 minutes at 4°C and resuspended with in 50 ul of PBS with 0.04% non-acetylated BSA. To isolate live cells, an OptiPrep™ Density Gradient Medium (Sigma, #D1556-250ML) was used. A 40% (w/v) iodixanol working solution was prepared by mixing 2 volumes of OptiPrep™ with 1 volume of 0.04% BSA in 1X PBS/DEPC-treated water. This working solution was used to create a 22% (w/v) iodixanol solution in the same buffer. The cell suspension was mixed with one volume of the working solution and 0.45 volume of the cell suspension via gentle inversion, transferred to a 15 mL conical tube, and topped up to 6 mL with the working solution. This solution was overlaid with 3 mL of the 22% iodixanol, and then with 0.5 mL of PBS with 0.04% BSA. Samples were centrifuged at 800 RCF for 20 minutes at 20°C. Viable cells were collected from the top interface, diluted in PBS with 0.04% BSA, and centrifuged at 300 RCF for 10 minutes at 4°C. The supernatant was discarded, and the cells were resuspended in PBS with 0.04% non-acetylated BSA to reach the desired concentration. Cells were loaded onto a 10× Chromium instrument (10× Genomics) and libraries were prepared using the Single Cell 3' Reagent Kit (V2 chemistry) (10× Genomics) according to the manufacturer's instructions. The sequencing coverage was approximately 100,000 reads per cell. Data analysis was performed using the Seurat package in R (*179*).

Cell proliferation assay

HT29, SW480, and HCT116 cell lines were seeded onto a 96-well flat-bottom plate at a density of 5000 cells/well and grown for 1 day in 100µl of DMEM with 10% FBS medium in a humidified 5% CO2 atmosphere at 37°C. After starvation in serum-free medium overnight, human IL26 recombinant protein (R&D Systems, #1375-IL-025) was added to the wells and incubated in medium containing 0.1% FBS for 48 hours. 100 µl of medium were removed and 10 µl of the cell proliferation reagent WST-1 (Roche, #11 644 807 001) were added. The plates were incubated for 2-3 hour. Wavelength measurements were performed between 420 and 480 nm.

Gel migration assay to determine DNA-binding ability of IL-26

Genomic zebrafish DNA was mixed with different cytokines at a final concentration of 3 ng/µl. Samples were loaded onto a 1.5% agarose gel for electrophoretic migration.

Antimicrobial assay

The following bacterial strains were used: *Pseudomonas aeruginosa*, *Escherichia coli*, and *Enterococcus faecalis*. Bacteria were cultured at 37°C overnight in trypticase soy broth with 10 mM NaCl. Samples were subcultured for an additional 3 hours to achieve mid–logarithmic phase growth. Bacterial concentrations were measured by spectrophotometry at 620 nm and diluted to a final concentration of 10^5 CFU/ml, after which they were incubated at 37°C for 24 hours under low-ionic-strength conditions (10 mM NaCl). Human or zebrafish IL-26 were added to these cultures to test their antimicrobial activity. After 24 hours, serial dilutions of bacterial cultures were plated onto lysogeny broth (LB) agar plates overnight. The number of colonies was counted visually.

Generation of germ-free larvae and co-housing experiments

Fertilized zebrafish eggs were treated with bleach (0.05%) for a maximum of 2 minutes at 3 to 4 hours post fertilization and then washed twice with sterile E3 medium for 5 minutes. Embryos were incubated in chlorine hypochlorite (0.003%) for 20 minutes. After washing, embryos were transferred to sterile E3 medium containing ampicillin (200 µg/mL), kanamycin (5 µg/mL), ceftazidime (200 µg/mL), and chloramphenicol (20 µg/mL) and placed at 28°C in isolated containers. The medium was renewed daily under sterile conditions until the day of

sample collection. Sterility was monitored every 2 days by incubating fish water in TBS media for 24 hours at 37°C. Cohousing experiments were performed by transferring GF larvae to containers with CV larvae, separated by a sterile strainer (Fisherbrand, #22363547).

Quantitative real-time PCR

10 guts per replicate were dissected and RNA was extracted using the Single Cell RNA Purification Kit (Norgen, #51800) following the manufacturer's instructions. Synthesis of cDNA was performed using the M-MLV Reverse Transcriptase Kit (Invitrogen, #28025013). qPCR was carried out using the Takyon™ Kit (Takyon, #UF-LPMT-C0701) on a Thermo ABI ViiA 7 Real-Time PCR System (Thermo Applied Biosystems). The primers used were as follows: *il26*: CCATAAATCCCTGCCGAGAGA, CACGCTTGAAGTCTGGGACA; *il20ra*: GGAGTACGCCATTTACGGGG, ACAGTGGTCTGAATCTGCCG; *il1b*: GAGACAGACGGTGCTGTTTA, GTAAGACGGCACTGAATCCA; *tnfa*: GGCCTTTTCTTCAGGTGGCT, AGCACTTGTTCCTCAGTCAGT; *il22*: TGCAGAATCACTGTAAACACGA, CTCCCCGATTGCTTTGTTAC; *il10*: TCACGTCATGAACGAGATCC, CCTCTTGCATTTCACCATATCC.

V. anguillarum Injections

Vibrio anguillarum strain 1669 was grown in TSA broth medium to OD600 of 1.5. The bacterial pellet from 9 mL of fully grown culture was resuspended in NaCl (9 g/L) with 0.35% formaldehyde and incubated overnight at 20°C. The suspension was then washed four times in NaCl (9 g/L) and resuspended in 800 µL of the same isotonic solution. For injections, 1.5 µL of this solution was added to 1 µL of water and 0.5 µL of phenol red. PBS was injected as a control.

HCR™ RNA-FISH

HCR probes for zebrafish *il26* and *nitr9* were purchased from Molecular Instruments. The staining was performed according to the manufacturer's guidelines with the following optimizations: guts were dissected and fixed in 4% paraformaldehyde for 1 hour at room temperature. After completing the staining protocol, the dissected guts were mounted with ProLong™ Gold Antifade Mountant (ThermoFisher, #P36931). Images were acquired using the Upright Spinning Disk Confocal Microscope (Roper/Zeiss) with a 63X objective (63x/1.4 OIL DICII PL APO, 420782-9900).

E. tarda infections

Edwarsiella tarda FL60 (provided by Dr. Phillip Klesius (USDA, Agricultural Research Service, Aquatic Animal Health Research Unit) were grown in TSB medium + tetracycline (15 ug/mL) at 28°C overnight. A 1:100 dilution was performed, and the bacteria were grown to reach OD600 = 0.250. The bacteria were then centrifuged at 3500 RCF for 5-10 minutes and resuspended in E3 water to achieve OD600 = 0.250. 6 ml of the bacterial suspension in E3 were added to six larvae for 5 hours at 28°C. Larvae were washed three times with E3 water. Survival was monitored every 12 hours for 3-days post-infection. Images were acquired with the THUNDER Imager Model Organism microscope (Leica). mCherry area and mean intensity were determined using ImageJ.

Statistical analysis

Statistical analyses were performed using RStudio or GraphPad Prism. Specific statistical tests and significance levels are detailed in the respective figure legends.

Discussion and perspectives

In this section, I will provide an in-depth discussion of the obtained results. To avoid redundancy with the previous chapter, I will only briefly summarize the results of my PhD and directly proceed to outline the planned experiments necessary to complete this project. Additionally, I will describe a series of interesting observations that were not included in the Results section and propose potential research directions that can emerge from this project.

1. IL-26 modulates gut epithelial homeostasis

Although IL-26 has been implicated in various inflammatory conditions, the absence of suitable animal models to study this cytokine has significantly hindered our understanding of its functions. For instance, IL-26 is overexpressed in the inflamed gut tissue of patients with IBD. However, it remains unclear whether IL-26 drives the inflammation and exacerbates its outcomes, suggesting that its targeting could attenuate the inflammatory response, or whether it is a physiological consequence of inflammation aimed at combating dysregulated microbial communities, implying that its supplementation could be beneficial to patients.

In this project, we report the generation of *il26*-deficientzebrafish as the first animal model to study the consequences of IL-26 loss-of-function. We show that the loss of IL-26 leads to elevated cell proliferation in gut epithelial cells during early life. To address the consequences of this heightened proliferation, we initially hypothesized that it might lead to differences in organ size. However, we found that the gut length of *il26*$^{-/-}$ larvae was similar to WT. Other possible effects include higher epithelial turnover or smaller epithelial cell size. To investigate whether the increased proliferation leads to faster epithelial turnover in *il26*$^{-/-}$, we plan to conduct EdU pulse-chase experiments.

The gut epithelium maintains a delicate equilibrium between cell proliferation and differentiation. One unclear outcome of the enhanced cell proliferation in *il26*$^{-/-}$ is whether it is compensated by a correspondingly faster differentiation process. We are investigating this by performing RNA velocity assays on our scRNA-seq dataset. RNA velocity is a technique that measures the rate of change in gene expression within individual cells by analyzing both spliced and unspliced mRNA. This method allows us to predict the future states of cells and the speed at which they transition to these states. This could help clarify whether epithelial

cells in *il26*$^{-/-}$ guts exhibit faster differentiation. Alternatively, it is possible that the increased proliferation compromises cell differentiation, potentially leading to a dysfunctional gut epithelium. Interestingly, we can detect differences in gene expression in differentiated epithelial subtypes between WT and *il26*$^{-/-}$. However, the extent to which these changes translate into functional differences remains to be explored.

The functions of IL-26 in epithelial cell differentiation could also manifest through altering the cell fate of ISCs towards certain epithelial cell types. Notably, IL-10, which shares the IL-10RB receptor subunit with IL-26, has been shown to suppress goblet cell fate in zebrafish larvae (*180*). Therefore, understanding the effects of IL-26 on epithelial cell differentiation requires further investigation.

Human IL26 was reported to mildly suppress proliferation in the epithelial cell line HT29 at concentrations of 10 and 100 ng/ml (*5*). However, we were unable to reproduce these results, even when using a wider range of concentrations (10 to 1000 ng/ml) and multiple gut epithelial cell lines, including SW480 and HCT116. These findings are in line with our conclusion that IL-26 modulates epithelial proliferation through interactions with the microbiota, which is absent in this *in vitro* culture system. This indicates that the effects of IL-26 protein injections on epithelial proliferation should be investigated *in vivo*. Consequently, we are exploring this by employing human and zebrafish IL-26 protein injections in zebrafish larvae and mouse models.

We revealed that IL-26 loss increased DNA damage accumulation in absorptive enterocytes in zebrafish larvae. To characterize the consequences of this phenomenon, we are assessing absorption by gavaging fluorescent lipids and proteins and measuring fluorescence intensity in gut epithelial cells. Additionally, we are conducting TUNEL analysis to determine whether the increased DNA damage leads to higher cell death. Finally, we are assessing the impact on tissue barrier integrity by gavaging larvae with FITC-dextran and quantifying fluorescence intensity in the body of the larvae.

Our findings that *il26*$^{-/-}$ larvae exhibit heightened proliferation and DNA damage in the gut raise important questions about the long-term effects of IL-26 loss. Notably, we observed a steady increase in *il26* expression in the gut up to 4 weeks post fertilization (wpf) (Fig. 1). Therefore, although we did not detect gross defects in adult *il26*$^{-/-}$ zebrafish, we are now characterizing proliferation and DNA damage in *il26*$^{-/-}$ guts across the lifespan.

Given that the effects of IL-26 loss on epithelial cells in larvae are microbiota-dependent, and considering that adult zebrafish share the same water system thereby possibly harboring similar microbiota, we speculate that these phenotypes may be rescued in adult fish. Profiling microbial communities in this context would be particularly insightful. Alternatively, if adult *il26*$^{-/-}$ continue to show increased proliferation and DNA damage, investigating IL-26 function in aging models would be worthwhile.

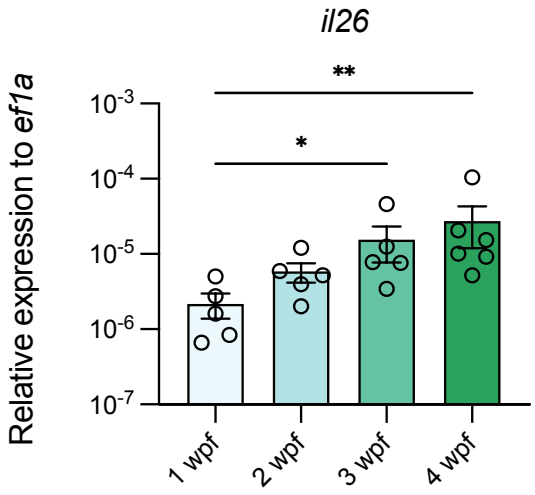

Fig. 1. *il26* expression across zebrafish development. qRT-PCR analysis of *il26* in dissected guts of WT zebrafish. Error bars show means ± SEM. Statistical significance was determined by Kruskal-Wallis test. **P* < 0.05, ***P* < 0.01, ****P* < 0.001, and *****P* < 0.0001.

2. Receptor-dependent versus -independent functions of zebrafish IL-26

To better understand the phenotypes observed in the gut epithelium of *il26*$^{-/-}$ larvae, we generated zebrafish deficient for the IL-26 receptor, *il20ra*$^{-/-}$. Using this model, we demonstrated that IL-26 suppresses proliferation and DNA damage in the larval gut independently of its receptor. This prompted us to investigate the involvement of receptor-independent functions of IL-26.

Human IL26 is an amphipathic 171-amino acid protein with 30 positively charged residues and an isoelectric point of 10.7. These properties enable receptor-independent functions, such as killing bacteria and binding to DNA (*92*). Zebrafish Il26 is an amphipathic 169-amino acid protein with 34 positively charged residues and an isoelectric point of 9.51. The similar physiochemical properties between human and zebrafish IL-26 proteins prompted

us to examine the conservation of IL-26 receptor-independent functions in zebrafish. We demonstrated that zebrafish Il26 can directly kill bacteria to similar levels as the human protein, indicating that the intrinsic bactericidal activity of human IL26 is conserved in zebrafish. However, in contrast to human IL26, the zebrafish protein did not bind to DNA. The specific structural and physiochemical differences between human and zebrafish IL-26 proteins that enable human IL26, but not zebrafish Il26, to bind DNA require further investigation.

Given that the antimicrobial activity of IL-26 is conserved in zebrafish and that IL-26 regulates proliferation and DNA damage in a receptor-independent manner, we hypothesized that IL-26 suppresses proliferation and DNA damage in gut epithelial cells through its antimicrobial function. One possible mechanism is through modulating the microbiota composition. To test this, we reared *il26*$^{-/-}$ GF and found that the absence of microbiota in *il26*$^{-/-}$ was sufficient to rescue the phenotypes to WT CV levels. In addition, co-housing-mediated microbiota transfer from WT to *il26*$^{-/-}$ restored the high proliferation and DNA damage in *il26*$^{-/-}$ to WT CV levels. These results support the hypothesis that an altered microbiota composition in *il26*$^{-/-}$ is responsible for the elevated proliferation and DNA damage. Overall, these data suggest that the loss of IL-26 antimicrobial activity leads to dysbiosis in the gut, which in turn results in higher proliferation and DNA damage in gut epithelial cells.

In order to confirm the dysbiosis in *il26*$^{-/-}$ guts, we plan to profile the microbiota by performing 16S rRNA-seq. Moreover, we plan to characterize microbiota composition under co-housing conditions. This could help pinpoint specific bacterial species, strains, or components driving the observed phenotypes in *il26*$^{-/-}$.

It is worth mentioning that in our co-housing setting, not only live bacteria are transferred, but also metabolites and other organisms. Therefore, to verify that co-housing *il26*$^{-/-}$ with WT rescues the phenotypes as a result of the transfer of live bacteria, we plan to perform experiments transferring medium treated with antibiotics or filtered medium that excludes bacteria and bacterial components but retains metabolites. This will help determine whether live bacteria, bacterial components, or metabolites are responsible for rescuing the phenotypes in *il26*$^{-/-}$ zebrafish.

Interestingly, we observed that cohousing WT GF with *il26*$^{-/-}$ CV did not result in increased cell proliferation and DNA damage in WT. This suggests that the microbiota of *il26*$^{-/-}$ is not sufficient to induce the phenotypes in WT larvae. Microbiota profiling in this condition could help identify the bacterial species that are failing to colonize WT larvae, indicating a potential role for these species in inducing cell proliferation and heightened DNA damage in *il26*$^{-/-}$ gut epithelial cells.

3. Gut innate lymphoid cells during early life

In addition to the role of IL-26 in shaping the microbiota, we show that microbial colonization induces *il26* expression in gut ILCs, indicating a bidirectional interaction between ILCs and the microbiota. This represents a major finding because, prior to this report, the presence and functional significance of ILCs in zebrafish larvae had not been demonstrated.

We demonstrate that microbiota induces *il26* expression in ILCs through MYD88-dependent TLR signaling. To clarify whether ILCs sense the microbiota directly via TLRs, we propose generating a knock-in line that specifically re-expresses *myd88* in ILCs in *myd88*$^{-/-}$ background by taking advantage of the ILC-specific markers *nitr9* or *nitr4a*. Unperturbed *il26* levels in this line compared to WT would confirm this hypothesis. Alternatively, intestinal epithelial cells could be responsible for sensing the microbiota and subsequently signaling to ILCs. To test this, *myd88* could be re-expressed specifically in intestinal epithelial cells in *myd88*$^{-/-}$ background by utilizing the well-characterized *cldn15la* promotor. However, this prospect remains outside the scope of this PhD thesis. Additionally, screening individual TLR ligands to determine which ones induce *il26* expression requires further characterization.

Interestingly, qPCR analysis of dissected guts up to 4 wpf showed an increase in *nitr9* expression at 3 wpf (Fig. 2). Whether this increased expression represents a higher number of ILCs in the gut or increased *nitr9* expression per cell remains to be resolved. Additionally, *nitr9* is predicted to be an activating cell surface receptor (*181*). Therefore, the functional consequences of higher *nitr9* expression warrant further investigation.

To facilitate the study of ILCs in zebrafish, we are creating *nitr4a:GFP-NTR* knock-in line. This will enable the visualization of zebrafish ILCs and allow for their targeted ablation upon metronidazole administration. By using this model, we can confirm ILCs as the source of IL-26 by ablating ILCs and measuring *il26* expression in the gut. Complementarily, we can

sort ILCs from the gut and analyze *il26* expression in this population versus other cell types present in the gut. This line will pave the way for further in-depth characterization of the role of ILCs, allowing to investigate the dynamics of ILC emergence and function in gut homeostasis and disease.

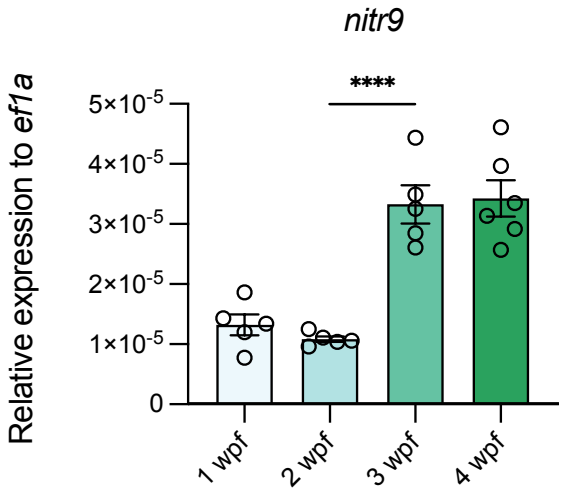

Fig. 2. *nitr9* expression across development. qRT-PCR analysis of *nitr9* in dissected guts of WT zebrafish. Error bars show means ± SEM. Statistical significance was determined by Kruskal-Wallis test. **P* < 0.05, ***P* < 0.01, ****P* < 0.001, and *****P* < 0.0001.

The expression of IL-26 was reported by lymphocytes other than ILCs (see section 6.2). Although we show that *il26* is primarily expressed by ILCs in 5-dpf larval guts, we cannot rule out the possibility that other cell types may produce *il26* later in life. To investigate the complete spectrum of *il26*-expressing cells, we are generating *il26:GFP* knock-in line. This will allow us to study the dynamics of IL-26 expression throughout the lifespan and under various immunological challenges.

4. IL-26 functions in disease models

We show that IL-26 confers protection against *E. tarda* gut bacterial infections. *il26*$^{-/-}$ larvae exhibit higher mortality, increased DNA damage accumulation in gut epithelial cells, and a compromised immune response in the gut. Our current efforts are focused on distinguishing between the protective effects mediated by the IL-26 receptor versus IL-26 direct antibacterial activity. More precisely, we are assessing the ability of rzIl26 to kill *E. tarda in vitro* and performing *E. tarda* infections in *il20ra*$^{-/-}$. Additionally, we are investigating the protective effects of rzIl26 injections against *E. tarda* infections. These experiments may open

new avenues for research into the potential usage of IL-26 as a therapeutic agent for combating bacterial infections.

To investigate the role of IL-26-microbiota interactions during *E. tarda* infections, we plan to infect WT and *il26*$^{-/-}$ under cohousing conditions. A protective effect of co-housing would suggest that a dysregulated microbiota in *il26*$^{-/-}$ contributes to the observed phenotypes.

While we show that *il26* is mainly expressed by ILCs in the developing gut at steady state, we did not address whether ILCs are the main the cellular sources of *il26* upon *E. tarda* infections. This could be tested by infecting *rag1*$^{-/-}$ and *il2rga*$^{-/-}$*prkdc*$^{-/-}$ zebrafish and measuring *il26* in the gut.

Notably, we observed that *E. tarda* infections induced *nitr4a* and *nitr9* expression in the gut 3-dpi (Fig. 3, A and B). Whether this increased expression of these ILC-markers is a consequence of an increased ILCs number in the gut remains to be determined.

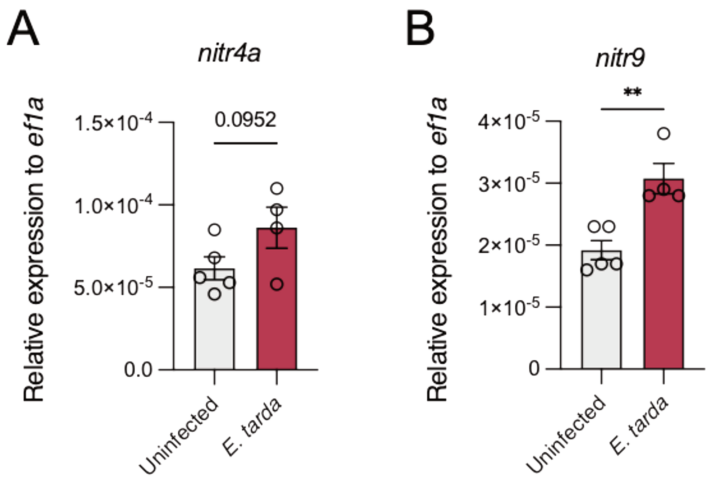

Fig. 3. *nitr4a* and *nitr9* expression upon *E. tarda* infections. qRT-PCR analysis of *nitr4a* (**A**) and *nitr9* (**B**) in dissected guts of WT larvae 3-dpi. Error bars show means ± SEM. Statistical significance was determined by Mann-Whitney test. **P* < 0.05, ***P* < 0.01, ****P* < 0.001, and *****P* < 0.0001.

In addition to the protective role of IL-26 in zebrafish *E. tarda* infections, IL-26 was shown to exert protective functions upon DSS-induced colitis in a humanized mouse model harboring the human *IL26* gene (hIL-26Tg) (*99*). Whether these protective functions of IL-26 in this mouse model are linked to the regulation of the microbiota and the modulation of proliferation and DNA damage in intestinal epithelial cells remain to be elucidated.

A notable observation we made was that rzIl26 injections upregulated antiviral gene expression in whole larvae at 5-hpi. This included genes such as myxovirus resistance protein a (*mxa*) and virus inhibitory protein, endoplasmic reticulum-associated, interferon-inducible (*viperin*) (Fig. 4, A and B). This suggests a role of IL-26 during viral infections. To explore this, we utilized Sindbis virus (SINV) as a viral infection model. SINV is an arthropod-borne virus that causes encephalitis in humans and is often used to study viral pathogenesis and immune responses (*182*). In fish, SINV infects several organs including the brain, spinal cord, liver, and gut (*183*, *184*).

Using this model, we found that inoculating 3-dpf larvae with SINV upregulated *il26* expression in whole larvae 2-days post-infection (dpi) (Fig. 4C). To test whether IL-26 overexpression could protect against SINV infections, we injected rzIl26 into 3-dpf larvae prior to SINV inoculation and measured viral loads in whole larvae. We observed that rzIl26 failed to reduce viral loads in whole larvae 2-dpi in contrast to the positive control, interferon phi 1 (Ifnphi1) (Fig. 4D).

To gain insight into the role of endogenous IL-26 in viral defense, we propose infecting *il26*$^{-/-}$ larvae with SINV and measure viral loads as well as survival rates. Additionally, investigating the function of IL-26 in other viral infections could further elucidate its broader antiviral properties.

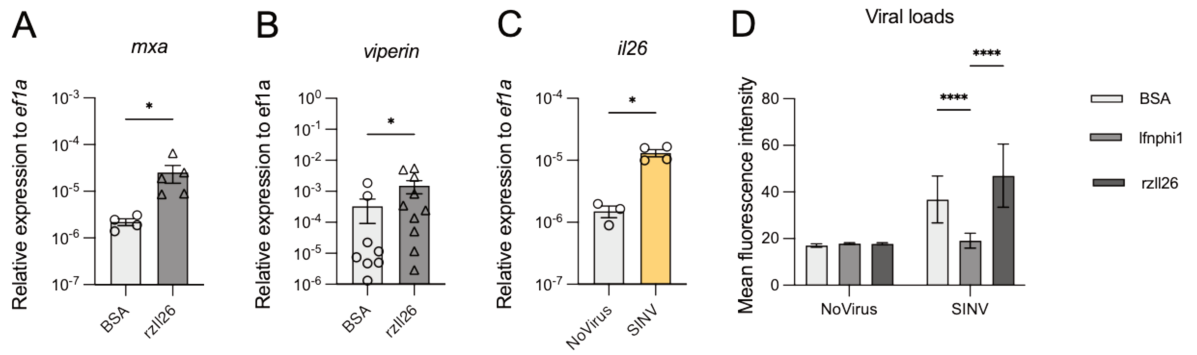

Fig. 4. The role of IL-26 during viral infections. qRT-PCR analysis of *mxa* (**A**) and *viperin* (**B**) in whole larvae 5-hpf with rzIl26. (**C**) qRT-PCR analysis of *il26* in whole larvae 2-dpi with SINV. (**D**) Viral loads in whole larvae 2-dpi. Error bars show means ± SEM. Statistical significance was determined by Mann-Whitney test (A-C) and 2way ANOVA (D). **P* < 0.05, ***P* < 0.01, ****P* < 0.001, and *****P* < 0.0001.

Finally, although this research project primarily focuses on the function of IL-26 in the gut, our findings open new avenues for investigating the role of IL-26 in regulating microbiota composition, cell proliferation, and DNA damage in other organs. This broader exploration could provide a more comprehensive understanding of IL-26's functions and its potential impact on overall health and disease.

References

1. S. Alatab, S. G. Sepanlou, K. Ikuta, H. Vahedi, C. Bisignano, S. Safiri, A. Sadeghi, M. R. Nixon, A. Abdoli, H. Abolhassani, V. Alipour, M. A. H. Almadi, A. Almasi-Hashiani, A. Anushiravani, J. Arabloo, S. Atique, A. Awasthi, A. Badawi, A. A. A. Baig, N. Bhala, A. Bijani, A. Biondi, A. M. Borzì, K. E. Burke, F. Carvalho, A. Daryani, M. Dubey, A. Eftekhari, E. Fernandes, J. C. Fernandes, F. Fischer, A. Haj-Mirzaian, A. Haj-Mirzaian, A. Hasanzadeh, M. Hashemian, S. I. Hay, C. L. Hoang, M. Househ, O. S. Ilesanmi, N. Jafari Balalami, S. L. James, A. P. Kengne, M. M. Malekzadeh, S. Merat, T. J. Meretoja, T. Mestrovic, E. M. Mirrakhimov, H. Mirzaei, K. A. Mohammad, A. H. Mokdad, L. Monasta, I. Negoi, T. H. Nguyen, C. T. Nguyen, A. Pourshams, H. Poustchi, M. Rabiee, N. Rabiee, K. Ramezanzadeh, D. L. Rawaf, S. Rawaf, N. Rezaei, S. R. Robinson, L. Ronfani, S. Saxena, M. Sepehrimanesh, M. A. Shaikh, Z. Sharafi, M. Sharif, S. Siabani, A. R. Sima, J. A. Singh, A. Soheili, R. Sotoudehmanesh, H. A. R. Suleria, B. E. Tesfay, B. Tran, D. Tsoi, M. Vacante, A. B. Wondmieneh, A. Zarghi, Z.-J. Zhang, M. Dirac, R. Malekzadeh, M. Naghavi, The global, regional, and national burden of inflammatory bowel disease in 195 countries and territories, 1990–2017: a systematic analysis for the Global Burden of Disease Study 2017. *The Lancet Gastroenterology & Hepatology* **5**, 17–30 (2020).

2. D. B. Graham, R. J. Xavier, Pathway paradigms revealed from the genetics of inflammatory bowel disease. *Nature* **578**, 527–539 (2020).

3. M. S. Silverberg, J. H. Cho, J. D. Rioux, D. P. B. McGovern, J. Wu, V. Annese, J.-P. Achkar, P. Goyette, R. Scott, W. Xu, M. M. Barmada, L. Klei, M. J. Daly, C. Abraham, T. M. Bayless, F. Bossa, A. M. Griffiths, A. F. Ippoliti, R. G. Lahaie, A. Latiano, P. Paré, D. D. Proctor, M. D. Regueiro, A. H. Steinhart, S. R. Targan, L. P. Schumm, E. O. Kistner, A. T. Lee, P. K. Gregersen, J. I. Rotter, S. R. Brant, K. D. Taylor, K. Roeder, R. H. Duerr, Ulcerative colitis–risk loci on chromosomes 1p36 and 12q15 found by genome-wide association study. *Nat Genet* **41**, 216–220 (2009).

4. D. Song, L. Lai, J. Lu, J. Tong, Z. Ran, Interleukin-26 Expression in Inflammatory Bowel Disease and Its Immunoregulatory Effects on Macrophages. *Front. Med.* **9**, 797135 (2022).

5. J. Dambacher, F. Beigel, K. Zitzmann, E. N. De Toni, B. Goke, H. M. Diepolder, C. J. Auernhammer, S. Brand, The role of the novel Th17 cytokine IL-26 in intestinal inflammation. *Gut* **58**, 1207–1217 (2009).

6. R. P. Donnelly, F. Sheikh, H. Dickensheets, R. Savan, H. A. Young, M. R. Walter, Interleukin-26: An IL-10-related cytokine produced by Th17 cells. *Cytokine & Growth Factor Reviews* **21**, 393–401 (2010).

7. D. Igawa, M. Sakai, R. Savan, An unexpected discovery of two interferon gamma-like genes along with interleukin (IL)-22 and -26 from teleost: IL-22 and -26 genes have been described for the first time outside mammals. *Molecular Immunology* **43**, 999–1009 (2006).

8. K. K. Reed, R. Wickham, Review of the Gastrointestinal Tract: From Macro to Micro. *Seminars in Oncology Nursing* **25**, 3–14 (2009).

9. D.-H. Liao, J.-B. Zhao, H. Gregersen, Gastrointestinal tract modelling in health and disease. *WJG* **15**, 169 (2009).

10. K. T. Patton, G. A. Thibodeau, *Anatomy & Physiology* (Mosby/Elsevier, St. Louis, Mo., 7th ed., 2010; http://books.google.com/books?id=LvRLAQAAIAAJ).

11. J. M. Allaire, S. M. Crowley, H. T. Law, S.-Y. Chang, H.-J. Ko, B. A. Vallance, The Intestinal Epithelium: Central Coordinator of Mucosal Immunity. *Trends in Immunology* **39**, 677–696 (2018).

12. A. S. Darwich, U. Aslam, D. M. Ashcroft, A. Rostami-Hodjegan, Meta-Analysis of the Turnover of Intestinal Epithelia in Preclinical Animal Species and Humans s.

13. C. L. Bevins, N. H. Salzman, Paneth cells, antimicrobial peptides and maintenance of intestinal homeostasis. *Nat Rev Microbiol* **9**, 356–368 (2011).

14. D. E. Jones, C. L. Bevins, Paneth cells of the human small intestine express an antimicrobial peptide gene. *J Biol Chem* **267**, 23216–23225 (1992).

15. H. F. Farin, J. H. Van Es, H. Clevers, Redundant Sources of Wnt Regulate Intestinal Stem Cells and Promote Formation of Paneth Cells. *Gastroenterology* **143**, 1518-1529.e7 (2012).

16. C. Wallaeys, N. Garcia-Gonzalez, C. Libert, Paneth cells as the cornerstones of intestinal and organismal health: a primer. *EMBO Mol Med* **15**, e16427 (2023).

17. M. E. Rothenberg, Y. Nusse, T. Kalisky, J. J. Lee, P. Dalerba, F. Scheeren, N. Lobo, S. Kulkarni, S. Sim, D. Qian, P. A. Beachy, P. J. Pasricha, S. R. Quake, M. F. Clarke, Identification of a cKit+ Colonic Crypt Base Secretory Cell That Supports Lgr5+ Stem Cells in Mice. *Gastroenterology* **142**, 1195-1205.e6 (2012).

18. A. S. Chikina, F. Nadalin, M. Maurin, M. San-Roman, T. Thomas-Bonafos, X. V. Li, S. Lameiras, S. Baulande, S. Henri, B. Malissen, L. Lacerda Mariano, J. Barbazan, J. M. Blander, I. D. Iliev, D. Matic Vignjevic, A.-M. Lennon-Duménil, Macrophages Maintain Epithelium Integrity by Limiting Fungal Product Absorption. *Cell* **183**, 411-428.e16 (2020).

19. J. W. Hickey, W. R. Becker, S. A. Nevins, A. Horning, A. E. Perez, C. Zhu, B. Zhu, B. Wei, R. Chiu, D. C. Chen, D. L. Cotter, E. D. Esplin, A. K. Weimer, C. Caraccio, V. Venkataraaman, C. M. Schürch, S. Black, M. Brbić, K. Cao, S. Chen, W. Zhang, E. Monte, N. R. Zhang, Z. Ma, J. Leskovec, Z. Zhang, S. Lin, T. Longacre, S. K. Plevritis, Y. Lin, G. P. Nolan, W. J. Greenleaf, M. Snyder, Organization of the human intestine at single-cell resolution. *Nature* **619**, 572–584 (2023).

20. J. M. H. Larsson, H. Karlsson, J. G. Crespo, M. E. V. Johansson, L. Eklund, H. Sjövall, G. C. Hansson, Altered O-glycosylation profile of MUC2 mucin occurs in active ulcerative

colitis and is associated with increased inflammation: *Inflammatory Bowel Diseases* **17**, 2299–2307 (2011).

21. M. Van der Sluis, B. A. E. De Koning, A. C. J. M. De Bruijn, A. Velcich, J. P. P. Meijerink, J. B. Van Goudoever, H. A. Büller, J. Dekker, I. Van Seuningen, I. B. Renes, A. W. C. Einerhand, Muc2-Deficient Mice Spontaneously Develop Colitis, Indicating That MUC2 Is Critical for Colonic Protection. *Gastroenterology* **131**, 117–129 (2006).

22. E. H. Kromann, A. P. Cearra, J. F. Neves, Organoids as a tool to study homeostatic and pathological immune–epithelial interactions in the gut. *Clinical and Experimental Immunology*, uxad118 (2024).

23. G. M. Jowett, I. Coales, J. F. Neves, Organoids as a tool for understanding immune-mediated intestinal regeneration and development. *Development* **149**, dev199904 (2022).

24. M. Biton, A. L. Haber, N. Rogel, G. Burgin, S. Beyaz, A. Schnell, O. Ashenberg, C.-W. Su, C. Smillie, K. Shekhar, Z. Chen, C. Wu, J. Ordovas-Montanes, D. Alvarez, R. H. Herbst, M. Zhang, I. Tirosh, D. Dionne, L. T. Nguyen, M. E. Xifaras, A. K. Shalek, U. H. von Andrian, D. B. Graham, O. Rozenblatt-Rosen, H. N. Shi, V. Kuchroo, O. H. Yilmaz, A. Regev, R. J. Xavier, T Helper Cell Cytokines Modulate Intestinal Stem Cell Renewal and Differentiation. *Cell* **175**, 1307-1320.e22 (2018).

25. Q. Hou, J. Huang, H. Ayansola, H. Masatoshi, B. Zhang, Intestinal Stem Cells and Immune Cell Relationships: Potential Therapeutic Targets for Inflammatory Bowel Diseases. *Front. Immunol.* **11**, 623691 (2021).

26. A. M. Mowat, W. W. Agace, Regional specialization within the intestinal immune system. *Nat Rev Immunol* **14**, 667–685 (2014).

27. G. A. Perry, J. G. Sharp, Characterization of proximal colonic lymphoid tissue in the mouse. *Anat. Rec.* **220**, 305–312 (1988).

28. R. L. Owen, A. J. Piazza, T. H. Ermak, Ultrastructural and cytoarchitectural features of lymphoreticular organs in the colon and rectum of adult BALB/c mice. *Am. J. Anat.* **190**, 10–18 (1991).

29. S. Ryu, M. Lim, J. Kim, H. Y. Kim, Versatile roles of innate lymphoid cells at the mucosal barrier: from homeostasis to pathological inflammation. *Exp Mol Med* **55**, 1845–1857 (2023).

30. A. Saez, R. Gomez-Bris, B. Herrero-Fernandez, C. Mingorance, C. Rius, J. M. Gonzalez-Granado, Innate Lymphoid Cells in Intestinal Homeostasis and Inflammatory Bowel Disease. *IJMS* **22**, 7618 (2021).

31. E. Vivier, D. Artis, M. Colonna, A. Diefenbach, J. P. Di Santo, G. Eberl, S. Koyasu, R. M. Locksley, A. N. J. McKenzie, R. E. Mebius, F. Powrie, H. Spits, Innate Lymphoid Cells: 10 Years On. *Cell* **174**, 1054–1066 (2018).

32. F. Ciccia, A. Accardo-Palumbo, R. Alessandro, A. Rizzo, S. Principe, S. Peralta, F. Raiata, A. Giardina, G. De Leo, G. Triolo, Interleukin-22 and interleukin-22–producing NKp44+ natural killer cells in subclinical gut inflammation in ankylosing spondylitis. *Arthritis & Rheumatism* **64**, 1869–1878 (2012).

33. S. Hue, P. Ahern, S. Buonocore, M. C. Kullberg, D. J. Cua, B. S. McKenzie, F. Powrie, K. J. Maloy, Interleukin-23 drives innate and T cell–mediated intestinal inflammation. *The Journal of Experimental Medicine* **203**, 2473–2483 (2006).

34. S. Buonocore, P. P. Ahern, H. H. Uhlig, I. I. Ivanov, D. R. Littman, K. J. Maloy, F. Powrie, Innate lymphoid cells drive interleukin-23-dependent innate intestinal pathology. *Nature* **464**, 1371–1375 (2010).

35. C. A. Lindemans, M. Calafiore, A. M. Mertelsmann, M. H. O'Connor, J. A. Dudakov, R. R. Jenq, E. Velardi, L. F. Young, O. M. Smith, G. Lawrence, J. A. Ivanov, Y.-Y. Fu, S. Takashima, G. Hua, M. L. Martin, K. P. O'Rourke, Y.-H. Lo, M. Mokry, M. Romera-Hernandez, T. Cupedo, L. E. Dow, E. E. Nieuwenhuis, N. F. Shroyer, C. Liu, R. Kolesnick, M. R. M. van den Brink, A. M. Hanash, Interleukin-22 promotes intestinal-stem-cell-mediated epithelial regeneration. *Nature* **528**, 560–564 (2015).

36. K. Gronke, P. P. Hernández, J. Zimmermann, C. S. N. Klose, M. Kofoed-Branzk, F. Guendel, M. Witkowski, C. Tizian, L. Amann, F. Schumacher, H. Glatt, A. Triantafyllopoulou, A. Diefenbach, Interleukin-22 protects intestinal stem cells against genotoxic stress. *Nature* **566**, 249–253 (2019).

37. Q. Zhu, D. Korenfeld, A. Suarez-Fueyo, S. Graham, L. Jin, S. Punit, R. Duffy, M. Puri, A. Caruso, C. Hu, Y. Tian, B. L. McRae, R. Kamath, L. Phillips, A. J. Schwartz-Sterman, S. Westmoreland, X. Cao, M. C. Levesque, Y. Bi, J. Paez-Cortez, R. Goenka, Epithelial dysfunction is prevented by IL-22 treatment in a Citrobacter rodentium-induced colitis model that shares similarities with inflammatory bowel disease. *Mucosal Immunology* **15**, 1338–1349 (2022).

38. E. Read, A. Peña-Cearra, D. Coman, G. M. Jowett, M. W. H. Chung, I. Coales, S. Syntaka, R. E. Finlay, R. Tachó-Piñot, S. Van Der Post, U. Naizi, L. B. Roberts, M. R. Hepworth, M. A. Curtis, J. F. Neves, Bi-directional signaling between the intestinal epithelium and type-3 innate lymphoid cells regulates secretory dynamics and interleukin-22. *Mucosal Immunology* **17**, 1–12 (2024).

39. E. Thursby, N. Juge, Introduction to the human gut microbiota. *Biochem J* **474**, 1823–1836 (2017).

40. G. P. Donaldson, S. M. Lee, S. K. Mazmanian, Gut biogeography of the bacterial microbiota. *Nat Rev Microbiol* **14**, 20–32 (2016).

41. Diversity of the Human Intestinal Microbial Flora | Science. https://www.science.org/doi/10.1126/science.1110591?url_ver=Z39.88-2003&rfr_id=ori:rid:crossref.org&rfr_dat=cr_pub%20%200pubmed.

42. J. F. Rawls, M. A. Mahowald, R. E. Ley, J. I. Gordon, Reciprocal Gut Microbiota Transplants from Zebrafish and Mice to Germ-free Recipients Reveal Host Habitat Selection. *Cell* **127**, 423–433 (2006).

43. X. Yang, L. Xie, Y. Li, C. Wei, More than 9,000,000 Unique Genes in Human Gut Bacterial Community: Estimating Gene Numbers Inside a Human Body. *PLoS ONE* **4**, e6074 (2009).

44. Host–microbiota interactions in inflammatory bowel disease | Nature Reviews Immunology. https://www.nature.com/articles/s41577-019-0268-7.

45. W. S. Garrett, G. M. Lord, S. Punit, G. Lugo-Villarino, S. K. Mazmanian, S. Ito, J. N. Glickman, L. H. Glimcher, Communicable Ulcerative Colitis Induced by T-bet Deficiency in the Innate Immune System. *Cell* **131**, 33–45 (2007).

46. M. Schaubeck, T. Clavel, J. Calasan, I. Lagkouvardos, S. B. Haange, N. Jehmlich, M. Basic, A. Dupont, M. Hornef, M. V. Bergen, A. Bleich, D. Haller, Dysbiotic gut microbiota causes transmissible Crohn's disease-like ileitis independent of failure in antimicrobial defence. *Gut* **65**, 225–237 (2016).

47. A. Couturier-Maillard, T. Secher, A. Rehman, S. Normand, A. D. Arcangelis, R. Haesler, L. Huot, T. Grandjean, A. Bressenot, A. Delanoye-Crespin, O. Gaillot, S. Schreiber, Y. Lemoine, B. Ryffel, D. Hot, G. Nùñez, G. Chen, P. Rosenstiel, M. Chamaillard, NOD2-mediated dysbiosis predisposes mice to transmissible colitis and colorectal cancer (2013). https://doi.org/10.1172/JCI62236.

48. L. Dianda, A. M. Hanby, N. A. Wright, A. Sebesteny, A. C. Hayday, M. J. Owen, T cell receptor-alpha beta-deficient mice fail to develop colitis in the absence of a microbial environment. *Am J Pathol* **150**, 91–97 (1997).

49. S. Kitajima, M. Morimoto, E. Sagara, C. Shimizu, Y. Ikeda, Dextran Sodium Sulfate-Induced Colitis in Germ-Free IQI/Jic Mice. *Exp. Anim.* **50**, 387–395 (2001).

50. Spatial Organization and Composition of the Mucosal Flora in Patients with Inflammatory Bowel Disease. https://doi.org/10.1128/jcm.43.7.3380-3389.2005.

51. International Inflammatory Bowel Disease Genetics Consortium, H. Huang, M. Fang, L. Jostins, M. Umićević Mirkov, G. Boucher, C. A. Anderson, V. Andersen, I. Cleynen, A. Cortes, F. Crins, M. D'Amato, V. Deffontaine, J. Dmitrieva, E. Docampo, M. Elansary, K. K.-H. Farh, A. Franke, A.-S. Gori, P. Goyette, J. Halfvarson, T. Haritunians, J. Knight, I. C. Lawrance, C. W. Lees, E. Louis, R. Mariman, T. Meuwissen, M. Mni, Y. Momozawa, M. Parkes, S. L. Spain, E. Théâtre, G. Trynka, J. Satsangi, S. Van Sommeren, S. Vermeire, R. J. Xavier, R. K. Weersma, R. H. Duerr, C. G. Mathew, J. D. Rioux, D. P. B. McGovern, J. H. Cho, M. Georges, M. J. Daly, J. C. Barrett, Fine-mapping inflammatory bowel disease loci to single-variant resolution. *Nature* **547**, 173–178 (2017).

52. A NOD2–NALP1 complex mediates caspase-1-dependent IL-1β secretion in response to Bacillus anthracis infection and muramyl dipeptide. https://doi.org/10.1073/pnas.0802726105.

53. The NLRP3 inflammasome mediates DSS-induced intestinal inflammation in Nod2 knockout mice - Benjamin Umiker, Hyun-Hee Lee, Julia Cope, Nadim J. Ajami, Jean-Philippe Laine, Christine Fregeau, Heidi Ferguson, Stephen E Alves, Nunzio Sciammetta, Melanie Kleinschek, Michael Salmon, 2019. https://journals.sagepub.com/doi/10.1177/1753425919826367?url_ver=Z39.88-2003&rfr_id=ori:rid:crossref.org&rfr_dat=cr_pub%20%200pubmed.

54. M. Van Der Vaart, J. J. Van Soest, H. P. Spaink, A. H. Meijer, Functional analysis of a zebrafish *myd88* mutant identifies key transcriptional components of the innate immune system. *Disease Models & Mechanisms*, dmm.010843 (2013).

55. S. Rakoff-Nahoum, J. Paglino, F. Eslami-Varzaneh, S. Edberg, R. Medzhitov, Recognition of Commensal Microflora by Toll-Like Receptors Is Required for Intestinal Homeostasis. *Cell* **118**, 229–241 (2004).

56. B. Deplancke, H. R. Gaskins, Microbial modulation of innate defense: goblet cells and the intestinal mucus layer123. *The American Journal of Clinical Nutrition* **73**, 1131S-1141S (2001).

57. A. A. Schoenborn, R. J. von Furstenberg, S. Valsaraj, F. S. Hussain, M. Stein, M. T. Shanahan, S. J. Henning, A. S. Gulati, The enteric microbiota regulates jejunal Paneth cell number and function without impacting intestinal stem cells. *Gut Microbes* **10**, 45–58 (2018).

58. F. Bäckhed, J. K. Manchester, C. F. Semenkovich, J. I. Gordon, Mechanisms underlying the resistance to diet-induced obesity in germ-free mice. *Proc Natl Acad Sci U S A* **104**, 979–984 (2007).

59. J. Petersson, O. Schreiber, G. C. Hansson, S. J. Gendler, A. Velcich, J. O. Lundberg, S. Roos, L. Holm, M. Phillipson, Importance and regulation of the colonic mucus barrier in a mouse model of colitis. *Am J Physiol Gastrointest Liver Physiol* **300**, G327–G333 (2011).

60. O. Pabst, H. Herbrand, M. Friedrichsen, S. Velaga, M. Dorsch, G. Berhardt, T. Worbs, A. J. Macpherson, R. Förster, Adaptation of solitary intestinal lymphoid tissue in response to microbiota and chemokine receptor CCR7 signaling. *J Immunol* **177**, 6824–6832 (2006).

61. V. Gaboriau-Routhiau, S. Rakotobe, E. Lécuyer, I. Mulder, A. Lan, C. Bridonneau, V. Rochet, A. Pisi, M. De Paepe, G. Brandi, G. Eberl, J. Snel, D. Kelly, N. Cerf-Bensussan, The Key Role of Segmented Filamentous Bacteria in the Coordinated Maturation of Gut Helper T Cell Responses. *Immunity* **31**, 677–689 (2009).

62. I. I. Ivanov, K. Atarashi, N. Manel, E. L. Brodie, T. Shima, U. Karaoz, D. Wei, K. C. Goldfarb, C. A. Santee, S. V. Lynch, T. Tanoue, A. Imaoka, K. Itoh, K. Takeda, Y. Umesaki, K. Honda, D. R. Littman, Induction of intestinal Th17 cells by segmented filamentous bacteria. *Cell* **139**, 485–498 (2009).

63. T. Sujino, M. London, D. P. Hoytema van Konijnenburg, T. Rendon, T. Buch, H. M. Silva, J. J. Lafaille, B. S. Reis, D. Mucida, Tissue adaptation of regulatory and intraepithelial CD4+ T cells controls gut inflammation. *Science* **352**, 1581–1586 (2016).

64. S. Hapfelmeier, M. A. E. Lawson, E. Slack, J. K. Kirundi, M. Stoel, M. Heikenwalder, J. Cahenzli, Y. Velykoredko, M. L. Balmer, K. Endt, M. B. Geuking, R. Curtiss, K. D. McCoy, A. J. Macpherson, Reversible Microbial Colonization of Germ-Free Mice Reveals the Dynamics of IgA Immune Responses. *Science* **328**, 1705–1709 (2010).

65. N. Powell, A. W. Walker, E. Stolarczyk, J. B. Canavan, M. R. Gökmen, E. Marks, I. Jackson, A. Hashim, M. A. Curtis, R. G. Jenner, J. K. Howard, J. Parkhill, T. T. MacDonald, G. M. Lord, The Transcription Factor T-bet Regulates Intestinal Inflammation Mediated by Interleukin-7 Receptor+ Innate Lymphoid Cells. *Immunity* **37**, 674–684 (2012).

66. R. J. Xavier, D. K. Podolsky, Unravelling the pathogenesis of inflammatory bowel disease. *Nature* **448**, 427–434 (2007).

67. A. Gutiérrez, R. Francés, A. Amorós, P. Zapater, M. Garmendia, M. Ndongo, R. Caño, R. Jover, J. Such, M. Pérez-Mateo, Cytokine association with bacterial DNA in serum of patients with inflammatory bowel disease. *Inflamm Bowel Dis* **15**, 508–514 (2009).

68. A. Gutiérrez, E. Holler, P. Zapater, L. Sempere, R. Jover, M. Pérez-Mateo, J. Schoelmerich, J. Such, R. Wiest, R. Francés, Antimicrobial peptide response to blood translocation of bacterial DNA in Crohn's disease is affected by NOD2/CARD15 genotype. *Inflamm Bowel Dis* **17**, 1641–1650 (2011).

69. A. Gutiérrez, P. Zapater, O. Juanola, L. Sempere, M. García, R. Laveda, A. Martínez, M. Scharl, J. M. González-Navajas, J. Such, R. Wiest, G. Rogler, R. Francés, Gut Bacterial DNA Translocation is an Independent Risk Factor of Flare at Short Term in Patients With Crohn's Disease. *Am J Gastroenterol* **111**, 529–540 (2016).

70. G. G. Kaplan, S. C. Ng, Understanding and Preventing the Global Increase of Inflammatory Bowel Disease. *Gastroenterology* **152**, 313-321.e2 (2017).

71. Z. Cai, S. Wang, J. Li, Treatment of Inflammatory Bowel Disease: A Comprehensive Review. *Front Med (Lausanne)* **8**, 765474 (2021).

72. E. Langholz, Review: Current trends in inflammatory bowel disease: the natural history. *Therap Adv Gastroenterol* **3**, 77–86 (2010).

73. N. Kakiuchi, K. Yoshida, M. Uchino, T. Kihara, K. Akaki, Y. Inoue, K. Kawada, S. Nagayama, A. Yokoyama, S. Yamamoto, M. Matsuura, T. Horimatsu, T. Hirano, N. Goto, Y. Takeuchi, Y. Ochi, Y. Shiozawa, Y. Kogure, Y. Watatani, Y. Fujii, S. K. Kim, A. Kon, K. Kataoka, T. Yoshizato, M. M. Nakagawa, A. Yoda, Y. Nanya, H. Makishima, Y. Shiraishi, K. Chiba, H. Tanaka, M. Sanada, E. Sugihara, T. Sato, T. Maruyama, H. Miyoshi, M. M. Taketo, J. Oishi, R. Inagaki, Y. Ueda, S. Okamoto, H. Okajima, Y. Sakai, T. Sakurai, H. Haga, S. Hirota, H. Ikeuchi, H. Nakase, H. Marusawa, T. Chiba, O. Takeuchi, S. Miyano, H. Seno, S. Ogawa, Frequent mutations that converge on the NFKBIZ pathway in ulcerative colitis. *Nature* **577**, 260–265 (2020).

74. S. Olafsson, R. E. McIntyre, T. Coorens, T. Butler, H. Jung, P. S. Robinson, H. Lee-Six, M. A. Sanders, K. Arestang, C. Dawson, M. Tripathi, K. Strongili, Y. Hooks, M. R. Stratton, M. Parkes, I. Martincorena, T. Raine, P. J. Campbell, C. A. Anderson, Somatic Evolution in Non-neoplastic IBD-Affected Colon. *Cell* **182**, 672-684.e11 (2020).

75. The landscape of somatic mutation in normal colorectal epithelial cells | Nature. https://www.nature.com/articles/s41586-019-1672-7.

76. R. W. Zhou, N. Harpaz, S. H. Itzkowitz, R. E. Parsons, Molecular mechanisms in colitis-associated colorectal cancer. *Oncogenesis* **12**, 48 (2023).

77. β-Catenin destruction complex: insights and questions from a structural perspective | Oncogene. https://www.nature.com/articles/1210055.

78. A. T. Mah, K. S. Yan, C. J. Kuo, Wnt pathway regulation of intestinal stem cells. *J Physiol* **594**, 4837–4847 (2016).

79. A. R. Moser, H. C. Pitot, W. F. Dove, A Dominant Mutation That Predisposes to Multiple Intestinal Neoplasia in the Mouse. *Science* **247**, 322–324 (1990).

80. L.-K. Su, K. W. Kinzler, B. Vogelstein, A. C. Preisinger, A. R. Moser, C. Luongo, K. A. Gould, W. F. Dove, Multiple Intestinal Neoplasia Caused by a Mutation in the Murine Homolog of the APC Gene. *Science* **256**, 668–670 (1992).

81. Y. Abuetabh, H. H. Wu, C. Chai, H. Al Yousef, S. Persad, C. M. Sergi, R. Leng, DNA damage response revisited: the p53 family and its regulators provide endless cancer therapy opportunities. *Exp Mol Med* **54**, 1658–1669 (2022).

82. S. P. Sharp, R. A. Malizia, T. Walrath, S. S. D'Souza, C. J. Booth, B. J. Kartchner, E. C. Lee, S. C. Stain, W. O'Connor, DNA damage response genes mark the early transition from colitis to neoplasia in colitis-associated colon cancer. *Gene* **677**, 299–307 (2018).

83. M. Prorok-Hamon, M. K. Friswell, A. Alswied, C. L. Roberts, F. Song, P. K. Flanagan, P. Knight, C. Codling, J. R. Marchesi, C. Winstanley, N. Hall, J. M. Rhodes, B. J. Campbell, Colonic mucosa-associated diffusely adherent afaC+ Escherichia coli expressing lpfA and pks are increased in inflammatory bowel disease and colon cancer. *Gut* **63**, 761–770 (2014).

84. J. C. Arthur, E. Perez-Chanona, M. Mühlbauer, S. Tomkovich, J. M. Uronis, T.-J. Fan, B. J. Campbell, T. Abujamel, B. Dogan, A. B. Rogers, J. M. Rhodes, A. Stintzi, K. W. Simpson, J. J. Hansen, T. O. Keku, A. A. Fodor, C. Jobin, Intestinal inflammation targets cancer-inducing activity of the microbiota. *Science* **338**, 120–123 (2012).

85. R. Hansen, J. M. Thomson, E. M. El-Omar, G. L. Hold, The role of infection in the aetiology of inflammatory bowel disease. *J Gastroenterol* **45**, 266–276 (2010).

86. Mutational signature in colorectal cancer caused by genotoxic pks+ E. coli | Nature. https://www.nature.com/articles/s41586-020-2080-8.

87. A. Knappe, S. Hör, S. Wittmann, H. Fickenscher, Induction of a Novel Cellular Homolog of Interleukin-10, AK155, by Transformation of T Lymphocytes with Herpesvirus Saimiri. *J Virol* **74**, 3881–3887 (2000).

88. K. F. Che, S. Tengvall, A. Lindén, Interleukin-26 in host defense and inflammatory disorders of the airways. *Cytokine & Growth Factor Reviews* **57**, 1–10 (2021).

89. J. R. Schoenborn, M. Dorschner, M. Sekimata, D. Santer, M. Shnyreva, D. R. Fitzpatrick, J. A. Stamatoyannopoulos, B. Wilson, Comprehensive epigenetic profiling identifies multiple distal regulatory elements directing Ifng transcription. (2008).

90. L. Dumoutier, E. Van Roost, G. Ameye, L. Michaux, J.-C. Renauld, IL-TIF/IL-22: genomic organization and mapping of the human and mouse genes. *Genes Immun* **1**, 488–494 (2000).

91. M. Shakhsi-Niaei, M. Drögemüller, V. Jagannathan, V. Gerber, T. Leeb, *IL 26* gene inactivation in *Equidae*. *Animal Genetics* **44**, 770–772 (2013).

92. S. Meller, J. Di Domizio, K. S. Voo, H. C. Friedrich, G. Chamilos, D. Ganguly, C. Conrad, J. Gregorio, D. Le Roy, T. Roger, J. E. Ladbury, B. Homey, S. Watowich, R. L. Modlin, D. P. Kontoyiannis, Y.-J. Liu, S. T. Arold, M. Gilliet, TH17 cells promote microbial killing and innate immune sensing of DNA via interleukin 26. *Nat Immunol* **16**, 970–979 (2015).

93. T. Hughes, B. Becknell, S. McClory, E. Briercheck, A. G. Freud, X. Zhang, H. Mao, G. Nuovo, J. Yu, M. A. Caligiuri, Stage 3 immature human natural killer cells found in secondary lymphoid tissue constitutively and selectively express the TH17 cytokine interleukin-22. *Blood* **113**, 4008–4010 (2009).

94. M. Cols, A. Rahman, P. J. Maglione, Y. Garcia-Carmona, N. Simchoni, H.-B. M. Ko, L. Radigan, A. Cerutti, D. Blankenship, V. Pascual, C. Cunningham-Rundles, Expansion of inflammatory innate lymphoid cells in patients with common variable immune deficiency. *Journal of Allergy and Clinical Immunology* **137**, 1206-1215.e6 (2016).

95. M. Cella, A. Fuchs, W. Vermi, F. Facchetti, K. Otero, J. K. M. Lennerz, J. M. Doherty, J. C. Mills, M. Colonna, A human natural killer cell subset provides an innate source of IL-22 for mucosal immunity. *Nature* **457**, 722–725 (2009).

96. N. Jaeger, R. Gamini, M. Cella, J. L. Schettini, M. Bugatti, S. Zhao, C. V. Rosadini, E. Esaulova, B. Di Luccia, B. Kinnett, W. Vermi, M. N. Artyomov, T. A. Wynn, R. J. Xavier, S. A. Jelinsky, M. Colonna, Single-cell analyses of Crohn's disease tissues reveal intestinal intraepithelial T cells heterogeneity and altered subset distributions. *Nat Commun* **12**, 1921 (2021).

97. L. C. Garner, A. Amini, M. E. B. FitzPatrick, M. J. Lett, G. F. Hess, M. Filipowicz Sinnreich, N. M. Provine, P. Klenerman, Single-cell analysis of human MAIT cell transcriptional, functional and clonal diversity. *Nat Immunol* **24**, 1565–1578 (2023).

98. V. Bosáková, B.-J. Ke, M. H. Kohoutková, I. Papatheodorou, F. Kafka, M. D. Zuani, S. Santhosh, F. Biscu, S. Abdurahiman, I. D. Greef, S. Verstockt, B. Verstockt, S. Vermeire,

R. J. Argüello, G. Matteoli, J. Frič, Unveiling the guardians: IL-26-expressing MAIT cells protect epithelial barrier function and are dysregulated in Crohn's disease. [Preprint] (2024). https://doi.org/10.1101/2024.06.02.597015.

99. D. Corridoni, A. Antanaviciute, T. Gupta, D. Fawkner-Corbett, A. Aulicino, M. Jagielowicz, K. Parikh, E. Repapi, S. Taylor, D. Ishikawa, R. Hatano, T. Yamada, W. Xin, H. Slawinski, R. Bowden, G. Napolitani, O. Brain, C. Morimoto, H. Koohy, A. Simmons, Single-cell atlas of colonic CD8+ T cells in ulcerative colitis. *Nat Med* **26**, 1480–1490 (2020).

100. K. Wolk, S. Kunz, K. Asadullah, R. Sabat, Cutting Edge: Immune Cells as Sources and Targets of the IL-10 Family Members? *The Journal of Immunology* **168**, 5397–5402 (2002).

101. Maturing dendritic cells are an important source of IL-29 and IL-20 that may cooperatively increase the innate immunity of keratinocytes | Journal of Leukocyte Biology | Oxford Academic. https://academic.oup.com/jleukbio/article-abstract/83/5/1181/6975457?redirectedFrom=fulltext&login=true.

102. J. M. Guerra-Laso, S. Raposo-García, S. García-García, C. Diez-Tascón, O. M. Rivero-Lezcano, Microarray analysis of Mycobacterium tuberculosis-infected monocytes reveals IL26 as a new candidate gene for tuberculosis susceptibility. *Immunology* **144**, 291–301 (2015).

103. V. Larochette, C. Miot, C. Poli, E. Beaumont, P. Roingeard, H. Fickenscher, P. Jeannin, Y. Delneste, IL-26, a Cytokine With Roles in Extracellular DNA-Induced Inflammation and Microbial Defense. *Front. Immunol.* **10**, 204 (2019).

104. M. Fujii, A. Nishida, H. Imaeda, M. Ohno, K. Nishino, S. Sakai, O. Inatomi, S. Bamba, M. Kawahara, T. Shimizu, A. Andoh, Expression of Interleukin-26 is upregulated in inflammatory bowel disease. *WJG* **23**, 5519 (2017).

105. F. Sheikh, V. V. Baurin, A. Lewis-Antes, N. K. Shah, S. V. Smirnov, S. Anantha, H. Dickensheets, L. Dumoutier, J.-C. Renauld, A. Zdanov, R. P. Donnelly, S. V. Kotenko, Cutting Edge: IL-26 Signals through a Novel Receptor Complex Composed of IL-20 Receptor 1 and IL-10 Receptor 2. *The Journal of Immunology* **172**, 2006–2010 (2004).

106. S. Hör, H. Pirzer, L. Dumoutier, F. Bauer, S. Wittmann, H. Sticht, J.-C. Renauld, R. De Waal Malefyt, H. Fickenscher, The T-cell Lymphokine Interleukin-26 Targets Epithelial Cells through the Interleukin-20 Receptor 1 and Interleukin-10 Receptor 2 Chains. *Journal of Biological Chemistry* **279**, 33343–33351 (2004).

107. R. P. Donnelly, F. Sheikh, H. Dickensheets, R. Savan, H. A. Young, M. R. Walter, Interleukin-26: An IL-10-related cytokine produced by Th17 cells. *Cytokine and Growth Factor Reviews* **21**, 393–401 (2010).

108. T. Itoh, R. Hatano, E. Komiya, H. Otsuka, Y. Narita, T. M. Aune, N. H. Dang, S. Matsuoka, H. Naito, M. Tominaga, K. Takamori, C. Morimoto, K. Ohnuma, Biological Effects of IL-

26 on T Cell–Mediated Skin Inflammation, Including Psoriasis. *Journal of Investigative Dermatology* **139**, 878–889 (2019).

109. Y.-H. Lin, Y.-H. Wang, Y.-J. Peng, F.-C. Liu, G.-J. Lin, S.-H. Huang, H.-K. Sytwu, C.-P. Cheng, Interleukin 26 Skews Macrophage Polarization Towards M1 Phenotype by Activating cJUN and the NF-κB Pathway. *Cells* **9**, 938 (2020).

110. J. Dambacher, F. Beigel, K. Zitzmann, E. N. De Toni, B. Göke, H. M. Diepolder, C. J. Auernhammer, S. Brand, The role of the novel Th17 cytokine IL-26 in intestinal inflammation. *Gut* **58**, 1207–1217 (2009).

111. C. Poli, J. F. Augusto, J. Dauvé, C. Adam, L. Preisser, V. Larochette, P. Pignon, A. Savina, S. Blanchard, J. F. Subra, A. Chevailler, V. Procaccio, A. Croué, C. Créminon, A. Morel, Y. Delneste, H. Fickenscher, P. Jeannin, IL-26 Confers Proinflammatory Properties to Extracellular DNA. *The Journal of Immunology* **198**, 3650–3661 (2017).

112. S. Meller, J. Di Domizio, K. S. Voo, H. C. Friedrich, G. Chamilos, D. Ganguly, C. Conrad, J. Gregorio, D. Le Roy, T. Roger, J. E. Ladbury, B. Homey, S. Watowich, R. L. Modlin, D. P. Kontoyiannis, Y. J. Liu, S. T. Arold, M. Gilliet, TH17 cells promote microbial killing and innate immune sensing of DNA via interleukin 26. *Nature Immunology* **16**, 970–979 (2015).

113. Y. Kumagai, O. Takeuchi, S. Akira, TLR9 as a key receptor for the recognition of DNA☆. *Advanced Drug Delivery Reviews* **60**, 795–804 (2008).

114. W. Nj, B. K, C. Jr, M. Bs, B. Wm, M. Jd, B. B, S. K, C. T, M. F, L. Jc, K. Ra, C. Dj, M. Tk, B. Ep, de W. M. R, Development, cytokine profile and function of human interleukin 17-producing helper T cells. *Nature immunology* **8** (2007).

115. M. Corvaisier, Y. Delneste, H. Jeanvoine, L. Preisser, S. Blanchard, E. Garo, E. Hoppe, B. Barré, M. Audran, B. Bouvard, J.-P. Saint-André, P. Jeannin, IL-26 Is Overexpressed in Rheumatoid Arthritis and Induces Proinflammatory Cytokine Production and Th17 Cell Generation. *PLOS Biology* **10**, e1001395 (2012).

116. S. Bogaert, D. Laukens, H. Peeters, L. Melis, K. Olievier, N. Boon, G. Verbruggen, J. Vandesompele, D. Elewaut, M. De Vos, Differential mucosal expression of Th17-related genes between the inflamed colon and ileum of patients with inflammatory bowel disease. *BMC Immunol* **11**, 61 (2010).

117. A. Goris, M. G. Marrosu, K. Vandenbroeck, Novel polymorphisms in the IL-10 related AK155 gene (chromosome 12q15). *Genes Immun* **2**, 284–286 (2001).

118. Polymorphisms in the interferon-γ/interleukin-26 gene region contribute to sex bias in susceptibility to rheumatoid arthritis. doi: 10.1002/art.11236.

119. M. S. Silverberg, J. H. Cho, J. D. Rioux, D. P. B. McGovern, J. Wu, V. Annese, J. P. Achkar, P. Goyette, R. Scott, W. Xu, M. M. Barmada, L. Klei, M. J. Daly, C. Abraham, T. M. Bayless, F. Bossa, A. M. Griffiths, A. F. Ippoliti, R. G. Lahaie, A. Latiano, P. Paré, D. D. Proctor, M. D. Regueiro, A. H. Steinhart, S. R. Targan, L. P. Schumm, E. O. Kistner, A. T. Lee, P. K.

Gregersen, J. I. Rotter, S. R. Brant, K. D. Taylor, K. Roeder, R. H. Duerr, Ulcerative colitis-risk loci on chromosomes 1p36 and 12q15 found by genome-wide association study. *Nature Genetics*, doi: 10.1038/ng.275 (2009).

120. P. Piñero, O. Juanola, A. Gutiérrez, P. Zapater, P. Giménez, A. Steinert, L. Sempere, J. M. González-Navajas, J. H. Niess, R. Francés, IL26 modulates cytokine response and anti-TNF consumption in Crohn's disease patients with bacterial DNA. *J Mol Med* **95**, 1227–1236 (2017).

121. P. L. Collins, S. Chang, M. Henderson, M. Soutto, G. M. Davis, A. G. McLoed, M. J. Townsend, L. H. Glimcher, D. P. Mortlock, T. M. Aune, Distal Regions of the Human IFNG Locus Direct Cell Type-Specific Expression. *The Journal of Immunology* **185**, 1492–1501 (2010).

122. E. M. Flores, A. T. Nguyen, M. A. Odem, G. T. Eisenhoffer, A. M. Krachler, The zebrafish as a model for gastrointestinal tract–microbe interactions. *Cellular Microbiology* **22** (2020).

123. R. Gerlai, From Genes to Behavior: The Question of Evolutionary Conservation and the Role of Ethology in the Analysis of the Zebrafish. *Front Neuroanat* **15**, 809967 (2021).

124. P. Pevzner, G. Tesler, Genome Rearrangements in Mammalian Evolution: Lessons From Human and Mouse Genomes. *Genome Res* **13**, 37–45 (2003).

125. P. Nalbant, C. Boehmer, L. Dehmelt, F. Wehner, A. Werner, Functional characterization of a Na+-phosphate cotransporter (NaP(i)-II) from zebrafish and identification of related transcripts. *Journal of Physiology* **520**, 79–89 (1999).

126. Z. Wang, J. Du, S. H. Lam, S. Mathavan, P. Matsudaira, Z. Gong, RMeseoarrchpahrtioclelogical and molecular evidence for functional organization along the rostrocaudal axis of the adult zebrafish intestine. (2010).

127. C. R. Lickwar, J. G. Camp, M. Weiser, J. L. Cocchiaro, D. M. Kingsley, T. S. Furey, S. Z. Sheikh, J. F. Rawls, Genomic dissection of conserved transcriptional regulation in intestinal epithelial cells. *PLoS Biol* **15**, e2002054 (2017).

128. K. N. Wallace, M. Pack, Unique and conserved aspects of gut development in zebrafish. *Developmental Biology* **255**, 12–29 (2003).

129. X. Wei, X. Tan, Q. Chen, Y. Jiang, G. Wu, X. Ma, J. Fu, Y. Li, K. Gang, Q. Yang, R. Ni, J. He, L. Luo, Extensive jejunal injury is repaired by migration and transdifferentiation of ileal enterocytes in zebrafish. *Cell Reports* **42**, 112660 (2023).

130. L. O. Jones, R. J. Willms, X. Xu, R. D. V. Graham, M. Eklund, M. Shin, E. Foley, Single-cell resolution of the adult zebrafish intestine under conventional conditions and in response to an acute Vibrio cholerae infection. *Cell Reports* **42**, 113407 (2023).

131. M. Peron, A. Dinarello, G. Meneghetti, L. Martorano, N. Facchinello, A. Vettori, G. Licciardello, N. Tiso, F. Argenton, The stem-like STAT3-responsive cells of zebrafish intestine are WNT/β-catenin dependent. *Development*, dev.188987 (2020).

132. N. Aghaallaei, F. Gruhl, C. Q. Schaefer, T. Wernet, V. Weinhardt, L. Centanin, F. Loosli, T. Baumbach, J. Wittbrodt, Identification, visualization and clonal analysis of intestinal stem cells in fish. *Development* **143**, 3470–3480 (2016).

133. S. Tavakoli, S. Zhu, P. Matsudaira, Cell clusters containing intestinal stem cells, line the zebrafish intestine intervillus pocket. *iScience* **25**, 104280 (2022).

134. J. Park, D. S. Levic, K. D. Sumigray, J. Bagwell, O. Eroglu, C. L. Block, C. Eroglu, R. Barry, C. R. Lickwar, J. F. Rawls, S. A. Watts, T. Lechler, M. Bagnat, Lysosome-Rich Enterocytes Mediate Protein Absorption in the Vertebrate Gut. *Developmental Cell* **51**, 7-20.e6 (2019).

135. J. Harper, A. Mould, R. M. Andrews, E. K. Bikoff, E. J. Robertson, The transcriptional repressor Blimp1/Prdm1 regulates postnatal reprogramming of intestinal enterocytes. *Proceedings of the National Academy of Sciences* **108**, 10585–10590 (2011).

136. V. Muncan, J. Heijmans, S. D. Krasinski, N. V. Büller, M. E. Wildenberg, S. Meisner, M. Radonjic, K. A. Stapleton, W. H. Lamers, I. Biemond, M. A. Van Den Bergh Weerman, D. O'Carroll, J. C. Hardwick, D. W. Hommes, G. R. Van Den Brink, Blimp1 regulates the transition of neonatal to adult intestinal epithelium. *Nature Communications* **2** (2011).

137. R. J. Willms, L. O. Jones, J. C. Hocking, E. Foley, A cell atlas of microbe-responsive processes in the zebrafish intestine. *Cell Reports* **38**, 110311 (2022).

138. T. Malonga, N. Vialaneix, M. Beaumont, BEST4 $^{+}$ cells in the intestinal epithelium. *American Journal of Physiology-Cell Physiology* **326**, C1345–C1352 (2024).

139. P. P. Hernández, P. M. Strzelecka, E. I. Athanasiadis, D. Hall, A. F. Robalo, C. M. Collins, P. Boudinot, J.-P. Levraud, A. Cvejic, Single-cell transcriptional analysis reveals ILC-like cells in zebrafish. *Sci. Immunol.* **3**, eaau5265 (2018).

140. J. M. Bates, E. Mittge, J. Kuhlman, K. N. Baden, S. E. Cheesman, K. Guillemin, Distinct signals from the microbiota promote different aspects of zebrafish gut differentiation. *Developmental Biology* **297**, 374–386 (2006).

141. W. Zac Stephens, A. R. Burns, K. Stagaman, S. Wong, J. F. Rawls, K. Guillemin, B. J. M. Bohannan, The composition of the zebrafish intestinal microbial community varies across development. *ISME J* **10**, 644–654 (2016).

142. S. E. Cheesman, J. T. Neal, E. Mittge, B. M. Seredick, K. Guillemin, Epithelial cell proliferation in the developing zebrafish intestine is regulated by the Wnt pathway and microbial signaling via Myd88. *Proc. Natl. Acad. Sci. U.S.A.* **108**, 4570–4577 (2011).

143. J. V. Troll, M. K. Hamilton, M. L. Abel, J. Ganz, J. M. Bates, W. Z. Stephens, E. Melancon, M. Van Der Vaart, A. H. Meijer, M. Distel, J. S. Eisen, K. Guillemin, Microbiota promote

secretory cell determination in the intestinal epithelium by modulating host Notch signaling. *Development* **145**, dev155317 (2018).

144. I. Semova, J. D. Carten, J. Stombaugh, L. C. Mackey, R. Knight, S. A. Farber, J. F. Rawls, Microbiota Regulate Intestinal Absorption and Metabolism of Fatty Acids in the Zebrafish. *Cell Host & Microbe* **12**, 277–288 (2012).

145. B. E. V. Koch, S. Yang, G. Lamers, J. Stougaard, H. P. Spaink, Intestinal microbiome adjusts the innate immune setpoint during colonization through negative regulation of MyD88. *Nat Commun* **9**, 4099 (2018).

146. J. Michael, S. L. Abbott, Infections Associated with the Genus Edwardsiella: the Role of Edwardsiella tarda in Human Disease. *Clinical Infectious Diseases* **17**, 742–748 (1993).

147. K. Bravo-Tello, N. Ehrenfeld, C. J. Solís, P. E. Ulloa, M. Hedrera, M. Pizarro-Guajardo, D. Paredes-Sabja, C. G. Feijóo, Effect of microalgae on intestinal inflammation triggered by soybean meal and bacterial infection in zebrafish. *PLoS ONE* **12**, e0187696 (2017).

148. L. Ye, M. Bae, C. D. Cassilly, S. V. Jabba, D. W. Thorpe, A. M. Martin, H.-Y. Lu, J. Wang, J. D. Thompson, C. R. Lickwar, K. D. Poss, D. J. Keating, S.-E. Jordt, J. Clardy, R. A. Liddle, J. F. Rawls, Enteroendocrine cells sense bacterial tryptophan catabolites to activate enteric and vagal neuronal pathways. *Cell Host & Microbe* **29**, 179-196.e9 (2021).

149. O. Rendueles, L. Ferrières, M. Frétaud, E. Bégaud, P. Herbomel, J.-P. Levraud, J.-M. Ghigo, A New Zebrafish Model of Oro-Intestinal Pathogen Colonization Reveals a Key Role for Adhesion in Protection by Probiotic Bacteria. *PLoS Pathog* **8**, e1002815 (2012).

150. S. Menanteau-Ledouble, A. Karsi, M. L. Lawrence, Importance of skin abrasion as a primary site of adhesion for Edwardsiella ictaluri and impact on invasion and systematic infection in channel catfish Ictalurus punctatus. *Vet Microbiol* **148**, 425–430 (2011).

151. M. E. Pressley, P. E. Phelan, P. Eckhard Witten, M. T. Mellon, C. H. Kim, Pathogenesis and inflammatory response to Edwardsiella tarda infection in the zebrafish. *Developmental & Comparative Immunology* **29**, 501–513 (2005).

152. M. Maronek, B. Gromova, R. Liptak, B. Konecna, M. Pastorek, B. Cechova, M. Harsanyova, J. Budis, D. Smolak, J. Radvanszky, T. Szemes, J. Harsanyiova, A. Kralova Trancikova, R. Gardlik, Extracellular DNA Correlates with Intestinal Inflammation in Chemically Induced Colitis in Mice. *Cells* **10**, 81 (2021).

153. F. Di Vincenzo, Y. Yadid, V. Petito, V. Emoli, L. Masi, D. Gerovska, M. J. Araúzo-Bravo, A. Gasbarrini, B. Regenberg, F. Scaldaferri, Circular and Circulating DNA in Inflammatory Bowel Disease: From Pathogenesis to Potential Molecular Therapies. *Cells* **12**, 1953 (2023).

154. B.-T. Hansen, G. Maschkowitz, R. Podschun, H. Fickenscher, The Kinocidin Interleukin-26 Shows Immediate Antimicrobial Effects Even to Multi-resistant Isolates. *Front. Microbiol.* **12**, 757215 (2021).

155. P. Qiu, T. Ishimoto, L. Fu, J. Zhang, Z. Zhang, Y. Liu, The Gut Microbiota in Inflammatory Bowel Disease. *Front. Cell. Infect. Microbiol.* **12**, 733992 (2022).

156. M. F. Zacarías-Fluck, L. Soucek, J. R. Whitfield, MYC: there is more to it than cancer. *Front. Cell Dev. Biol.* **12**, 1342872 (2024).

157. L. Mao, X. Ling, J. Chen, Cyclin H Regulates Lung Cancer Progression as a Carcinoma Inducer. *Computational and Mathematical Methods in Medicine* **2021**, 1–11 (2021).

158. H. Patel, R. Abduljabbar, C.-F. Lai, M. Periyasamy, A. Harrod, C. Gemma, J. H. Steel, N. Patel, C. Busonero, D. Jerjees, J. Remenyi, S. Smith, J. J. Gomm, L. Magnani, B. Győrffy, L. J. Jones, F. Fuller-Pace, S. Shousha, L. Buluwela, E. A. Rakha, I. O. Ellis, R. C. Coombes, S. Ali, Expression of CDK7, Cyclin H, and MAT1 Is Elevated in Breast Cancer and Is Prognostic in Estrogen Receptor–Positive Breast Cancer. *Clinical Cancer Research* **22**, 5929–5938 (2016).

159. C. Peng, Y. Yang, L. Ji, P. Yang, X. Yang, Y. Zhang, Cyclin H predicts the poor prognosis and promotes the proliferation of ovarian cancer. *Cancer Cell Int* **20**, 316 (2020).

160. F. Sadeghi, M. Asgari, M. Matloubi, M. Ranjbar, N. Karkhaneh Yousefi, T. Azari, M. Zaki-Dizaji, Molecular contribution of BRCA1 and BRCA2 to genome instability in breast cancer patients: review of radiosensitivity assays. *Biol Proced Online* **22**, 23 (2020).

161. I. E. Wassing, F. Esashi, RAD51: Beyond the break. *Seminars in Cell & Developmental Biology* **113**, 38–46 (2021).

162. P. Bohanes, M. J. LaBonte, H.-J. Lenz, A Review of Excision Repair Cross-complementation Group 1 in Colorectal Cancer. *Clinical Colorectal Cancer* **10**, 157–164 (2011).

163. A. L. Alvers, S. Ryan, P. J. Scherz, J. Huisken, M. Bagnat, Single continuous lumen formation in the zebrafish gut is mediated by *smoothened* -dependent tissue remodeling. *Development* **141**, 1110–1119 (2014).

164. C. Crosnier, N. Vargesson, S. Gschmeissner, L. Ariza-McNaughton, A. Morrison, J. Lewis, Delta-Notch signalling controls commitment to a secretory fate in the zebrafish intestine. *Development* **132**, 1093–1104 (2005).

165. D. Zhang, V. S. Golubkov, W. Han, R. G. Correa, Y. Zhou, S. Lee, A. Y. Strongin, P. D. S. Dong, Identification of Annexin A4 as a hepatopancreas factor involved in liver cell survival. *Developmental Biology* **395**, 96–110 (2014).

166. T. Jiang, Y. Li, X. Huang, P. Jayakumar, T. R. Billiar, M. Deng, Activation of TLR9 signaling suppresses the immunomodulating functions of CD55lo fibroblastic reticular cells during bacterial peritonitis. *Front. Immunol.* **15**, 1337384 (2024).

167. P. Parroche, G. Roblot, F. Le Calvez-Kelm, I. Tout, M. Marotel, M. Malfroy, G. Durand, J. McKay, M. Ainouze, C. Carreira, O. Allatif, A. Traverse-Glehen, M. Mendiola, J. J. Pozo-Kreilinger, C. Caux, M. Tommasino, N. Goutagny, U. A. Hasan, TLR9 re-expression in

cancer cells extends the S-phase and stabilizes p16INK4a protein expression. *Oncogenesis* **5**, e244–e244 (2016).

168. V. Jovasevic, E. M. Wood, A. Cicvaric, H. Zhang, Z. Petrovic, A. Carboncino, K. K. Parker, T. E. Bassett, M. Moltesen, N. Yamawaki, H. Login, J. Kalucka, F. Sananbenesi, X. Zhang, A. Fischer, J. Radulovic, Formation of memory assemblies through the DNA-sensing TLR9 pathway. *Nature* **628**, 145–153 (2024).

169. S. Nayar, J. K. Morrison, M. Giri, K. Gettler, L. Chuang, L. A. Walker, H. M. Ko, E. Kenigsberg, S. Kugathasan, M. Merad, J. Chu, J. H. Cho, A myeloid–stromal niche and gp130 rescue in NOD2-driven Crohn's disease. *Nature* **593**, 275–281 (2021).

170. L. Petrie-Hanson, C. Hohn, L. Hanson, Characterization of rag1 mutant zebrafish leukocytes. *BMC Immunol* **10**, 8 (2009).

171. C. Yan, Q. Yang, D. Do, D. C. Brunson, D. M. Langenau, Adult immune compromised zebrafish for xenograft cell transplantation studies. *EBioMedicine* **47**, 24–26 (2019).

172. I. Frans, C. W. Michiels, P. Bossier, K. A. Willems, B. Lievens, H. Rediers, *Vibrio anguillarum* as a fish pathogen: virulence factors, diagnosis and prevention. *Journal of Fish Diseases* **34**, 643–661 (2011).

173. X.-D. Li, L. She, H. H. Alanazi, Y. Xu, S. Guo, Q. Xiong, H. Jiang, K. Mo, J. Wang, D. P. Chupp, H. Zan, Z. Xu, Y. Sun, N. Xiong, N. Zhang, Z. Xie, W. Jiang, X. Zhang, Y. Liu, Direct Activation of Toll-like Receptor 4 Signaling in Group 2 Innate Lymphoid Cells Contributes to Inflammatory Responses of Allergic Diseases. [Preprint] (2022). https://doi.org/10.22541/au.166563550.01016211/v1.

174. S. Okuzumi, J. Miyata, H. Kabata, T. Mochimaru, S. Kagawa, K. Masaki, M. Irie, H. Morita, K. Fukunaga, TLR7 Agonist Suppresses Group 2 Innate Lymphoid Cell–mediated Inflammation via IL-27–Producing Interstitial Macrophages. *Am J Respir Cell Mol Biol* **65**, 309–318 (2021).

175. I. Marafini, I. Monteleone, D. Di Fusco, M. L. Cupi, O. A. Paoluzi, A. Colantoni, A. Ortenzi, R. Izzo, S. Vita, E. De Luca, G. Sica, F. Pallone, G. Monteleone, TNF-α Producing Innate Lymphoid Cells (ILCs) Are Increased in Active Celiac Disease and Contribute to Promote Intestinal Atrophy in Mice. *PLoS ONE* **10**, e0126291 (2015).

176. E. Wienholds, S. Schulte-Merker, B. Walderich, R. H. A. Plasterk, Target-selected inactivation of the zebrafish rag1 gene. *Science* **297**, 99–102 (2002).

177. M. D. Robinson, D. J. McCarthy, G. K. Smyth, edgeR: a Bioconductor package for differential expression analysis of digital gene expression data. *Bioinformatics* **26**, 139–140 (2010).

178. G. Yu, L.-G. Wang, Y. Han, Q.-Y. He, clusterProfiler: an R Package for Comparing Biological Themes Among Gene Clusters. *OMICS* **16**, 284–287 (2012).

179. Y. Hao, T. Stuart, M. H. Kowalski, S. Choudhary, P. Hoffman, A. Hartman, A. Srivastava, G. Molla, S. Madad, C. Fernandez-Granda, R. Satija, Dictionary learning for integrative, multimodal and scalable single-cell analysis. *Nat Biotechnol* **42**, 293–304 (2024).

180. R. A. Morales, S. Rabahi, O. E. Diaz, Y. Salloum, B. C. Kern, M. Westling, X. Luo, S. M. Parigi, G. Monasterio, S. Das, P. P. Hernández, E. J. Villablanca, Interleukin-10 regulates goblet cell numbers through Notch signaling in the developing zebrafish intestine. *Mucosal Immunology* **15**, 940–951 (2022).

181. S. Wei, J. Zhou, X. Chen, R. N. Shah, J. Liu, T. M. Orcutt, D. Traver, J. Y. Djeu, G. W. Litman, J. A. Yoder, The zebrafish activating immune receptor Nitr9 signals via Dap12. *Immunogenetics* **59**, 813–821 (2007).

182. S. Adouchief, T. Smura, J. Sane, O. Vapalahti, S. Kurkela, Sindbis virus as a human pathogen-epidemiology, clinical picture and pathogenesis. *Rev Med Virol* **26**, 221–241 (2016).

183. Y. P. Ahearn, J. J. Saredy, D. F. Bowers, The Alphavirus Sindbis Infects Enteroendocrine Cells in the Midgut of Aedes aegypti. *Viruses* **12**, 848 (2020).

184. Imaging of viral neuroinvasion in the zebrafish reveals that Sindbis and chikungunya viruses favour different entry routes | Disease Models & Mechanisms | The Company of Biologists. https://journals.biologists.com/dmm/article/10/7/847/2497/Imaging-of-viral-neuroinvasion-in-the-zebrafish.

Annexes

In this section, I will describe my contributions to two published original research articles.

Annex 1: Interleukin-10 regulates goblet cell numbers through Notch signaling in the developing zebrafish intestine

Abstract

interleukin-10 (IL-10) is a critical immunomodulatory cytokine in the gut, as evidenced by the development of spontaneous colitis in *IL10*-deficientmice. The role of IL-10 in cell fate determination within intestinal epithelial cells has not been fully explored. In this study, we show the expression of IL-10 and its receptor complex in the developing zebrafish gut as early as 3-days post-fertilization (dpf). *il10*-deficientlarvae exhibited higher levels of pro-inflammatory cytokine expression and a greater number of intestinal goblet cells compared to wild-type larvae. The expansion of goblet cells is mediated by decreased Notch signaling as a result of IL-10 loss. The effect of IL-10 on goblet cell fate was further demonstrated using murine organoids suggesting conservation across species. This research uncovers a previously unrecognized IL-10-Notch pathway that regulates goblet cell homeostasis in the developing zebrafish intestine.

My contribution

The emergence of differentiated intestinal cell types in zebrafish happens around 74-120-hours post-fertilization (hpf). To gain insights into the developmental stage at which IL-10 might affect epithelial differentiation, I quantified *il10* gene expression levels by qPCR in zebrafish larval guts from 72-hpf or 3-dpf up to the stages where the intestine becomes fully functional, 5- and 7-dpf (Fig. 1a). I found that *il10* is expressed to higher levels at 3-dpf compared to 5- and 7-dpf (Fig. 1b), suggesting a role for IL-10 signaling in gut homeostasis during early developmental stages.

ARTICLE OPEN

Check for updates

Interleukin-10 regulates goblet cell numbers through Notch signaling in the developing zebrafish intestine

Rodrigo A. Morales[1,2]✉, Soraya Rabahi[3], Oscar E. Diaz[1,2], Yazan Salloum[3], Bianca C. Kern[1,2], Mikaela Westling[1,2], Xinxin Luo[1,2], Sara M. Parigi[1,2], Gustavo Monasterio[1,2], Srustidhar Das[1,2], Pedro P. Hernández[3] and Eduardo J. Villablanca[1,2]✉

Cytokines are immunomodulatory proteins that orchestrate cellular networks in health and disease. Among these, interleukin (IL)-10 is critical for the establishment of intestinal homeostasis, as mutations in components of the IL-10 signaling pathway result in spontaneous colitis. Whether IL-10 plays other than immunomodulatory roles in the intestines is poorly understood. Here, we report that *il10*, *il10ra*, and *il10rb* are expressed in the zebrafish developing intestine as early as 3 days post fertilization. CRISPR/Cas9-generated *il10*-deficient zebrafish larvae showed an increased expression of pro-inflammatory genes and an increased number of intestinal goblet cells compared to WT larvae. Mechanistically, Il10 promotes Notch signaling in zebrafish intestinal epithelial cells, which in turn restricts goblet cell expansion. Using murine organoids, we showed that IL-10 modulates goblet cell frequencies in mammals, suggesting conservation across species. This study demonstrates a previously unappreciated IL-10-Notch axis regulating goblet cell homeostasis in the developing zebrafish intestine and may help explain the disease severity of IL-10 deficiency in the intestines of mammals.

Mucosal Immunology (2022) 15:940–951; https://doi.org/10.1038/s41385-022-00546-3

INTRODUCTION

The intestine is a semi-permeable and highly regenerative tissue responsible for nutrient and water absorption while keeping the host protected from environmental and microbiota challenges. The control of these functions is orchestrated by complex cellular crosstalk between intestinal epithelial cells and tissue-resident immune cells, among others. In this regard, cytokines, and particularly IL-10, have been considered key mediators in the maintenance of intestinal homeostasis and function.[1] This has been demonstrated in mice defective in IL-10 signaling, which develop spontaneous colitis.[2] In humans, mutations in the IL-10 signaling genes *IL10*, *IL10RA*, and *IL10RB* are strongly associated with a very early onset of inflammatory bowel diseases (VEO-IBD),[3,4] which is characterized by clinical manifestations in children before 6 years of age, and a significant number of cases occurring in infants younger than 1 year.[5] VEO-IBD has a strong genetic component compared to the 5–10% familial cases observed in adult inflammatory bowel diseases (IBD).[6] In addition, VEO-IBD is phenotypically distinct from adult IBD and is characterized by extensive colitis, growth failure, and unresponsiveness to conventional therapies.[6] Common clinical manifestations in children with VEO-IBD include bloody diarrhea and mucous stool,[7] suggesting altered goblet cell activity.

Intestinal immune cells, including macrophages, B cells, and T cells, are the predominant IL-10 producers and responders. IL-10 signaling in intestinal macrophages is critical to maintaining intestinal homeostasis, as conditional deletion of IL-10Rα in $CX3CR1^{+}$ macrophages is sufficient to trigger spontaneous colitis in mice.[8] Interestingly, intestinal epithelial cells also express IL-10 receptors and are therefore equipped to mount a cellular response upon IL-10R stimulation[9–11] In this regard, IL-10 deficiency in myeloid cells results in impaired regeneration of the epithelium following damage, whereas administration of recombinant IL-10 promotes intestinal epithelial cell proliferation in vivo.[12] Furthermore, IL-10 promotes intestinal stem cell (ISC) proliferation in organoid cultures,[13] suggesting an intrinsic role of IL-10 signaling in intestinal epithelial cells (IEC) differentiation. In line with this, specific IL-10R deficiency on IECs results in goblet cell hyperplasia in the colon of adult mice.[14] Altogether, the combined evidence not only shows that IL-10 signaling can modulate IEC differentiation but also raises the possibility that early-stage intestinal development is impaired in individuals with mutations in the IL-10 signaling pathway, which may lead to the phenotypes observed in VEO-IBD.

The intestinal tract develops at early embryonic stages from the endodermal germinal layer. It is initially formed as a flat tube of epithelial and mesenchymal cells that proliferate and stratify in a synchronic fashion, which results in the morphogenesis of the villi and crypts. At the bottom of the crypt, intestinal stem cells are constantly self-renewing and giving rise to specialized epithelial cells with either absorptive or secretory functions. The main drivers of intestinal stem cell differentiation include the orchestrated activity of signaling pathways such as Wingless/Int-1 (Wnt), bone morphogenetic proteins (BMP), and Notch,

[1]Division of Immunology and Allergy, Department of Medicine Solna (MedS), Karolinska Institutet and University Hospital, 17176 Stockholm, Sweden. [2]Center for Molecular Medicine (CMM), 17176 Stockholm, Sweden. [3]Institut Curie, PSL Research University, INSERM U934, CNRS UMR3215, Development and Homeostasis of Mucosal Tissues Group, 75248 Paris, France. ✉email: rodrigo.morales@ki.se; eduardo.villablanca@ki.se

Received: 2 February 2022 Revised: 20 June 2022 Accepted: 27 June 2022
Published online: 15 July 2022

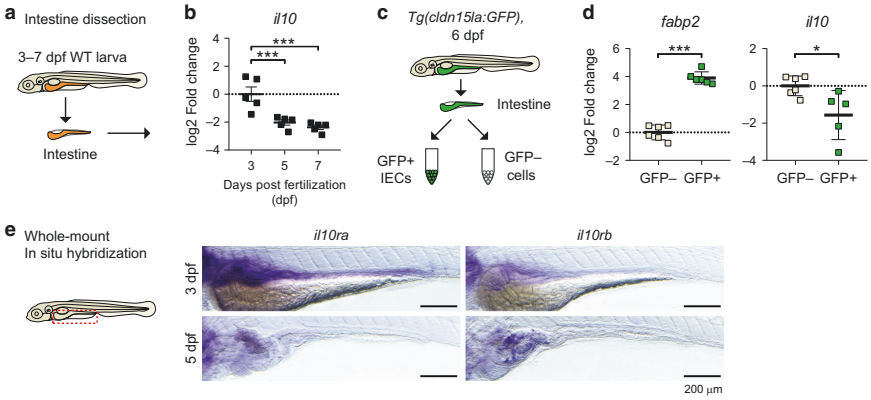

Fig. 1 Early expression of *il10* during intestinal development in zebrafish larvae. a Diagram showing intestine extractions of wild-type (WT) larvae, from 3 to 7 days post fertilization (dpf). **b** Expression of *il10* transcripts measured by qRT-PCR. Each dot represents independent experiments with a pool of 20 intestines used for RNA extraction ($N = 5$). **c** Sorting strategy for the isolation of intestinal epithelial cells. Intestines from *Tg(cldn15la:GFP)* larvae were extracted from the body, disaggregated to cell suspensions, and FACS sorted based on the expression of GFP. GFP^+ and GFP^- cell collections were subsequently used for RNA transcriptomic analyses. **d** Transcriptomic expression analyses from sorted GFP^+ and GFP^- cells by qRT-PCR. Each dot represents an individual sorting experiment with around 30,000 cells collected ($N = 6$). **e** Whole-mount in situ hybridization for the genes *il10ra* and *il10rb* in 3dpf and 5dpf zebrafish larvae. Representative pictures of the stainings at each developmental stage are shown. Scale bar = 200 µm. One-way ANOVA with Fisher's LSD multiple comparisons test was performed in **b**, while two-tailed *t*-tests were performed in **d** (*$p < 0.05$; ***$p < 0.001$).

which antagonize each other to promote or attenuate cell replication.[15,16] Particularly, Notch signaling plays a critical function in stem cell maintenance and regulation of secretory cell differentiation across species.[17–19] In mice, Paneth and goblet cells are expanded after Notch inhibition,[20] and the lack of Notch target genes, such as *hairy/enhancer of split 1* (*Hes1*) show a skewed epithelial cell differentiation towards the secretory lineage.[21,22] By contrast, continuous Notch activation by over-expression of the Notch intracellular domain (NICD) results in the expansion of the intestinal stem cell pool and impaired secretory-IEC differentiation.[23] Expression of the Notch1 and Notch 2 receptors and their main target genes *Hes1*, *Hes5*, and *Hes6* have been detected in the dividing cells within the intestinal crypt.[24] Interestingly, the Notch pathway regulates T cell function,[25] including the production of IL-10 by Th1 cells.[26] However, whether IL-10 signaling regulates tissue differentiation by controlling Notch or other stem cell-related pathways remains unknown.

Zebrafish have been successfully used to model key biological processes associated with intestinal disorders, as physiological and cellular features are highly conserved between fish and humans.[27] Using zebrafish, we and others have addressed the impact of dietary compounds,[28] environmental pollutants[29] and IBD risk genes[30] in intestinal homeostasis, highlighting zebrafish as a powerful tool to investigate the function of genetics in intestinal development. The zebrafish ortholog for the human *IL10* gene[31] shows a conserved immunomodulatory function.[32,33] Here, we took advantage of zebrafish to investigate the effect of IL-10 signaling in the developing intestine. Using CRISPR/Cas9 we generated Il10 mutants, which combined with histological and immunological stainings, transcriptional analysis and fluorescent transgenic reporters enabled us to investigate the intestinal cell composition of IL-10-deficient larvae. We found that IL-10 deficiency resulted in an increased number of goblet cells, which was independent of the microbiota. Mechanistically, the increase in goblet cells was associated with a decreased activity of intestinal Notch signaling, and ectopic Notch signaling activation restored alcian blue$^+$ goblet cell numbers in IL-10-deficient larvae. Moreover, IL-10 treatment in mouse small intestine (SI) organoids led to decreased frequencies of goblet cells and increased Notch activity, which suggests an evolutionarily conserved IL-10-Notch axis that regulates intestinal goblet cell differentiation across vertebrates.

RESULTS

Zebrafish *il10* is expressed during early intestinal development

The development of the larval zebrafish intestine, after the formation of the tube and lumen between 30 and 52 hours post fertilization (hpf), can be divided into an early stage of high proliferation and polarization of the intestinal epithelium (52–74hpf), followed by a later stage of tissue compartmentalization and the emergence of differentiated intestinal cell types (74–120 hpf).[34,35] To gain insights into the developmental stage in which Il10 might control zebrafish intestinal organogenesis, we analyzed *il10* transcript levels in zebrafish larvae starting at 72 hpf or 3 days post fertilization (dpf) until the stage in which a functional intestine is appreciated (5dpf and 7dpf). Using qRT-PCR to analyze *il10* transcript levels from dissected zebrafish larval intestines (Fig. 1a), we found higher transcript levels of *il10* in 3dpf intestines, compared to 5dpf and 7dpf (Fig. 1b). Dissected intestines contain intestinal epithelial cells (IECs) among other intestine-associated cells that interact with IECs, therefore we sought to determine which group of cells was responsible for *il10* expression. We then FACS-sorted epithelial cells versus the rest by using the zebrafish reporter line *Tg(cldn15la:GFP)* (Fig. 1c), in which the *cldn15la* promoter drives GFP expression exclusively in intestinal epithelial cells.[36] qPCR analysis from sorted cells showed that *il10* expression was not detectable in GFP^+ cells but in GFP^- intestine-associated cells (Fig. 1d). To gain insights into a potential active IL-10 signaling in intestinal cells, we analyzed the expression of the orthologs for the receptors of *il10*, defined as *il10ra* and *il10rb* in the zebrafish database ZFIN. Whole-mount in situ hybridizations (WISH) showed that both *il10ra* and *il10rb* genes were expressed in the zebrafish developing intestine at 3dpf, while *il10rb* was predominantly expressed at 5dpf (Figs. 1e and S1). Altogether, these results suggest that *il10* signaling may act in zebrafish intestinal cells during early developmental stages.

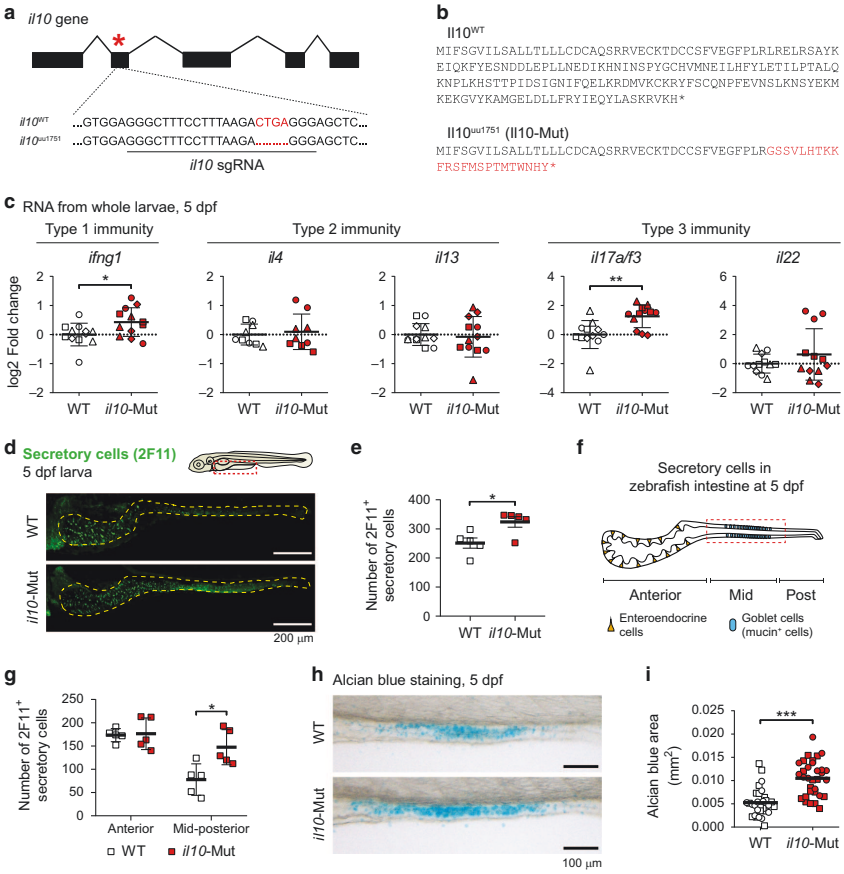

Fig. 2 Increased pro-inflammatory expression and alcian blue$^+$ goblet cells in *il10* mutant zebrafish larvae. a Schematic for the mutation generated in the zebrafish *il10* gene (*il10*^{uu1751}, -4bp) by CRISPR/Cas9. **b** Predicted protein sequences for Il10 in WT and *il10*-Mut individuals, according to the DNA sequences obtained. **c** Whole-body expression levels of type 1, type 2, and type 3 cytokines in WT (white symbols) and *il10*-Mut larvae (red symbols) by qRT-PCR. Each dot represents a pool of 5–10 larvae collected in 3–4 independent experiments. **d** Whole-mount immunofluorescence staining in 5dpf WT and *il10*-Mut larvae using the pan-secretory marker antibody 2F11. Scale bar = 100 µm. **e** Quantification of 2F11$^+$ cells in the intestines of WT and *il10*-Mut larvae. Each dot represents individual larvae collected in 2 independent experiments. **f** Diagram for the larval zebrafish intestinal tract showing the location of Goblet cells in the mid-intestinal region. **g** Stratification of the number of 2F11$^+$ cells in the anterior or mid-posterior intestines of WT and *il10*-Mut larvae ($N = 5$). **h** Alcian blue (ab) staining on 5dpf WT and *il10*-Mut larvae. **i** Automatic quantifications of the ab-stained area in the mid intestines of WT and *il10*-Mut larvae. Each dot corresponds to an individual larva collected in two independent experiments. Different symbol shapes represent independent experiments in **c** and **i**. Two-tailed student *t* tests were used for the comparisons in **c**, **e**, **g** and **i**. (*$p < 0.05$; **$p < 0.01$; ***$p < 0.001$).

Altered immune and intestine-associated profiles in *il10* mutant larvae

Next, we aimed to determine whether *il10* can modulate the development of the larval zebrafish intestine by using loss-of-function genetic approaches. Using CRISPR/Cas9,[37] we generated a 4 bp deletion in the exon 2 of the zebrafish *il10* gene (*il10*^{uu1751}) (Fig. 2a), predicted to generate a premature stop codon (Fig. 2b). *il10*$^{uu1751/uu1751}$ mutant fish (hereinafter referred to as *il10*-Mut) did not show any apparent morphological or developmental defect while in homozygosis in larva (Fig. S2a), reached adulthood and were fertile (Fig. S3a, b). Analysis of selected type 1, 2, and 3 cytokines by qPCR from the whole larvae at 5dpf revealed that type 2 cytokines (*il4* and *il13*) and the type 3 cytokine *il22* were comparable whereas *ifng1* (type 1) and *il17a/f3* (type 3) were significantly elevated in *il10*-Mut larvae compared to wild-type (WT, *il10*$^{wt/wt}$) larvae (Figs. 2c and S2b). Thus, Il10 deficiency results in altered pro-inflammatory cytokine levels in the whole larvae. We then sought to investigate whether Il10 deficiency affects the development of the intestinal tract. Absorptive and secretory cells, namely enteroendocrine and goblet cells, can be distinguished by 5dpf in zebrafish larvae.[18] To analyze enteroendocrine and goblet cells, we performed whole-mount immunofluorescence using the pan-secretory marker antibody 2F11.[18] By 5dpf, the *il10*-Mut larvae showed a higher number of secretory cells in the intestine compared to WT (Fig. 2d, e). Secretory cells in the zebrafish larvae are differentially distributed along the anterior-distal intestine,[34]

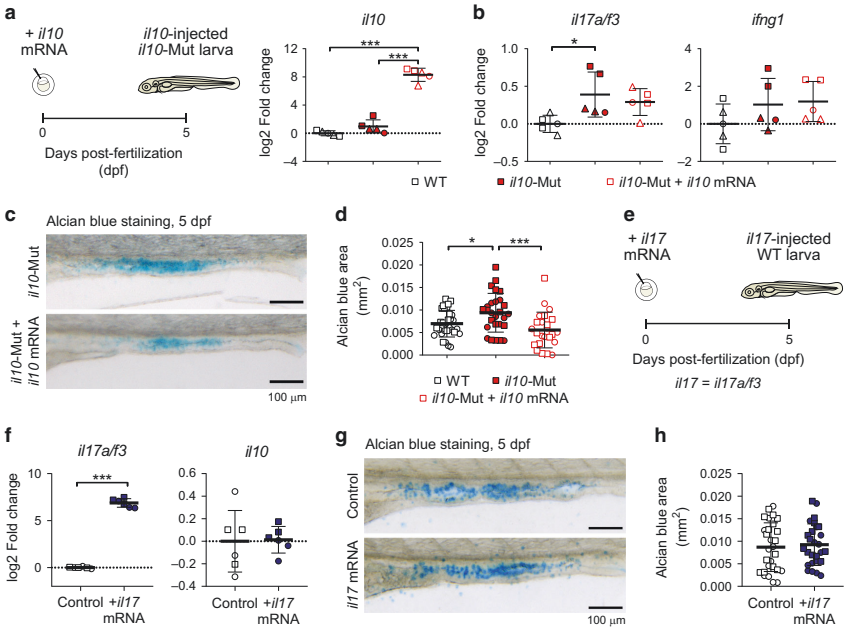

Fig. 3 Altered alcian blue$^+$ goblet cell homeostasis in *il10* mutant larvae is rescued after *il10* mRNA administration. a Experimental strategy for *il10* rescue experiments and expression levels of *il10* mRNA at 5dpf. **b** Whole-body expression levels of *il17a/f3* and *ifng1* by qRT-PCR. Each dot represents a pool of 5–10 larvae collected in three independent experiments. **c** Alcian blue stainings on 5dpf WT, *il10*-Mut larva controls and injected with *il10* mRNA. Scale bar = 100 µm. **d** Quantification for the ab-stained area in the *il10* mRNA-injected *il10*-KO larvae, compared to control *il10*-KO and WT larvae. $N = 2$ independent experiments. **e** Experimental strategy for the injection and analysis of *il17* (*il17a/f3*) mRNA-injected WT zebrafish embryos. **f** Whole-body expression levels of *il17a/f3* and *il10* by qPCR. Dots represent pools of 5–10 larvae collected in 2 independent experiments. **g** Alcian blue stainings on 5dpf control and *il17*-injected WT larvae. Scale bar = 100 µm. **h** Quantification of the ab-stained area of control and *il17*-injected larvae. $N = 2$ independent experiments. Each independent experiment is shown with a different symbol shape in **a**, **b**, **d**, **f** and **h**. One-way ANOVA was used for statistical analysis in **a**, **b** and **d**, whereas two-tailed student t-test were used in **f** and **h** (*$p < 0.05$; ***$p < 0.001$).

with enteroendocrine cells being concentrated in the anterior intestine and mucin-producing goblet cells in the mid intestine (Fig. 2f). Therefore, we further stratified 2F11$^+$ cells based on location. We observed that the number of 2F11$^+$ secretory cells in the mid-posterior, but not in the anterior segment, was significantly increased in *il10*-Mut compared to WT (Fig. 2g). The increase in secretory cells in the mid-posterior segment prompted us to hypothesize that goblet cells are increased in *il10*-Mut compared to WT larvae. In line with our hypothesis, whole-mount alcian blue (ab) staining labeling mucin production as an indicator of ab$^+$ goblet cell abundance in the mid intestine, displayed a higher staining area in 5dpf *il10*-Mut larvae compared to WT (Fig. 2h–i). Area measurements were complemented with ab intensity and stained length (Fig. S2c), showing an overall increase of the ab$^+$ signal detected in *il10*-Mut larvae. Likewise, whole-mount staining with fluorescently labeled wheat germ agglutinin (WGA), which binds to the N-acetylglucosamine present in the mucus produced by goblet cells[34] showed that the number of WGA$^+$ goblet cells in the mid intestine was increased in 5dpf *il10*-Mut larvae, compared to WT (Fig. S2d, e), further confirming that *il10*-deficiency results in goblet cell hyperplasia within the developing zebrafish embryo. To analyze if absorptive intestinal populations were affected in *il10*-Mut larvae, we used neutral red to stain a subset of mid intestine absorptive enterocytes with acidified lysosomes, namely lysosome-rich enterocytes (LREs).[38–40] Area, intensity and length analysis from neutral red-stained enterocytes in 5dpf larvae did not show differences between WT and *il10*-Mut (Fig. S2f, g), suggesting no impairments in the differentiation of absorptive intestinal lineages. Further, to determine whether the increased number of goblet cells in *il10*-Mut zebrafish was age-dependent, we analyzed different intestinal regions from >1-year-old WT and *il10*-Mut zebrafish (Fig. S3c). Ab staining on paraffin-embedded intestinal sections showed a higher number of goblet cells per villus area in *il10*-Mut larvae, compared to WT (Fig. S3d, e). Altogether, our results point towards a disbalance in both pro-inflammatory cytokine expression and the abundance of goblet cells in *il10*-deficient zebrafish.

The abundance of intestinal goblet cells depends on *il10*

To determine whether the phenotypes observed in the *il10*-Mut were dependent on Il10 signaling rather than off-target effects we performed rescue experiments using an in vitro-generated version of the zebrafish *il10* mRNA. Injection of the full *il10* mRNA at 1-cell stage resulted in a significant increase of *il10* transcripts in the whole 5dpf larvae (Fig. 3a). *il10* mRNA-injected *il10*-Mut 5dpf larvae showed a non-significant reduction of *il17a/f3* transcript levels compared to *il10*-Mut, whereas *ifng1* levels were comparable (Fig. 3b). In addition, the average ab-stained area was reduced in the intestines of *il10* mRNA-injected *il10*-Mut larvae compared to *il10*-Mut, reaching comparable levels to those of WT larvae (Fig. 3c, d). A recent publication showed that IL-17 signaling on intestinal epithelial cells promotes goblet cell differentiation.[41]

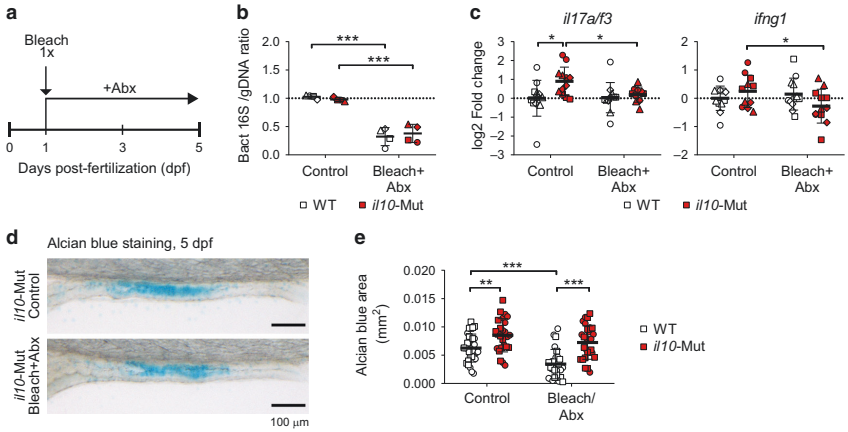

Fig. 4 Increased alcian blue^{+} goblet cells in *il10* mutant larvae are independent of the microbiota. a Diagram showing bleach (sodium hypochlorite 0.004%) plus antibiotic (Abx) treatment in zebrafish embryos/larvae (Abx: Ampicillin 100 µg/mL, Kanamycin 5 µg/mL). **b** Quantification of bacterial 16S DNA levels over zebrafish genomic DNA measured by PCR. Each dot corresponds to a pool of 2 larvae from 4 independent experiments. **c** Transcriptomic expression analysis of cytokines from treated larvae by qRT-PCR. Each dot represents a pool of 8–10 larvae collected from 4 independent experiments (**d**, **e**) Alcian blue staining and analysis on 5dpf WT and *il10*-Mut larvae treated with Bleach+Abx and controls ($N = 2$ independent experiments). Scale bar = 100 µm. Independent experiments are shown with different symbol shapes in **b**, **c** and **e**. Two-way ANOVAs with Fisher's LSD multiple comparisons tests were performed in **b**, **c** and **e** (*$p < 0.05$; **$p < 0.01$; ***$p < 0.001$).

To assess the role of Il17 signaling on the increased goblet cell numbers observed in *il10*-Mut larvae, we analyzed the abundance of intestinal goblet cells in WT larvae injected with an in vitro-generated *il17* (*il17a/f3*) mRNA at 1-cell stage (Fig. 3e). While *il17a/f3* transcripts were high in 5dpf *il17*-injected larvae (Fig. 3f), ab analysis did not show differences in the ab-stained area between *il17a/f3* mRNA-injected and control larvae (Fig. 3g, h), suggesting that the abundance of goblet cells does not depend on Il17 signaling in zebrafish larvae. To further confirm our findings, we measured the ab-stained area in a second CRISPR/Cas9-generated mutant line for the *il10* gene, this time containing a 17 bp insertion replacing 3 bp (+14 bp total insertion) in exon 3 (*il10*^{uu1762}, referred to as *il10*-Mut2), which is predicted to generate a premature stop codon (Fig. S4a, b). Similar to the *il10*-Mut, we observed increased staining for ab in 5dpf *il10*-Mut2 larvae compared to WT (Fig. S4c, d). Altogether, these results indicate that *il10* modulates ab^{+} goblet cell differentiation, but not cytokine expression, in zebrafish larvae.

Increased goblet cells in *il10* mutant larvae are microbiota-independent

Previous findings suggest that goblet cell differentiation is dependent on the microbiota.[42] To investigate a potential role of the microbiota in the phenotypes observed in *il10*-Mut larvae, we established a protocol to reduce bacterial loads in zebrafish embryos (Fig. 4a). Briefly, 24–28 hpf embryos were treated with E3 water containing 0.004% sodium hypochlorite (bleach) for 5 min, and then they were incubated in the presence of an antibiotic cocktail (Abx, Ampicillin and Kanamycin) from 1dpf to 5dpf. We confirmed a reduction of total bacterial loads after bleach+Abx treatments in larvae by comparing bacterial 16S versus targeted zebrafish genomic DNA amplification levels by PCR (Fig. 4b). Bleach + Abx-treated 5dpf *il10*-Mut larvae showed a reduced expression of both *il17a/f3* and *ifng1*, compared to non-treated siblings (Fig. 4c), suggesting that cytokine modulation is microbiota-dependent. On the other hand, ab levels remained enhanced in *il10*-Mut compared to WT larvae, regardless of the reduced bacterial load (Fig. 4d, e). These results indicate that the increased ab^{+} goblet cells observed in *il10*-Mut larvae are independent of the bacterial microbiota.

Impaired Notch signaling in the intestines of *il10* mutant larvae

To gain insights into the potential mechanisms by which *il10* modulates goblet cell numbers in zebrafish larvae, we analyzed the activity of signaling pathways involved in goblet cell differentiation, such as Notch,[18] RAR,[28] and ARP/ASCL factors.[43,44] For this purpose, we dissected intestines from 5dpf WT and *il10*-Mut larvae (Fig. 5a) and we analyzed the expression of Goblet cell markers and key target genes for the above-mentioned signaling pathways by qRT-PCR. We did not observe differences in the expression of the RAR signaling target gene *cyp26a1*, the ARP/ASCL-associated genes *atoh1a* and *ascl1a*, nor in the expression of the goblet cell markers *agr2* and *muc2.1* (Fig. S5a). In addition, we did not detect differences in the expression of *olfm4.2*, ortholog for the mammalian stem cell marker Olfm4, nor in the expression of the teleost intestinal progenitor marker *sox9b* (Fig. S5b). However, we found a reduction in the intestinal expression levels of *her6* and *her9*, both Notch target genes described as the ortholog of human *HES1* and *HES5*, respectively (Fig. 5b). To confirm our observations, we combined the *il10*-Mut fish with the Notch activity reporter *Tg(tp1:EGFP)*,[45] which detects Notch-responding cells in the larval intestinal tract.[46] In vivo imaging of the intestines of 5dpf *Tg(tp1:EGFP)* larvae in a WT and *il10*-Mut background proved that the number of GFP^{+} cells in the intestines of *il10*-Mut reporters was lower compared to WT (Fig. 5c, d), thus demonstrating an impaired Notch activity in *il10*-Mut larval intestines. In mammals, intracellular IL-10 downstream signaling relies predominantly on the activity of the transcription factor Stat3,[47] and the zebrafish intestine was shown to contain Stat3-responsive cells with progenitor-like features.[48] To determine whether Stat3 activity is impaired in the intestines of *il10*-Mut larvae, we crossed *il10*-Mut with the Stat3 activity reporter *Tg(7xStat3:EGFP)*.[48] Imaging and quantification of the number of

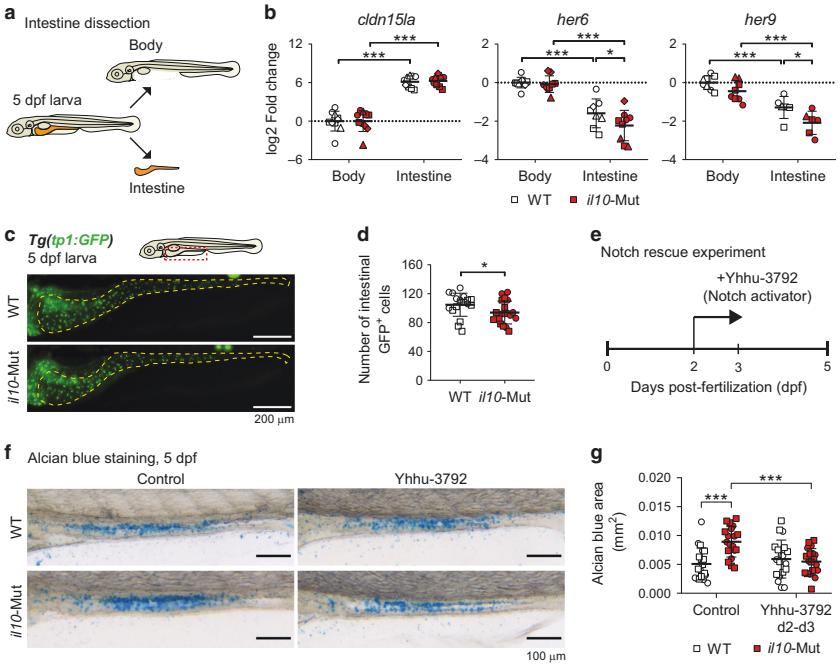

Fig. 5 Decreased Notch signaling activity in the intestines of *il10* mutant larvae. a Schematics showing the body-intestine tissue collection for RNA expression analyses. **b** qRT-PCR for intestinal (*cldn15la*) and Notch signaling pathway markers (*her6* and *her9*). Each dot represents a pool of 10 separated intestines and body remnants collected from 4 independent experiments. **c** Representative images of *Tg(tp1:GFP)* in WT or *il10*-Mut genetic backgrounds. Scale bar = 200 µm. **d** Quantification of the number of *tp1*:GFP$^+$ cells in the intestines of WT or *il10*-Mut individuals. Each dot corresponds to 1 larva. Two independent experiments were performed. **e** Schematics for the rescue experiments in which *il10*-Mut larvae are exposed to the Notch activator Yhhu-3792. **f** Representative pictures of alcian blue stainings from 5dpf WT and *il10*-Mut larvae after treatment with Yhhu-3792. Scale bar = 100 µm. **g** Quantification of the ab-stained area after Yhhu-3792. Each dot represents individual larvae collected from two independent experiments. Independent experiments are shown with different symbol shapes in **b**, **d** and **g**. Two-way ANOVAs with Fisher's LSD multiple comparisons tests were performed in **b** and **g**, while a two-tailed t-test was performed in **d** (*$p < 0.05$; ***$p < 0.001$).

intestinal GFP$^+$ cells showed no differences between WT and *il10*-Mut larvae (Fig. S5c, d), suggesting that Stat3 signaling is not affected in *il10*-Mut larvae.

It has been previously shown that Notch signaling controls secretory cell differentiation in a time-specific manner, particularly during the phase of intestinal proliferation and polarization between 64–74 hpf.[49] We validated these findings by using the γ-secretase/Notch inhibitor DAPT at 2 different time points: from 48 to 72 hpf (hereinafter referred to as 2–3 dpf) and from 72 to 120 hpf (referred to as 3–5 dpf, Fig. S6a). We found that Notch inhibition during 2-3dpf led to an increased ab-stained area in WT larvae, while 3–5 dpf inhibition did not modulate ab levels (Fig. S6b, c). Additionally, we tested goblet cell abundance after inhibiting Stat3 signaling with the Jak2/Stat3 inhibitor AG-490[48] and found a reduced ab-stained area in AG-490-treated compared to control larvae, at both 2-3dpf and 3–5dpf time points (Fig. S6d–f). These results are opposite to our observations in *il10*-Mut larvae and suggest that Stat3 signaling is unlikely to play a role in the goblet cell hyperplasia observed in *il10*-Mut larvae. Therefore, we sought to determine whether boosting Notch activity between 2–3dpf restores ab-stained area to normal levels in *il10*-Mut larvae. For this purpose, we took advantage of the Notch activator Yhhu-3792[50] and tested its activity in zebrafish larvae. Incubation of WT larvae with 1 µM of Yhhu-3792 was sufficient to upregulate the expression of *her6* transcripts (Fig. S7a, b). We then analyzed goblet cell abundance in WT and *il10*-Mut larvae exposed or not to 1 µM of Yhhu-3792 at 2-3 dpf (Fig. 5e). Yhhu-3792 treatment of *il10*-Mut larvae resulted in reduced ab-stained area compared to vehicle-treated *il10*-Mut and comparable to WT larvae (Fig. 5f, g). As expected, Yhhu-3792 treatments in *il10*-Mut larvae at 3–5dpf did not result in changes in the ab-stained area (Fig. S7c–e). These results indicate that the increased abundance of goblet cells in *il10*-Mut larvae is restored by activating Notch signaling in a specific temporal window.

IL-10 enhances Notch signaling and restricts mucin production in mouse small intestine organoids

To address whether our findings in zebrafish can be translated to mammals, we used a 3D murine small intestine (SI) organoid system which models key features of intestinal differentiation and development in vitro.[51] We isolated crypts from wild-type C57/Bl6 mice and we cultured them in EGF-, Noggin-, and R-Spondin-containing media (ENR medium; see methods) supplemented or not with recombinant murine IL-10 for 4 days (Fig. 6a). Crypt domains per organoid and organoid areas were comparable between treatments on day 4 (d4) of treatment (Fig. S8a-c). However, transcriptional analyses of d4 organoids showed that IL-10 treatment increased the expression of the stem cell-related

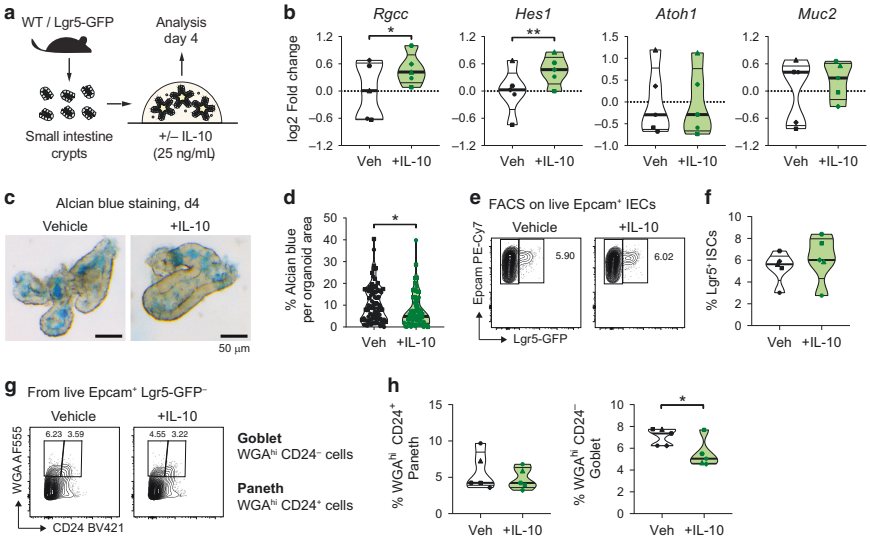

Fig. 6 Enhanced Notch signaling and decreased goblet cell frequencies in mouse small intestine organoids treated with IL-10. **a** Schematics for mouse SI organoid cultures. Organoids were grown in ENR media (containing EGF, Noggin, and R-Spondin) supplemented with recombinant murine IL-10 or BSA (Vehicle control). **b** RNA expression analysis by qRT-PCR from organoids treated with IL-10. Each dot represents SI organoids generated from an individual mouse ($N = 5$ independent mice). **c** Alcian blue staining of SI organoids in vehicle- and IL-10-treated organoids. Scale bar = 50 μm. **d** Percentage of the ab-stained area from the total organoid area. Dots represent single organoids imaged from 2 independent experiments/mice. **e** Flow cytometry analysis of organoids generated from SI crypts of Lgr5-GFP mice. Representative contour plots showing the percentage of intestinal stem cells (Epcam$^+$ Lgr5-GFP$^+$ cells) are shown. **f** Frequency of Lgr5$^+$ intestinal stem cells (ISCs) after IL-10 treatments. Dots represent pools of organoids collected from 5 different mice. **g** Representative contour plots of WGA/CD24 stainings on disaggregated organoids treated with IL-10. **h** Frequencies of goblet cells (Epcam$^+$ Lgr5-GFP$^-$ WGA^{hi} CD24$^-$) and paneth cells (Epcam$^+$ Lgr5$^-$ WGA^{hi} CD24$^+$) from vehicle and IL-10-treated SI organoids. $N = 5$ independent mice. Independent experiments are represented by different symbol shapes in **b**, **d**, **f** and **h**. Conventional two-tailed *t*-test was performed in **d**, whereas paired two-tailed *t* tests were performed in **b**, **f** and **h** (*$p < 0.05$, **$p < 0.01$).

gene *Rgcc* and the Notch target gene *Hes1*, compared to vehicle-treated organoids (Fig. 6b). Similar to zebrafish, we did not observe differences in the expression of the secretory cell differentiation driver *Atoh1* and the goblet cell marker *Muc2* (Fig. 6b), nor in additional markers for intestinal stem cells (*Olfm4*) and other secretory cell types including enteroendocrine (*Chga*), tuft (*Dclk1*) and Paneth cells (*Lyz1*) (Fig. S8d). Further, we did not find differences in the expression levels of the intestinal differentiation marker *Krt20* and the Wnt member gene *Wnt3* (Fig. S8d). To analyze goblet cells abundance in control and IL-10-treated organoids, we modified the zebrafish ab staining protocol to perform whole-mount staining in matrigel-embedded SI organoids (see methods). IL-10-treated SI organoids exhibited a reduced percentage of ab staining per organoid area when compared to vehicle-treated organoids (Fig. 6c, d). To confirm our findings and expand our analysis to additional intestinal cell populations, we performed flow cytometry analysis of d4 SI organoids generated from Lgr5-GFP mice[52] and stained with Epcam (Fig. S9a, b), together with WGA and CD24 to detect intestinal stem and secretory cells populations, as previously described.[53,54] IL-10 treatments did not affect the frequency of organoid ISCs (defined as live Epcam$^+$ Lg5-GFP$^+$ cells, Fig. 6e, f). However, IL-10 treatments reduced specifically the frequencies of goblet cells (defined as live Epcam$^+$ Lgr5-GFP$^-$ WGA^{hi} CD24$^-$ cells), while Paneth cells (live Epcam$^+$ Lgr5-GFP$^-$ WGA^{hi} CD24$^+$ cells) remained unaltered (Fig. 6g, h). Further, immunofluorescence stainings of d4 SI organoids with WGA and the Paneth cell marker Lysozyme (Lyz)[55] confirmed the presence of a group of WGA$^+$ Lyz$^-$ cells corresponding to goblet cells (white arrows on Fig. S9c), and its reduction after IL-10 treatments (Fig. S9d). Therefore, these results conclude that IL-10 signaling in intestinal epithelial cells modulates goblet cell frequencies across vertebrates through the activation of Notch signaling.

DISCUSSION

How IL-10 signaling controls intestinal immune homeostasis has been an active area of research over the past two decades. However, due to the viviparous nature of the sample sources such as humans and mice, many of these studies were performed in adult specimens, and studies understanding the role of cytokines in intestinal development remain elusive. The ex utero embryonic development and the transparency of the zebrafish larva made it an ideal model to investigate the role of cytokines in the development of intestinal mucosal immunology. Here, we combined zebrafish and mouse organoids to demonstrate that IL-10 signaling controls goblet cell homeostasis in a mechanism involving Notch signaling. Thus, we provided additional evidence showing that cytokines can act beyond leukocytes to orchestrate tissue development and that zebrafish is an excellent model organism to investigate the development and maturation of intestinal mucosal barrier functions.

The relationship between IL-10 signaling and goblet cell function has been a matter of study over the past years. An early study showed that *Muc2* was predominantly overexpressed but aberrantly sulfated in the colon of IL-10 deficient mice.[56] This was

further addressed in a later report, which showed alterations in the colonic mucus layer of IL-10 deficient mice, specifically a thicker adherent mucus layer which was however more permeable to bacteria[57]. In line with a role in orchestrating epithelial homeostasis, IL-10R signaling disruption specifically in intestinal epithelial cells (IECs) skewed IEC differentiation towards goblet cells over absorptive enterocytes.[14] Moreover, using mouse organoids treated with recombinant IL-10 it was proposed that goblet cell modulation could be a consequence of altered intestinal stem cell (ISC) maintenance and/or differentiation.[13] However, how IL-10 signaling might control goblet cell homeostasis, whether IL-10 signaling acts directly on ISC, and if such cytokine-IEC crosstalk occurs early in development remained elusive. Using zebrafish, our study proposes that IL-10 signaling regulates intestinal goblet cell homeostasis early in intestinal development in a mechanism involving Notch signaling and without affecting the ISC pool. The latter was investigated in murine organoids and zebrafish, using the Lgr5 reporter mice and zebrafish markers such as *olfm4.2*, the ortholog of the mammalian stem cell marker *OLFM4* and a potential marker for intestinal stem cells in adult zebrafish.[58] In addition, we did not observe differences in the teleost intestinal progenitor marker *sox9b*,[48,59,60] nor in the proportion of absorptive neutral red$^+$ lysosome-rich enterocytes (LREs), suggesting that *il10* deficiency in zebrafish leads to a specific increase in goblet cells in the larval mid intestine.

We found a temporal correlation between intestinal *il10* expression and Notch activity in controlling secretory cell differentiation. Further, our data highlighted IL-10 signaling as a potential upstream regulator of Notch activity in the zebrafish intestine, which helped to explain the increase of goblet cells observed in *il10*-Mut larvae. Although the inhibition of Notch activity at the peak of intestinal *il10* expression(2-3dpf) recapitulated the phenotypes observed in *il10*-Mut larvae, rescue experiments are needed to directly link Notch as a downstream effector of IL-10 signaling. To rescue Notch activity, a previous study used transgenic animals that overexpressed the Notch intracellular domain (NICD), leading to a permanent activation of Notch signaling.[42] In our approach, we used a novel synthetic Notch signaling activator Yhhu-3792[50] which allowed us to rescue Notch signaling specifically at the 2-3dpf time window. Since intestinal ab$^+$ goblet cells were restored to WT levels in *il10*-Mut after Yhhu-3792-mediated Notch activation at 2-3dpf, our data strongly suggest that early expression of *il10* is key in controlling goblet cell homeostasis in zebrafish larvae through the regulation of Notch activity. Although Stat3 could serve as a potential link between IL-10 and Notch signaling, as previously reported on monocytes,[61] our data suggest a Stat3-independent mechanism linking both signals. An alternative mechanism could be PI3K/Akt signaling, previously described to be activated by IL-10,[62,63] or other members of the Stat family which can be activated by IL-10, such as Stat1 and Stat5.[47] However, further studies will be required to find the exact mechanisms which might explain the connection between *il10* and Notch signaling in the intestine of zebrafish.

Our results from mouse small intestine (SI) organoids revealed that the IL-10-Notch axis is also present in mammals and further confirms its independence from the microbiota. Although we did not find differences in the transcript levels for secretory cell markers in organoids, it is possible that these changes may be visible at a protein level, as observed in zebrafish. In addition, SI organoids do not show elevated numbers of goblet cells under normal sterile growth conditions, thus the addition of inducers of goblet cell differentiation, such as type 2 cytokines or Notch inhibitors[64] would be needed to potentially visualize its regulation by IL-10. Nevertheless, our results from SI organoids match previous findings from single-cell transcriptomic analysis of mouse intestinal organoids, which showed an increased *Rgcc* expression after IL-10 treatments.[13] Given that both *Rgcc* and *Hes1* are used as markers for intestinal progenitors in mice,[65] there is the possibility that IL-10 is modulating the intestinal stem cell (ISC) pool. However, we did not observe changes in Epcam$^+$ Lgr5-GFP$^+$ ISCs in our organoid settings after IL-10 treatments. Therefore, the decreased average in the ab-stained area from IL-10-treated organoids, as well as the decreased frequency of Epcam$^+$ Lgr5-GFP$^-$ WGA^{hi} CD24$^-$ cells observed by FACS, indicate that goblet cell homeostasis is specifically modulated by IL-10 in mice. Deeper analyses, focusing on specific intestinal cell populations, are required to better elucidate if IL-10 signaling impacts the specification of intestinal precursors to a secretory lineage or acts directly on goblet cells to control its function.

Our study might have implications for a better understanding of pediatric IBD, as mutations in IL-10 signaling pathway-associated genes are frequent in very-early onset (VEO) IBD cases, and dysregulation of mucus biosynthesis and goblet cell numbers are classic features of IBD. Thus, it is likely that defective IL-10 signaling may contribute to the severity of VEO-IBD by affecting early intestinal epithelial cell development, which may impact subsequent processes such as microbiota colonization. The fact that IL-10 can act beyond immune responses and directly control the differentiation of IECs raises several points to be considered in clinical studies. First, it suggests that aberrant immune responses are not the only driving cause for the development of VEO-IBD in patients carrying mutations in IL-10 signaling-related genes, which explains their resistance to immunosuppressive therapies[66] and improving defective intestinal development and differentiation might also be considered for therapeutics.[67] Second, although alterations in mucus and goblet cells are observed in active VEO-IBD cases,[7,68] there is no clear information about the intestinal cell composition before the onset of the disease and with no active inflammation, which could change the view on the causal factors and the physiological consequences of IBD pathogenesis. Third, despite the lack of clinical evidence directly linking IL-10 signaling, goblet cells, and VEO-IBD, data from experimental models support this idea, and further investigation needs to be conducted to better understand how these factors play a role in the initiation of the disease.

Thus, we propose the existence of an IL-10-Notch axis in the early development of intestinal epithelial cells which regulates mucin production, goblet cell differentiation, and is conserved across vertebrates.

MATERIAL AND METHODS

Animals

Zebrafish (*Danio rerio*, AB strain) were reared and kept in the Karolinska Institutet (KI) Zebrafish Core Facility and the Institut Curie Animal Facility, according to standard protocols. Ethical permits used for zebrafish husbandry were Nr 5756/17 (to Eduardo Villablanca), 14049/19 (to KI Zebrafish Core Facility), and APAFiS #21197-2019062521156746-v2 (To Pedro Hernandez). Zebrafish embryos were collected by natural spawning of adults and were kept at 28 °C in E3 water. The zebrafish line *TgBAC(cldn15la-GFP)*^{pd1034}, [36] referred to in the text as *Tg(cldn15la:GFP)*, was provided by Prof. Michael Bagnat (Duke University Medical Center, USA); the line *Tg(Tp1bglob:eGFP)*^{um14}, [45] referred in the manuscript as *Tg(tp1:EGFP)* was kindly provided by Prof. Olov Andersson (Department of Cell and Molecular Biology CMB, Karolinska Institutet, Sweden); and the line *Tg(7xStat3-Hsv.Ul23:EGFP)*,[48] referred in the manuscript as *Tg(7xStat3:EGFP)*, was kindly provided by Prof. Francesco Argenton (Università degli Studi di Padova, Italy).

Wild-type mice (*Mus musculus*, C57/Bl6 strain) were purchased from Charles River Laboratories or Taconic and were kept in the Comparative Medicine facility from Karolinska University Hospital (AKM). The transgenic strain *Lgr5-EGFP-IRES-creERT2*,[52] referred to in the text as Lgr5-GFP, was maintained in a C57/Bl6 background at the Comparative Medicine facility from Karolinska Institutet (KM-B). All mice used for experiments were 6–10 weeks old. Animals were handled according to protocols approved by the Stockholm Regional Ethics Committee (Nr 3227-2017 and

6778-2020). All experiments were performed following the national and institutional guidelines and regulations.

Isolation of fluorescent intestinal epithelial cells from zebrafish larvae

To acquire the intestinal epithelial population, approximately 100 of 6dpf *TgBAC(cldn15la:GFP)* zebrafish larvae were collected for the FACS experiment, then intestines were dissected and placed into PBS on ice with a maximum dissection time of 2 h. Intestine dissociation was performed using TrypLE Express (Gibco, Cat. No. 12605028) for 1 h at 37 °C, pipetting up and down every 10 min to support digestion. Digested samples were spun at 1500 g for 5 min at 4 °C and washed twice with PBS 1× before being resuspended together with PBS 1× and 10% FBS (fetal bovine serum). Filtered cells were immediately subjected to FACS at Institut Curie Flow Cytometry Platform using the Sony SH800 Cell Sorter. Dead cells were excluded from analysis using the combination of Calcein Blue (Invitrogen, Cat. No. 65-0855-39) and Propidium Iodide viability stains (Sigma-Aldrich, Cat. No. P4864). Non-transgenic and single transgenic controls (pools of 10 dissected guts) were prepared as above and used for gating and compensation. RNA isolation was done using on average 30,000 GFP^+ or GFP^- sorted cells with the Single-Cell RNA Purification Kit from Norgen Biotek Corp and reverse transcribed using Superscript IV Reverse Transcriptase (Life Technologies, Cat. No. 18090050) following the manufacturer's instructions.

Whole-mount in situ hybridization in zebrafish larvae

Portions of the coding sequences for the ZFIN-annotated orthologs of the human *IL10RA* (Gene name: *il10ra*, Gene ID: 777651, ENSEMBL ID: ENSDARG00000100383) and *IL10RB* genes (Gene name: *il10rb*, Gene ID: 619391, ENSDARG00000078042) were amplified by PCR using the primers from Table S1, and subsequently cloned into a pCRII-TOPO vector (Invitrogen, Cat. No. 450640). Probe and control RNA sequences were synthesized in vitro by using T7 and SP6 RNA polymerases and subsequently purified by Lithium chloride (LiCl) precipitation. Whole-mount in situ hybridizations were performed in 3 dpf and 5 dpf zebrafish larvae as previously described[30] with the following modifications. Permeabilization was done by treating fixed larvae with 10 µg/mL of Proteinase K (Qiagen, Cat. No. 19131) prepared in PBS supplemented with Tween-20 0.1% and DMSO 1% for 30 minutes at room temperature. Pre-hybridization was done at 60 °C for at least 3 h in Hybridization media (HM, Formamide 50%, Sodium citrate solution 5×, citric acid 9.2 mM, Heparin 50 µg/mL, RNAse-free yeast tRNA 500 µg/mL). Probe hybridization was done using 500 µL of HM containing 4 ng/mL of either probe or control RNA, and samples were incubated overnight at 60 °C. Anti-dig-AP antibody (Roche, Cat. No. 1109327493) was diluted 1:3000 in PBS supplemented with Tween-20 0.1%, sheep serum 2%, and bovine serum albumin (BSA) 2 mg/mL. Development of probe hybridizations was done by diluting NBT-BCIP stock solution (Roche, Cat. No. 11681451001) 1:50 in alkaline phosphatase buffer (Tris-HCl 100 mM pH 9.5, $MgCl_2$, NaCl, Tween-20 0.1%). After 3 h of developing, samples were washed extensively with PBS plus Tween-20 0.1%, fixed in PFA 4%, washed again in PBS Tween-20 0.1%, and subsequently dehydrated in Methanol and stored at −80 °C for at least one night, to allow clearing of background signal. Larvae were rehydrated, transferred to Glycerol 85%, and imaged using a Nikon SMZ25 stereoscope equipped with a DS-Fi3 camera.

Generation of *il10*-Mut zebrafish lines

The zebrafish coding sequence for the ortholog of the human *IL10* gene (Gene name: *il10*, Gene ID: 553957, ENSEMBL ID: ENSDARG00000078147)[31] was targeted by CRISPR/Cas9[37] with specific sgRNAs (Table S1). For the maintenance of wild-type and *il10* mutant stocks, zebrafish embryos coming from the incross of heterozygous *il10* individuals were raised, and genotyping was performed once they reached adulthood by fin-clipping a portion of the tail fin. The $il10^{uu1751}$ mutation created a restriction enzyme site for EcoNI, which is absent in wild-type fish. Carriers of the $il10^{uu1751}$ mutation were screened by PCR followed by enzymatic digestion with EcoNI. Zebrafish carrying the $il10^{uu1762}$ mutation were screened by PCR using combinations of primers in which the forward primer was specific for either the WT or mutant sequence. Primers used for genotyping are shown in Table S1.

Cloning of the zebrafish *il10* and *il17a/f3* genes and rescue experiments

The coding sequences for the zebrafish *il10* and *il17a/f3* genes were amplified by PCR using specific primers for both genes (Table S1) and then cloned in a pCR2.1-TOPO vector (Invitrogen, Cat. No. 450641). In vitro-transcribed mRNA was synthesized using the T7 mMessage mMachine kit (Invitrogen, Cat. No. AM1344), following the manufacturer's guidelines. For injections, 1nL of 200 ng/µL of in vitro-transcribed mRNA was co-injected with 0.5% of Rhodamine-Dextran MW10000 (Invitrogen, Cat. No. D1824) in 1-cell stage wild-type or *il10*-Mut embryos. Embryos injected with 0.5% Rhodamine-dextran were used as control. At 2dpf, Rhodamine-positive embryos were selected and used for subsequent analysis.

Body-intestine isolation in zebrafish larva

Larvae from 3 dpf to 5 dpf were euthanized by overdosing them with MS-222 and intestines were isolated mechanically with the use of needles to pierce the tissue and extract the intestines. Around 10 intestines and their respective bodies were collected for analysis.

RNA extraction and qRT-PCR from zebrafish samples

For zebrafish samples, up to 10 tissue samples (i.e. whole larvae, intestines, or body carcasses) were pooled and collected in Trizol reagent (Invitrogen, Cat. no. 10296010), and tissues were homogenized by pipetting the samples repeatedly through 23G and 27G needles. Total RNA was extracted following Trizol manufacturer's instructions. Synthesis of cDNA was performed using the iScript cDNA synthesis kit (BioRad, Cat. No. 1708841). Quantitative PCR was performed using iTaq Universal SYBR Green supermix (BioRad, Cat. No. 1725124), as previously reported.[69] Primers used for zebrafish qRT-PCR analysis are found in Table S2.

Bleach and antibiotic treatments in zebrafish larvae

Zebrafish embryos between 24–28 hpf were treated with chlorine hypochlorite (0.04%) for 5 minutes and then washed twice with sterile E3 medium for 5 min. After washing, embryos were left in sterile E3 medium containing Ampicillin 100 µg/mL and Kanamycin 5 µg/mL and placed at 28 °C in isolated containers. Media was renewed every day in sterile conditions until the day of sample collection. For the quantification of bacterial loads, genomic DNA from 2 larvae per condition was extracted by (heat-basic), and PCR against 16S All Bacteria[30] and zebrafish gDNA (for *il23r* gene) was performed. PCR products were run in a 2% agarose gel, and band intensities were measured in Fiji/ImageJ (NIH).

Alcian blue, neutral red stainings and quantifications in zebrafish larvae

Stainings for Neutral red (Sigma, Cat. No. N4638) and Alcian blue (Sigma, Cat. No. B8438) in 5dpf zebrafish larvae were performed as previously described.[70] Alcian blue-stained larvae were additionally treated with H_2O_2 1.5%/KOH 0.5% to remove pigments before imaging. Larvae were mounted in a lateral position using 1% low-gelling point agarose (Sigma, Cat. No. A9414), and RGB images were acquired using a Nikon SMZ25 stereoscope equipped with a DS-Fi3 camera. Images were cropped to keep the mid-intestine section. Automatic unbiased analyses of the Alcian blue-stained area in the intestine of individual larvae were performed in Fiji/ImageJ software (NIH) using "Colour Deconvolution 1.7" and selecting the "Alcian blue & H" vector to identify the Alcian blue-stained area. For the automatic detection of the Neutral red-stained area, the function "Color Threshold" was used. The length of the alcian blue- and neutral red-stained regions were measured manually in randomized images.

Immunofluorescence staining in zebrafish larvae

Immunostaining was performed on whole larvae at 5 days post fertilization. Paraformaldehyde at 4% was used to fix zebrafish larvae overnight at 4 °C. The samples were then washed with distilled water. For whole-mount 2F11 immunostaining, fixed larvae were permeabilized with cold 100% acetone for 20 min at 4 °C before being washed three times with PBST (PBS supplemented with 0,5% Triton-X-100). Samples were further permeabilized with 1 mg/mL Collagenase from *Clostridium histolyticum* (Cat. No. C2139) for 2 h at room temperature. Samples were then washed with PBST and blocked with 10% of FBS/PBST at room temperature for more than 2 h. The primary mouse monoclonal 2F11 antibody (1:200; Abcam, Cat. No. ab71286) was diluted in blocking solution and incubated at 4 °C for more than 24 h. Following primary antibody incubation, the samples were washed with PBST solution and incubated for at least 2 h with secondary anti-mouse Alexa Fluor 488 antibody (1:500; Invitrogen, Cat. No. A11001) at room temperature in the dark. For whole-mount WGA staining, larvae were washed in distilled water for 1 h at

room temperature, permeabilized with cold 100% acetone form 20 minutes at −20 °C, and washed with PBST. Larvae were incubated in Alexa Fluor 555-conjugated Wheat Germ Agglutinin (1:5000 from 5 mg/mL stock; Invitrogen, Cat. No. W32464) overnight at 4 °C and washed extensively with PBST. Imaging was performed using the Zeiss Axio Zoom.V16 stereoscope or the Zeiss LSM800 confocal microscope and analyzed with ImageJ software.

Chemical treatments in larval zebrafish

At 2 days post fertilization, pools of 10 larvae per milliliter were exposed to the Notch/γ-secretase inhibitor DAPT (50 µM; Tocris, Cat. No. 2634), the Jak2/Stat3 inhibitor Tyrphostin AG-490 (50 µM; Sigma-Aldrich, Cat. No. T3434), or the Notch activator Yhhu-3792 (Tocris, Cat. No. 6599), or. As a control for Notch activity induced by Yhhu-3792, RNA was extracted from treated larvae and the expression levels of the Notch downstream gene *her6* were measured by qRT-PCR.

Fluorescent reporter imaging and analysis

The fluorescent reporters for Notch activity *Tg(tp1:GFP)* and Stat3 activity *Tg(7xStat3:EGFP)*, in either wild-type or *il10*^{uu1751} genetic background, were imaged at 5dpf in an SMZ25 stereoscope equipped with a CoolLed laser set and a DS-Fi3 camera (Nikon), focusing on the intestinal region. Z-stacks were merged in Fiji/ImageJ software, and the number of GFP^{+} cells in the intestinal region was counted manually in Fiji/ImageJ.

Dissection, sectioning, and staining of adult zebrafish intestines

Zebrafish older than 1 year of age were euthanized with an overdose of MS-222. Intestines were collected and fixed in neutral buffered formalin (Sigma, Cat. No. HT-501128) overnight at room temperature, and subsequently transferred to ethanol 70% for at least 24 h. Tissues were dehydrated and embedded in paraffin, and 10 µm sections were collected and stained with alcian blue. Briefly, tissue sections were deparaffinized and rehydrated to PBS, and incubated in 3% alcian blue solution (Sigma) for 5 min. After staining, tissues were counterstained with nuclear fast red (Sigma, Cat. No. N3020). Images were acquired in a Nikon SMZ25 stereoscope and quantifications of goblet cells per villus area were performed using QuPath 0.2.3 (University of Edinburgh, UK).

Mouse intestinal organoid cultures

Mouse organoids were generated from crypts derived from the entire small intestine (SI). Briefly, SIs from WT mice were collected and flushed with PBS, cut opened longitudinally, and subsequently cut into five pieces of similar size. Tissue pieces were placed in PBS and were vigorously shaken to remove mucus. Tissue pieces were then transferred to cold PBS-EDTA 10 mM and incubated for 1 h in ice. After incubation, SI villi were removed by gentle scraping of the luminal side using two glass slides. Then SI crypts were scraped from the tissue pieces by applying stronger pressure with the glass slides and collected in recipient tubes filled with cold PBS. Collected crypts were centrifuged for 5 min at 300 × *g* and 4 °C, and then quantified using an upright microscope by placing 10 µL of crypt solution on a glass slide. The basic culture medium (ENR) contained advanced DMEM/F12, 1× penicillin/streptomycin, 1x Glutamax (Thermo Fisher Scientific), 10 mM HEPES (Thermo Fisher Scientific), 1x B27 supplement (Life Technologies, Cat. No.17504044), 1× N2 supplement (Life Technologies, Cat. No. 17504048), 1mM N-acetylcysteine (NAC, from Sigma, Cat. No. A9165) and was supplemented with 50 ng/mL of recombinant murine epidermal growth factor (EGF, from R&D, Cat. No. 2028-EG), 250 ng/mL recombinant murine R-Spondin (R&D, Cat. No. 3474-RS) and 100 ng/mL recombinant murine Noggin (Peprotech, Cat. No. 250-38). SI crypts were resuspended in 30–40% basic culture medium with 60–70% Matrigel (Corning, Cat. No. 356231) and 20 µl containing approximately 500 crypts were plated in a pre-warmed flat-bottom 48-well plate (Sarstedt, Cat. No. 83.3923). The plate was placed at 37 °C and allowed to solidify for 15 min before 200 µl of ENR medium (containing the different stimuli) was overlaid. The medium was replaced every 2 days with fresh medium and cultures were maintained at 37 °C in fully humidified chambers containing 5% CO_2. During the first 2 days of culture, the ENR medium was supplemented with 10 µM of the ROCK inhibitor Y-27632 (Sigma, Cat. No. Y0503). For organoid in vitro stimulation, 25 ng/mL of recombinant murine IL-10 (Peprotech, Cat. No. 210-10) diluted in 0.1% bovine serum albumin (BSA, Sigma) was added in the ENR medium for the entire duration of the organoid cultures. Control organoids were supplemented with a similar volume of 0.1% BSA vehicle. Each condition was plated in technical triplicates. On day 4 of culture, crypt domains per IL-10-treated or vehicle-treated organoids were quantified in 2–3 wells/condition Each dot in the quantification plot represents one mouse and an average of 2–3 technical replicates.

Alcian blue stainings on mouse SI organoids

The Alcian blue protocol used for the staining of mouse SI organoids was adapted from the protocol used for whole-mount Alcian blue stainings in zebrafish. Organoids were collected after 4 days of culture, washed 5 times with cold PBS-BSA 0.1%, and replated in a new Matrigel stock in 24-well plates, to remove debris from the initial culture. After Matrigel gelification, organoids were fixed in PFA 4% for 45 minutes, washed twice with PBS-BSA 0.1%, and washed twice with acidic ethanol (70% Ethanol supplemented with 1% HCl). Organoids were stained with Alcian blue solution (Sigma, Cat. No. B8438) for 1 h at room temperature. After the incubation, stained organoids were washed extensively with acidic ethanol and were left overnight in acidic ethanol at 4 °C, to remove excessive staining from the Matrigel. Once the Matrigel became clear, organoids were washed with PBS-BSA 0.1% and imaged using the Nikon SMZ25 system.

RNA extraction from mouse organoids and qRT-PCR

After 4 days of culture, treated organoids were harvested and Matrigel was removed by consecutive washes with cold PBS-BSA 0.1%. Cleaned organoids were resuspended in RLT-plus buffer supplemented with 1% β-Mercaptoethanol, and RNA extraction was performed using the RNeasy extraction kit (Qiagen, Cat. No. 74136), following the manufacturer's instructions. Similar to zebrafish samples, synthesis of cDNA was performed using the iScript cDNA synthesis kit (BioRad), and quantitative PCR was performed using iQ SYBR Green mix (BioRad). Primers used for mouse qRT-PCR analysis are found in Table S2.

Flow cytometry from organoid cell suspensions

For flow cytometry experiments, SI organoids were generated from crypts extracted from Lgr5-GFP mice. After 4 days of treatment, organoids were harvested and washed 5 times with cold PBS-BSA 0.1%. Organoids were disaggregated to single cells by incubating with TrypLE supplemented with DNase I for 5 min at 37 °C. Cells were incubated in Fc block (1:1000; Invitrogen, Cat. No. 14-0161-85) and Fixable Viability Dye eFluor 780 (1:1000; eBioscience, Cat. No. 65-0865-14) for 15 min at 4 °C, and subsequently stained with anti-Epcam PE-Cy7 (1:200; BioLegend, Cat. No. 118215), anti-CD24 BV421 (1:200; BioLegend, Cat. No. 101825) and WGA Alexa Fluor 555 (1:5000; Invitrogen) for 1 h at 4 °C. Flow cytometry was performed using an LSRFortessa flow cytometer (BD Biosciences, USA), and analysis was perfumed using FlowJo v10 (Treestar, USA).

Immunostaining of small intestine organoids

For immunofluorescence experiments, Matrigel-embedded isolated crypts extracted from small intestines of WT mice were plated in pre-warmed 8-well 15 µm glass-bottom chambers (Ibidi, Cat. No. 80826) and cultured as described above. On day 4 of culture, organoids were fixed in PBS-buffered Paraformaldehyde 4% for 45 minutes, permeabilized with Triton X-100 0.5% for 30 minutes and treated with Glycine 0.1 M for 1 h to block free aldehyde groups. Organoids were incubated in blocking solution (Normal goat serum 5%, Triton X-100 0.25%, BSA 0.1% in PBS) for 30 min before incubating with WGA Alexa Fluor 555 (1:5000, Invitrogen) and rabbit polyclonal anti-Lysozyme Ab-1 (1:200; Thermo Scientific, Cat. No. RB-372-A) overnight at 4 °C. After 3 washes with PBS-BSA 0.1%, organoids were incubated with goat anti-rabbit Alexa Fluor 647 (1:1000; Invitrogen, Cat. No. A21244) overnight at 4 °C. On the final day of staining, organoid nuclei were stained with DAPI (1 µg/mL, Molecular Probes, Cat. No. D1306) for 30 min at room temperature, washed, and kept in PBS until imaging within 0–3 days. Images from stained organoids were acquired in a Zeiss LSM800 confocal microscope (Zeiss, Germany) and analyzed using ImageJ.

Statistical analysis

Quantitative data were analyzed using GraphPad Prism v8.0 software (GraphPad, San Diego, CA, USA). Group comparisons were considered statistically significant when they reached a *p*-value below 0.05.

REFERENCES

1. Friedrich, M., Pohin, M. & Powrie, F. Cytokine networks in the pathophysiology of inflammatory bowel disease. *Immunity* **50**, 992–1006 (2019).
2. Kühn, R., Löhler, J., Rennick, D., Rajewsky, K. & Müller, W. Interleukin-10-deficient mice develop chronic enterocolitis. *Cell* **75**, 263–274 (1993).
3. Nambu, R. et al. A systematic review of monogenic inflammatory bowel disease. *Clin. Gastroenterol. Hepatol.* **20**, e653–e663 (2021).
4. Shim, J. O. & Seo, J. K. Very early-onset inflammatory bowel disease (IBD) in infancy is a different disease entity from adult-onset IBD; one form of interleukin-10 receptor mutations. *J. Hum. Genet.* **59**, 337–341 (2014).
5. Shim, J. O. Recent advance in very early onset inflammatory bowel disease. *Pediatr. Gastroenterol. Hepatol. Nutr.* **22**, 41–49 (2019).
6. Peloquin, J. M., Goel, G., Villablanca, E. J. & Xavier, R. J. Mechanisms of pediatric inflammatory bowel disease. *Annu Rev. Immunol.* **34**, 31–64 (2016).
7. Bequet, E. et al. Incidence and phenotype at diagnosis of very-early-onset compared with later-onset paediatric inflammatory bowel disease: a population-based study [1988-2011]. *J. Crohns Colitis* **11**, 519–526 (2017).
8. Zigmond, E. et al. Macrophage-restricted interleukin-10 receptor deficiency, but not IL-10 deficiency, causes severe spontaneous colitis. *Immunity* **40**, 720–733 (2014).
9. Denning, T. L. et al. Expression of IL-10 receptors on epithelial cells from the murine small and large intestine. *Int. Immunol.* **12**, 133–139 (2000).
10. Papoutsopoulou, S. et al. Impact of interleukin 10 deficiency on intestinal epithelium responses to inflammatory signals. *Front. Immunol.* **12**, 690817 (2021).
11. Kominsky, D. J. et al. IFN-γ-mediated induction of an apical IL-10 receptor on polarized intestinal epithelia. *J. Immunol.* **192**, 1267–1276 (2014).
12. Quiros, M. et al. Macrophage-derived IL-10 mediates mucosal repair by epithelial WISP-1 signaling. *J. Clin. Investig.* **127**, 3510–3520 (2017).
13. Biton, M. et al. T helper cell cytokines modulate intestinal stem cell renewal and differentiation. *Cell* **175**, 1307–1320.e1322 (2018).
14. Jenkins, B. R. et al. Loss of interleukin-10 receptor disrupts intestinal epithelial cell proliferation and skews differentiation towards the goblet cell fate. *FASEB J.* **35**, e21551 (2021).
15. Pinto, D. & Clevers, H. Wnt control of stem cells and differentiation in the intestinal epithelium. *Exp. Cell Res.* **306**, 357–363 (2005).
16. He, X. C. et al. BMP signaling inhibits intestinal stem cell self-renewal through suppression of Wnt-beta-catenin signaling. *Nat. Genet.* **36**, 1117–1121 (2004).
17. Guo, Z. & Ohlstein, B. Stem cell regulation. Bidirectional Notch signaling regulates Drosophila intestinal stem cell multipotency. *Science* **350**, aab0988 (2015).
18. Crosnier, C. et al. Delta-Notch signalling controls commitment to a secretory fate in the zebrafish intestine. *Development* **132**, 1093–1104 (2005).
19. van Es, J. H. et al. Notch/gamma-secretase inhibition turns proliferative cells in intestinal crypts and adenomas into goblet cells. *Nature* **435**, 959–963 (2005).
20. VanDussen, K. L. et al. Notch signaling modulates proliferation and differentiation of intestinal crypt base columnar stem cells. *Development* **139**, 488–497 (2012).
21. Jensen, J. et al. Control of endodermal endocrine development by Hes-1. *Nat. Genet.* **24**, 36–44 (2000).
22. Ueo, T. et al. The role of Hes genes in intestinal development, homeostasis and tumor formation. *Development* **139**, 1071–1082 (2012).
23. Fre, S. et al. Notch signals control the fate of immature progenitor cells in the intestine. *Nature* **435**, 964–968 (2005).
24. Schröder, N. & Gossler, A. Expression of Notch pathway components in fetal and adult mouse small intestine. *Gene Expr. Patterns* **2**, 247–250 (2002).
25. Dell'Aringa, M. & Reinhardt, R. L. Notch signaling represents an important checkpoint between follicular T-helper and canonical T-helper 2 cell fate. *Mucosal Immunol.* **11**, 1079–1091 (2018).
26. Rutz, S. et al. Notch regulates IL-10 production by T helper 1 cells. *Proc. Natl Acad. Sci. USA* **105**, 3497–3502 (2008).
27. Nayar, S. et al. A myeloid-stromal niche and gp130 rescue in NOD2-driven Crohn's disease. *Nature* **593**, 275–281 (2021).
28. Jijon, H. B. et al. Intestinal epithelial cell-specific RARα depletion results in aberrant epithelial cell homeostasis and underdeveloped immune system. *Mucosal Immunol.* **11**, 703–715 (2018).
29. Diaz, O. E. et al. Perfluorooctanesulfonic acid modulates barrier function and systemic T-cell homeostasis during intestinal inflammation. *Dis. Model Mech.* **14**, dmm049104 (2021).
30. Kaya, B. et al. Lysophosphatidic acid-mediated GPR35 Signaling in CX3CR1. *Cell Rep.* **32**, 107979 (2020).
31. Zhang, D. C., Shao, Y. Q., Huang, Y. Q. & Jiang, S. G. Cloning, characterization and expression analysis of interleukin-10 from the zebrafish (*Danio rerion*). *J. Biochem Mol. Biol.* **38**, 571–576 (2005).
32. Harjula, S. E., Ojanen, M. J. T., Taavitsainen, S., Nykter, M. & Rämet, M. Interleukin 10 mutant zebrafish have an enhanced interferon gamma response and improved survival against a Mycobacterium marinum infection. *Sci. Rep.* **8**, 10360 (2018).
33. Bottiglione, F. et al. Zebrafish IL-4-like cytokines and IL-10 suppress inflammation but only IL-10 is essential for gill homeostasis. *J. Immunol.* **205**, 994–1008 (2020).
34. Wallace, K. N., Akhter, S., Smith, E. M., Lorent, K. & Pack, M. Intestinal growth and differentiation in zebrafish. *Mech. Dev.* **122**, 157–173 (2005).
35. Ng, A. N. et al. Formation of the digestive system in zebrafish: III. Intestinal epithelium morphogenesis. *Dev. Biol.* **286**, 114–135 (2005).
36. Alvers, A. L., Ryan, S., Scherz, P. J., Huisken, J. & Bagnat, M. Single continuous lumen formation in the zebrafish gut is mediated by smoothened-dependent tissue remodeling. *Development* **141**, 1110–1119 (2014).
37. Varshney, G. K. et al. A high-throughput functional genomics workflow based on CRISPR/Cas9-mediated targeted mutagenesis in zebrafish. *Nat. Protoc.* **11**, 2357–2375 (2016).
38. Oehlers, S. H. et al. A chemical enterocolitis model in zebrafish larvae that is dependent on microbiota and responsive to pharmacological agents. *Dev. Dyn.* **240**, 288–298 (2011).
39. Park, J. et al. Lysosome-rich enterocytes mediate protein absorption in the vertebrate gut. *Dev. Cell* **51**, 7–20.e26 (2019).
40. Chuang, L. S. et al. Zebrafish modeling of intestinal injury, bacterial exposures and medications defines epithelial. *Dis. Model. Mech.* **12**, dmm037432 (2019).
41. Lin, X. et al. IL-17RA-signaling in Lgr5^{+} intestinal stem cells induces expression of transcription factor ATOH1 to promote secretory cell lineage commitment. *Immunity* **55**, 237–253.e238 (2022).
42. Troll, J. V. et al. Microbiota promote secretory cell determination in the intestinal epithelium by modulating host Notch signaling. *Development* **145**, dev155317 (2018).
43. Roach, G. et al. Loss of ascl1a prevents secretory cell differentiation within the zebrafish intestinal epithelium resulting in a loss of distal intestinal motility. *Dev. Biol.* **376**, 171–186 (2013).
44. Reuter, A. S. et al. Identification of an evolutionarily conserved domain in Neurod1 favouring enteroendocrine versus goblet cell fate. *PLoS Genet.* **18**, e1010109 (2022).
45. Parsons, M. J. et al. Notch-responsive cells initiate the secondary transition in larval zebrafish pancreas. *Mech. Dev.* **126**, 898–912 (2009).
46. Lickwar, C. R. et al. Genomic dissection of conserved transcriptional regulation in intestinal epithelial cells. *PLoS Biol.* **15**, e2002054 (2017).
47. Ouyang, W. & O'Garra, A. IL-10 family cytokines IL-10 and IL-22: from basic science to clinical translation. *Immunity* **50**, 871–891 (2019).
48. Peron, M. et al. The stem-like Stat3-responsive cells of zebrafish intestine are Wnt/β-catenin dependent. *Development* **147**, dev188987 (2020).
49. Tham, E. R., Briggs, L. & Murrell, G. A. Ultrasound changes after rotator cuff repair: is supraspinatus tendon thickness related to pain? *J. Shoulder Elb. Surg.* **22**, e8–e15 (2013).
50. Lu, H. et al. A novel 2-phenylamino-quinazoline-based compound expands the neural stem cell pool and promotes the hippocampal neurogenesis and the cognitive ability of adult mice. *Stem Cells* **36**, 1273–1285 (2018).
51. Sato, T. et al. Single Lgr5 stem cells build crypt-villus structures in vitro without a mesenchymal niche. *Nature* **459**, 262–265 (2009).
52. Barker, N. et al. Identification of stem cells in small intestine and colon by marker gene Lgr5. *Nature* **449**, 1003–1007 (2007).
53. Cornick, S., Kumar, M., Moreau, F., Gaisano, H. & Chadee, K. VAMP8-mediated MUC2 mucin exocytosis from colonic goblet cells maintains innate intestinal homeostasis. *Nat. Commun.* **10**, 4306 (2019).
54. Ludikhuize, M. C. et al. Mitochondria define intestinal stem cell differentiation downstream of a FOXO/Notch axis. *Cell Metab.* **32**, 889–900.e887 (2020).
55. Sato, T. et al. Paneth cells constitute the niche for Lgr5 stem cells in intestinal crypts. *Nature* **469**, 415–418 (2011).
56. Makkink, M. K. et al. Fate of goblet cells in experimental colitis. *Dig. Dis. Sci.* **47**, 2286–2297 (2002).
57. Johansson, M. E. et al. Bacteria penetrate the normally impenetrable inner colon mucus layer in both murine colitis models and patients with ulcerative colitis. *Gut* **63**, 281–291 (2014).
58. Li, C. et al. celsr1a is essential for tissue homeostasis and onset of aging phenotypes in the zebrafish. *Elife* **9**, e50523 (2020).
59. Aghaallaei, N. et al. Identification, visualization and clonal analysis of intestinal stem cells in fish. *Development* **143**, 3470–3480 (2016).
60. Willms, R. J., Jones, L. O., Hocking, J. C. & Foley, E. A cell atlas of microbe-responsive processes in the zebrafish intestine. *Cell Rep.* **38**, 110311 (2022).
61. Hildebrand, D. et al. The interplay of Notch signaling and STAT3 in TLR-activated human primary monocytes. *Front. Cell. Infect. Microbiol.* **8**, 241 (2018).
62. Zhu, Y. P., Brown, J. R., Sag, D., Zhang, L. & Suttles, J. Adenosine 5′-monophosphate-activated protein kinase regulates IL-10-mediated anti-inflammatory signaling pathways in macrophages. *J. Immunol.* **194**, 584–594 (2015).
63. Antoniv, T. T. & Ivashkiv, L. B. Interleukin-10-induced gene expression and suppressive function are selectively modulated by the PI3K-Akt-GSK3 pathway. *Immunology* **132**, 567–577 (2011).

64. Parmar, N. et al. Intestinal-epithelial LSD1 controls goblet cell maturation and effector responses required for gut immunity to bacterial and helminth infection. *PLoS Pathog.* **17**, e1009476 (2021).
65. Wang, Y. et al. Single-cell transcriptome analysis reveals differential nutrient absorption functions in human intestine. *J. Exp. Med.* **217**, e20191130 (2020).
66. Zhu, L. et al. IL-10 and IL-10 receptor mutations in very early onset inflammatory bowel disease. *Gastroenterol. Res.* **10**, 65–69 (2017).
67. Villablanca, E. J., Selin, K. & Hedin, C. R. H. Mechanisms of mucosal healing: treating inflammatory bowel disease without immunosuppression? *Nat. Rev. Gastroenterol. Hepatol.* https://doi.org/10.1038/s41575-022-00604-y. Online ahead of print (2022).
68. Kelsen, J. R., Russo, P. & Sullivan, K. E. Early-onset inflammatory bowel disease. *Immunol. Allergy Clin. N. Am.* **39**, 63–79 (2019).
69. Diaz, O. E. et al. Retinoic acid induced cytokines are selectively modulated by liver X receptor activation in zebrafish. *Reprod. Toxicol.* **93**, 163–168 (2020).
70. Oehlers, S. H. et al. Chemically induced intestinal damage models in zebrafish larvae. *Zebrafish* **10**, 184–193 (2013).

ACKNOWLEDGEMENTS

We would like to thank all the Villablanca lab members for their constant feedback on the project. We thank the KI Zebrafish Core Facility and the Institut Curie Animal Facility staff for their expert support in the maintenance of zebrafish lines and stocks. E.J.V. was supported by grants from the Swedish Research Council, VR grant K2015-68X-22765-01-6, 2018-02533, and 2021-01277. Formas grant nr. FR-2016/0005, Cancerfonden (19 0395 Pj), Ruth and Richard Julin Foundation, and the Wallenberg Academy Fellow program (2019.0315). P.P.H. was supported by Labex DEEP (ANR-11-LBX-0044, ANR-10-IDEX- 0001-02 PSL), FRM (AJE201905008718), Ville de Paris (2020 DAE 78). R.A.M. was supported by ANID Becas Chile (74200049) and by funds from the Marcus Borgström Foundation.

AUTHOR CONTRIBUTIONS

Idea conception and experimental design: R.A.M., S.D., P.P.H., E.J.V. Experiment execution and data analysis: R.A.M., S.R., O.E.D., Y.S., M.W., B.C.K., X.L., G.M., S.M.P., S.D. Manuscript preparation: R.A.M., E.J.V. All authors have revised and accepted the final version of the manuscript.

FUNDING

Open access funding provided by Karolinska Institute.

COMPETING INTERESTS

The authors declare no competing interests.

ADDITIONAL INFORMATION

Supplementary information The online version contains supplementary material available at https://doi.org/10.1038/s41385-022-00546-3.

Correspondence and requests for materials should be addressed to Rodrigo A. Morales or Eduardo J. Villablanca.

Annex 2: Definitive hematopoiesis is dispensable to sustain erythrocytes and macrophages during zebrafish ontogeny

Abstract:

Blood cells originate through multiple sequential waves from distinct hematopoietic sources throughout development in organisms from flies to humans. The contribution and role of these ontogenetically different hematopoietic waves to embryonic blood cells and tissue regeneration during development are not well understood. In this study, we show that definitive hematopoietic progenitors contribute minimally to the formation of erythrocytes and macrophages during early developmental stages. Additionally, we demonstrate that primitive macrophages are recruited earlier to injury sites and are essential for tissue regeneration during early larval stages, in contrast to definitive macrophages. These findings underscore the essential role of primitive hematopoiesis in ensuring the availability of blood cells needed to maintain tissue homeostasis and integrity during early development.

My contribution

We revealed that the ablation of definitive macrophages does not compromise the regenerative capacity of zebrafish larvae in a tail fin injury model. To determine whether the deficiency of definitive macrophages affects cell proliferation in the injured fin, I performed EdU staining and I found that the absence of definitive macrophages does not affect the number of proliferating cells in the blastema post-injury (Figures S3F and S3G).

iScience

CellPress
OPEN ACCESS

Article

Definitive hematopoiesis is dispensable to sustain erythrocytes and macrophages during zebrafish ontogeny

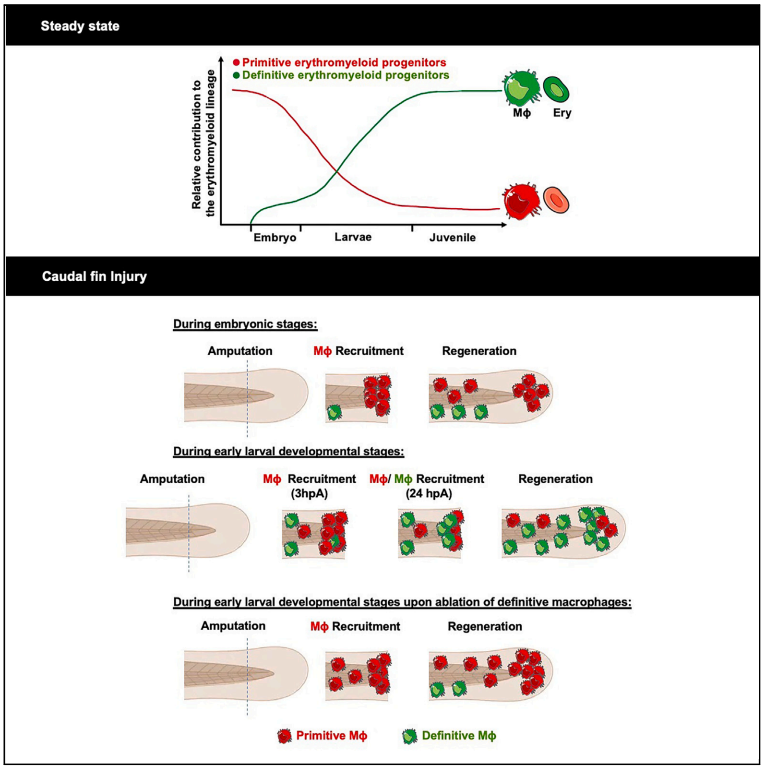

Ramy Elsaid, Aya Mikdache, Keinis Quintero Castillo, ..., Gwendoline Gros, Carmen G. Feijoo, Pedro P. Hernández

ramy.elsaid@curie.fr (R.E.)
pedro.hernandez-cerda@curie.fr (P.P.H.)

Highlights

Primitive hematopoiesis gives rise to and sustains embryonic erythromyeloid lineages

Primitive macrophages are recruited earlier to the site of injury

Ablation of larval definitive macrophages does not impair tail fin regeneration

Primitive macrophages depletion impairs tail fin regeneration in zebrafish larvae

Elsaid et al., iScience 27, 108922
February 16, 2024
https://doi.org/10.1016/j.isci.2024.108922

iScience

CellPress
OPEN ACCESS

Article

Definitive hematopoiesis is dispensable to sustain erythrocytes and macrophages during zebrafish ontogeny

Ramy Elsaid,[1,*] Aya Mikdache,[1] Keinis Quintero Castillo,[2] Yazan Salloum,[1] Patricia Diabangouaya,[1,3] Gwendoline Gros,[1,3] Carmen G. Feijoo,[2] and Pedro P. Hernández[1,4,*]

SUMMARY

In all organisms studied, from flies to humans, blood cells emerge in several sequential waves and from distinct hematopoietic origins. However, the relative contribution of these ontogenetically distinct hematopoietic waves to embryonic blood lineages and to tissue regeneration during development is yet elusive. Here, using a lineage-specific "switch and trace" strategy in the zebrafish embryo, we report that the definitive hematopoietic progeny barely contributes to erythrocytes and macrophages during early development. Lineage tracing further shows that ontogenetically distinct macrophages exhibit differential recruitment to the site of injury based on the developmental stage of the organism. We further demonstrate that primitive macrophages can solely maintain tissue regeneration during early larval developmental stages after selective ablation of definitive macrophages. Our findings highlight that the sequential emergence of hematopoietic waves in embryos ensures the abundance of blood cells required for tissue homeostasis and integrity during development.

INTRODUCTION

Hematopoiesis is a complex biological process by which all mature blood lineages are generated. In mammals, hematopoiesis originates from distinct blood progenitors that emerge during development through an endothelial-to-hematopoietic transition mechanism (EHT),[1–3] resulting in a layered organization of the immune system.[4] As in mammals, zebrafish hematopoiesis also consists of multiple waves that emerge at distinct anatomical locations.[4] In the zebrafish embryo, primitive hematopoiesis emerges intra-embryonically directly from mesoderm around 11 h postfertilization (hpf) in the rostral blood island (RBI) and the posterior lateral mesoderm (PLM) and generates primitive erythrocytes and myeloid cells.[4,5] Other definitive or endothelial-derived hematopoietic waves are also produced in the developing organism.[4] One of them is a transient wave that emerges from the posterior blood island (PBI) at 24–30 hpf via EHT and gives rise to erythro-myeloid progenitors (EMPs) like those in mammals.[6–8] At 36 hpf, other waves of HSCs and HSC-independent progenitors emerge from the dorsal aorta (DA) via EHT.[1,3] These DA-derived hematopoietic progenitors then migrate to the caudal hematopoietic tissue (CHT), the fetal liver counterpart in zebrafish.[9] Therefore, due to its similarity to mammalian hematopoiesis, the zebrafish is an excellent model to study the ontogeny of different hematopoietic waves during development.

Although it is well characterized that blood cells are produced in sequential and overlapping waves,[4] little is known about their contribution to different hematopoietic lineages during development. Recently, independent reports support the notion that definitive hematopoiesis sustains embryonic blood lineages.[8,10–12] However, primitive hematopoietic progenitors give rise also to the erythromyeloid lineage, and it is yet unknown to what extent these progenitors contribute to embryonic blood lineages. This is mainly due to the lack of specific markers for primitive hematopoietic progenitors in mammals.[4,7,13,14]

The difficulty in accurately tracing the output of each wave in mammalian animal models has hindered the full understanding of immune cell ontogeny. In this study, we used the unique strengths of the zebrafish embryo to perform temporarily resolved lineage tracing combined with live imaging to investigate the embryonic erythromyeloid lineage ontogeny *in vivo*. We unveiled that embryonic erythromyeloid lineages originate from primitive hematopoietic progenitors with a delayed contribution from definitive hematopoietic waves to the erythromyeloid lineage till the larval developmental stage. We further showed that primitive macrophages were recruited to the damage site earlier than their definitive counterparts. Our results also suggest that primitive macrophages maintain tissue regeneration during early larval developmental stages after selective ablation of definitive macrophages. Combined, our study reveals that the sequential emergence of hematopoietic waves ensures the abundance of macrophages and erythrocytes required for tissue homeostasis and integrity during development.

[1]Institut Curie, PSL Research University CNRS UMR 3215, INSERM U934, 26 Rue d'Ulm, 75248 Paris Cedex 05, France
[2]Fish Immunology Laboratory, Faculty of Life Science, Andres Bello University, Santiago 8370146, Chile
[3]These authors contributed equally
[4]Lead contact
*Correspondence: ramy.elsaid@curie.fr (R.E.), pedro.hernandez-cerda@curie.fr (P.P.H.)
https://doi.org/10.1016/j.isci.2024.108922

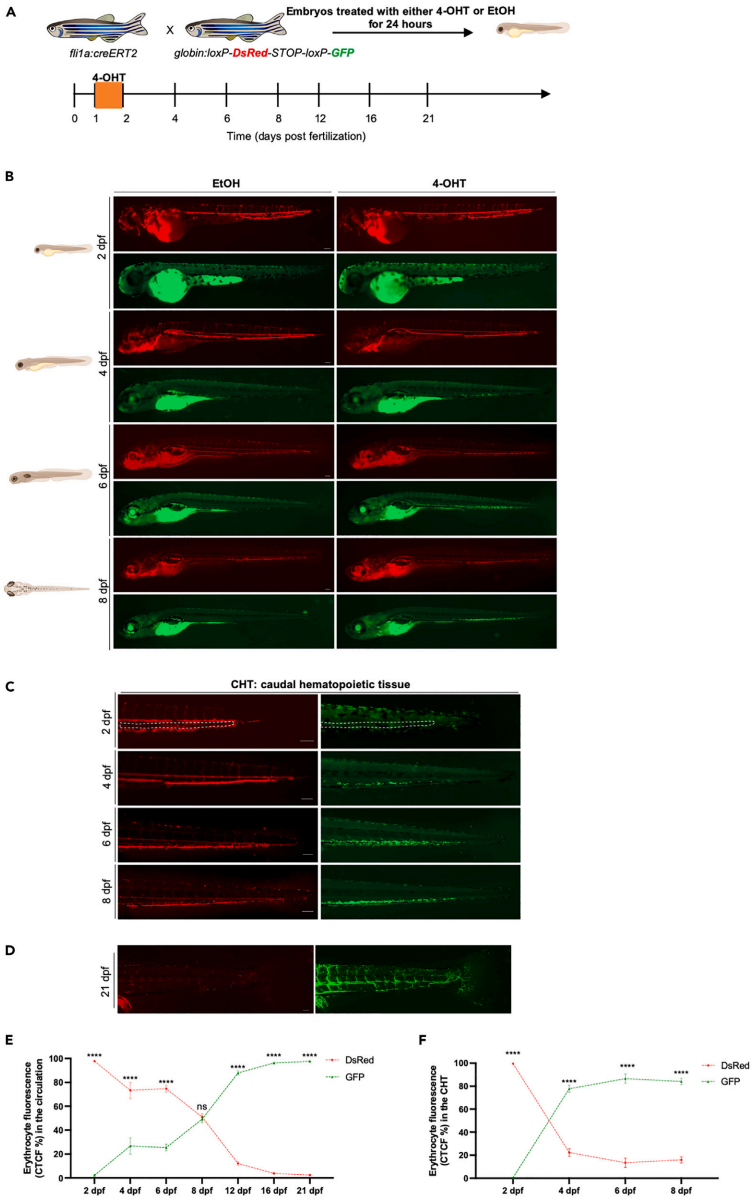
A
Embryos treated with either 4-OHT or EtOH
for 24 hours
fli1a:creERT2
X
globin:loxP-DsRed-STOP-loxP-GFP
4-OHT
0 1 2 4 6 8 12 16 21
Time (days post fertilization)
B
EtOH
4-OHT
2 dpf
4 dpf
6 dpf
8 dpf
C
CHT: caudal hematopoietic tissue
2 dpf
4 dpf
6 dpf
8 dpf
D
21 dpf
E
Erythrocyte fluorescence (CTCF %) in the circulation
DsRed
GFP
ns
2 dpf 4 dpf 6 dpf 8 dpf 12 dpf 16 dpf 21 dpf
F
Erythrocyte fluorescence (CTCF %) in the CHT
DsRed
GFP
2 dpf 4 dpf 6 dpf 8 dpf

Figure 1. Tracing the contribution of definitive hematopoietic waves to the erythroid lineage in the embryo and early larvae

(A) Scheme of the 4-OHT-inducible transgenic lines used to assess the contribution of definitive hematopoietic waves to the erythroid lineage.

(B) Fluorescent images of EtOH non-switched controls (left) and 4-OHT-induced (right) *Tg(fli1a:creERT2;globin:Switch)* embryos and larvae (2 dpf–8 dpf). Scale bars, 100 μm. Quantification of erythrocytes in circulation are shown in (E).

(C) Fluorescent images of 4-OHT-induced *Tg(fli1a:creERT2;globin:Switch)* embryos and larvae (2–8 dpf) in the CHT region. Non-switched primitive erythrocytes (left) and definitive erythrocytes (right). Scale bars, 100 μm. quantification of erythrocytes in the CHT are shown in (F).

(D) Fluorescent images of 4-OHT-induced *Tg(fli1a:creERT2;globin:Switch)* (21 dpf) in the circulation. Scale bar, 100 μm. Non-switched primitive erythrocytes (left) and definitive erythrocytes (right). Quantification of erythrocytes in the circulation is shown in (E).

(E) Quantification of DsRed and GFP fluorescence intensity percentage in the circulation was measured over a time course of 2–21 dpf. (2 dpf n = 6; 4 dpf n = 4; 6 dpf n = 5; 8 dpf n = 4; 12 dpf; 16 dpf n = 6 and 21 dpf n = 5). Mean ± SEM of the $DsRed^+$ and GFP^+ corrected total cell fluorescence (CTCF) percentage at each time point is shown. Two-way ANOVA with Sidak's multiple comparison was used for this analysis. ****$p \leq 0.0001$.

(F) Quantification of DsRed and GFP fluorescence intensity percentage in the CHT was measured over a time course of 2–8 dpf. (2 dpf n = 6; 4 dpf n = 4; 6 dpf n = 5; and 8 dpf n = 4). Mean ± SEM of the $DsRed^+$ and GFP^+ corrected total cell fluorescence (CTCF) percentage at each time point is shown. two-way ANOVA with Sidak's multiple comparison was used for this analysis. ****$p \leq 0.0001$.

RESULTS

Primitive hematopoietic progenitors sustain erythrocytes during embryonic development

As all definitive hematopoietic progenitors originate from hemogenic endothelium (HE) as early as 24 hpf,[1,3,6,8,10,15] while primitive progenitors originate directly from mesoderm in zebrafish,[1,3,16,17] we set up a strategy to distinguish between primitive and definitive hematopoietic progenitors based on their tissue of origin. We used the endothelial-specific tamoxifen-inducible transgenic line Tg(*fli1a:CreERT2*)[18] in combination with different hematopoietic lineage-specific switch and trace lines.[19] Our inducible labeling strategy at 24 hpf will label exclusively definitive hematopoietic progenitors as they emerge from the HE without labeling primitive hematopoietic progenitors. To assess the efficiency of our labeling strategy, we combined the Tg(*fli1a:CreERT2*) line with two different independent transgenic lines, the lymphocyte-specific Tg(lck:loxP-DsRedx-loxP-GFP)[8,20] line (Figure S1A) and the Tg(coro1a:loxP-DsRedx-loxP-GFP) line which labels all leukocytes[13,21] (Figure S1D). We found that 80% of thymocytes in the thymus, which have only a definitive hematopoietic origin,[8,22] were labeled using either the Tg(lck:loxP-DsRedx-loxP-GFP) (Figures S1B and S1C) or the Tg(coro1a:loxP-DsRedx-loxP-GFP) lines (Figures S1E and S1F), indicating the high labeling efficiency of our system.

To determine the origin of erythrocytes during embryonic development and early larval stages, we combined the Tg(*fli1a:CreERT2*) line with the erythrocyte-specific Tg(α/βa2-globin:loxP-DsRedx-loxP-GFP) line (referred to hereafter as globin:switch).[8,17] In double transgenic zebrafish, 4-OH-tamoxifen (4-OHT) induces cre recombination and removes the DsRed cassette, leading to permanent GFP expression in fli1a+-derived erythroid progeny (Figure 1A). To determine the contribution of definitive hematopoietic progenitors to erythropoiesis during early stages of development, we exposed embryos to either 4-OHT or ethanol (EtOH) starting at 24 hpf to label the aortic-endothelium-derived definitive hematopoietic progenitors,[1,3,8] and then monitored GFP+ definitive erythrocytes via live imaging (Figure 1B, Videos S1, S2, S3, S4, S5, S6, S7, and S8). Primitive hematopoietic progenitors robustly generated erythrocytes from early embryonic stages (Figure 1B). In contrast, GFP+ definitive erythrocytes started to emerge after 2 dpf, accumulated in the CHT region starting at 4 dpf (Figure 1C) and their contribution to the erythrocyte pool was not appreciable until later larval developmental stages (~12 dpf, Figures 1C–1F).

These results indicate that erythrocytes emerge in a layered organization during embryonic and early larval stages as in mammals,[23] and that primitive hematopoietic progenitors generate a sufficient number of erythrocytes to sustain embryonic survival and tissue homeostasis.[24]

Embryonic macrophages originate exclusively from primitive hematopoietic progenitors

To assess the contribution of definitive hematopoietic progenitors to the embryonic macrophage pool, we marked the latter by combining the Tg(*fli1a:CreERT2*) line with the macrophage-specific Tg(mpeg1:LoxP-DsRedx-LoxP-GFP-NTR) line (referred to hereafter as mpeg1:switch).[25,26] As aforementioned, 4-OHT-induced cre recombination leads to permanent GFP expression in fli1a+-derived macrophages progeny (Figure 2A). Using this system, embryonic microglia cells, which are known to be of primitive hematopoietic origin in zebrafish,[7,13] were not labeled, indicating the precision of this labeling system (Figures S2A and S2B). While primitive macrophages contributed robustly to the embryonic macrophage pool, we found that definitive hematopoietic progenitors minimally contribute to macrophages during early developmental stages, akin to erythrocytes ontogeny (Figure 2B). We showed further that GFP+ definitive macrophages started to emerge after 2 dpf and gradually increased in numbers in the CHT region (Figures 2B and 2E) with a delayed modest contribution to the macrophage pool in the periphery starting after 4 dpf (Figures 2B–2D). GFP+ definitive macrophages contributed robustly to peripheral macrophages by 16 dpf, suggesting distinct differentiation kinetics of primitive and definitive macrophages throughout development (Figure 2C).

Altogether, our lineage tracing experiments show that aortic endothelium-derived hematopoietic progenitors are barely contributing to embryonic erythroid and myeloid lineages (Figures 1 and 2).

Ontogenetically distinct macrophages are differentially recruited to the site of injury

It has been recently reported that distinct macrophage subpopulations play different roles to promote tail regeneration after amputation.[27,28] However, whether ontogenetically distinct macrophages display different functions and recruitment behaviors to the site of injury remains

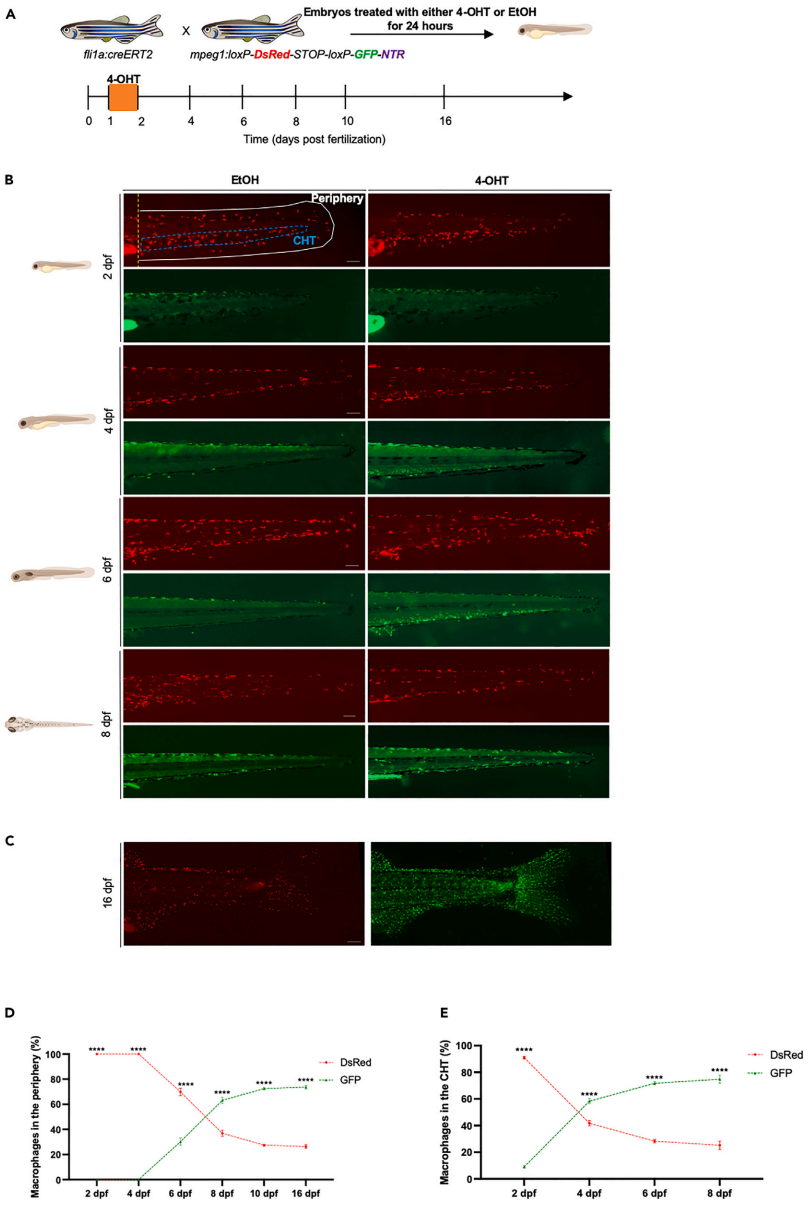
A
Embryos treated with either 4-OHT or EtOH
for 24 hours
fli1a:creERT2
X
mpeg1:loxP-DsRed-STOP-loxP-GFP-NTR
4-OHT
0 1 2 4 6 8 10 16
Time (days post fertilization)
B
EtOH
4-OHT
Periphery
CHT
2 dpf
4 dpf
6 dpf
8 dpf
C
16 dpf
D
Macrophages in the periphery (%)
DsRed
GFP
2 dpf 4 dpf 6 dpf 8 dpf 10 dpf 16 dpf
E
Macrophages in the CHT (%)
DsRed
GFP
2 dpf 4 dpf 6 dpf 8 dpf

Figure 2. Tracing the contribution of definitive hematopoietic waves to macrophages in the embryo and early larvae

(A) Scheme of the 4-OHT-inducible transgenic lines used to assess the contribution of definitive hematopoietic waves to the macrophage lineage.

(B) Fluorescent images of EtOH non-switched controls (left) and 4-OHT-induced (right) *Tg(fli1a:creERT2;mpeg1:Switch)* embryos and larvae (2–8 dpf). Macrophages were considered as peripheral macrophages (white area) or CHT-resident macrophages (blue area). Scale bars, 100 μm. Quantification of macrophages in the periphery and the CHT are shown in (D) and (E) respectively.

(C) Fluorescent images of 4-OHT-induced *Tg(fli1a:creERT2;mpeg1:Switch)* (16 dpf) in the periphery. Scale bar, 500 μm. Non-switched primitive macrophages (left) and definitive macrophages (right). Quantification of macrophages in the periphery is shown in (D).

(D) Quantification of DsRed and GFP macrophage number in the periphery was measured over a time course of 2–16 dpf. (2 dpf n = 6; 4 dpf n = 11; 6 dpf n = 7; 8 dpf n = 4; 10 dpf n = 5 and 16 dpf n = 5). Mean ± SEM of the $DsRed^+$ and GFP^+ macrophage number at each time point is shown. two-way ANOVA with Sidak's multiple comparison was used for this analysis. ****$p \leq 0.0001$.

(E) Quantification of DsRed and GFP macrophage number in the CHT was measured over a time course of 2–8 dpf. (2 dpf n = 6; 4 dpf n = 11; 6 dpf n = 7; and 8 dpf n = 4). Mean ± SEM of the $DsRed^+$ and GFP^+ macrophage number at each time point is shown. Two-way ANOVA with Sidak's multiple comparison was used for this analysis. ****$p \leq 0.0001$.

poorly understood. Therefore, we sought to analyze if macrophages of distinct origins are recruited in a differential manner to the damage site at different developmental stages. Using the same labeling strategy (Figure 2A), we analyzed macrophages recruitment to the damaged site in embryos (2 dpf) and larvae (5 dpf) since our lineage tracing experiments showed a different abundance of ontogenetically distinct macrophages at these developmental stages (Figure 2). In embryos, we observed that primitive macrophages were recruited to the site of injury at 24 h post amputation (hpa) and 48 hpa (Figures 3A and 3B; Figure S3A). We then analyzed macrophage recruitment to the damage site in larvae, where both primitive and definitive macrophage populations coexist in the periphery. We did not observe differences in the recruitment of both primitive and definitive macrophages to the damage site 24 hpa with a slight increase in the number of definitive macrophages 48 hpa (Figures 3C and 3E; Figure S3B). Altogether, these results suggest that primitive macrophages can alone modulate tail fin regeneration during embryonic stages while both macrophage populations are recruited to the damaged site in the larvae.

Previous reports showed that the first recruited macrophages play an important role in proper tail fin regeneration,[28–30] therefore, we further analyzed which macrophage population is recruited first to the site of injury. We found that primitive macrophages are recruited earlier than their definitive counterparts showed by the reduced number of definitive macrophages recruited to the site of injury from 3 to 12 hpa (Figures 3E and 3F). In addition, primitive macrophages manifested signs of active phagocytosis activity as early as 3 hpa evidenced by the appearance of vacuoles in their cell bodies (Figure 3D). Since our observation of a delay in the recruitment of definitive macrophages could be the result of differences in the number of primitive and definitive macrophages in the periphery at the time of injury, we attempted to normalize their numbers. Data were normalized by dividing the number of each recruited macrophage subpopulation by their total number in the tail of the same larvae.[28] After normalization, we still observed that primitive macrophages are recruited earlier compared to their definitive counterparts with a reduced recruitment of definitive macrophages at 3, 6, and 12 hpa, when compared to their primitive counterparts (Figure 3F). These data indicate that primitive macrophages, as the first arrivals to the damage site, may have a specific role in the regeneration process after amputation during development.

Selective ablation of definitive macrophages does not impair tail fin regeneration during early larval developmental stages

To evaluate the contribution of ontogenetically distinct macrophages to tail fin regeneration, we used the mpeg1 switch line *Tg(mpeg1:loxP-dsRed-loxP-eGFP-NTR)* that allows selective ablation of macrophages based on their origin. In this line, the expression of bacterial nitroreductase (NTR) is under the control of the *mpeg1* promoter.[26] Thus, the NTR will be expressed exclusively in the traced macrophages, thereby, traced macrophages could be ablated by metronidazole (MTZ) treatment[31] (Figure 4A). To assess the efficiency of the NTR-MTZ system, we quantified the number of primitive and definitive macrophages in the tail after treatment with either DMSO or MTZ for 48 h from 4 to 6 dpf. We found that while primitive macrophages were not affected by the MTZ treatment, definitive macrophages were significantly reduced after 48 h of MTZ treatment (Figures S3C and S3D).

We next performed tail fin amputation in 5 dpf larvae that were treated with either DMSO or MTZ from 4 to 6 dpf to ensure ablation of definitive macrophages through the regeneration process. While primitive macrophage numbers and recruitment were not affected during the regeneration process, definitive macrophages were significantly reduced during the first 48 hpa but recovered by 72 hpa (Figures 4B–4E; Figure S3E). Next, we analyzed macrophage recruitment to the site of injury in MTZ-treated larvae from 24 to 72 hpa. We normalized the number of recruited macrophages by the number of total macrophages in the tail at their respective time points, and we observed a decrease in the number of recruited definitive macrophages during the first 48 hpa, indicating the efficiency of the MTZ-mediated selective ablation of definitive macrophages (Figure 4F). We then performed tail fin regeneration analysis and observed no differences in the regenerated tail fin area between larvae treated with either DMSO or MTZ (Figures 4G and 4H). Furthermore, cell proliferation was not altered in the regenerated tail of 72 hpa larvae with either DMSO or MTZ (Figures S3F and S3G).

To determine if this observation could be replicated in the absence of definitive macrophages, we analyzed tail fin regeneration in *cmyb*-deficient zebrafish that lack HSCs, have impaired definitive hematopoiesis and have reduced numbers of definitive macrophages.[7,32,33] We found no differences in regeneration efficiency, measured by the tail fin area, between *cmyb*-deficient and wild-type larvae (Figures 4I and 4J). Our results, thus, indicate that primitive macrophages recruitment to the damage site is not affected and tail fin regeneration is not impaired when definitive macrophages are depleted.

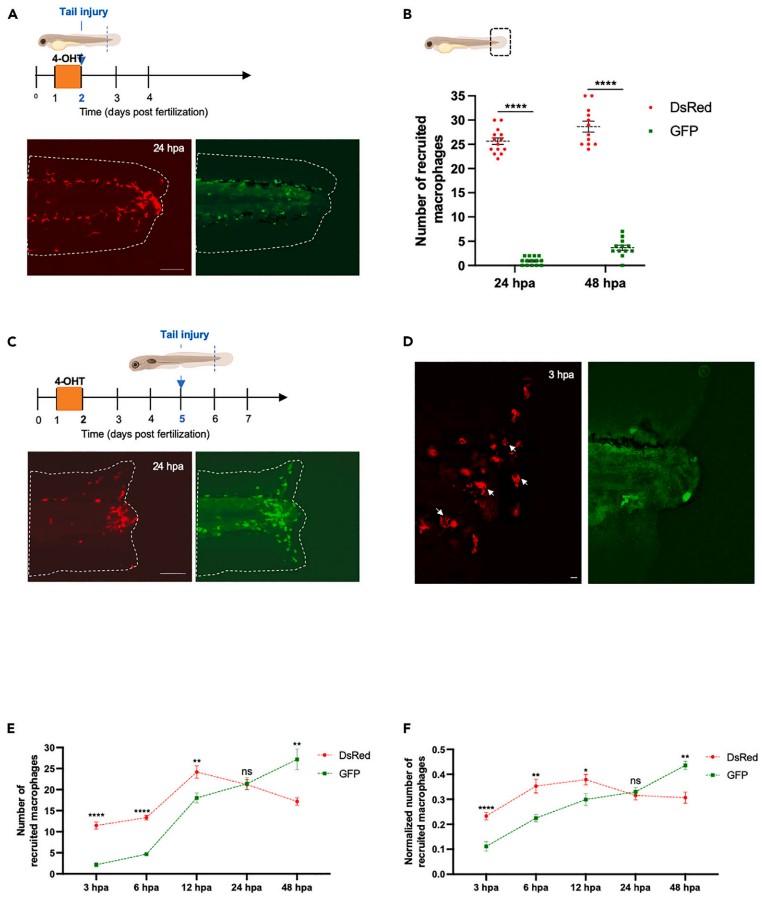

Figure 3. Ontogenetically distinct macrophages exhibit different migration behavior and recruitment after tissue injury during early developmental stages

(A) Diagram showing the amputation plan, tail fin of *Tg(fli1a:creERT2;mpeg1:Switch)* were amputated at 2 dpf and macrophages recruitment to the site of injury was analyzed. Representative images are shown at 24 hpa. Scale bar: 100μm.

(B) Diagram showing the counting region in the larvae. Quantification of DsRed and GFP macrophage number at the site of injury at 24 hpa (n = 14) and 48 hpa (n = 12). Mean ± SEM of the $DsRed^+$ and GFP^+ macrophage number at each time point is shown. ****$p \leq 0.0001$.

(C) Diagram showing the amputation plan, tail fin of *Tg(fli1a:creERT2;mpeg1:Switch)* were amputated at 5 dpf and macrophages recruitment to the site of injury was analyzed. Representative images are shown at 24 hpa. Scale bar: 100μm.

(D) Tail fin of *Tg(fli1a:creERT2;mpeg1:Switch)* were amputated at 5 dpf and macrophages recruitment to the site of injury was analyzed. Representative images are shown at 3 hpa. White arrows indicate the primitive macrophages with big vacuoles. Scale bar: 10μm.

(E) Quantification of DsRed and GFP macrophage number at the site of injury at 3 hpa (n = 13); 6 hpa (n = 6); 12 hpa (n = 6); 24 hpa (n = 10); and 48 hpa (n = 6). Mean ± SEM of the $DsRed^+$ and GFP^+ macrophage number at each time point is shown. ns, $p > 0.05$; **$p \leq 0.01$; ****$p \leq 0.0001$.

(F) Quantification of dsRed and GFP macrophage number at the site of injury at 3 hpa (n = 13); 6 hpa (n = 6); 12 hpa (n = 6); 24 hpa (n = 10) and 48 hpa (n = 6). Mean ± SEM of the $DsRed^+$ and GFP^+ macrophage number at each time point is shown. Quantification was normalized by the number of total macrophages in the tail of the respective larvae (the sum of peripheral, CHT and recruited macrophages of distinct origins). ns, $p > 0.05$; *$p \leq 0.05$; **$p \leq 0.01$; ****$p \leq 0.0001$.

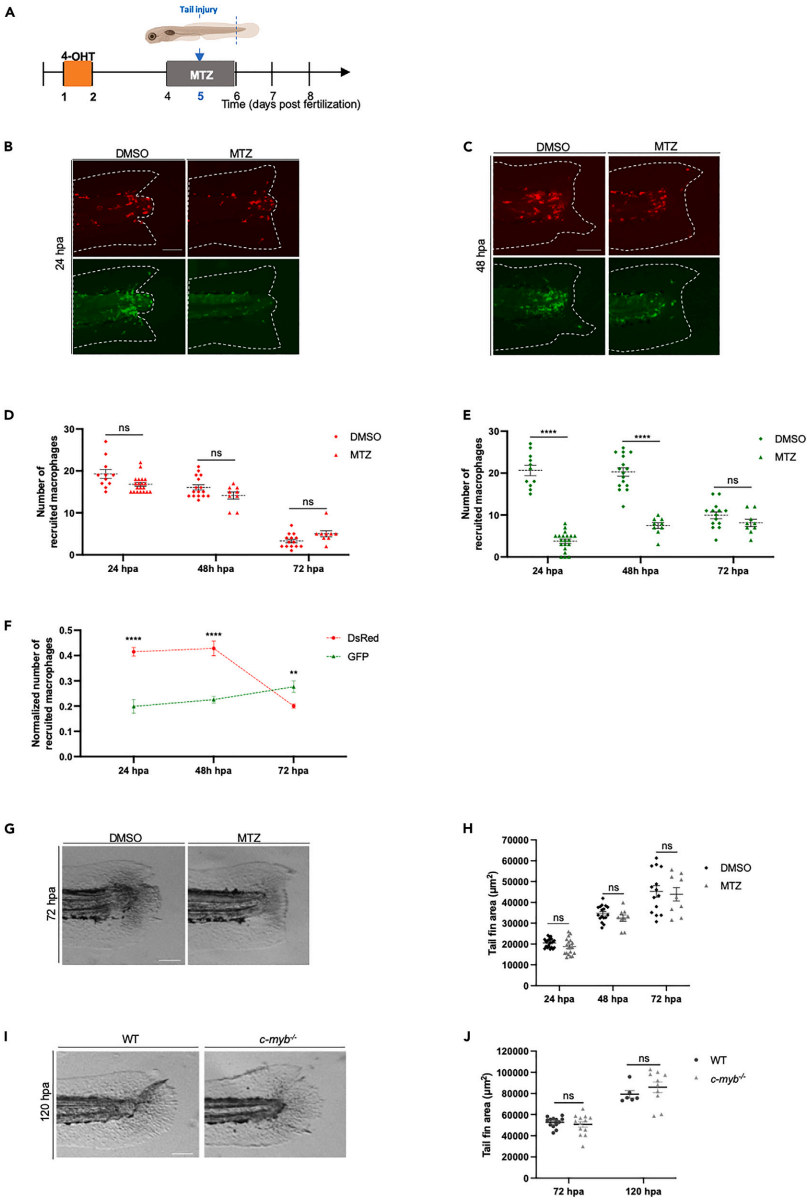
A
Tail injury
4-OHT
MTZ
1 2 4 5 6 7 8
Time (days post fertilization)
B
DMSO
MTZ
24 hpa
C
DMSO
MTZ
48 hpa
D
Number of recruited macrophages
ns
DMSO
MTZ
24 hpa
48h hpa
72 hpa
E
Number of recruited macrophages
****
ns
DMSO
MTZ
24 hpa
48h hpa
72 hpa
F
Normalized number of recruited macrophages
****
**
DsRed
GFP
24 hpa
48h hpa
72 hpa
G
DMSO
MTZ
72 hpa
H
Tail fin area (μm²)
ns
DMSO
MTZ
24 hpa
48 hpa
72 hpa
I
WT
c-myb-/-
120 hpa
J
Tail fin area (μm²)
ns
WT
c-myb-/-
72 hpa
120 hpa

Figure 4. Selective ablation of definitive macrophages does not impair tail fin regeneration in early larvae

(A) Diagram showing the macrophage ablation and tail fin amputation plan.

(B and C) Switched *Tg(fli1a:creERT2;mpeg1:Switch)* larvae were treated with DMSO as a control, or metronidazole (MTZ) to ablate definitive macrophages. Treatments were performed from 4 to 6 dpf and tail fins were amputated at 5 dpf. Representative images are shown 24 hpa in (B) and 48 hpa in (C). Scale bars: 100 μm.

(D) Quantification of DsRed recruited macrophage number in the tail region at 24, 48 and 72 hpa in larvae treated at 4 dpf with either DMSO or MTZ for 48 h (24 hpa: DMSO = 11, MTZ = 20; 48 hpa: DMSO n = 16, MTZ n = 9; 72 hpa: DMSO n = 14, MTZ n = 9). Mean ± SEM of the $DsRed^+$ macrophage number is shown. ns, $p > 0.05$.

(E) Quantification of GFP recruited macrophage number in the tail region at 24, 48, and 72 hpa in larvae treated at 4 dpf with either DMSO or MTZ for 48 h (24 hpa: DMSO = 11, MTZ = 20; 48 hpa: DMSO n = 16, MTZ n = 9; 72 hpa: DMSO n = 14, MTZ n = 9). Mean ± SEM of the GFP^+ macrophage number is shown. ns, $p > 0.05$; ****$p \leq 0.0001$.

(F) Quantification of DsRed and GFP macrophage number at the site of injury at 24, 48 and 72 hpa. Quantification was normalized by the number of total macrophages in the tail of the respective larvae (the sum of peripheral, CHT and recruited macrophages of distinct origins). **$p \leq 0.01$; ****$p \leq 0.0001$.

(G) Representative images of regenerating tail fins of larvae at 72 hpa. Larvae were treated with either DMSO or MTZ. Scale bars: 100 μm.

(H) Tail fin area quantification of regenerating tail fins at 24, 48 and 72 hpa in larvae treated with either DMSO or MTZ (24 hpa: DMSO n = 21, MTZ n = 20; 48 hpa: DMSO n = 17, MTZ n = 9; 72 hpa: DMSO n = 14, MTZ n = 9). Mean ± SEM of the tail fin area is shown. ns, $p > 0.05$.

(I) Representative images of regenerating tail fins of $cmyb^{null}$ and WT larvae at 120 hpa. Scale bars: 100 μm.

(J) Tail fin area quantification of regenerating tail fins of $cmyb^{null}$ and WT larvae at 72 hpa and 120 hpa (72 hpa: $cmyb^{null}$ n = 13, WT n = 13; 120 hpa: $cmyb^{null}$ n = 10, WT n = 6). Mean ± SEM of the tail fin area is shown. ns, $p > 0.05$.

Depletion of primitive macrophages impairs tail fin regeneration in early larvae

To characterize the role of primitive macrophages in tail fin regeneration during early larval developmental stages, we chemically depleted them at 48 hpf, before the maturation of their definitive counterparts as previously reported in zebrafish[34] (Figure 5A). In line with previous studies,[28,29,34] intravenous injection of L-clodronate at 48 hpf efficiently depleted macrophages in 5 dpf zebrafish larvae (Figures 5B and 5C). Thus, we performed tail fin amputation and regeneration analysis in L-clodronate injected larvae and compared them with L-PBS injected controls (Figures 5D and 5E). We found fewer macrophages at the injury site in L-clodronate injected fish compared to L-PBS injected controls (Figure 5F), suggesting primitive macrophage ablation at 72 and 120 hpa. In contrast to the selective ablation of definitive macrophages (Figure 4), depletion of primitive macrophages impaired tail fin regeneration, as measured by the tail fin area, at 72 hpa and 120 hpa (Figures 5D and 5E). These observations suggest that primitive macrophage depletion leads to tail fin regeneration defects, highlighting the functional differences among macrophages based on their ontogeny. Overall, these results shed light on the critical role of early recruited primitive macrophages during tail fin regeneration in early zebrafish larvae.

DISCUSSION

Two major waves of hematopoietic progenitors are generated during embryogenesis: the primitive and the definitive waves. Both waves generate erythromyeloid progenitors during embryogenesis, however, having a dual source of blood progenitors makes it difficult to assess accurately each wave contribution to blood lineages in homeostasis and upon tissue injury. Therefore, the lack of specific markers to identify different populations from the same blood lineage according to their origin and function has hindered the full understanding of immune cell ontogeny.

Here, we classified hematopoietic waves according to their site of origin and tracked them during homeostasis and upon recruitment to the site of injury. Our study shows that the hematopoietic system follows a layered strategy to provide a timely supply of innate immune cells and erythrocytes. Under steady-state conditions, we found that the contribution of definitive hematopoietic progenitors to embryonic erythromyeloid lineage is limited. This is of particular interest as none of the lineage tracing strategies performed in mice, despite their elegant designs, are specific to definitive hematopoietic waves. Our results also complement the recently reported observations that HSCs have a delayed contribution to the lymphomyeloid lineage during development.[10]

In addition, as timely recruitment of macrophages to the damage site is important to ensure proper tail fin regeneration,[27–30] we found that the primitive macrophages are the first responders after tail fin injury showed by their active phagocytic activity as early as 3 hpa and their earlier recruitment than their definitive counterparts. The difference in recruitment behavior between primitive and definitive macrophages could be due to that the primitive macrophages are more sensitive to damage sensing and/or a consequence of the immaturity of definitive macrophages at early developmental stages. However, we delineated that definitive macrophages regenerate following their depletion but are not required for tail regeneration during early developmental stages. These intriguing results suggest that embryos and early larvae adopt a layered ontogeny of macrophages to ensure their abundance for a timely contribution to tissue regeneration. Further studies are needed to determine the molecular signatures of these ontogenetically distinct populations accounting for their different behaviors.

A significant discovery from our study highlights the key role of primitive macrophages in orchestrating tissue regeneration. Depletion of primitive macrophages during early developmental stages had a negative impact on the regeneration of tail fins. In contrast, the selective ablation of definitive macrophages did not hinder tail fin regeneration. This conclusion is supported by additional experiments, where we independently targeted either the definitive or primitive macrophage populations using two distinct methods and then analyzed the regrowth of tail fins in amputated larvae. These results underscore the remarkable capacity of primitive macrophages to facilitate timely tissue regeneration.

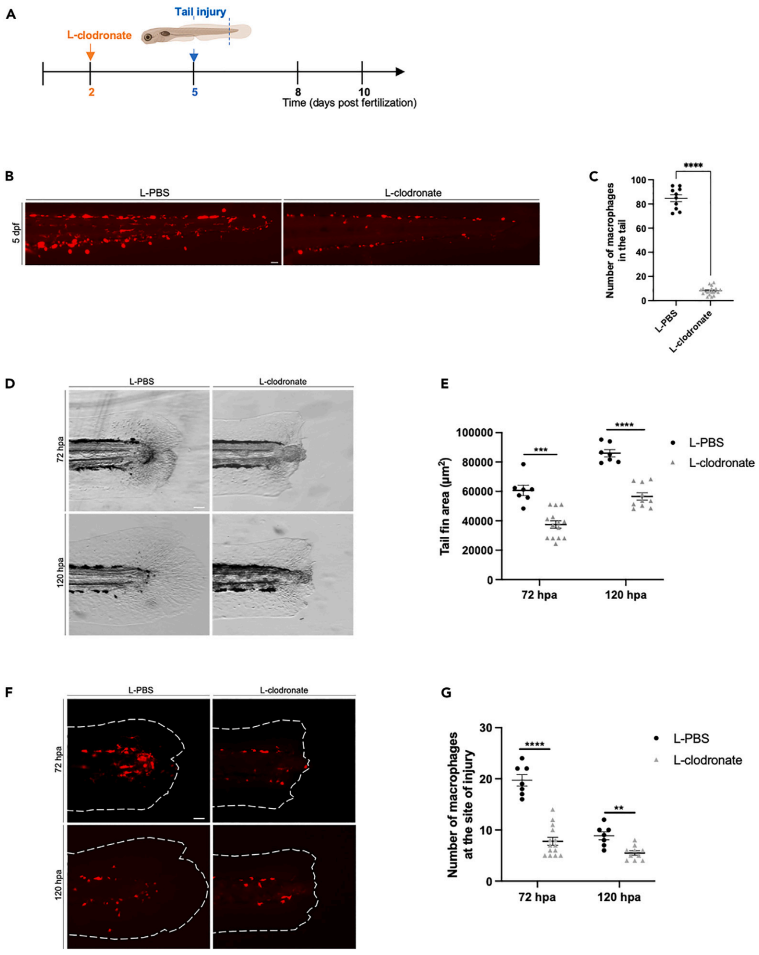

Figure 5. Depletion of primitive macrophages impair tail fin regeneration in early larvae

(A) Diagram showing the macrophage depletion using L-clodronate injection and tail fin amputation plan.

(B) *Tg(mpeg1:*Switch) larvae were injected at 48 hpf with L-PBS as a control, or L-clodronate (L-clo) to deplete primitive macrophages. Representative images are shown at 5 dpf. Scale bars: 100 µm.

(C) Quantification of DsRed macrophage number in the tail region at 5 dpf in larvae injected with either L-PBS (n = 10) or L-clo (n = 18). Mean ± SEM of the $DsRed^{+}$ macrophage number is shown. ****$p \leq 0.0001$.

(D) Representative images of regenerating tail fins of larvae at 72 and 120 hpa. Larvae were injected with either L-PBS or L-clodronate. Scale bars: 100 µm.

(E) Tail fin area quantification of regenerating tail fins at 72 and 120 hpa in larvae injected with either L-PBS or L-clodronate (72 hpa: L-PBS n = 7, L-clo n = 14; 72 hpa: L-PBS n = 7, L-clo n = 10). Mean ± SEM of the tail fin area is shown. ***$p \leq 0.001$; ****$p \leq 0.0001$.

(F) Representative images of the macrophages recruitment to the site of injury at 72 and 120 hpa in larvae injected with either L-PBS or L-clo. Scale bars: 100 µm.

(G) Quantification of the number of macrophages at the site of injury at 72 and 120 hpa (72 hpa: L-PBS = 7, L-clo n = 14; 120 hpa: L-PBS = 7, L-clo n = 10). Mean ± SEM of the macrophage number is shown. **$p \leq 0.01$; ****$p \leq 0.0001$.

In conclusion, our study provides insights into the ontogeny of the erythromyeloid lineage during embryonic/early larval developmental stages. Our findings support the notion that embryos show a sequential emergence of hematopoietic waves to ensure the abundance of macrophages required for tissue homeostasis and regeneration during a crucial developmental time window. In line with our results, it has been recently reported in mice[11,35–37] and in zebrafish[8,10] that embryonic and adult HSCs do not give rise to several blood subtypes at steady state, upon ablation of mature blood cells, and in response to immune challenge. These observations indicate that ensuring a rapid response to stress to maintain tissue homeostasis in an HSC-independent manner might be a conserved mechanism between species throughout their life.

Limitations of the study

fli1a is expressed in mature thrombocytes[38] and is expressed also at 10 hpf in the lateral mesoderm.[39] Therefore, we used an inducible system to label all definitive hematopoietic progenitors as they emerge from hemogenic endothelium at 24 hpf. Using our labeling strategy, we could not distinguish distinct definitive hematopoietic progenitors as they all share the expression of *fli1a*$^{+}$ as they go through EHT,[1,3,10]therefore, better tools are required. Furthermore, in our study, we were not able to selectively ablate the primitive macrophage population because of lacking a specific marker to the primitive hematopoietic progenitors and their progeny. In addition, we were unable to guarantee that all definitive hematopoietic progenitors were successfully labeled. According to the tracing result that ~80% of thymocytes were labeled, there is still a remaining ~20% of cells that likely derived from unlabeled definitive progenitors due to the incomplete *loxP* recombination.

STAR★METHODS

Detailed methods are provided in the online version of this paper and include the following:

- KEY RESOURCES TABLE
- RESOURCE AVAILABILITY
  - Lead contact
  - Materials availability
  - Data and code availability
- EXPERIMENTAL MODEL AND STUDY PARTICIPANT DETAILS
  - Zebrafish
  - Transgenic lines
- METHOD DETAILS
  - Fluorescence microscopy
  - Image analysis
  - CreER-loxP cell labelling (lineage tracing)
  - Macrophage ablation and drug treatments
  - Tail fin amputation
  - Quantification of tail fin regeneration
  - Quantification of tail macrophages
  - Cell proliferation analysis
- QUANTIFICATION AND STATISTICAL ANALYSIS

SUPPLEMENTAL INFORMATION

Supplemental information can be found online at https://doi.org/10.1016/j.isci.2024.108922.

ACKNOWLEDGMENTS

We thank the Developmental Biology Curie imaging facility (PICT-IBiSA@BDD, Paris, France, UMR3215/U934) members of the France-BioImaging national research infrastructure for their help and advice. We also thank the members of the animal facility of Institut Curie for zebrafish care. We also thank Yohanns Bellaiche and all the members of the Hernandez lab for thoughtful and valuable discussions. We are grateful to Nadia Mercader for providing the Tg(*fli1a:CreERT2*), we also thank Zilong Wen for providing all the immune and blood lineage switch lines used in this study. This work was supported by the Institut Curie, Inserm, CNRS, the Ville de Paris emergence program (2020 DAE 78), FRM amorçage (AJE201905008718), ATIP-Avenir starting grant R21045DS and the Laboratoire d'Excellence (Labex) DEEP (ANR-11- LBX-0044, ANR-10-IDEX- 0001-02 PSL), ECOS-ANID C22S01-220029. R.E. was supported by the Springboard postdoctoral fellowship from Institut Curie and Labex DEEP.

AUTHOR CONTRIBUTIONS

Conceptualization: R.E. and P.P.H.; Methodology and data collection: R.E., A.M., K.C., Y.S., P.D., and G.G.; Writing - original draft: R.E.; Writing - review and editing: R.E. and P.P.H.; Funding Acquisition: P.P.H.

DECLARATION OF INTERESTS

The authors declare no competing interests.

Received: March 8, 2023
Revised: September 23, 2023
Accepted: January 12, 2024
Published: January 17, 2024

REFERENCES

1. Bertrand, J.Y., Chi, N.C., Santoso, B., Teng, S., Stainier, D.Y.R., and Traver, D. (2010). Haematopoietic stem cells derive directly from aortic endothelium during development. Nature *464*, 108–111.
2. Boisset, J.-C., van Cappellen, W., Andrieu-Soler, C., Galjart, N., Dzierzak, E., and Robin, C. (2010). In vivo imaging of haematopoietic cells emerging from the mouse aortic endothelium. Nature *464*, 116–120.
3. Kissa, K., and Herbomel, P. (2010). Blood stem cells emerge from aortic endothelium by a novel type of cell transition. Nature *464*, 112–115.
4. Elsaid, R., Soares-da-Silva, F., Peixoto, M., Amiri, D., Mackowski, N., Pereira, P., Bandeira, A., and Cumano, A. (2020). Hematopoiesis: A Layered Organization Across Chordate Species. Front. Cell Dev. Biol. *8*, 606642.
5. Herbomel, P., Thisse, B., and Thisse, C. (2001). Zebrafish Early Macrophages Colonize Cephalic Mesenchyme and Developing Brain, Retina, and Epidermis through a M-CSF Receptor-Dependent Invasive Process. Dev. Biol. *238*, 274–288.
6. Bertrand, J.Y., Kim, A.D., Violette, E.P., Stachura, D.L., Cisson, J.L., and Traver, D. (2007). Definitive hematopoiesis initiates through a committed erythromyeloid progenitor in the zebrafish embryo. Development *134*, 4147–4156.
7. Ferrero, G., Mahony, C.B., Dupuis, E., Yvernogeau, L., Di Ruggiero, E., Miserocchi, M., Caron, M., Robin, C., Traver, D., Bertrand, J.Y., and Wittamer, V. (2018). Embryonic Microglia Derive from Primitive Macrophages and Are Replaced by cmyb-Dependent Definitive Microglia in Zebrafish. Cell Rep. *24*, 130–141.
8. Tian, Y., Xu, J., Feng, S., He, S., Zhao, S., Zhu, L., Jin, W., Dai, Y., Luo, L., Qu, J.Y., and Wen, Z. (2017). The first wave of T lymphopoiesis in zebrafish arises from aorta endothelium independent of hematopoietic stem cells. J. Exp. Med. *214*, 3347–3360.
9. Murayama, E., Kissa, K., Zapata, A., Mordelet, E., Briolat, V., Lin, H.-F., Handin, R.I., and Herbomel, P. (2006). Tracing hematopoietic precursor migration to successive hematopoietic organs during zebrafish development. Immunity *25*, 963–975.
10. Ulloa, B.A., Habbsa, S.S., Potts, K.S., Lewis, A., McKinstry, M., Payne, S.G., Flores, J.C., Nizhnik, A., Feliz Norberto, M., Mosimann, C., and Bowman, T.V. (2021). Definitive hematopoietic stem cells minimally contribute to embryonic hematopoiesis. Cell Rep. *36*, 109703.
11. Patel, S.H., Christodoulou, C., Weinreb, C., Yu, Q., da Rocha, E.L., Pepe-Mooney, B.J., Bowling, S., Li, L., Osorio, F.G., Daley, G.Q., and Camargo, F.D. (2022). Lifelong multilineage contribution by embryonic-born blood progenitors. Nature *606*, 747–753.
12. Stachura, D.L., and Traver, D. (2011). Chapter 4 - Cellular Dissection of Zebrafish Hematopoiesis. In Methods in Cell Biology The Zebrafish: Cellular and Developmental Biology, B. Part, H.W. Detrich, M. Westerfield, and L.I. Zon, eds. (Academic Press), pp. 75–110.
13. Xu, J., Zhu, L., He, S., Wu, Y., Jin, W., Yu, T., Qu, J.Y., and Wen, Z. (2015). Temporal-Spatial Resolution Fate Mapping Reveals Distinct Origins for Embryonic and Adult Microglia in Zebrafish. Dev. Cell *34*, 632–641.
14. McGrath, K.E., Frame, J.M., and Palis, J. (2015). Early hematopoiesis and macrophage development. Semin. Immunol. *27*, 379–387.
15. Henninger, J., Santoso, B., Hans, S., Durand, E., Moore, J., Mosimann, C., Brand, M., Traver, D., and Zon, L. (2017). Clonal fate mapping quantifies the number of haematopoietic stem cells that arise during development. Nat. Cell Biol. *19*, 17–27.
16. Herbomel, P., Thisse, B., and Thisse, C. (1999). Ontogeny and behaviour of early macrophages in the zebrafish embryo. Development *126*, 3735–3745.
17. Ganis, J.J., Hsia, N., Trompouki, E., de Jong, J.L.O., DiBiase, A., Lambert, J.S., Jia, Z., Sabo, P.J., Weaver, M., Sandstrom, R., et al. (2012). Zebrafish globin Switching Occurs in Two Developmental Stages and is Controlled by the LCR. Dev. Biol. *366*, 185–194.
18. Sánchez-Iranzo, H., Galardi-Castilla, M., Sanz-Morejón, A., González-Rosa, J.M., Costa, R., Ernst, A., Sainz de Aja, J., Langa, X., and Mercader, N. (2018). Transient fibrosis resolves via fibroblast inactivation in the regenerating zebrafish heart. Proc. Natl. Acad. Sci. USA *115*, 4188–4193.
19. Carney, T.J., and Mosimann, C. (2018). Switch and Trace: Recombinase Genetics in Zebrafish. Trends Genet. *34*, 362–378.
20. Langenau, D.M., Ferrando, A.A., Traver, D., Kutok, J.L., Hezel, J.-P.D., Kanki, J.P., Zon, L.I., Look, A.T., and Trede, N.S. (2004). In vivo tracking of T cell development, ablation, and engraftment in transgenic zebrafish. Proc. Natl. Acad. Sci. USA *101*, 7369–7374.
21. Li, L., Yan, B., Shi, Y.-Q., Zhang, W.-Q., and Wen, Z.-L. (2012). Live Imaging Reveals Differing Roles of Macrophages and Neutrophils during Zebrafish Tail Fin Regeneration. J. Biol. Chem. *287*, 25353–25360.
22. Elsaid, R., Meunier, S., Burlen-Defranoux, O., Soares-da-Silva, F., Perchet, T., Iturri, L., Freyer, L., Vieira, P., Pereira, P., Golub, R., et al. (2021). A wave of bipotent T/ILC-restricted progenitors shapes the embryonic thymus microenvironment in a time-dependent manner. Blood *137*, 1024–1036.
23. Soares-da-Silva, F., Freyer, L., Elsaid, R., Burlen-Defranoux, O., Iturri, L., Sismeiro, O., Pinto-do-Ó, P., Gomez-Perdiguero, E., and Cumano, A. (2021). Yolk sac, but not hematopoietic stem cell-derived progenitors, sustain erythropoiesis throughout murine embryonic life. J. Exp. Med. *218*, e20201729.
24. Palis, J. (2014). Primitive and definitive erythropoiesis in mammals. Front. Physiol. *5*, 3.
25. Lin, X., Zhou, Q., Zhao, C., Lin, G., Xu, J., and Wen, Z. (2019). An Ectoderm-Derived Myeloid-like Cell Population Functions as Antigen Transporters for Langerhans Cells in Zebrafish Epidermis. Dev. Cell *49*, 605–617.e5.
26. Ellett, F., Pase, L., Hayman, J.W., Andrianopoulos, A., and Lieschke, G.J. (2011). mpeg1 promoter transgenes direct macrophage-lineage expression in zebrafish. Blood *117*, e49–e56.
27. Wynn, T.A., and Vannella, K.M. (2016). Macrophages in Tissue Repair, Regeneration, and Fibrosis. Immunity *44*, 450–462.
28. Morales, R.A., and Allende, M.L. (2019). Peripheral Macrophages Promote Tissue Regeneration in Zebrafish by Fine-Tuning the Inflammatory Response. Front. Immunol. *10*, 253.
29. Nguyen-Chi, M., Laplace-Builhé, B., Travnickova, J., Luz-Crawford, P., Tejedor, G., Lutfalla, G., Kissa, K., Jorgensen, C., and Djouad, F. (2017). TNF signaling and macrophages govern fin regeneration in zebrafish larvae. Cell Death Dis. *8*, e2979.
30. Petrie, T.A., Strand, N.S., Yang, C.T., Rabinowitz, J.S., and Moon, R.T. (2014). Macrophages modulate adult zebrafish tail fin regeneration. Development *141*, 2581–2591.
31. Curado, S., Stainier, D.Y.R., and Anderson, R.M. (2008). Nitroreductase-mediated cell/tissue ablation in zebrafish: a spatially and temporally controlled ablation method with applications in developmental and regeneration studies. Nat. Protoc. *3*, 948–954.
32. Soza-Ried, C., Hess, I., Netuschil, N., Schorpp, M., and Boehm, T. (2010). Essential role of *c-myb* in definitive hematopoiesis is evolutionarily conserved. Proc. Natl. Acad. Sci. USA *107*, 17304–17308.
33. He, S., Chen, J., Jiang, Y., Wu, Y., Zhu, L., Jin, W., Zhao, C., Yu, T., Wang, T., Wu, S., et al. (2018). Adult zebrafish Langerhans cells arise from hematopoietic stem/progenitor cells. Elife *7*, e36131.
34. Travnickova, J., Tran Chau, V., Julien, E., Mateos-Langerak, J., Gonzalez, C., Lelièvre, E., Lutfalla, G., Tavian, M., and Kissa, K. (2015). Primitive macrophages control HSPC mobilization and definitive haematopoiesis. Nat. Commun. *6*, 6227.
35. Gomez Perdiguero, E., Klapproth, K., Schulz, C., Busch, K., Azzoni, E., Crozet, L., Garner, H., Trouillet, C., de Bruijn, M.F., Geissmann, F., and Rodewald, H.R. (2015). Tissue-resident macrophages originate from yolk-sac-derived erythro-myeloid progenitors. Nature *518*, 547–551.

36. Yokomizo, T., Ideue, T., Morino-Koga, S., Tham, C.Y., Sato, T., Takeda, N., Kubota, Y., Kurokawa, M., Komatsu, N., Ogawa, M., et al. (2022). Independent origins of fetal liver haematopoietic stem and progenitor cells. Nature *609*, 779–784.

37. Fanti, A.-K., Busch, K., Greco, A., Wang, X., Cirovic, B., Shang, F., Nizharadze, T., Frank, L., Barile, M., Feyerabend, T.B., et al. (2023). Flt3- and Tie2-Cre tracing identifies regeneration in sepsis from multipotent progenitors but not hematopoietic stem cells. Cell Stem Cell *30*, 207–218.e7.

38. Jagadeeswaran, P., Lin, S., Weinstein, B., Hutson, A., and Kim, S. (2010). Loss of GATA1 and gain of FLI1 expression during thrombocyte maturation. Blood Cells Mol. Dis. *44*, 175–180.

39. Hsia, N., and Zon, L.I. (2005). Transcriptional regulation of hematopoietic stem cell development in zebrafish. Exp. Hematol. *33*, 1007–1014.

40. Schindelin, J., Arganda-Carreras, I., Frise, E., Kaynig, V., Longair, M., Pietzsch, T., Preibisch, S., Rueden, C., Saalfeld, S., Schmid, B., et al. (2012). Fiji: an open-source platform for biological-image analysis. Nat. Methods *9*, 676–682.

41. Renaud, O., Herbomel, P., and Kissa, K. (2011). Studying cell behavior in whole zebrafish embryos by confocal live imaging: application to hematopoietic stem cells. Nat. Protoc. *6*, 1897–1904.

42. Pei, W., Tanaka, K., Huang, S.C., Xu, L., Liu, B., Sinclair, J., Idol, J., Varshney, G.K., Huang, H., Lin, S., et al. (2016). Extracellular HSP60 triggers tissue regeneration and wound healing by regulating inflammation and cell proliferation. NPJ Regen. Med. *1*, 16013–16111.

STAR★METHODS

KEY RESOURCES TABLE

REAGENT or RESOURCE	SOURCE	IDENTIFIER
Chemicals, peptides, and recombinant proteins		
(Z)-4-Hydroxytamoxifen (4-OHT)	Sigma	Cat# H7904
Ethyl 3-aminobenzoate methane sulfonate salt (Tricaine)	Sigma	Cat# A5040
Dimethyl sulfoxide (DMSO)	Sigma	Cat# D5879
Metronidazole (MTZ)	Sigma	Cat# M1547
5-ethynyl-2′-deoxyuridine (EdU)	ThermoFisher SCIENTIFIC	Cat #C10340
L-clodronate	LIPOSOMA	www.clodronateliposomes.org
rowheadExperimental models: Organisms/strains		
Zebrafish Tg(fli1a: CreER^{T2})	Sánchez-Iranzo et al., [18]	ZFIN: ZDBTGCONSTRCT-170711-8
Zebrafish Tg(mpeg1:LoxP-DsRedx-LoxP-GFP-NTR)	Lin et al., [25]	ZFIN: ZDB-ALT-191122-8
Tg(coro1a:loxP-DsRedx-loxP-GFP)	Xu et al., [13]	ZFIN: ZDB-TGCONSTRCT-160114-1
Tg(globin:loxP-DsRedx-loxP-GFP)	Tian et al., [8]	ZFIN: ZDB-TGCONSTRCT-180702-2
Tg(lck:loxP-DsRedx-loxP-GFP)	Tian et al., [8]	ZFIN: ZDB-TGCONSTRCT-180702-3
Tg(cmyb$^{+/-}$;kdrl:Cre^{+} ; ßactin:Switch-DsRed^{+})	Ferrero et al., [7]	N/A
Software and algorithms		
ImageJ	Schindelin et al.[40]	https://imagej.nih.gov/ij/
Prism 9	GraphPad	https://www.graphpad.com/

RESOURCE AVAILABILITY

Lead contact

Further information and requests for scripts, resources, and reagents should be directed to and will be fulfilled by lead contact, Pedro P. Hernández (pedro.hernandez-cerda@curie.fr).

Materials availability

This study did not generate new unique reagents. The data sets generated during the current study are available from the corresponding authors upon request.

Data and code availability

- Data sets reported in this paper will be shared by the lead contact upon request.
- Any additional information required to reanalyze the data reported in this paper is available from the lead contact upon request.
- This paper does not report original code.

EXPERIMENTAL MODEL AND STUDY PARTICIPANT DETAILS

Zebrafish

Embryonic and adult zebrafish (Danio rerio) were maintained at 28°C on a 14-hour light/10-hour dark cycle. The collected embryos were raised in fish water containing 0.01% methylene blue to prevent fungal growth. All fish are housed in the fish facility of our laboratory, which was built according to the local animal welfare standards. Animal care and use for this study were performed in accordance with the recommendations of the European Community (2010/63/UE) for the care and use of laboratory animals. Experimental procedures were specifically approved by the ethics committee of the Institut Curie CEEA-IC #118 (Authorization number - APAFiS#21197-2019062521156746-v2 - given by National Authority) in compliance with the international guidelines." Embryo and Larval zebrafish were studied before the onset of sexual differentiation and their sex can therefore not be determined.

Transgenic lines

The following lines of the AB stain were used: Tg(fli1a: CreERT2),[18] Tg(mpeg1:LoxP-DsRedx-LoxP-GFP-NTR),[25]Tg(coro1a:loxP-DsRedx-loxP-GFP),[13] Tg(globin:loxP-DsRedx-loxP-GFP),[8] Tg(lck:loxP-DsRedx-loxP-GFP)[8] and Tg(cmyb$^{+/-}$; kdrl:Cre+; ßactin:Switch-DsRed+)[7] *cmyb*^{null} embryos were identified at 5 dpf based on the absence of HSC-derived *DsRed*$^{+}$ thymocytes.

METHOD DETAILS

Fluorescence microscopy

Zebrafish embryos, larvae and adults were anesthetized with 0.01% tricaine (A5040, Sigma) and mounted in 2.5% 2.5% methylcellulose in 35-mm imaging dishes (MatTek) as described previously.[41] Fluorescent imaging was performed with either Zeiss Axio Zoom V.16 upright microscope with an AxioCam HRm Zeiss camera and Zeiss Zen 3.3 software or with Leica thunder imaging system with Leica LAS-X software. Fluorescence was detected with dsRed and green fluorescent protein (GFP) filters.

Image analysis

All images were analyzed using FIJI software.[40]

CreER-loxP cell labelling (lineage tracing)

Zebrafish embryos at 24 hpf were treated with 5 μM 4-OHT (H7904, Sigma) for 24 hours. Controls were incubated in the equivalent amount of Ethanol solution during the same period. Light exposure was avoided by using foil to cover the plates as 4-OHT is light sensitive. After treatment, embryos were washed with fresh embryo medium and placed back in incubator. From 5 dpf, larvae were transferred to the fish facility nursery where they were kept and fed. Embryos were raised for further analysis at different developmental stages.

Macrophage ablation and drug treatments

The Tg(fli1CreERT2;mpeg1:loxP-DsRedx-loxP-GFP-NTR) embryos were immersed in system water containing 10 mM metronidazole (M1547, Sigma) for 48 hours, which caused an acute depletion of GFP-NTR^{+} cells. The medium containing the MTZ was changed every 24 hours. Controls were incubated in the equivalent amount of DMSO solution during the same period. Light exposure was avoided by using foil to cover the plates as MTZ is light sensitive. Zebrafish were further analyzed by fluorescence imaging at different developmental time points. For primitive macrophage ablation using L-clodronate injection, the larvae were anesthetized in 0.016% Tricaine and microinjected with 5 nl of liposome encapsulated clodronate (www.clodronateliposomes.org) in the posterior caudal vein in the Urogenital Opening region at 48 hpf. Control embryos were similarly injected with liposome-PBS (L-PBS).

Tail fin amputation

2 and 5 dpf larvae were anesthetized with 0.01% tricaine and amputated with a sterile scalpel. The amputation was performed by using the posterior section of the ventral pigmentation gap in the tail fin as a reference, and immediately after amputation larvae were incubated in either E3 medium, or in MTZ in case of macrophage ablation at 28°C.

Quantification of tail fin regeneration

At 24-, 48- and 72-hours post amputation or dpa (6,7- and 8-days post fertilization, respectively), larvae were mounted in 2.5% methylcellulose, and regenerating tail fins were imaged in bright field. Tail fin area was measured from the anterior section of the ventral tail fin gap to the end of the regenerating fin, as previously described,[42] using FiJi software. Tail fin areas were calculated and expressed in square micrometers (um^{2}).

Quantification of tail macrophages

Macrophages were quantified based on their location in the tail (periphery vs CHT) (Figure 2B) in non-amputated larvae. In amputated larvae, recruited macrophages to the site of injury were quantified. Normalization of recruited macrophage numbers was obtained by dividing the number of recruited macrophage subpopulation by their total number in the tail of the same larvae (periphery, CHT and recruited macrophages).[28] We have factored the labelling efficiency in our quantification data analysis in Figures 3 and 4.

Cell proliferation analysis

For cell proliferation analysis, EdU analysis was performed in 72 hpa larvae previously fixed in 4% PFA and dehydrated with methanol, using Click-iT EdU cell proliferation kit for imaging, Alexa Fluor 647 dye. Stained larvae were imaged using fluorescence microscopy and analyzed using FIJI.

QUANTIFICATION AND STATISTICAL ANALYSIS

Statistical analyses were performed by the GraphPad Prism software (Prism 9). All experiments with only two groups and one dependent variable were compared using an unpaired t-test with Welch's correction. Two-way ANOVA with Sidak's multiple comparison was used for this analysis. Statistical data show mean ± s.e.m. Each dot plot value represents an independent embryo, and every experiment was conducted three times independently. The corrected total cell fluorescence (CTCF) was calculated using the formula 'Integrated density whole – (area whole embryo x mean fluorescence background)'. This formula is loosely based on a method described for calculating cell-fluorescence.[10] To calculate the CTCF percentage for DsRed+ cells, the CTCF value of DsRed was divided by the total summation of CTCF values for both DsRed and GFP in each larvae. The same was done for calculating CTCF percentage for GFP+ cells.

Figure S1. Labeling strategy and the labeling efficiency of using thymocytes as a positive read out with *lck*:switch and *coro1a*:switch transgenic lines, Related to Figure 1.

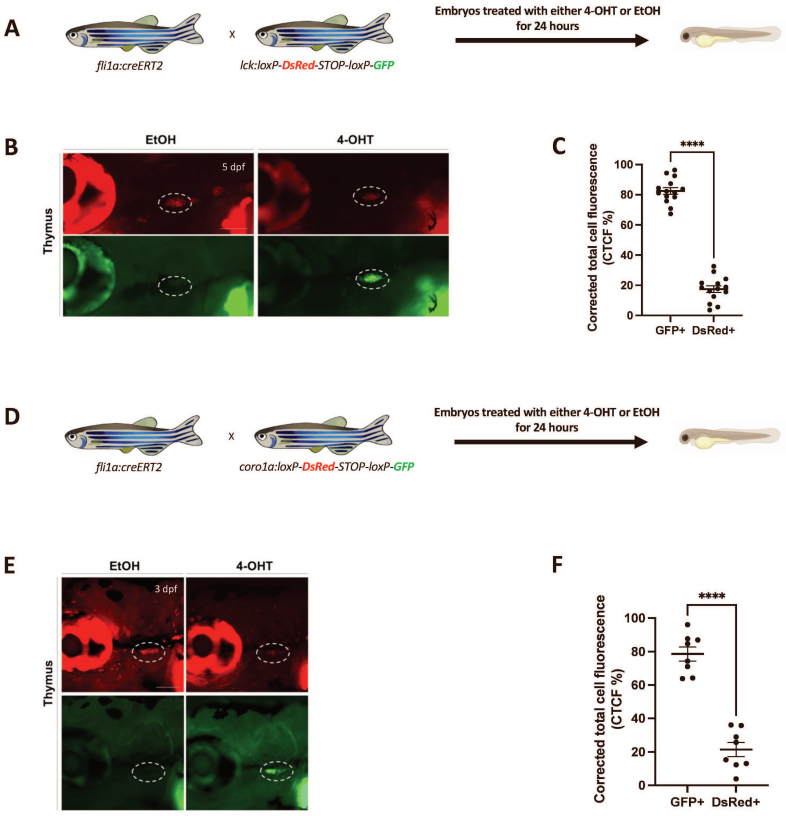

Figure S2. Quantification of GFP+ microglia in the head region at 2 dpf embryos, Related to Figure 2.

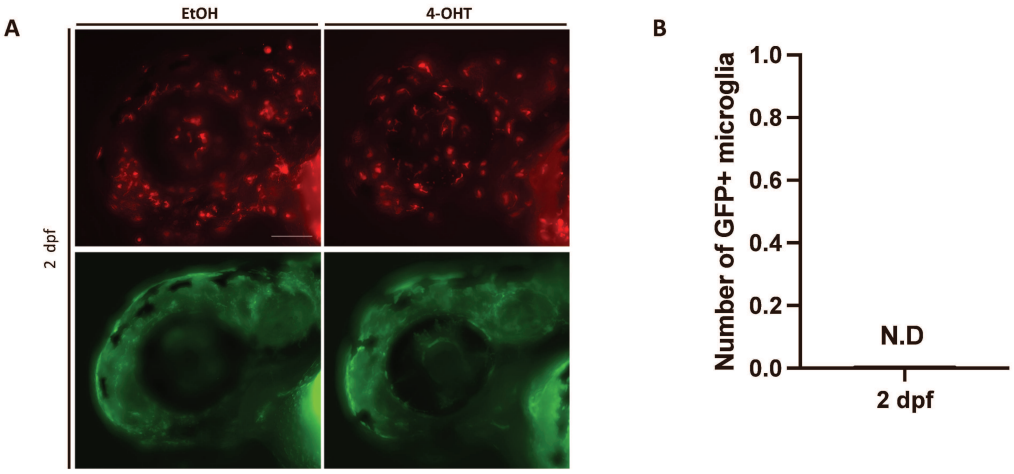

Figure S3. Ontogenetically distinct macrophages recruitment after tail injury at different developmental stages, Related to Figure 3 and 4.

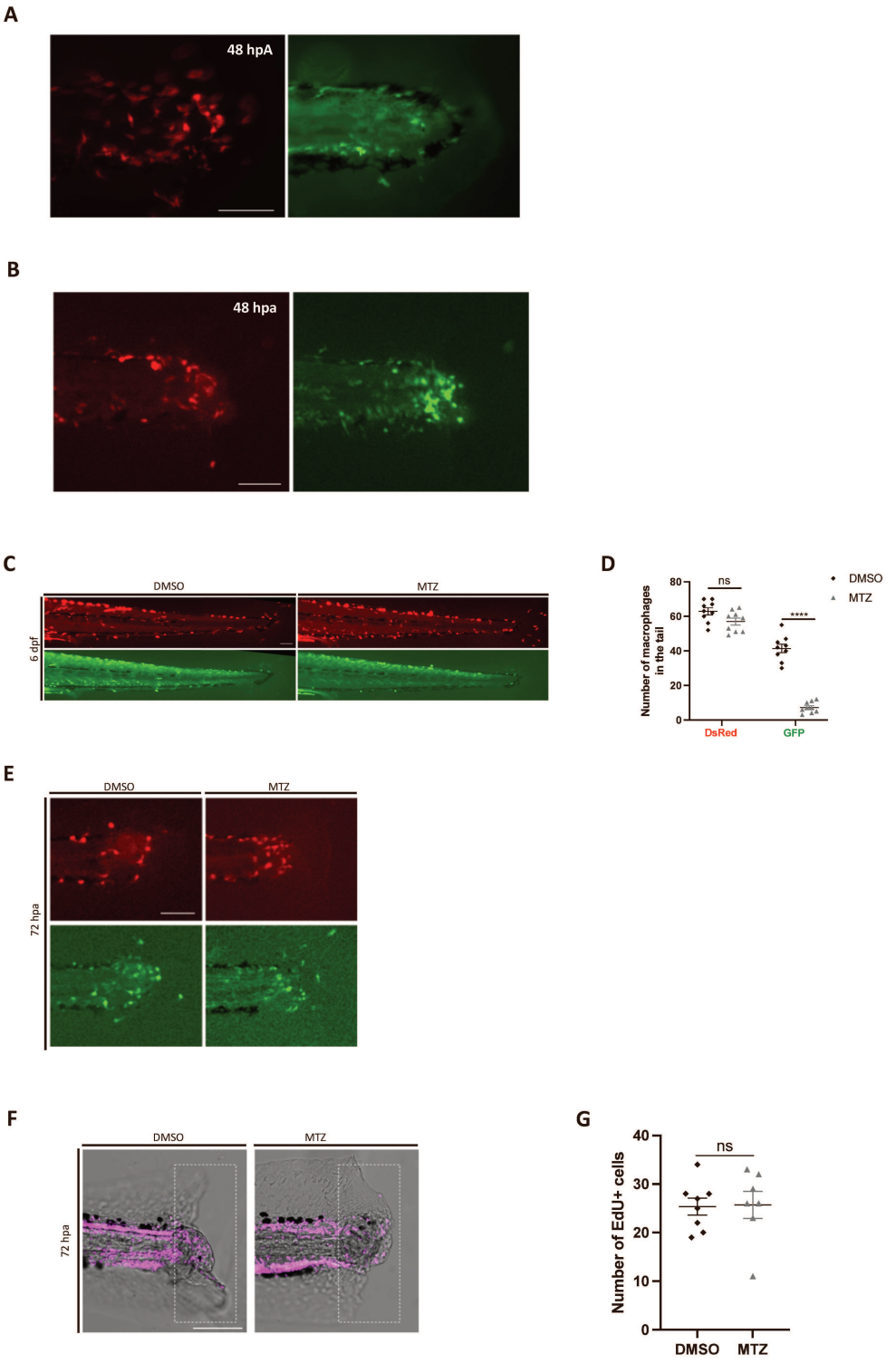

Figure S1. Labeling strategy and the labeling efficiency of using thymocytes as a positive read out with *lck*:switch and *coro1a*:switch transgenic lines. Related to Figure 1.

(A) Scheme of the 4-OHT-inducible *Tg(fli1a:creERT2;lck:Switch)* line used to assess the efficiency of the labelling strategy.

(B) Fluorescent images of EtOH non-switched controls (left) and 4-OHT-induced (right) *Tg(fli1a:creERT2;lck:Switch)* thymocytes at 5 dpf larvae. Representative images are shown. Scale bars, 100 µm.

(C) Quantification of DsRed and GFP fluorescence intensity percentage in the thymic region was measured at 5dpf (n=14). Mean ± SEM of the $DsRed^+$ and GFP^+ corrected total cell fluorescence (CTCF) percentage is shown. ****p≤ 0.0001

(D) Scheme of the 4-OHT-inducible *Tg(fli1a:creERT2; coro1a:Switch)* line used to assess the efficiency of the labelling strategy.

(E) Fluorescent images of EtOH non-switched controls (left) and 4-OHT-induced (right) *Tg(fli1a:creERT2;coro1a:Switch)* thymocytes at 3 dpf embryos. Representative images are shown. Scale bars, 100 µm.

(F) Quantification of DsRed and GFP fluorescence intensity percentage in the thymic region was measured at 3dpf (n=8). Mean ± SEM of the $DsRed^+$ and GFP^+ corrected total cell fluorescence (CTCF) percentage is shown. ****p≤ 0.0001

Figure S2. Quantification of GFP+ microglia in the head region at 2 dpf embryos. related to Figure 2.

(A) Fluorescent images of EtOH non-switched controls (left) and 4-OHT-induced (right) *Tg(fli1a:creERT2;mpeg1:Switch)* head regions in the developing embryos at 2 dpf. Representative images are shown. Scale bar: 100µm.

(B) Quantification of GFP+ macrophage number in the head at 2 dpf (n=6). Mean ± SEM of the GFP^+ macrophage numbers are shown.

Figure S3. Ontogenetically distinct macrophages recruitment after tail injury at different developmental stages. related to Figure 3 and 4.

(A) Tail fin of *Tg(fli1a:creERT2;mpeg1:Switch)* were amputated at 2 dpf and macrophage recruitment to the site of injury was analyzed. Representative images are shown at 48 hpa. Scale bar: 100µm.

(B) Tail fin of *Tg(fli1a:creERT2;mpeg1:Switch)* were amputated at 5 dpf and macrophage recruitment to the site of injury was analyzed. Representative images are shown at 48 hpa. Scale bar: 100µm.

(C) Switched *Tg(fli1a:creERT2;mpeg1:Switch)* larvae were treated with DMSO as a control, or metronidazole (MTZ) to ablate definitive macrophages. Treatments were performed from 4 to 6 dpf. Representative images are shown at 6 dpf. Scale bars: 100 µm.

(D) Quantification of DsRed and GFP macrophage number in the tail region 48 hours after DMSO (n=9) or MTZ treatments (n=9). Mean ± SEM of the $DsRed^+$ and GFP^+ macrophage numbers are shown. ****p ≤ 0.0001.

(E) Switched *Tg(fli1a:creERT2;mpeg1:Switch)* larvae were treated with DMSO or MTZ. Treatments were performed from 4 to 6 dpf and tail fins were amputated at 5 dpf. Representative images are shown 72 hpa. Scale bars: 100 µm.

(F) Cell proliferation was measured by EdU assay at 72 hpa. Red dots represent EdU^+ cells. Representative images are shown at 72 hpa of larvae treated with DMSO as a control, or metronidazole (MTZ) to ablate definitive macrophages. Scale bar: 100µm.

(G) Numbers of EdU^+ cells in switched *Tg(fli1a:creERT2;mpeg1:Switch)* larvae that were treated with DMSO (n=8) or MTZ (n=7). Unpaired t-test with Welch's correction was used for the analysis.

RÉSUMÉ

Les études d'association pangénomiques humaines ont identifié l'Interleukine-26 (IL-26) comme un facteur de risque génétique pour les maladies inflammatoires de l'intestin. Cependant, ses fonctions *in vivo* restent largement inexplorées en raison de l'absence de l'IL-26 chez les rongeurs. De manière intéressante, le poisson-zèbre possède un homologue unique du gène IL-26 humain.

En utilisant des larves de poisson-zèbre, nous avons découvert que l'IL-26 supprime la prolifération et les dommages à l'ADN dans les cellules épithéliales intestinales. De plus, nous avons mis en évidence que la colonisation microbienne de l'intestin induit l'expression de l'IL-26 dans les cellules lymphoïdes innées (ILC), identifiant ainsi un nouveau circuit entre le microbiote, les ILC et l'épithélium. Cela éclaire de nouvelles voies thérapeutiques potentielles pour les maladies impliquant des réponses immunitaires dysrégulées dans le tractus gastro-intestinal.

MOTS CLÉS

Homéostasie intestinale, scRNA-seq, infection bactérienne, sans germes

ABSTRACT

Human genome-wide association studies have identified interleukin-26 (IL-26) as a risk locus for inflammatory bowel diseases (IBD). However, the *in vivo* functions of this cytokine remain largely uncharacterized largely due to its absence in rodents. Interestingly, the zebrafish possesses a unique homolog of the human IL-26 gene.

Using zebrafish larvae, we found that IL-26 suppresses proliferation and DNA damage in intestinal epithelial cells. Moreover, we uncovered that microbial colonization of the gut induces IL-26 expression in innate lymphoid cells (ILCs), identifying a new circuit between microbiota, ILCs, and the epithelium. This sheds a light on potential therapeutic avenues for diseases involving dysregulated immune responses in the gastrointestinal tract.

KEYWORDS

Gut homeostasis, scRNA-seq, bacterial infection, germ-free